

Exploring the Influence of Entropy on Dynamic Macromolecular Ligation

Zur Erlangung des akademischen Grades eines

DOKTORS DER NATURWISSENSCHAFTEN

(Dr. rer. nat.)

der KIT-Fakultät für Chemie und Biowissenschaften

des Karlsruher Instituts für Technologie (KIT)

genehmigte

DISSERTATION

von

Dipl.-Chem. Kai Pahnke

aus

Nagold, Deutschland

KIT-Dekan: Prof. Dr. Willem M. Klopper

Referent: Prof. Dr. Christopher Barner-Kowollik

Korreferent: Prof. Dr. Manfred Wilhelm

Tag der mündlichen Prüfung: 22.07.2016

Die vorliegende Arbeit wurde im Zeitraum von Februar 2013 bis Juni 2016 im Rahmen einer Kollaboration zwischen dem KIT und der Evonik Industries AG unter der Betreuung von Prof. Dr. Christopher Barner-Kowollik durchgeführt

Only entropy comes easy.

Anton Chekhov

ABSTRACT

The present thesis reports a novel, expedient linker species as well as previously unforeseen effects of physical molecular parameters on reaction entropy and thus equilibria with extensive implications on diverse fields of research via the study of dynamic ligation chemistries, especially in the realm of macromolecular chemistry.

A set of experiments investigating the influence of different physical molecular parameters on reaction or association equilibria is designed. Initially, previous findings of a mass dependant effect on the reaction entropy – resulting in a more pronounced debonding of heavier or longer species – are reproduced and expanded to other dynamic ligation techniques as well as further characterization methods, now including a rapid and catalyst-free Diels–Alder reaction. The effects are evidenced via high temperature nuclear magnetic resonance spectroscopy (HT NMR) as well as temperature dependent size exclusion chromatography (TD SEC) and verified via quantum chemical *ab initio* calculations.

Next, the impact of chain mobility on entropic reaction parameters and thus the overall bonding behavior is explored via the thermoreversible ligation of chains of similar mass and length, comprising isomeric butyl side-chain substituents with differing steric demands. The employed chains are synthesized via activators regenerated by electron-transfer (ARGET) atom transfer radical polymerization (ATRP), a controlled reversible deactivation radical polymerization (RDRP) technique. As the more mobile species are undergoing significantly higher degrees of chain cleavage, chain stiffness is demonstrated to have a similar impact on reaction equilibria as adduct masses, again verified via HT NMR and TD SEC as well as corroborating computational calculations.

Furthermore, the universal applicability of the explored entropic effects is evidenced not only for reversible covalent chemistries, yet also for non-covalent, supramolecular associations via the investigation of the dissociation characteristics of differently sized associates. Polymer blocks are synthesized via another RDRP technique – reversible addition-fragmentation chain-transfer (RAFT) polymerization – and selectively associated via the hydrogen bonding of cyanuric acid with Hamilton wedge functional end-groups. The

dissociation constants of the self-assembled diblock polymers are quantified via NMR titration methods, verifying the occurrence of entropic mass effects also within non-covalent ligation methods.

Finally, the impact of the ligation position on the (de-)bonding characteristics of adducts in otherwise similar (chain) molecules of the same overall length – their building blocks again synthesized via ARGET ATRP or RAFT techniques – is explored. Both covalent step-growth adducts, studied via TD SEC, as well as non-covalent diblock associates, characterized via NMR titration, are considered and the results are interpreted via computational calculations of geometrical model systems. While at central bonding sites an entropically favored chain cleavage is observed, terminal ligation of molecules leads to relatively unfavorable scission of the dynamic linkage as established for analogous small molecular adducts.

In addition, the computationally-driven design and implementation of dithiooxalates in a di-functional hetero Diels–Alder linker is described. The obtained linker enables mild, rapid, efficient, and thermoreversible linkage of diverse dienes, characterized via UV/Vis spectroscopy, (HT) NMR, high-resolution electrospray ionization mass spectrometry (ESI-MS) as well as TD SEC, rendering it a promising candidate for application in polymer science and organic chemistry as well as industry, the latter also due to its straightforward and cost effective synthesis from readily available starting materials.

ZUSAMMENFASSUNG

Die vorliegende Arbeit beschreibt einen neuartigen, vorteilhaften Vernetzer sowie die Untersuchung von dynamischen – vor allem makromolekularen – Verknüpfungsmethoden. Dabei wurden bisher unbekannte Auswirkungen von physikalischen Molekülparametern auf die Entropie und damit auch Gleichgewichte von chemischen Reaktionen beobachtet und untersucht, die zu weitreichenden Auswirkungen auf verschiedenste Forschungsgebiete führen.

Ein experimenteller Aufbau zur Untersuchung des Einflusses von verschiedenen physikalischen Molekülparametern auf Reaktions- oder Assoziationsgleichgewichte wird entworfen. Zunächst werden vorausgegangene Befunde eines Masseneffekts auf die Reaktionsentropie – welcher eine stärker ausgeprägte Entknüpfung von schwereren und längeren Addukten zur Folge hat – reproduziert und auf andere Charakterisierungsmethoden sowie chemische Verknüpfungsarten wie eine schnelle und katalysatorfreie Hetero-Diels–Alder-Reaktion übertragen. Die Effekte werden mittels Hochtemperatur-Kernresonanzspektroskopie (HT NMR) sowie temperaturabhängiger Größenausschlusschromatographie (TD SEC) aufgezeigt und mit Hilfe von quantenchemischen *ab initio*-Berechnungen verifiziert.

Im nächsten Schritt wird der Einfluss der Kettenmobilität oder -steifigkeit auf entropische Reaktionsparameter und dadurch auf das Gesamtbindungsverhalten untersucht, indem Kettenmoleküle von gleicher Masse und Länge mit isomeren Butylseitenketten unterschiedlichen sterischen Anspruchs thermoreversibel verknüpft werden. Die eingesetzten Ketten werden mittels *activators regenerated by electrontransfer* (ARGET) Atom Transfer radikalischer Polymerisation (ATRP), einer kontrollierten reversibel deaktivierenden radikalischen Polymerisation (RDRP), synthetisiert. Abermals werden die Proben per HT NMR und TD SEC sowie computergestützten Berechnungen untersucht. Da die weniger steifen Ketten einem signifikant höheren Anteil an Kettenspaltung unterlaufen, kann ein vergleichbar großer Einfluss der Kettensteifigkeit wie der zuvor beschriebene der Kettenmasse und -länge auf Reaktionsgleichgewichte aufgezeigt werden.

Um die universelle Einsetzbarkeit der erforschten entropischen Effekte nicht nur für kovalente, sondern auch für nicht-kovalente, supramolekulare Assoziationsarten nachzuweisen, wurde das Dissoziationsverhalten verschieden großer Assoziate untersucht. Die dafür benötigten Polymerblöcke wurden mittels einer weiteren RDRP-Technik – der reversiblen Additions-Fragmentierungs Kettentransfer- (RAFT) Polymerisation – synthetisiert und selektiv über die Wasserstoffbrückenbindung von Cyanursäure- und Hamilton Wedge funktionalen Endgruppen assoziiert. Die Dissoziationskonstanten der selbstorganisierten Diblockpolymere werden per NMR-Titrationsmethoden quantifiziert und belegen den entropischen Masseneffekt auch für nicht-kovalente Verknüpfungsmethoden.

Schließlich wird der Einfluss der reversiblen Verknüfungsposition auf die Bindungscharakteristika ansonsten gleichartiger (Ketten-) Molekülen der gleichen Gesamtlänge untersucht. Die benötigten polymeren Bausteine werden abermals mittels ARGET ATRP- oder RAFT-Methoden synthetisiert. Sowohl kovalente Stufenwachstumsaddukte, untersucht per TD SEC, als auch nicht-kovalente Diblockassoziate, charakterisiert mittels NMR-Titration, wurden berücksichtigt und die gewonnenen Ergebnisse mit Hilfe von computergestützten Berechnungen an geometrischen Modellsystemen interpretiert. Während an mittelständigen Verknüfungsstellen ein entropisch bevorzugter Kettenbruch zu beobachten ist, führt die dynamische Anbindung von kleinen Molekülen an terminale Bindungsstellen zu einer relativ benachteiligten Abspaltung, die vergleichbar mit analogen niedermolekularen Bindungscharakteristika ist.

Zusätzlich wird die computerunterstützte Planung, Synthese und Untersuchung eines Dithiooxalat-difunktionalen Hetero-Diels–Alder-Vernetzers beschrieben. Der gewonnene Vernetzer erlaubt die milde, schnelle, effiziente und thermoreversible Verknüpfung verschiedenster Diene, charakterisiert und belegt mittels UV/Vis Spektroskopie, (HT) NMR, hochauflösender Elektrospray-Ionisierungs-Massenspektrometrie (ESI-MS) sowie TD SEC. Die positiven Ergebnisse sowie seine unkomplizierte und wirtschaftliche Synthese aus leicht verfügbaren Ausgangsstoffen machen den neuartigen Vernetzer zu einem vielversprechenden Kandidaten für Anwendungen in den Polymerwissenschaften, der organischen Chemie sowie der Industrie.

PUBLICATIONS

Publications Arising from this Thesis

[4] *A Mild, Efficient and Catalyst-Free Thermoreversible Ligation System Based on Dithiooxalates*

K. Pahnke, N. L. Haworth, J. Brandt, U. Paulmann, C. Richter, F. G. Schmidt, A. Lederer, M. L. Coote, C. Barner-Kowollik, *Polym. Chem.* **2016**, *7*, 3244-3250.

[3a] *Entropy-Driven Selectivity for Chain Scission: Where Macromolecules Cleave*

K. Pahnke, J. Brandt, G. Gryn'ova, C. Y. Lin, O. Altintas, F. G. Schmidt, A. Lederer, M. L. Coote, C. Barner-Kowollik, *Angew. Chem. Int. Ed.* **2016**, *55*, 1514-1518.

[3b] *Entropisch bedingte Selektivität der Kettenspaltung oder: Wo Makromoleküle sich trennen*

K. Pahnke, J. Brandt, G. Gryn'ova, C. Y. Lin, O. Altintas, F. G. Schmidt, A. Lederer, M. L. Coote, C. Barner-Kowollik, *Angew. Chem.* **2016**, *128*, 1537-1541.

[2] *Entropic Effects on the Supramolecular Self-Assembly of Macromolecules*

K. Pahnke, O. Altintas, F. G. Schmidt, C. Barner-Kowollik, *ACS Macro Lett.* **2015**, *4*, 774-777.

[1] *Entropy Driven Chain Effects on Ligation Chemistry*

K. Pahnke, J. Brandt, G. Gryn'ova, P. Lindner, R. Schweins, F. G. Schmidt, A. Lederer, M. L. Coote, C. Barner-Kowollik, *Chem. Sci.* **2015**, *6*, 1061-1074.

Patents Arising from this Thesis

- [1] *Neuartige Hetero-Diels-Alder-Vernetzer und deren Verwendung in reversibel vernetzenden Polymersystemen*

F. G. Schmidt, U. Paulmann, C. Richter, M. Inhestern, C. Meier, C. Barner-Kowollik, **K. Pahnke**, M. A. Sanz, S. Umbreen, IP-Nr. to be advised.

Additional Publications

- [1] *Consecutive Modular Ligation as an Access Route to Palladium Containing Polymers*

C. Lang, **K. Pahnke**, C. Kiefer, A. S. Goldmann, P. W. Roesky, C. Barner-Kowollik, *Polym. Chem.* **2013**, *4*, 5456-5462.

TABLE OF CONTENTS

1	Introduction	1
2	Theory and Background	5
2.1	Polymer Chemistry	6
2.1.1	History of Polymer Chemistry.....	6
2.1.2	Polymer Properties	7
2.1.3	Chain-Growth Polymerization	11
2.1.4	Step-Growth Polymerization	13
2.1.5	Advanced Polymerization Methods	16
	Atom Transfer Radical Polymerization.....	17
	Reversible Addition-Fragmentation Chain-Transfer Polymerization	18
2.2	Dynamic Ligation Systems.....	21
2.2.1	Diels–Alder Reactions	22
2.2.2	Hydrogen Bonding	28
2.3	Thermodynamics of Chemical Equilibria	33
2.3.1	Classical and Statistical Thermodynamics.....	33
2.3.2	Computational Assessment of Reactions	37
3	Entropic Effects on Chemical Equilibria	41
3.1	Motivation	41
3.2	Mass/Length Effect on Dynamic Reactions.....	45
3.2.1	Experimental Design	45
3.2.2	Computational Studies	46
3.2.3	High Temperature NMR.....	50
3.2.4	Temperature Dependent SEC.....	54
3.2.5	Summary.....	55
3.3	Chain Stiffness Effect on Reaction Equilibria	57

3.3.1	Experimental Design	57
3.3.2	Computational Studies	58
3.3.3	High Temperature NMR	61
3.3.4	Temperature Dependent SEC.....	67
3.3.5	Summary.....	68
3.4	Entropic Effects on Non-Covalent Ligation	71
3.4.1	Experimental Design	72
3.4.2	NMR Measurements.....	74
3.4.3	Summary.....	76
3.5	Effect of the Ligation Position on Reactions	79
3.5.1	Experimental Design	79
3.5.2	Computational Studies	80
3.5.3	NMR Titration of Hydrogen-Bonding Specimen.....	81
3.5.4	Temperature Dependent SEC of Covalently Bonded Materials	84
3.5.5	Summary.....	87
3.6	Conclusions.....	89
4	Excursion: Dithiooxalates as Thermoreversible Linkers	91
4.1	Motivation	91
4.2	Computational Guidance	93
4.3	Design of a Novel Diels–Alder Linker.....	96
4.4	UV/Vis Kinetics Studies.....	97
4.5	Transfer to Reversible Polymer Ligation	101
4.5.1	Step-Growth Polymerization of Difunctional Dienes	101
4.5.2	Demonstration of Thermoreversible Bonding Character	103
4.6	Conclusions.....	106
5	Concluding Remarks and Outlook	107
6	Experimental Section	111
6.1	Materials.....	111

6.2	Methods and Instruments	113
6.3	Synthetic Procedures	117
6.3.1	Syntheses from Section 3.2 and 3.3.....	117
6.3.2	Syntheses from Section 3.4	124
6.3.3	Syntheses from Section 3.5	130
6.3.4	Syntheses from Chapter 4	133
6.4	Computational Data	138
6.4.1	Computational Data from Section 3.2 and 3.3.....	138
6.4.2	Computational Data from Chapter 4	142
	Bibliography	159
	List of Schemes, Figures and Tables	173
	Schemes.....	173
	Figures	177
	Tables	184
	List of Abbreviations.....	187
	Curriculum Vitae.....	191
	Publications and Conference Contributions	193
	Publications Arising from this Thesis.....	193
	Patents Arising from this Thesis	194
	Additional Publications	194
	Invited Talk and Conference Contributions.....	194
	Acknowledgements	197
	Declaration.....	199

1

INTRODUCTION

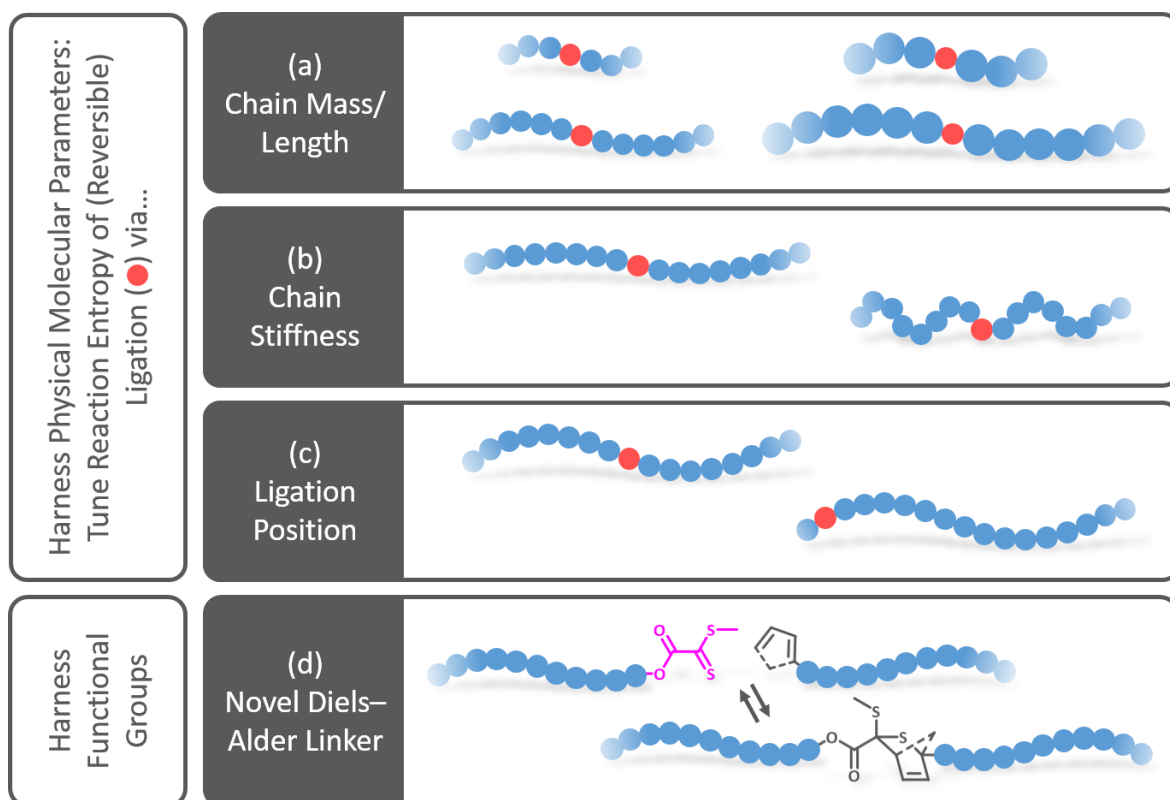
The ever ongoing efforts and progress in chemistry, biology, physics or science in general enables the design and employment of new or revisited materials with novel, adaptive characteristics.¹ For many years, for example plastic materials have largely been inexpensive, lightweight and durable, yet at the same time inherently passive materials with certain mechanical or chemical characteristics. Only recently, progress in chemistry and polymer science allowed for the integration of stimuli-responsive and smart abilities, leading to the introduction of more dynamic materials and enabling the design and emergence of new material classes with added tailor-made functionality and value.¹⁻⁶ The aforementioned smart materials, often based on basic principles adopted from nature, entail the capability to respond on-demand to physical or chemical stimuli from their environment such as altered temperature, changed solvents, redox potentials, pH values, irradiation with light and also magnetic or electric fields via, e.g., a change in conformation or bonding.^{2, 3, 5, 7-19} As a result, a wide field of applications of intelligent materials in sensors and switches, self-healing or shape-memorizing polymers, biomimetic and drug-delivery systems amongst others is possible, leading to great interest especially in the fields of

aerospace and biomedical materials, but also products of everyday use as for example in the automotive industry.^{1, 2, 5, 7, 20-25} One very popular avenue to create smart materials is the integration of dynamic covalent or supramolecular bonds in the chemical composition of a material. Thus, a reversible bonding or debonding on demand of the microscopic structure of so-called dynamats – or in the case of polymeric materials dynamers – via diverse stimuli is enabled.^{1, 5, 26} In doing so, self-healing, -assembling or -immolative species can be realized.^{5, 27-34} The example of self-healing materials is one of the great challenges in materials science of recent years, as it addresses the very important topic of material lifetime, durability and recyclability, leading to, e.g., sustainable, resource-efficient and lightweight materials with high mechanical strengths for applications such as aircraft or automotive manufacturing as well as in less and in-accessible areas such as medical and aerospace technology.^{1, 4, 5, 22, 35-37} With the ongoing progress and increasing use of dynamic chemistries in materials science, an in-depth understanding of the underlying principles of bonding is of great importance. While there is a great variety of possible dynamic covalent as well as non-covalent interactions such as Diels–Alder chemistry, the reversible cleavage of nitroxides or disulfide bridges, dynamic vitrimers formed via transesterification, metathesis or vinylogous urethanes, hydrogen bonding, metal-ligand interactions, pi stacking etc., their chemical integration in target molecules and compounds remains challenging.^{5, 6, 26, 36, 38-47} Consequently, a more general method to tune bonding attributes via physical molecular parameters is desired to facilitate the adjustment of dynamic properties. Furthermore, differences in observed (de-)bonding attributes in several studies of similar chemical linkage units can be accounted for in an altered molecular context to guarantee the desired material properties in the final product.

Polymer chemistry with its versatile synthetic methods for well-defined molecules provides for a multitude of possibilities to investigate the influence of altered physical molecular parameters on ligation sites. For example, reversible deactivation radical polymerization (RDRP) of various monomers allows for high end-group fidelity, as well as very variable and precisely adjustable molecular characteristics such as mass, length, stiffness, bulkiness etc. The click-inspired, efficient, high yielding and robust nature of selected dynamic catalyzed or catalyst-free Diels–Alder cycloadditions in combination with their thermoreversibility – in numerous cases at expedient temperatures – renders them a prime example of covalent

dynamic chemistry.^{5, 48-51} The combination of both polymer and Diels–Alder chemistry has been demonstrated to result in materials of great academic as well as industrial interest and – together with additional non-covalent examples of reversible ligation via hydrogen bonding – forms the basis of the present thesis.

The main part of the thesis investigates the different possibilities of manipulating dynamic equilibria of covalent or supramolecular association chemistries via non-enthalpic, i.e., entropic means. Hence, the possibility to harness physical parameters of (macro-) molecules in order to alter reaction entropies and thus equilibrium positions are experimentally as well as theoretically explored. More specifically, the influence of the molecular mass of ligated building blocks in covalently – and later on supramolecularly – joint adducts is investigated at first (Scheme 1-1 (a)). Subsequently, also the impact of intramolecular mobility or stiffness and finally of the ligation position inside a molecule itself is highlighted (Scheme 1-1 (b) and (c)).



Scheme 1-1 Overview of the investigated possibilities to adjust the reaction entropy and thus equilibrium of (reversible) covalent or non-covalent ligation sites via altering (a) chain mass or length, (b) chain stiffness or (c) the ligation position of adducts as well as a schematic depiction of the novel self-reporting dithiooxalate hetero Diels–Alder linker (d) with valuable ligation properties.

Additionally, an offshoot of the project allows for the establishment and characterization of a novel, self-reporting, simple to synthesize and low-cost hetero Diels–Alder linker comprising dithiooxalates (Scheme 1-1 (d)) in an attempt to expand the toolbox of dynamic ligation chemistries with mild and efficient reaction properties. Thereby, the quest for beneficial ligation methods for applications in, e.g., polymer and organic chemistry as well as materials science is pursued further.

The newly established effects studied in the present thesis provide for a basis and deepen the understanding of previously unforeseen physical influences on covalent and non-covalent linkage mechanisms. Thus, the current work expands a mainly enthalpic research area via entropic contributions in – especially macromolecular – ligation chemistry and their impact on various research fields such as polymer synthesis and degradation, synthetic biochemistry and ligation chemistry in general is discussed. To further extend the possibilities of dynamic ligation tools, a very efficient all-purpose and industrially feasible Diels–Alder linker was designed and investigated.

2

THEORY AND BACKGROUND

The following chapter introduces a literature review of the basic principles relevant for a general understanding of the present dissertation. In order to not go beyond the scope of the thesis, it is designed to give a general overview and background information on its topics, theories and employed methods, while not being exhaustive. To begin with, the development of polymer chemistry (Section 2.1.1), leading to an understanding of polymer properties (Section 2.1.2), common polymerization techniques (Sections 2.1.3 and 2.1.4) as well as advanced polymerization techniques (Section 2.1.5) enabling the generation of defined polymer chains suitable for the studies at hand, are summarized. Next, the employed examples of dynamic covalent as well as non-covalent ligation methods (Section 1.1) are highlighted. Finally, essential concepts of chemical thermodynamics and computational chemistry (Section 1.1) are summarized. For more details regarding particular topics, the reader is referred to the relevant literature.

2.1 Polymer Chemistry

The current section describes the emergence and importance of polymer chemistry, underlying molecular principles leading to macromolecular characteristics and different basic as well as advanced polymerization techniques for the generation of defined polymeric materials.

2.1.1 History of Polymer Chemistry

Natural polymeric materials have been utilized by humankind since millennia, for instance natural fibers such as silk or cotton, cellulose in the form of wood or papyrus, natural rubber, polysaccharides etc. Besides other biopolymers, without one very specific polymer – our DNA (deoxyribonucleic acid) – life as we know it would not even be possible at all. In the course of the 19th century, first synthetically modified natural polymers were discovered and industrially produced due to their enhanced and tunable properties profiles. The most prominent examples are vulcanized rubber, developed by Charles Goodyear in the 1840s, or diverse nitrocellulose products, investigated by Christian Schönbein and Alexander Parks, amongst others, and successfully commercialized in the form of celluloid by John W. Hyatt in 1868.⁵²⁻⁵⁵ The first purpose-made fully synthetic plastic, a thermoset produced in a polycondensation of formaldehyde and phenol, was discovered in 1872 by Adolf v. Baeyer and commercialized in the early 20th century as Bakelite by Leo Baekeland.⁵⁶⁻⁵⁸ Nowadays common vinylic monomers, e.g., styrene or vinyl chloride, were known since the early 19th century but their use in a targeted polymerization was not discovered until the beginning of the 20th century.^{59, 60} Despite unfamiliar polymer characteristics being described at least since the beginning of the 19th century, the fundamental understanding of polymers and their properties was only established around 1930. Although Hermann Staudinger fought for his conviction of a chain-like macromolecular structure of polymers consisting of covalently linked repeating units, for many years the misconception of polymers being colloids – an aggregation of small molecules with the supposed ability to crystallize, if they were sufficiently purified – was commonly spread in the scientific world.^{61, 62} Additional efforts of other scientists such as Herman Mark, investigating natural macromolecules via crystallography, Werner Kuhn and Hans Kuhn with statistical descriptions of chain molecules or Wallace Carothers exploring

polycondensation reactions in the late 1920s to obtain step-growth polymers such as nylon or neoprene substantiated Staudinger's theses, finally leading to the bestowing of Staudinger with the Nobel Prize in 1953.^{54, 62} During World War II, shortages of resources led to expedited developments in polymer science to enable access to synthetic rubber and insulating materials. After World War II, the now extensive and sustained progress in polymer science in combination with economic growth allowed for countless novel developments and enabled a mass-production of plastic convenience products via, for example, the coordinative polymerization of ethylene or propylene with the help of metalorganic catalysts, discovered by Karl Ziegler and Giulio Natta, earning them the Nobel Prize in 1963.^{58, 63, 64} Since then, the growing demand for polymeric materials with their versatile characteristics and high availability drove the worldwide production of plastics to ever higher numbers, from 1.5 million tons in 1950 to 311 million tons in 2014.⁶⁵ Nonetheless, novel developments in polymer and organic chemistry, as for instance controlled polymerization techniques as well as the revisiting of established methods such as dynamic thermoreversible Diels–Alder adduct formation lead to more and more tailor-made materials, for example with abilities to be responsive to external stimuli, self-healing, shape memorizing, immolative etc., demonstrating the abilities, possibilities and challenges for upcoming generations of chemists and materials scientists.^{3-5, 24, 66, 67}

2.1.2 Polymer Properties

Polymers exhibit unique properties due to their chain-like macromolecular structure and typical molecular weights in the range of 10^3 - 10^6 g · mol⁻¹. To further define their characteristics, some basic definitions and classifications have to be introduced first. A description of the size of molecules can be obtained via the degree of polymerization DP_n , which is the mass of the polymer $M_{polymer}$ divided by the mass of the incorporated monomeric units $M_{monomer}$ (equation 2-1), thus resulting in the number of polymerized monomer molecules:

$$DP_n = \frac{M_{polymer}}{M_{monomer}} \quad 2-1$$

The more or less controlled characteristics of different polymerization techniques (refer to Sections 2.1.3-2.1.5) lead to a distribution of different chain lengths and masses in standard

syntheses. Accordingly, an average molecular weight of a sample can be observed, e.g. via light scattering, viscosimetry, end-group analysis or size exclusion chromatography. The number averaged molecular weight (M_n , equation 2-2; n_i : number of molecules of weight M_i) and weight averaged molecular weight (M_w , equation 2-3; w_i : weight fraction of molecules of weight M_i) are the most commonly determined values:⁵⁸

$$M_n = \frac{\sum_i n_i M_i}{\sum_i n_i} \quad 2-2$$

$$M_w = \frac{\sum_i w_i M_i}{\sum_i w_i} \quad 2-3$$

As a result of the higher weighting of molecules of higher masses in M_w , a mass discrimination of smaller molecules can be observed in contrast to M_n . A quantification of the width of the chain mass or length distribution of polymer species – for example to determine the degree of control in a polymerization – is typically specified via the ratio of M_w/M_n to yield the dispersity \mathcal{D} (equation 2-4):

$$\mathcal{D} = \frac{M_w}{M_n} \quad 2-4$$

One method to categorize different types of polymers is to consider their thermal and mechanical properties. In doing so, three main groups of polymers can be specified: Thermoplasts are non-cross-linked – thus linear or branched – meltable and mostly soluble macromolecules which are amorphous or partially crystalline. With varying network density, cross-linked polymers – which cannot be molten or dissolved – can be divided into two subspecies: Less cross-linked elastic and amorphous elastomers which can significantly swell in appropriate solvents, and highly cross-linked, rigid and mechanically robust thermosets.^{54, 58} Other possible substructures are for example cyclic or branched polymers.⁵⁴ While said properties allow for a general classification of polymeric materials, their individual nature can differ significantly for different employed monomers or monomer mixtures. A homopolymer is formed from one type of monomer or – more generally speaking – includes only similar repeating units. Accordingly, copolymers consist of two or more types of repeating units which can be arranged in various constitutional isomers such as random, statistical, alternating, block or graft copolymers.^{54, 68-71} If the employed monomers contain one or more stereogenic centers, tacticity arises with side-chain substituents having different stereo-configurations such as iso-, syndio- or atactic

behavior, depending on the polymerization method and also monomer species. Due to such a more or less ordered orientation of the side-groups, drastically altered bulk material properties can arise, e.g., as a result of higher degrees of crystalline domains in isotactic samples, they feature increased glass transition temperatures (T_g) and thus elevated viable application temperatures.^{54, 58, 60, 72} Besides constitution and configuration, the conformation, i.e., the spatial arrangement of a single polymer chain due to bond rotation as well as intra- and intermolecular interactions – thus being also highly dependent on the employed solvent – is of great importance for the macroscopic behavior of polymers. When employing a random walk algorithm with $n \rightarrow \infty$ steps to theoretically model a freely-jointed polymer chain with segments of the bond length l , the averaged square of the end-to-end distance $\langle r^2 \rangle$ can be obtained via equation 2-5 and its root mean square (RMS) $\langle r^2 \rangle^{1/2}$ accordingly via equation 2-6:⁵⁴

$$\langle r^2 \rangle = n \cdot l^2 \quad 2-5$$

$$\langle r^2 \rangle^{1/2} = n^{1/2} \cdot l \quad 2-6$$

One immediate observation is the RMS end-to-end distance being shorter than the contour length, which equals the product of n and l , indicating the coiled nature of chain molecules. Such a simplified approach is obviously not capable to reflect complex factors as for example excluded volume, fixed bond and rotation angles or rotation potentials. By adding further restrictions such as bond rotation with a fixed bond angle θ and steric considerations – due to its complex theoretical assessment often simplified by an experimental steric parameter σ of typically 1.5 to 2.5 – the RMS end-to-end distance with hindered rotation and fixed bond angles $\langle r^2 \rangle_0$ can be described via equation 2-7:⁵⁴

$$\langle r^2 \rangle_0 = \sigma \cdot n \cdot l^2 \cdot \left(\frac{1 - \cos\theta}{1 + \cos\theta} \right) \quad 2-7$$

The ratio of the mean square restricted vs. the freely jointed end-to-end distances enable a description of chain stiffness via the characteristic ratio C_∞ (equation 2-8) with typical values ranging from 3 (very flexible) to up to 20 (very rigid):^{54, 73}

$$C_\infty = \frac{\langle r^2 \rangle_0}{\langle r^2 \rangle} \quad 2-8$$

In an attempt to provide for a simplified, yet realistic description of chains, an equivalent freely-jointed chain with N steps of increased segment length l_k while keeping the original contour length $Nl_k = nl$ as well as the original end-to-end distance can be utilized to indicate increasing restrictions of the conformation and thus stiffness with increasing segment lengths via equation 2-9:^{54, 58}

$$\langle r^2 \rangle_0 = N \cdot l_k^2 \quad 2-9$$

Kuhn could validate the model via successive auxiliary segment vectors which exhibit the same probability for all possible bond angles. The Kuhn length l_k as well as the number of equivalent steps N can be described with the help of C_∞ via equation 2-10 or 2-11, respectively:⁵⁴

$$l_k = l \cdot C_\infty \quad 2-10$$

$$N = \frac{n}{C_\infty} \quad 2-11$$

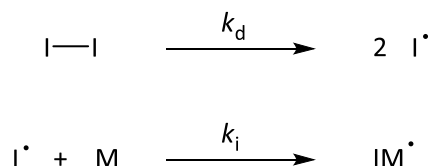
In order to provide more descriptive values for chain stiffness and to specify different polymer conformations from coil to rod, the rather complex persistence length l_p can be consulted. Per definition, l_p is the length necessary between two points on a chain to lose the correlation of the orientation of the chain tangents. In other words, the correlation of the chain direction decreases exponentially from 1 at the starting point to 0 after l_p . Geometrically speaking, l_p describes the sum of projections of segment vectors l_j with $j > i$ on the direction of l_i (equation 2-12):^{54, 58}

$$l_p \equiv l \sum_{j=i+1}^{\infty} \langle \cos\theta_{i,j} \rangle \quad 2-12$$

Several mathematical transformations and approximations in combination with $\langle r^2 \rangle_0$ and the Kuhn length enable the consideration of two extreme cases: for chain lengths much longer than l_p , the model converges with the freely-jointed one and l_p equals $l_k/2$, while for a very rigid chain molecule with a persistence length longer than its contour length, its end-to-end distance naturally equals the latter.⁵⁸ Typical values of l_p range from 1-3 nm for polyolefins to 10 nm for polyparaphenylene or even higher for DNA.⁷³

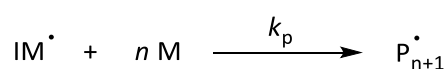
2.1.3 Chain-Growth Polymerization

An alternative method to classify polymers is via their synthesis mechanisms.⁷⁴ One very common technique is the chain-growth polymerization, where an initiator activates a monomer. The created active center is able to bind to another monomer while at the same time transferring its active properties to the newly bound repeating unit or link and so on, rapidly adding up to a chain molecule, generating material of high molecular weight. The active species or center can be a radical, anion or cation, resulting in a radical, anionic or cationic polymerization.⁵⁴ Conventional free radical polymerization (FRP) is the most popular polymerization technique due to very simple reaction conditions and a broad variety of applicable unsaturated monomers. The latter contain – mostly vinylic – C=C double bonds which are able to undergo homolytic cleavage of π -bonds, resulting in cheap manufacturing costs. (Radical) Chain-growth polymerizations can be divided into three to four basic steps.^{54, 58} Initiation takes place when radicals are formed from an initiator, e.g., via its homolysis due to heat, irradiation or in a redox process (Scheme 2-1, top), and subsequently the so-formed radicals add to a monomer (Scheme 2-1, bottom):



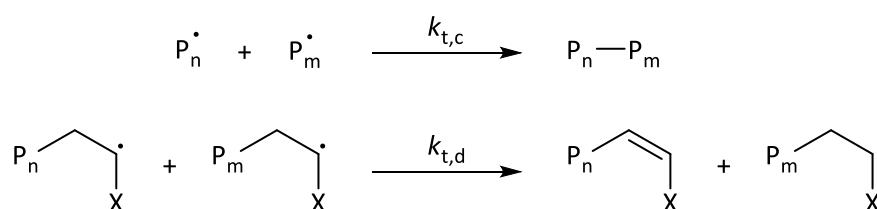
Scheme 2-1 Two-step initiation process in free radical polymerization, top: initial radical formation via homolysis of an initiator, bottom: addition of the monomer to the initiator radical.

The decomposition reaction of the initiator comprises rate coefficients k_d of typically 10^{-5} s^{-1} .⁵⁸ The radical concentration throughout a free radical polymerization usually lies in the order of $10^{-7} \text{ mol L}^{-1}$. Most often, the initial radical formation reaction is much slower than the subsequent very rapid 2nd order addition to a monomer, rendering the radical formation the rate-determining step. During the following rapid chain-growth or propagation, further monomer units are added to the growing macroradical (Scheme 2-2):



Scheme 2-2 Propagation of a (macro-)radical species with monomer molecules in a radical polymerization.

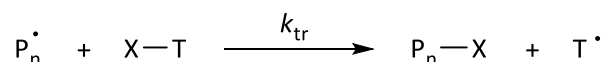
Examples for rate coefficients k_p for the propagation are $10^4 \text{ L mol}^{-1} \text{ s}^{-1}$ for rapidly polymerizing acrylates or $10^2 \text{ L mol}^{-1} \text{ s}^{-1}$ for methacrylates, demonstrating the effect of secondary vs. tertiary radical stability on the propagation rate.^{75, 76} Finally, irreversible termination reactions lead to the deactivation of the active centers, depending on the monomer and reaction conditions via two possible pathways: In the first one, radical-radical combination of two growing chain species or a propagating macroradical with a low molecular one result in an inactive polymer chain of combined weight (Scheme 2-3, top). The second pathway proceeds via hydrogen abstraction from a macroradical to another one, leading to two terminated chains via so-called disproportionation (Scheme 2-3, bottom).



Scheme 2-3 Termination reactions in radical polymerization, top: recombination of radical species, bottom: disproportionation of two macroradicals.

In contrast to propagation where only one radical species is involved, the kinetics of the termination steps are quadratically connected to the radical concentration. Thus, termination events exhibit a more pronounced dependency on radical concentration, utilizable for the establishment of modern reversible deactivation radical polymerization methods (refer to Section 2.1.5). Termination rate coefficients k_t for acrylates are in the order of $10^8 \text{ L mol}^{-1} \text{ s}^{-1}$ but can vary greatly due to the increasing viscosity with conversion.⁷⁶ As a result of the rapidly forming macroradicals and their more and more restricted diffusion, the fast termination reactions become diffusion controlled, potentially leading to an autoacceleration or Trommsdorff-Norrish effect due to the undamped exothermic propagation. Although the chain-length dependency of k_t was subject to many detailed studies, its theoretical understanding and experimental investigation remains challenging, yet crucial, as k_t also defines, e.g., polymer sizes.⁷⁷ Because of the statistical nature of chain termination, free radical polymerization leads to a broad variety of chain lengths and thus also a broad molecular weight distribution and dispersity values of usually 1.5 to 2. Another reaction channel leading to further unreactive chain species is the chain

transfer between a propagating chain and small molecules such as solvent and monomer species or transfer agents as well as between polymer chains themselves. Here, a propagating chain abstracts an atom from another molecule via homolysis, leading to the formation of a dead chain and a freshly formed radical (Scheme 2-4).



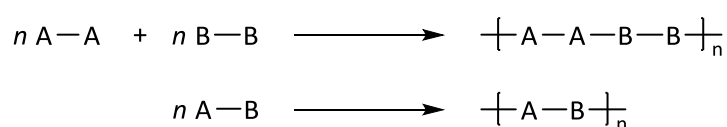
Scheme 2-4 Chain transfer of an active center from a propagating chain to another molecule.

As a new radical is generated in the course of this reaction, the propagation is not terminated and the new radical can re-initiate with further monomer. Therefore, also long-chain branching of polymers occurs if the molecule of which an atom is abstracted is a chain species.⁵⁴ Such intermolecular chain transfer is especially observed if tertiary – and thus more stabilized – radicals are formed, as, e.g., in the case of polyacrylates, where the tertiary backbone hydrogen is preferably cleaved.^{54, 78} However, for polyacrylates as well as polyethylene, the intramolecular chain transfer is probably more pronounced, leading to so-called backbiting via a six-membered transition state and thus short-chain branching.^{79, 80} Accordingly, the position of an abstraction event depends on the stabilization of the formed radical species and can hence be mainly suppressed if no labile atoms are present as for example in methacrylates.⁵⁴ β -scission of non-terminal radical species can additionally result in macromonomer species and a further broadening of the molecular weight distribution.^{81, 82}

2.1.4 Step-Growth Polymerization

Another important polymerization method yielding numerous everyday life products such as polyesters, polycarbonate, polyurethanes etc. is the step-growth polymerization via common and efficient condensation or addition reactions of di- or multifunctional species. In polycondensation reactions, alike their underlying small molecular organic reactions, a small molecule is cleaved upon polymerization which has to be removed in order to shift the reaction equilibrium to the polymerization. For example, the esterification of carboxylic acids with alcohols proceeds via the elimination of water. In contrast, (poly-)additions such as the reaction of isocyanates with alcohols to form urethanes are not leading to the cleavage of small molecules. Dissimilar to chain-growth reactions where single monomer

units are added to a growing chain, in step-growth polymerizations all monomers have – at least more or less, as chain-length effects are discussed in the literature and the present thesis – the same reactivity and form adducts with their reaction partners, thus step-wise activation leads to a step-wise propagation of chains.^{51, 54, 83} Linear polymerization occurs if the functional groups A and B, which are able to undergo condensation or addition, are either incorporated in two difunctional monomers A-A and B-B or in one difunctional monomer A-B. In the first case where the functionalities are incorporated in two different monomer units, equimolar ratios of both monomers have to be employed to allow for an efficient step-growth as otherwise at some point of the reaction all available functional groups are of one type and the reaction is stopped. In both cases, the reaction of two monomer species leads to the formation of a bifunctional dimer which can again react with another mono-, di-, trimer etc. (Scheme 2-5).



Scheme 2-5 Schematic depiction of the step-growth polymerization of A-A- plus B-B-type (top) or of A-B-type monomers (bottom).

To further understand the principle of step-growth polymerizations and to enable simple predictions of chain dimensions, the conversion p and degree of polymerization DP_n in equimolar reaction mixtures have to be defined. Via the number of monomers N_0 initially present at the beginning of the reaction and the number of monomers N_t after a polymerization time t , the conversion can be deduced via equation 2-13:^{54, 58}

$$p = \frac{N_0 - N_t}{N_0} = 1 - \frac{N_t}{N_0} \quad 2-13$$

In combination with the degree of polymerization being the ratio of N_0 to N_t , Carothers equation is obtained in equation 2-14:

$$DP_n = \frac{N_0}{N_t} = \frac{1}{1 - p} \quad 2-14$$

Evidently, very high conversion values have to be achieved to be able to obtain polymeric material with a reasonable DP_n (Figure 2-1), highlighting the importance of very efficient reactions to enable step-growth polymerizations.

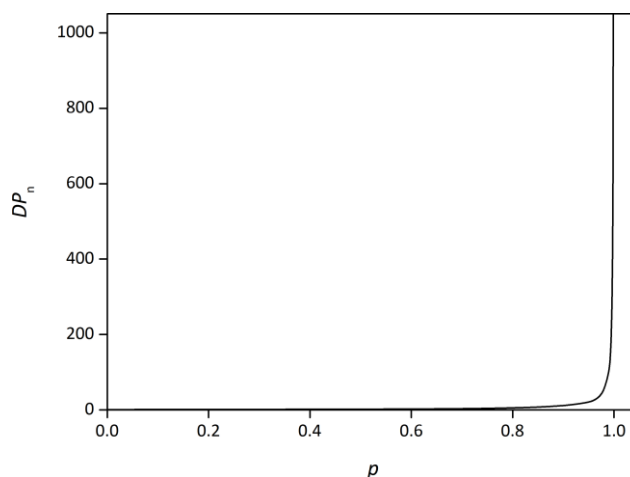


Figure 2-1 Degree of polymerization DP_n vs. conversion p in a step-growth polymerization.

If no equimolar reaction mixture is present, that is, if the ratio r of the numbers of functional groups N_A to N_B is not 1, Carothers equation can be transformed to resemble the more general equation 2-15:⁵⁴

$$DP_n = \frac{1 + r}{1 + r - 2 \cdot r \cdot p} \quad 2-15$$

The general Carothers equation demonstrates the significance of equimolar reaction mixtures if high molecular material is desired, as, e.g., already an r value of 0.99 results in a highest achievable DP_n of 199 for 100 % conversion. Then again, such a behavior allows for the facile adjustment of chain-lengths via the ratio of monomers.

Due to the aforementioned assumption of equal reactivity in all polymerization steps disregarding the chain length, kinetic considerations are also simplified with one effective rate coefficient for the – potentially catalyzed – elementary reaction of -A with -B functional groups of the concentration $[A]$ and $[B]$. The reaction rate is specified via equation 2-16, where the catalyst concentration $[Cat.]$ can be regarded as constant and thus combined with the rate coefficient k .⁵⁴

$$-\frac{d[A]}{dt} = k' \cdot [A] \cdot [B] \cdot [Cat.] = k \cdot [A] \cdot [B] \quad 2-16$$

In the favorable case of equimolar reaction mixtures and thus $[A] = [B] = c$, equation 2-16 can be simplified to resemble equation 2-17:

$$-\frac{dc}{dt} = k \cdot c^2 \quad 2-17$$

After integration of equation 2-17 from $c = c_0$ to c and from starting time $t = 0$ to t , in combination with Carothers equation 2-14 and $c_0/c = N_0/N$, the degree of polymerization is given by equation 2-18, demonstrating its proportionality to time:^{54, 58}

$$DP_n = \frac{1}{1-p} = k \cdot t \cdot c_0 + 1 \quad 2-18$$

Accordingly, for known rate coefficients and starting concentrations, the targeted molecular weight can be adjusted via the reaction time.

Statistical theories, e.g., as first described by Flory, additionally enable the theoretical investigation of weight-averaged molecular properties and associated values such as the dispersity \mathcal{D} (equation 2-19):⁵⁴

$$\mathcal{D} = \frac{\bar{M}_w}{\bar{M}_n} = 1 + p \quad 2-19$$

With conversion values of conveniently near to 1, linear step-growth polymerizations exhibit a dispersity of approximately 2.

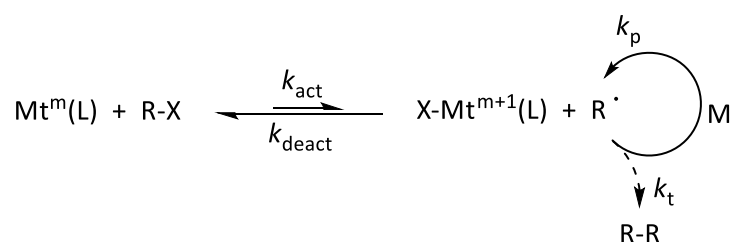
2.1.5 Advanced Polymerization Methods

Free radical polymerization is by far the most commonly employed method to industrially synthesize polymeric material, as it allows for facile reaction conditions, tolerates functional groups and impurities, can be performed in large scale etc. On the other hand, due to its non-controlled characteristics, no defined end-group fidelity, chain-lengths or at least narrow chain-length distributions can be achieved. Therefore, it is only capable to serve for the generation of bulk material, but not for materials with advanced properties. In contrast, anionic polymerization is the model example of a living polymerization comprising no termination reaction and thus a linear evolution of molar mass with conversion, quantitative end-group fidelity and perfectly controllable chain lengths.⁸⁴ Thus, also blockcopolymers can be obtained via the simple addition of another monomer type after completion of the first block. However, the high demands of anionic polymerization techniques on the reaction conditions as well as a limited number of feasible monomer species strongly restrict their employment in standard and large scale syntheses. Accordingly, researchers tried to combine the advantages of free radical polymerization with the ones from anionic polymerization techniques to yield the so-called reversible

deactivation radical polymerization (RDRP) methods.^{66, 85} The underlying principle of RDRP techniques is the temporary deactivation of the radical species via, e.g., a reversible coupling, redox equilibrium or the degenerative transfer into a non-reactive radical species. Thereby, the termination step of the radical polymerization is greatly diminished, while the achievable reaction rates are still acceptable due to the quadratic concentration dependency of k_t on the radical concentration and the only linear influence on the propagation rate k_p (refer to Section 2.1.3). In the following sections, with atom transfer radical polymerization (ATRP) and reversible addition-fragmentation chain-transfer (RAFT) polymerization, two of the most popular and wide-spread RDRP techniques are introduced.

Atom Transfer Radical Polymerization

Atom transfer radical polymerization (ATRP) is a RDRP technique adapted from the atom transfer radical addition known from organic chemistry where it is employed to form carbon-carbon bonds between alkyl halides and alkene species via a transition metal catalyst.⁸⁶ ATRP was independently introduced by the research groups of Sawamoto and Matyjaszewski in 1995 and is subject to constant investigations and enhancements to date.⁸⁶⁻⁸⁹ The basic principle of ATRP is the reversible deactivation of radical species via a redox cycle, transforming it into a temporarily dormant species which cannot undergo termination events. The initiator species in ATRP are organic halides (R-X) which are able to undergo a homolysis due to a single electron transfer from a transition metal catalyst or activator Mt to the halogen atom (Scheme 2-6).⁵⁴



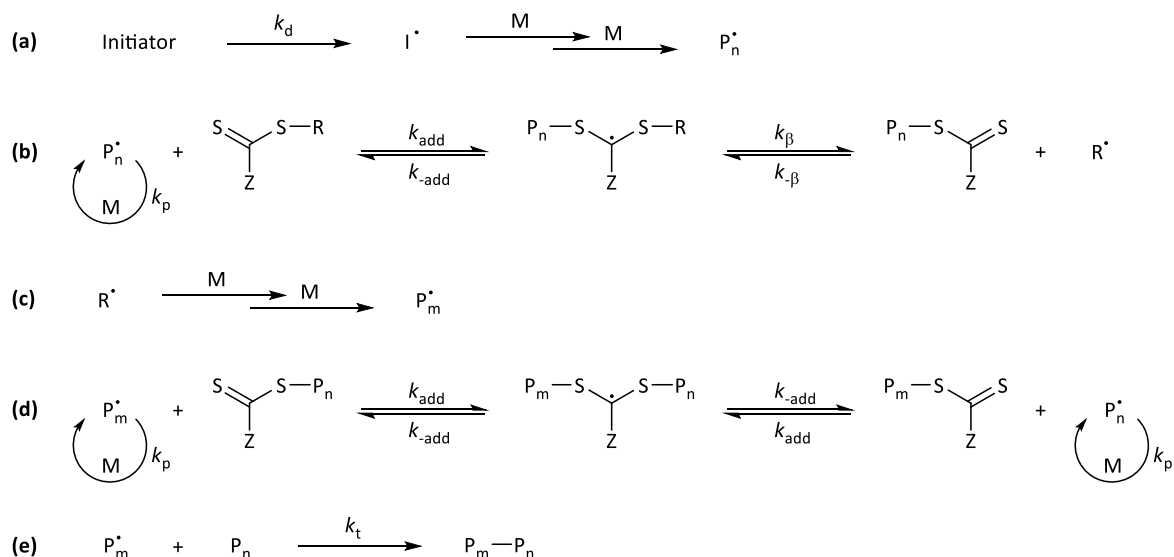
Scheme 2-6 General mechanism for ATRP techniques enabling a reversible deactivation of a (propagating) radical species. Mt: transition metal activator with oxidation number m , L: ligand, R-X: organic halide, M: monomer.

Although also other transition metals than copper can be used, ligand- (L) stabilized $\text{Cu}^{\text{I}}/\text{Cu}^{\text{II}}$ redox systems are the most widely employed ones due to their expedient and versatile reaction properties.⁸⁸ The formed radical can undergo chain-growth polymerization and

add a wide range of monomer species M until the redox process is reversed and the radical species is trapped as a halide again. To enable good control over the polymerization, i.e., highly restrict the bimolecular termination processes, the redox equilibrium has to be shifted to the side of the dormant organic halide, at the same time reducing the polymerization rate. Consequently, the achieved polymer chains bear halide end-groups which can straightforwardly be utilized to functionalize or ligate the macromolecules. To account for a decreased control and end-group fidelity at high conversion rates and reduce the oxygen sensitivity of the activator while at the same time reducing the necessary amount of transition metal species – which may be problematic due to possible cytotoxicity or other unwanted effects in the final product – different improvements of the ATRP method were established.⁸⁸ In activators regenerated by electron transfer (ARGET) ATRP, for instance, the use of an excess of a reducing agent leads to the continuous regeneration of the activator species.⁹⁰ Another interesting development is the investigation of light-induced ATRP mechanisms, enabling spatial and temporal control over the polymerization reaction. Besides examples with transition metal catalysts such as iridium-based photocatalysts or the copper-catalyzed photoRDRP, also metal-free approaches could be realized via organic photoredox systems.⁹¹⁻⁹⁴

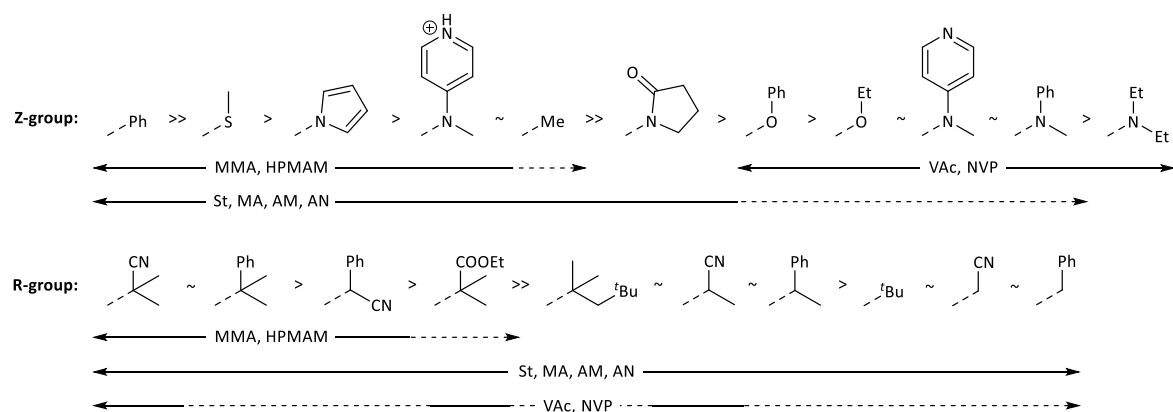
Reversible Addition-Fragmentation Chain-Transfer Polymerization

Reversible addition-fragmentation chain-transfer (RAFT) polymerization – nowadays with ATRP the most commonly employed RDRP method – was first discovered by researchers at CSIRO (Australia) in 1998 while investigating dithioester transfer agents in free radical polymerizations.^{54, 95, 96} Analogous observations for xanthates as reversible transfer agents could be obtained by French researchers and were patented as macromolecular design via the interchange of xanthates (MADIX) technique at the same time.⁹⁷ Actually, RAFT polymerizations are free radical polymerizations where a specialized reversible transfer or, in other words, RAFT agent is added. After initiation of the chain-growth reaction via standard initiators (Scheme 2-7 (a)), the RAFT agent – for example a dithioester, trithiocarbonate or xanthate – adds to the radical species in the pre-equilibrium (Scheme 2-7 (b)), causing a dormant state of the propagating chain radical.



Scheme 2-7 Mechanistic scheme of the RAFT polymerization process with (a) initiation, (b) pre-equilibrium, (c) re-initiation, (d) main equilibrium and (e) termination.

Thus, the radical transfer reduces the probability of termination, with highly active transfer agents leading to a quasi-elimination of termination events as nearly all chains are in the dormant state. The main equilibrium (Scheme 2-7 (d)) not only serves to reduce termination, but also enables a more uniform chain growth via the constant degenerative exchange of propagating chains.⁹⁸ As the overall radical concentration in RAFT polymerizations is not decreased in comparison to FRP – at least for well-chosen R-groups with comparable radical reactivity as the macroradicals (Scheme 2-7 (c)) – the reaction rate should also not be reduced.⁵⁴ Nevertheless, while RAFT polymerizations are faster than other RDRP techniques with lowered radical concentrations as for example ATRP or nitroxide mediated polymerization (NMP), induction periods and retardation effects lead to decreased reaction rates, probably due to relatively stable intermediate radicals or their termination.⁹⁸ To reduce these deviations from the ideal behavior, R- and stabilizing Z-groups have to be carefully selected to match the reactivity of the desired monomer (Scheme 2-8). With appropriate RAFT agents and due to the robustness and tolerance of RAFT polymerizations towards functional groups, a large variety of monomers such as styrene or (meth-)acrylates, but also vinyl acetate or acrylic acid can be polymerized in a controlled manner, generating polymers with interesting end-group functionality due to the incorporated RAFT agents.⁹⁸ Some of them enable rapid RAFT hetero Diels–Alder (HDA) reactions of dithioesters with dienes for macromolecular ligation, suitable for complex architectures or thermoresponsive materials (refer to Section 2.2.1).^{11, 50, 69, 99}

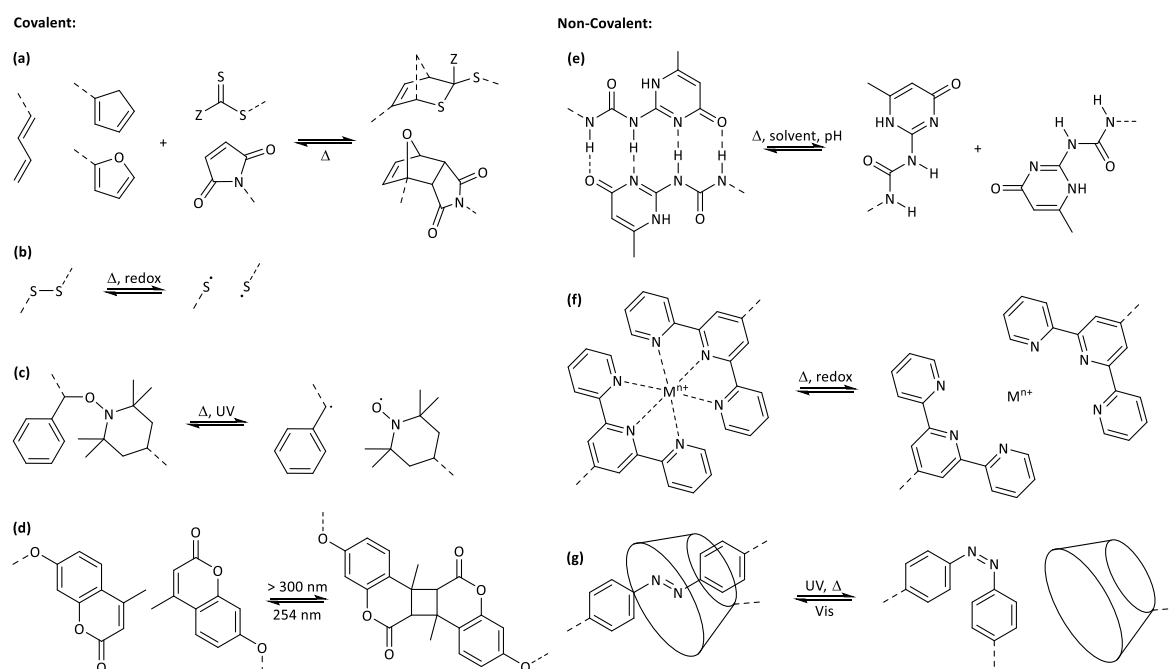


Scheme 2-8 Schematic depiction of appropriately chosen R- and Z-groups for RAFT polymerizations of controlled (—) or limited controlled (---) character, employing various monomers (MMA: methyl methacrylate, HPMAM: N-(2-hydroxypropyl)methacrylamide, Vac: vinyl acetate, NVP: N-vinylpyrrolidone, St: styrene, MA: methyl acrylate, AM: acrylamide, AN: acrylonitrile). Adapted with permission from Reference¹⁰⁰. Copyright 2012 American Chemical Society.

Additionally, because of the insensitivity of RAFT processes, also diverse other functionalities can selectively be inserted at the α - or ω -position of the final polymer via tailor-made R- and Z-groups of the employed RAFT agent, with especially the R-group approach leading to outstanding results.³² Due to typically high RAFT agent to initiator ratios, nearly all polymer chains are initiated by an R-group radical (Scheme 2-7 (c)), leading to a very high degree of α -functionality even for terminated chains.⁹⁸

2.2 Dynamic Ligation Systems

Covalent and non-covalent reversible chemical linkage allows for the generation of dynamic materials with the ability to respond to certain external stimuli, e.g., via the entropically forced shift of ligation equilibria at elevated temperatures to the opened adduct.¹⁰¹ Especially in the case of hydrogen bonding, the solvent properties plays an important role in the degree of association, resulting in tunable bonding behavior not only by means of temperature, but also via the employed solvent. Besides temperature and solvents, other triggers such as light, electric fields, redox potentials etc. can be included with appropriate linkage sites (Scheme 2-9).^{14, 16, 19, 39, 41, 50, 102-107}

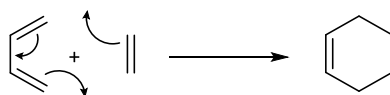


Scheme 2-9 Examples for dynamic covalent and non-covalent chemical linkage methods such as thermo-, redox- or photoresponsive (a) Diels–Alder reactions, (b) disulfide bridges, (c) alkoxyamines, (d) coumarin photodimerization, (e) hydrogen bonding, (f) metal-ligand complexation or (g) host-guest interactions.

When incorporated in, e.g., polymeric materials, such an adjustable bonding behavior enables interesting adaptive materials with for example self-healing properties, facilitated recyclability, mimicked protein folding behavior, the ability to re-shape networks or to design targeted drug delivery systems amongst others.^{4, 5, 7, 17, 46, 102, 108-110} In the following sections, the two dynamic ligation techniques employed in the current thesis – covalent thermoreversible Diels–Alder reactions and non-covalent hydrogen bonding – are introduced.

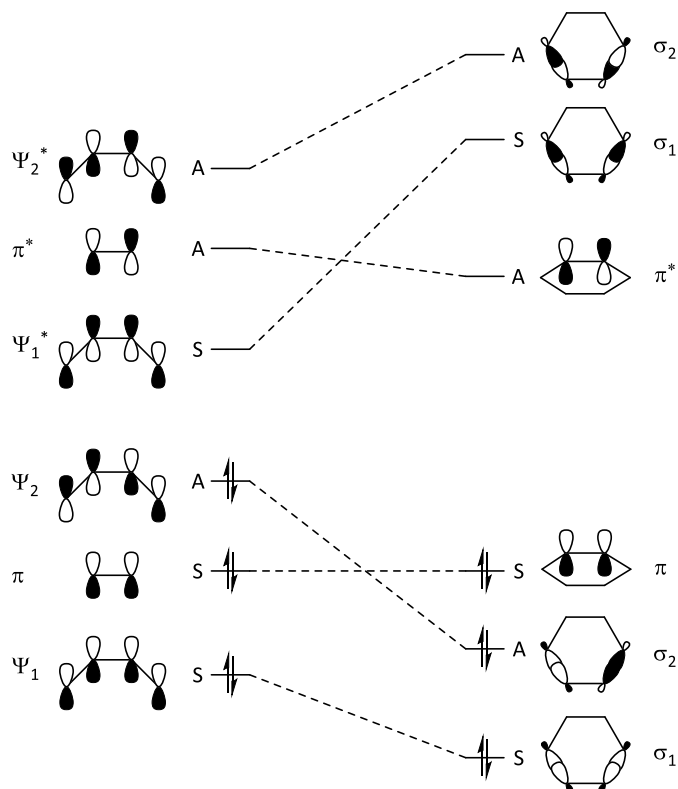
2.2.1 Diels–Alder Reactions

Diels–Alder reactions are pericyclic [4+2] cycloadditions of dienes with dienophiles, i.e., alkenes or their heteroatom analogues to form six-membered cyclohexene derivatives (formally depicted in Scheme 2-10), described by Otto Diels and Kurt Alder in 1928.¹¹¹⁻¹¹³



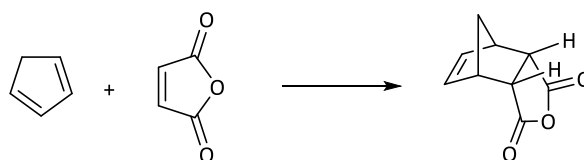
Scheme 2-10 Formal scheme of a pericyclic [4+2] Diels–Alder cycloaddition of a diene with a dienophile resulting in the formation of cyclohexene-analogue six-membered rings.

Although also radical pathways are probable for some specific reactants, the pericyclic process is the dominating mechanism for Diels–Alder reactions.¹¹² Thermodynamically speaking, two π -bonds are transformed into two energetically more favorable σ -bonds, greatly overcompensating the loss of diene conjugation.^{112, 114} The thermally allowed character of Diels–Alder reactions is defined in the Woodward–Hoffmann rules, stating that $(4n+2)$ participating electrons are required, leading to an energetically lowered ground state and no additional energy barrier, as no excitation is necessary (Scheme 2-11).¹¹⁵⁻¹¹⁷



Scheme 2-11 Correlation diagram of the [4+2] cycloaddition of 1,3-butadiene and ethylene.

In order to allow for a straightforward reaction in accordance with the frontier molecular orbital (FMO) theory, electron poor dienophiles are combined with electron rich dienes in Diels–Alder reactions of normal electron demand to ensure suitable interactions of the highest occupied molecular orbital (HOMO) of the diene with the lowest unoccupied molecular orbital (LUMO) of the dienophile.^{113, 117} The HOMO-LUMO gap and thus the reaction barrier is adjustable via different electron withdrawing or pushing substituents at the reactants, at the same time enabling a tuning of reaction rates.¹¹² Accordingly, also Diels–Alder reactions of inverse electron demand are feasible, where appropriately chosen reactants allow the interaction of the dienophile HOMO with the diene LUMO, but the aforementioned normal electron demand is more commonly employed, for example in the popular reaction of cyclopentadiene with maleic anhydride or its derivatives (Scheme 2-12):^{39, 118}



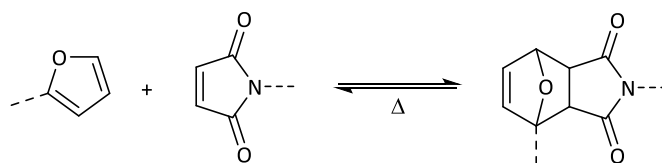
Scheme 2-12 Diels–Alder reaction of cyclopentadiene and maleic anhydride and the kinetically preferred *endo* product.

The concerted mechanism of pericyclic cycloadditions leads to a high stereospecificity, but no pronounced diastereospecificity.^{113, 117} While especially for inflexible, e.g., cyclic dienophiles the formation of the kinetically favored *endo* adduct with the dienophile substituent orientated in the direction of the diene π -system in the transition state is preferred – probably due to secondary orbital interactions – bulky substituents or altered reaction conditions can result in the generation of the sterically and thermodynamically favored *exo* product.^{112, 119} In general, no absolute selectivity occurs under standard conditions. FMO theory can also be utilized to investigate the regioselectivity of Diels–Alder reactions, adjustable by the diene substituent position as well as Lewis acid catalysts which are able to alter the orbital coefficients of polar functional groups.^{113, 117} In addition, chiral auxiliaries can be employed to enable enantioselective reaction control, for example in the total synthesis of natural substances.¹²⁰

In terms of kinetics, the configuration of the participating diene is of great importance, as it has to exist in a cisoid configuration to undergo a Diels–Alder reaction. Therefore, open-

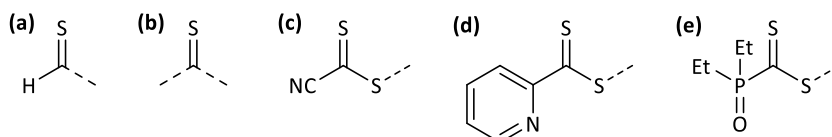
chain dienes – whose conformation equilibrium lies predominantly on the transoid side – exhibit slower reaction rates as dienes with a sterically or geometrically forced cisoid conformation, for instance 2,3-dimethyl-1,3-butadiene or cyclopentadiene.¹²¹⁻¹²³ While solvent polarity is not playing an overly important role in Diels–Alder kinetics due to the unpolar transition state, reactions in water proceed significantly faster due to hydrophobic interactions and thus a closer proximity of reactants.¹²⁴ As a result, even unreactive open-chain dienes which otherwise require a catalyst and elevated temperatures in organic media to be able to undergo Diels–Alder conjugation in an expedient time frame are able to undergo a rapid uncatalyzed Diels–Alder reaction at ambient temperature in water as solvent.^{125, 126}

The application of heteroatom substituted reactants can be employed to complement the characteristics in hetero Diels–Alder (HDA) reactions via the generation of heterocycles as well as altered reactivities. Examples for hetero dienophiles are aldehydes, imines, azo- or nitroso-compounds, dithioesters and many others, but also hetero dienes can be used such as α,β -unsaturated carbonyls and thiocarbonyls, 2-azabutadiene, etc.¹²⁷⁻¹²⁹ Specialized HDA reactions enable fast reaction times under mild conditions and reasonable retro reaction temperatures as for example in the RAFT HDA method or in a reaction of cyanodithioesters with cyclopentadiene.^{11, 22, 69, 130-132} As all thermally allowed cycloadditions are able to undergo a cycloreversion in combination with the increasing impact of entropy at elevated temperatures, the Diels–Alder reaction can be reversed in a retro reaction at adjustable temperatures depending on the reactants.^{39, 113, 133} The reversible character of the Diels–Alder ligation can be utilized to obtain self-healing or other adaptive materials such as organic sheets or thermoresponsive surface modifications and adhesives.^{5, 134, 135} Nevertheless, only few reactant combinations which result in a degradation-free retro Diels–Alder (rDA) reaction at feasible temperatures – yet still allowing for stable adducts under ambient conditions or at slightly elevated application temperatures – are known. The most commonly employed Diels–Alder reactants amongst thermoreversible materials is the pairing of furan- and maleimide-functionalities (Scheme 2-13), which can conveniently be inserted in diverse chemical systems, but exhibits relatively slow forward and retro reactions, even at elevated temperatures.



Scheme 2-13 Diels–Alder Reaction of furan and maleimides functional species.

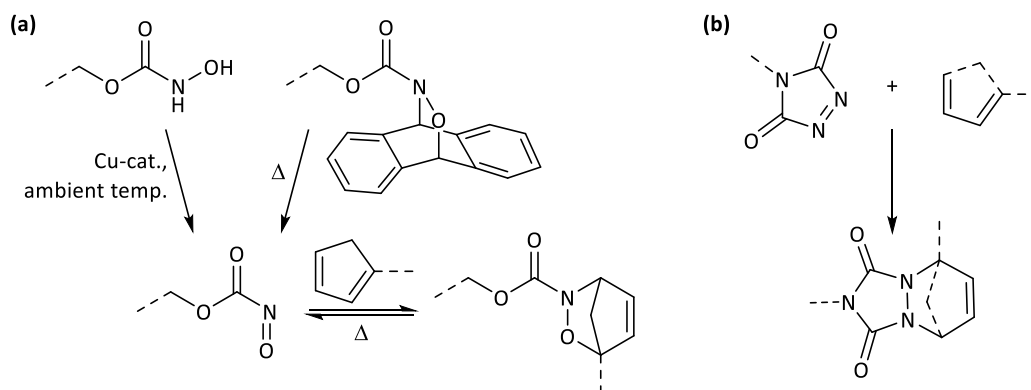
Typical reaction times for the forward reaction of furan with maleimides are hours at elevated temperatures of 60–80 °C or up to days at ambient temperature while significant amounts of retro reaction are observable from approximately 100–130 °C on.^{27, 136} Thiocarbonyl dienophiles can be utilized to obtain enhanced forward and retro reactivity. However, their increased reactivity also favors side-reactions as in the case of thioaldehydes, thioketones or highly activated dithioesters such as cyanodithioesters (Scheme 2-14 (a-c)), which is why they are mostly utilized in a trapped or precursor state and released *in situ*.^{132, 137, 138} Cyanodithioesters, for example, can be dynamically protected via the addition of cyclopentadiene, as otherwise dimerization and other side-reactions occur.^{132, 139–141} Upon heating of the protected cyanodithioester, an immediate rDA reaction can be observed from approximately 70 °C on, releasing the volatile cyclopentadiene and providing the deprotected dithioester. The latter can then be subject to other rapid and catalyst-free HDA reactions within minutes with various dienes such as cyclopentadiene-functional polymer chains, dimethylbutadiene or sorbic derivatives during cooling.^{22, 132, 142}



Scheme 2-14 Examples of thiocarbonyl compounds as dienophiles: (a) thioaldehydes, (b) thioketones, (c) activated dithioesters as well as (d) pyridinyl- or (e) phosphoryl-substituted dithioesters suitable for Lewis acid activation.

A useful technique to balance the dienophile reactivity is the employment of pyridinyl- or phosphoryl-groups at the dithioester (Scheme 2-14 (d) and (e)) which are not highly activating the dienophile towards HDA or side-reactions, yet can be transformed to strongly electron withdrawing and thus activating groups via the addition of Lewis acids.^{50, 51, 130, 143} Thereby, very rapid reactions with dienes at ambient conditions are possible. At the same time, similar compounds with appropriate R-groups can be utilized as transfer agents in RAFT polymerizations (refer to Section 2.1.5), thus enabling the formation of defined

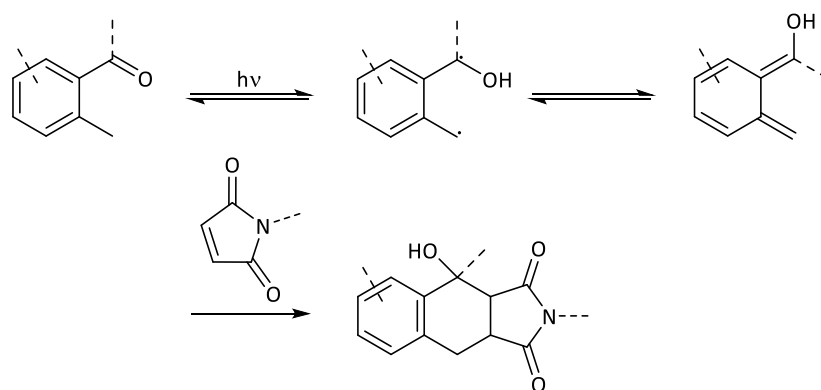
polymer block lengths with high dithioester end-group fidelity for a subsequent RAFT HDA reaction with diene functional species.^{50, 69, 144} Other examples for hetero dienophiles enabling efficient and rapid HDA reactions are highly reactive nitroso-compounds (Scheme 2-15 (a)) as well as triazolinediones (Scheme 2-15 (b)) which are nitrogen-derivatives of a maleimide.^{145, 146}



Scheme 2-15 Hetero Diels–Alder reactions via (a) nitrosocarbonyl or (b) triazolinedione hetero dienophiles.

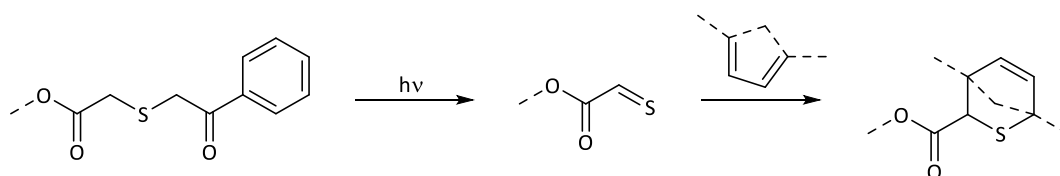
Nitrosocarbonyls can be formed *in situ* via, for example, thermally induced transformations or catalyzed pathways under ambient conditions, enabling thermoreversible HDA reactions with, e.g., cyclopentadiene functionalities. Triazolinediones allow very fast, yet irreversible conjugation of cyclic or open-chain dienes within seconds at ambient temperature.

As a result of the extraordinary efficiency of many Diels–Alder reactions with high yields, no side-product formation and thus a facile purification, available starting materials as well as a robust and orthogonal operability, they are amongst the revisited reactions comprising click-characteristics as introduced by Sharpless in 2001.⁴⁸ Another interesting development in the fields of Diels–Alder reactions is the light-induced generation of reactive species in order to allow for spatiotemporal control, for example to enable a precise surface patterning or biocompatible ligation.^{147, 148} One method is the light-triggered and reversible generation of a so-called photoenol species from *ortho*-methylphenyl ketones which can then undergo a rapid and uncatalyzed Diels–Alder reaction with, e.g., maleimides (Scheme 2-16).¹⁴⁹⁻¹⁵² Thanks to the reversible formation of the reactive photoenol species upon irradiation, the reactivity is switchable. Thus, unwanted side-reactions are minimized and no protecting groups are necessary, while reactivity can be re-gained for, e.g., subsequent functionalization steps via further irradiation events.^{153, 154}



Scheme 2-16 Light-triggered photoenol-formation from *o*-methylphenyl ketones and subsequent Diels–Alder reaction with a maleimide species.

An alternative possibility to achieve photo-controlled Diels–Alder reactions is the *in situ* generation of thioaldehydes via photolysis of phenacyl sulfides (Scheme 2-17).¹³⁸



Scheme 2-17 Photo-induced formation of thioaldehydes from phenacyl sulfides and their Diels–Alder reaction with dienes.

Due to the very high reactivity of thioaldehydes, they allow for rapid reaction rates, but at the same time undergo reactions with a variety of nucleophiles such as amines, hydroxylamines and thiols besides self-condensation.¹⁵⁵⁻¹⁵⁷ Thereby, also other functional groups can be trapped, leading to a high versatility, yet also numerous possible side-reactions.

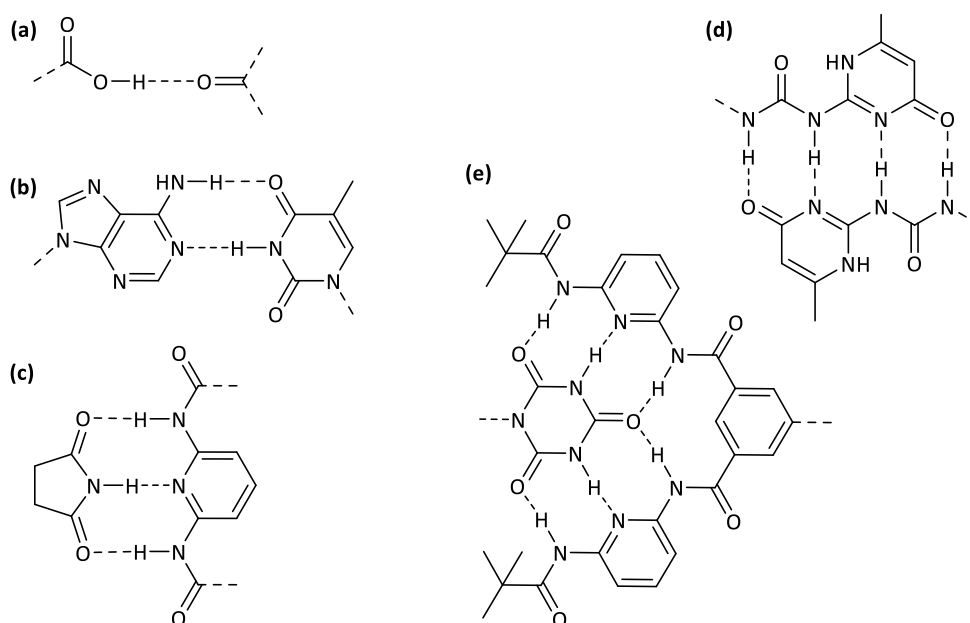
In conclusion, the versatile and robust chemistry of Diels–Alder reactions allows for a wide range of possible applications such as the formation of complex (macro-)molecular architectures, surface patterns of high resolution, thermoresponsive materials, etc. Consequently, Diels–Alder reactions are not only one of the most commonly employed methods to produce dynamic covalent materials, but will undergo constant future research for the generation of further knowledge and opportunities. Currently, one big challenge is the design of easily accessible and stable reactant pairings which allow for a fast, preferably catalyst-free and orthogonal switching between closed and opened adduct species at expedient processing temperatures for the establishing of, e.g., cost-efficient and durable

self-healing materials or organic sheets.^{5, 6, 22, 158} Another emerging field for synthetic chemists as well as theoreticians is the investigation of further refined λ -orthogonal photo-induced ligation methods such as the photoenol approach stated above to achieve more dimensions of control over the reactivity of participating species.¹⁴⁸ Accordingly, the detailed knowledge of the influence of different molecular parameters – e.g., substituents, but also physical ones as demonstrated by Guimard *et al.* in 2013 – on the bonding behavior is crucial for a targeted adjustment of desired reactivity in different applications.⁸³

2.2.2 Hydrogen Bonding

Classical chemistry mainly treats the formation and characterization of covalently bonded individual molecules. In contrast, supramolecular research – inspired by nature – combines fields of chemistry, physics, as well as biology to describe and establish inter- and intramolecular interactions of well-adjustable association characteristics via non-covalent means.^{159, 160} Thereby, a manifold of self-assembling and dynamic structures is obtainable, leading to the term “supramolecule” due to the defined characteristics of assembled multimolecular systems, comparable with the tertiary or quaternary structure of proteins.¹⁶¹ In 1987, the great impact of such a field of research was highlighted by the awarding of the Nobel Prize to three pioneers in supramolecular chemistry, namely Jean-Marie Lehn, Donald J. Cram and Charles J. Pedersen.¹⁶² Examples for non-covalent bonds suitable for supramolecular association are van der Waals, specialized host-guest and donor-acceptor interactions or hydrogen and halogen bonding.^{102, 163-165} Originating from, e.g., metal-ligand coordination, the three-dimensional structure of biomacromolecules and the studies of natural as well as synthetic recognition units, supramolecular chemistry can now be utilized for the formation of complex molecular architectures and constitutes an important technique towards artificial proteins or enzymes and other intra- and intermolecularly folded or associated structures.^{32, 46, 102, 161} In doing so, also beneficial material attributes can be realized via incorporating supramolecular binding motifs in, e.g., the side- or main-chains of polymeric materials to allow for outstanding mechanical strengths as inherently observed in Kevlar and Nylon or to generate dynamic, stimuli-responsive material characteristics such as self-healing abilities and processible networks.^{26, 159, 166, 167} Due to flexible synthetic procedures, its often directional and orthogonal bonding character, adjustable binding strengths or association constants K_a of,

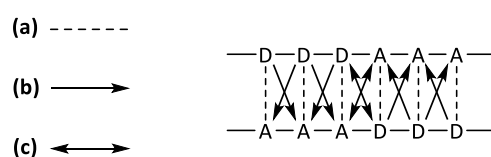
e.g., 10^2 to 10^{12} M^{-1} and diverse stimuli-responsiveness, hydrogen bonding is one of the most commonly employed supramolecular ligation methods.¹⁶⁸⁻¹⁷¹ Hydrogen bonding bases on the interaction of positively polarized hydrogen atoms, covalently bound to electronegative atoms such as nitrogen, oxygen or fluorine, and the free electron pair of another electronegative atom of the same or a different molecule. Accordingly, it is highly dependent on the polarity and protic character of solvents with polar and protic ones leading to drastically lowered association strengths. Thus, to achieve strongly conjugating interactions in hydrogen bonding, preferably apolar and aprotic solvents are employed. With approximately 7.5 kJ mol^{-1} per hydrogen bond, its strength lies below covalent bonds (some 100 kJ mol^{-1}), but above van der Waals interactions (few kJ mol^{-1}) and can be substantially increased via the combination of multiple bonding sites (Scheme 2-18).^{171, 172}



Scheme 2-18 Examples for (a) single, (b) two-centered, (c) triple, (d) quadruple and (e) multiple hydrogen-bonding interactions.

While for instance adenine-thymine pairings as naturally occurring in DNA (Scheme 2-18 (b)) with two-centered hydrogen bonding motifs exhibit association constants of $1.7 \cdot 10^2 \text{ M}^{-1}$, the quadruple hydrogen-bonding unit ureidopyrimidinone (UPy, Scheme 2-18 (d)) has a self-dimerization constant of more than 10^7 M^{-1} (both in chloroform).¹⁵⁹ Such high association capabilities of self-complementary binding motifs can easily be utilized for the reversible formation of linear supramolecular polymers or networks as performed by Meijer and co-workers via UPy di- or multifunctional species.¹⁷³

Another important factor influencing the bond strengths of hydrogen bonding units is the repulsive secondary interaction of neighboring opposing donor with donor (D) or acceptor with acceptor (A) groups, resulting in more attractive interactions between two recognition units if less alteration of D and A species is present on either side of the association pairing (Scheme 2-19).^{170, 171} However, unique donor-acceptor sequences and geometries can be harnessed to achieve a higher selectivity and thus orthogonality of specific recognition units.



Scheme 2-19 Schematic depiction of (a) hydrogen bonding, (b) attractive and (c) repulsive secondary interactions between donor (D) and acceptor (A) species.

As a result, self-dimerization can be excluded and thus selective intra- or intermolecular association of differently functionalized groups is viable. A popular example, named after Hamilton *et al.*, is the hexafunctional Hamilton wedge (Scheme 2-18 (e)) which allows for distinctive heteroassociation ($K_a \approx 10^5 \text{ M}^{-1}$) of barbiturates or cyanurates.¹⁷⁴ Thereby, alternating supramolecular polymers of cyanurate and Hamilton wedge α,ω -difunctional building blocks or selective point-folding of polymer chains as a step towards the synthesis of artificial proteins is feasible amongst others.^{175, 176} Another example of hetero-complementary binding motifs employed in polymer chemistry to supramolecularly associate diblock polymers are symmetrical in combination with asymmetrical oligoamides.¹⁷⁷ They allow for selective binding of polymer chains with an exceptionally strong association constant $K_a = 3.3 \cdot 10^7 \text{ M}^{-1}$, equivalent to an association enthalpy of 56 kJ mol^{-1} , yet can easily be separated via the addition of a protic solvent, thus enabling, e.g., the facile formation of nanoporous materials from phase-separated supramolecular diblock copolymers.¹⁷⁸ Further improvements of association characteristics can be achieved via the pre-organization of recognition units in geometrically suitable and rigid systems to minimize bond rotation and dissociation events or, generally speaking, the entropic driving forces of a disassembly.¹⁷⁹

As demonstrated above, the large toolbox of diverse hydrogen bonding units allows for a multitude of association properties for the generation of tailor-made (supra-)molecules

and materials with remarkable dynamic and stimuli-responsive characteristics. The reversible and highly dynamic hydrogen bond can be utilized to generate, e.g., self-healing or recyclable materials, self-assembly of complex macromolecular architectures, materials of tunable viscosity and phase transition behavior, pH- and solvent-responsive aggregates in biomedical applications as well as specific conjugation of recognition units amongst others.^{23, 32, 164, 171, 180-182} With the ongoing progress in the research area of dynamic bonding, further potential is about to be unlocked, enabling a more and more specified understanding and application of supramolecular techniques such as hydrogen bonding.

2.3 Thermodynamics of Chemical Equilibria

2.3.1 Classical and Statistical Thermodynamics

Thermodynamics is the study of energy or its transfer in chemical or physical processes.

The fundamental laws of thermodynamics are:

0. If two systems without direct connection are both in equilibrium with a third one, they are also in equilibrium with each other,
1. Closed systems have a constant intrinsic energy,
2. Heat is not freely transferring from a colder to a warmer system,
3. At absolute zero, a perfect crystal has zero entropy.

Enthalpy H is the amount of energy which is transferred to the system in the form of heat q under constant pressure p . With U being the intrinsic energy and V the volume, the enthalpy is defined by equation 2-20:

$$H = U + p \cdot V \quad 2-20$$

The intrinsic energy is dependent on the temperature, thus also the enthalpy is temperature dependent, yet its temperature dependency can typically be neglected for small changes of temperature.¹⁸³ As all parameters in equation 2-20 are state functions, also H is a state function which only depends on the initial and final state of the system. The standard enthalpy of a process or reaction $\Delta_R H^\ominus$ is similarly defined as the enthalpy, considering one process under standard conditions. Due to enthalpy's state function characteristics, Hess's law arises which states that the difference of standard enthalpies of a reaction $\Delta_R H^\ominus$ is a composite of the standard enthalpies of the formal formation of the individual reactants. In a spontaneous process, part of its energy is transferred to the surrounding system and thus an increasing entropy S – again a state function – is introduced (equation 2-21):

$$S = \frac{d q_{rev}}{T} \quad 2-21$$

Entropy occurs due to the number of energetically possible microstates W or, in other words, accessible energy levels, defined by the Boltzmann equation 2-22 with k_B being the Boltzmann constant ($1.38066 \cdot 10^{-23} \text{ J K}^{-1}$):

$$S = k_B \cdot \ln W \quad 2-22$$

Similar to the standard reaction enthalpies, standard reaction entropies $\Delta_R S^\ominus$ are accessible via the difference of the entropy values of products and reactants. Spontaneous chemical reactions at constant temperature T and p occur in the direction of the minimal free enthalpy G (equation 2-23) of a system (equation 2-24):

$$G = H - T \cdot S \quad 2-23$$

$$dG = dH - T \cdot dS \quad 2-24$$

The free reaction enthalpy $\Delta_R G$ is defined as the slope of the free enthalpy as a function of the extent of reaction ξ or the difference between the chemical potentials μ of products b and reactants a (equation 2-25):¹⁸³

$$\Delta_R G = \left(\frac{dG}{d\xi} \right)_{p,T} = \mu_b - \mu_a \quad 2-25$$

For $\mu_a = \mu_b$, the free reaction enthalpy $\Delta_R G = 0$, i.e., the reaction is in its equilibrium state. With $\mu_a > \mu_b$, $\Delta_R G$ is negative and the exergonic forward reaction occurs, while with $\mu_a < \mu_b$, $\Delta_R G$ is positive or the endergonic retro reaction is observed. With the help of the chemical potential of ideal gases, the universal gas constant R ($8.314 \text{ J mol}^{-1} \text{ K}^{-1}$) and the standard free reaction enthalpy $\Delta_R G^\ominus$, the free reaction enthalpy can be further interpreted, resulting in a logarithmic dependency of $\Delta_R G$ on the reaction quotient Q_R (equation 2-26) which is the ratio of activities of products and reactants:¹⁸³

$$\Delta_R G = \Delta_R G^\ominus + R \cdot T \cdot \ln Q_R \quad 2-26$$

Similar to enthalpy and entropy, the (standard) free reaction enthalpy can again be obtained via the difference between product and reactant values. For appropriate conditions, the aforementioned activities can be approximately equalized with partial pressures or the concentrations of participating species. For $\Delta_R G = 0$, Q_R equals the equilibrium constant K (equation 2-27).¹⁸⁴

$$R \cdot T \cdot \ln K = -\Delta_R G^\ominus \quad 2-27$$

Thus, equilibrium constants and the respective composition of a reaction mixture can be calculated from available thermodynamic data. Enthalpy and entropy contribute to K

according to the Boltzmann distribution of available energy levels for molecules. With the standard free reaction enthalpy being:

$$\Delta_R G^\ominus = \Delta_R H^\ominus - T \cdot \Delta_R S^\ominus \quad 2-28$$

the equilibrium constant K can be written as:

$$K = e^{-\Delta_R H^\ominus/RT} \cdot e^{\Delta_R S^\ominus/R} \quad 2-29$$

demonstrating the interplay of enthalpy and entropy values. For example, enthalpy values of one prefix can be counteracted by entropy values of the same prefix or vice versa. The equilibrium position can be shifted via the temperature dependent distribution of molecules over energy levels, as can be seen in the Van't-Hoff equation 2-30:¹⁸³

$$\frac{d \ln K}{d T} = \frac{\Delta_R H^\ominus}{R \cdot T^2} \quad 2-30$$

Accordingly, with increasing temperature, exothermic reactions – i.e., $\Delta_R H < 0$ – are shifted to the reactant side of the equilibrium, as K decreases. Such a behavior results from the decreased gain of entropy of the system and thus a loss of driving force due to a decreasing value for $-\Delta_R H^\ominus/T$ (refer to equation 2-28).

Statistical thermodynamics allows the combination and investigation of microscopic and macroscopic properties of systems and molecules. Here, partition functions describe the limited number of quantized thermally feasible microstates of, e.g., molecules as a product of translational (trans), rotational (rot) and vibrational (vib) as well as electronic (e) contributions. Said contributions depend on the degrees of freedom M of a molecule, summing up to, for example, its energy ε :¹⁸³

$$\varepsilon = \varepsilon^{trans} + \varepsilon^{rot} + \varepsilon^{vib} + \varepsilon^e \quad 2-31$$

The complete description of microstates is only possible by quantum mechanics, with classical mechanics as the limiting case for high energies.¹⁸⁵ Thus, the properties of investigated molecules can be obtained via solving the time-dependent Schrödinger equation 2-32:

$$\hat{H}\Psi_n = i\hbar \frac{\partial \Psi_n}{\partial t} \quad 2-32$$

The Schrödinger equation includes the wave function Ψ_n of a system with n states, Hamilton operator \hat{H} , Planck constant \hbar , time t and imaginary unit i . In applying \hat{H} on the wave function, the (kinetic and potential) energy of a system is characterized.¹⁸⁵ For special cases as molecules in their ground state, a stationary, time-independent Schrödinger equation can be deduced. For equilibrated systems with finite volume V and defined number of particles or sub-systems N , microcanonical ensembles of adequate size can be defined. Here, the fluctuation of quantized energies due to exchange events between different hypothetical sub-systems can be summarized to result in the ensemble average intrinsic energy $\langle \varepsilon \rangle$ which is equal to the time averaged energy of isolated sub-systems.¹⁸⁶ For large systems with $N \rightarrow \infty$, only the most probable distribution of energies ε_i contributes to its average value. The probability p_i for a sub-system to be in a particular state i is given by the number n_i of systems in such a state divided by N . Thus, $\langle \varepsilon \rangle$ is the ratio of the total energy ε_{total} to N or the sum of products of p_i and ε_i .¹⁸⁴

$$\langle \varepsilon \rangle = \frac{\varepsilon_{total}}{N} = \sum_i p_i \cdot \varepsilon_i \quad 2-33$$

The most probable distribution p_i is given by the Boltzmann distribution:

$$p_i = \frac{\exp(-\varepsilon_i/k_B \cdot T)}{\sum_i \exp(-\varepsilon_i/k_B \cdot T)} = \frac{\exp(-\beta \cdot \varepsilon_i)}{Q} \quad 2-34$$

The temperature dependent term $1/k_B T$ can be abbreviated with β while the denominator Q is called canonical partition function which allows for the calculation of all thermodynamic functions of a system.^{184, 185} Besides intrinsic energy and entropy, also free energy, (free) enthalpy as well as the pressure can be calculated and further ascribed to the average energies of the translational, rotational, vibrational or electric degrees of freedom M , defined via:

$$\langle \varepsilon^M \rangle = -\frac{1}{Q^M} \cdot \left(\frac{\partial Q^M}{\partial \beta} \right)_V \quad 2-35$$

To obtain these values, the canonical partition function has to be divided into the contributions of the different degrees of freedom Q^M , depending on the nature of the investigated molecule.¹⁸³

2.3.2 Computational Assessment of Reactions

While similar quantum chemical methods as introduced below are employed in the course of the current thesis in order to predict and identify the underlying microscopic causes of entropic effects in macromolecular ligation chemistry (Chapter 3) as well as to support the choice and synthesis of a novel hetero Diels–Alder linker (Chapter 4), the corresponding calculations were performed by collaboration partners under the supervision of Prof. Michelle Coote at the Australian National University (Canberra). Thus, the section at hand shall only provide for an introductory presentation of the general methodology to enable a more facile understanding of the reader.

Computational chemistry can serve as a tool to model chemical problems, for example structures or transition states and their molecular energies, enabling an investigation of reactions. But also vibrational frequencies, NMR spectra, bond properties, molecular orbitals and many other fields of interest are accessible in a theoretical way.¹⁸⁷ Based on the laws of physics – in part or fully – computational studies can be utilized to obtain qualitative and quantitative insights without the need for experiments.

Computational chemistry of molecules can be divided into two large sections: molecular mechanics and electronic structure theory.¹⁸⁷ Molecular mechanics methods treat the interactions of nuclei via classical physics, employing force fields. Potential energies dependent on the relative position of atoms in combination with atom parameters and fitting the employed equations to experimental data is used to evaluate bond lengths, angles and vibrational frequencies. After establishing parametric functions, molecular mechanics are computationally inexpensive, yet electronic effects have to be included for each system – thus, there is no generally applicable method. In addition, processes such as bond scission or formation cannot be treated in molecular mechanics.¹⁸⁷ In contrast, quantum mechanical calculations should in principle allow for the universal solution of countless chemical problems. While quantum mechanics originated at the beginning of the 20th century, their complexity prohibited a facile employment on the majority of chemical questions.¹⁸³ The ever increasing computational power enabling faster and faster approximation and iterative optimization of quantum mechanical equations in addition to the progress in theoretical physics and chemistry led to the establishment of expedient techniques to theoretically assess larger molecules.¹⁸⁸ Still, exact solutions of the

Schrödinger equation 2-32 are only feasible for the smallest possible chemical systems, e.g, the hydrogen atom.¹⁸³ Therefore, electronic structure methods aim for mathematically approximated solutions of the Schrödinger equation for problems at hand. Besides parametrized semi-empirical methods, *ab initio* calculations are not including experimental parameters, yet only quantum mechanical laws and the physical constants of the speed of light, charges and masses of nuclei and electrons as well as the Planck constant.¹⁸⁷ As a result of the particular approximations taken and the size of the investigated system or molecule, the computational cost or duration of calculations as well as their accuracy may differ drastically, wherefore a careful selection of quantum chemical models has to be considered to obtain qualitative or even quantitative results in a convenient time span. These so-called model chemistries are theoretical models which allow for the approximate solution of the Schrödinger equation for a given structure and should reproduce its exact solution as good as possible while being generally applicable. Due to different constraints such as a less expedient approximation of wave functions with increasing system size vs. the overall (computational) efficiency of model chemistries, different combinations of methods and basis sets are formed to provide model chemistries for different applications and computer generations. A method defines the theoretical procedure of approximation or, in other words, the level of theory. Common examples are the numerical iterative Hartree-Fock (HF) self-consistent field method, Becke-style 3-parameter density functional theory with Lee-Yang-Parr correlation functional (B3LYP) or different orders of the Møller-Plesset perturbation theory (abbreviated with, for instance, MP2 or MP4).^{183, 189-191} The basis set mathematically characterizes the molecular orbitals, with larger basis sets resulting in more accurate results at the cost of longer computation times.¹⁸⁷

With appropriately chosen model chemistries, the energy of a specified molecule can be obtained via single point calculations, representing one specific point – defined by the supplied molecular geometry – on the potential energy surface. To perform a geometry optimization of an initially indicated structure and thus determine the energetically most favorable arrangement of atoms in space for a target molecule, the minima of the potential energy surface is located via the fulfillment of convergence criteria. For optimized reactant and product compounds of a reaction, the calculation of their energies allows, e.g., for the determination of the thermodynamic parameters of the reaction in question. To account

for altered molecular and reaction properties in solution, often the method of a self-consistent reaction field (SCRF) is employed. Here, a continuous reaction field with a defined dielectric constant is modeled and the molecule under investigation is placed in a cavity within this field. Thereby, more or less stabilizing effects are introduced due to the interaction of molecule dipoles and the solvent field.¹⁸⁷

In summary, computational *ab initio* methods can be harnessed to calculate diverse molecular parameters such as the thermodynamic values of reactions without the need for any experimental data. Such studies are especially valuable if the experiments in question cannot be actually conducted or if general insights and first studies of feasibility are desired to guide further experimental work. In addition, quantum chemistry allows for the determination and ascription of microscopic effects which cannot be isolated via macroscopic factors.

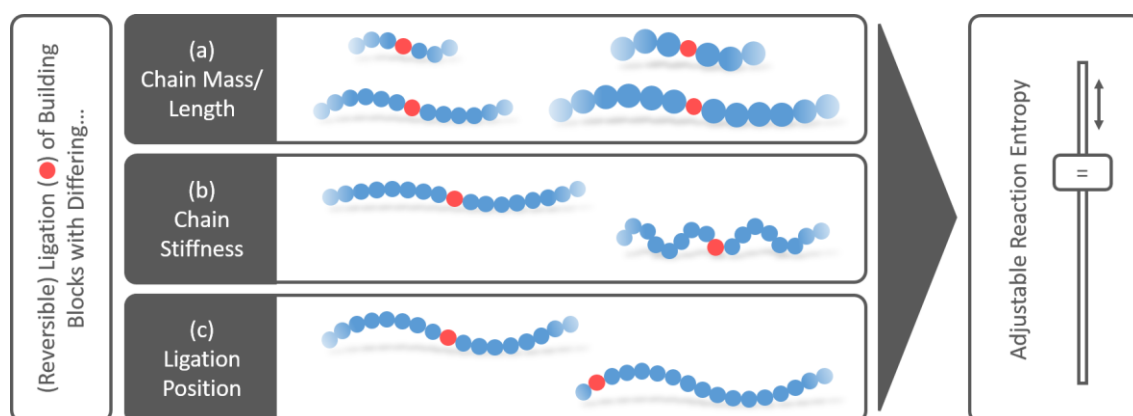
3

ENTROPIC EFFECTS ON CHEMICAL EQUILIBRIA

3.1 Motivation

Recently, more and more dynamic chemistries are being employed for the design of stimuli-responsive materials, aiming at the generation of smart materials, for example self-healing, self-assembling, recyclable, switchable or immolative ones amongst a multitude of possibilities.^{4, 5, 13, 15, 30, 33, 47, 109, 158, 166, 192-199} Such dynamic chemistries include, e.g., reversible covalent bonding via Diels–Alder reactions, boronic esters, alkoxyamines, oximes or disulfide links, as well as supramolecular association via hydrogen bonding, π - π -stacking or metal-ligand interactions.^{14, 22, 26, 27, 38-41, 46, 47, 51, 83, 99, 123, 132, 144, 166, 169, 197, 200-219} To generate a manifold of diverse association pairings necessary for different applications with variable requirements regarding bond strengths, association rates, retro reaction or dissociation temperatures etc., novel and possibly complex chemistries have to be

identified, investigated and established to insert the desired functionality into a target compound. Typically, tuning of the bonding parameters is established via enthalpic parameters, i.e., the modification of the electronic structure of the reactants via different, e.g., electron withdrawing or pushing, substituents in order to alter HOMO-LUMO interactions and thus bond strengths or cleavage temperatures.^{113, 117} A factor which is mainly untouched by the efforts of synthetic chemists when tuning bonding parameters of established reactions is the entropy of the reactive system, although its impact is evident in the Gibbs equation ($\Delta G = \Delta H - T \cdot \Delta S$).¹⁸³ While the somehow related topic of enthalpy-entropy compensation is discussed in several cases of intermolecular binding, stating that small losses of enthalpic interactions lead to higher entropy values and *vice versa*, thus counteracting any changes in the free energy, it is more focused on the different interactions of the recognition units of ligated molecules.²²⁰⁻²²² Accordingly, it is not isolating for similar bonding conditions while generating different entropic values of the residual respective specimen. Granted, the entropy of involved species cannot easily be modified in larger extents for a given phase and number of small molecules, but entropy values of different macromolecular species can vary substantially. Not only can macromolecules enormously differ in length and molecular weight, they can also be composed of variable backbones of different steric mobility and thus chain stiffness (Scheme 3-1).



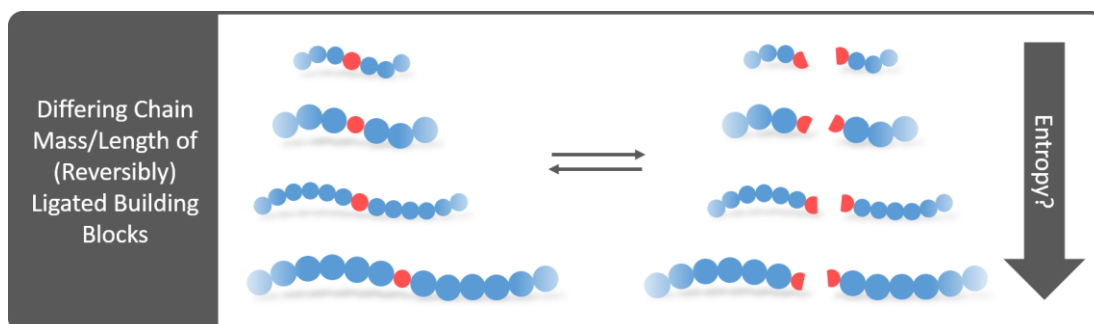
Scheme 3-1 General scheme of entropic influences on dynamic reaction equilibria via physical molecular parameters such as (a) molecular weight and length, (b) chain stiffness or (c) the ligation position inside a molecule.

These factors substantially determine the amount of translational, rotational or vibrational entropy of a system which sums up to its total entropy, rendering polymers a perfect

platform for an investigation of the influence of physical molecular parameters on entropy and thus also the Gibbs free energy. Consequently, particularly in the fields of macromolecular ligation, reaction or association parameters and equilibria should not only be tunable via different or differently substituted functional groups, but also via the physical properties of the ligated molecule in total while keeping the actual ligation chemistry unaltered (Scheme 3-1). This way, established chemistries may well be left unmodified while bonding and material properties can be changed via different macromolecular characteristics as for example individual chain length or simply exchangeable side-chain substituents. In addition, it should be kept in mind that all – i.e., also “non-dynamic” – chemical reactions underlie an equilibrium which is more or less shifted to one side, leading to a universal applicability of entropic effects to all reactions or associations involving macromolecular species. Actually, first studies exploring the thermoreversible Diels–Alder bonding of macromolecules or irreversible thermal degradation of polymers with differing chain lengths support the assumption of entropic effects.^{51, 83, 223} These preliminary findings allow for an initial explanation of different reported retro reaction temperatures for identical functional groups incorporated in dissimilar molecules and highlight the importance of further, more detailed studies.^{27, 108, 200} In the following sections of the current chapter, different possibilities of molecular parameters (Scheme 3-1) influencing reaction entropy and thus Gibbs free energy and the macroscopic equilibrium position at a given temperature are being investigated experimentally as well as in theoretical calculations, leading to the establishment of entropic effects on macromolecular reactions.

3.2 Mass/Length Effect on Dynamic Reactions

An obvious choice for parameters with an influence on entropy is the weight or length of the examined species, as these factors greatly affect the translational and rotational entropy of a given molecule. Thus, the first section on entropic effects treats the impact of macromolecular mass or length of reversibly connected adducts on covalent (retro) reaction parameters (Scheme 3-2).*



Scheme 3-2 Reversibly ligated building blocks of differing length or mass.

3.2.1 Experimental Design

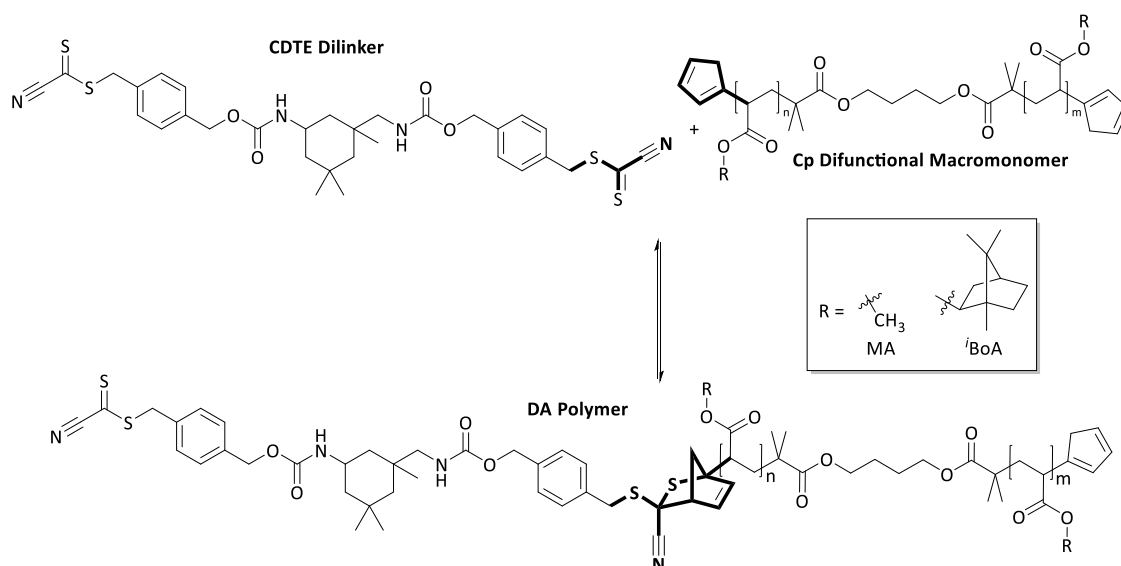
Chain length and mass of a functional molecule can be defined in a facile way for polymers via controlled polymerization methods (refer to, e.g., Section 2.1.5) and the application of different side-chain substituents. Reversible deactivation radical polymerization methods as for example activator regenerated by electron transfer (ARGET) atom transfer radical polymerization (ATRP) allow for the straightforward generation of polymer chains of adjustable and reproducible lengths with high end-group fidelity.²²⁴ Although small amounts of unreactive species with lost end-group functionality cannot be completely excluded due to irreversible chain termination processes still operational to minor degrees in such relatively controlled polymerization techniques, their proportion in the entire sample and impact on measurements or the comparability of different similarly synthesized samples is negligible when a careful adjustment of reaction parameters such

* Parts of the current section are reproduced or adapted from K. Pahnke, J. Brandt, G. Gryn'ova, P. Lindner, R. Schweins, F. G. Schmidt, A. Lederer, M. L. Coote, C. Barner-Kowollik, *Chem. Sci.* **2015**, *6*, 1061-1074, with permission from The Royal Society of Chemistry. J. Brandt carried out the TD SEC and SANS measurements. G. Gryn'ova conducted the quantum chemical calculations. P. Lindner and R. Schweins helped with the SANS measurements. F. G. Schmidt, A. Lederer and M. L. Coote helped with discussions. C. Barner-Kowollik motivated and supervised the project and contributed to the scientific discussions.

as low conversion and quantitative post-polymerization functionalization methods are employed.⁹⁰ Therefore, polymers resemble an ideal and facile model platform when investigating the impact of physical molecular parameters on their reactivity, while entropy and its diverse effects are essential for all kinds of reaction and association equilibria and thus the demonstrated investigations should be generally applicable and transferrable. A favorable ligation method (not only) in the realm of polymer chemistry are Diels–Alder (DA) reactions due to their possible efficiency, lack of side-products and – especially for the studies at hand where bond cleavage at defined positions is envisaged – in several cases due to their thermoreversible character at experimentally accessible temperatures (refer to Section 2.2.1).^{5, 39, 48-50, 225, 226} Via the combination of polymers with thermoreversible Diels–Alder ligation, various model compounds comprising dynamically connected macromolecular building blocks of different length or mass were realized. The individual degree of bonding of the generated thermoreversible DA adducts at different temperatures was monitored via high temperature nuclear magnetic resonance spectroscopy (HT NMR, Section 3.2.3) as well as temperature dependent size exclusion chromatography (TD SEC, Section 3.2.4). To derive and clarify initial assumptions and to generate a fundamental understanding of the impact of the underlying entropic factors on reaction parameters, quantum chemical *ab initio* calculations were employed (Section 3.2.2).

3.2.2 Computational Studies

Quantum chemical *ab initio* as well as density functional theory calculations via the Gaussian 09 software package – performed by collaboration partners at the Australian National University (Canberra) – led to first insights into the occurrence and the basic principles of effects of physical molecular parameters on reaction entropy and thus the Gibbs free energy of the reversible cycloaddition of a cyanodithioester (CDTE) dienophile dilinker and differently sized and substituted cyclopentadiene (Cp) functional polymer chains.²²⁷ As a result of computational constraints, the theoretical calculation of enthalpy and entropy could only be realized for model reactions with building block chain lengths of $n = m = 0-2$ (Scheme 3-3), nevertheless yielding valuable information on the entropic causes of the observed effects. While the final data is provided in the Experimental Section, refer to the original publication for full details on the theoretical methodology.¹⁴²



Scheme 3-3 Model DA reaction of CDTE linkers plus Cp functional polymers with side-chain substituents of different masses studied using quantum chemistry. Fragments in bold correspond to the reaction center in the ONIOM-like approximation. Adapted from Ref.¹⁴² – Published by The Royal Society of Chemistry.

Due to the size of the analyzed specimen, another approximation – known to be valid for small molecules, but not quantitative for larger, e.g., polymeric systems – had to be utilized to gain nonetheless realistic and expedient qualitative trends: The reactant and product species were considered in their minimum energy conformation in a solvent field, while gas-phase translational, rotational and vibrational entropic fractions of the (de-)bonding process were adjusted via their additional solvation energy proportions.⁸³

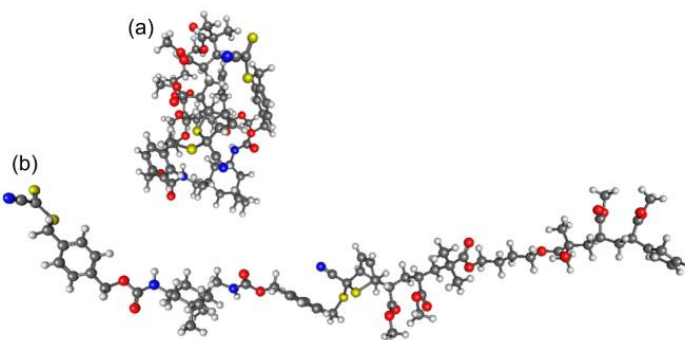


Figure 3-1 Optimized geometries of the DA adducts of CDTE and Cp difunctional poly(methyl acrylate) (with $n = m = 2$) corresponding to (a) the lowest energy conformation and (b) the extended chain conformation. Reproduced from Ref.¹⁴² – Published by The Royal Society of Chemistry.

In addition, optimized linear extended chain conformations based on the lowest energy optimized core molecule were investigated for modelling of longer vs. shorter chains (Figure 3-1), as the steric properties of polymer side-chains are likely to prevent a globular organization as observed for the oligomers, thus leading to a linear structure with

entropically very different attributes. The obtained globular and extended linear structures were then tested in relation to their differences in reaction entropy for the proceeding (retro) DA reaction between dienophile linker and diene-functional polymer species with poly(methyl acrylate) (PMA) or poly(isobornyl acrylate) (PⁱBoA) backbones (Figure 3-2).

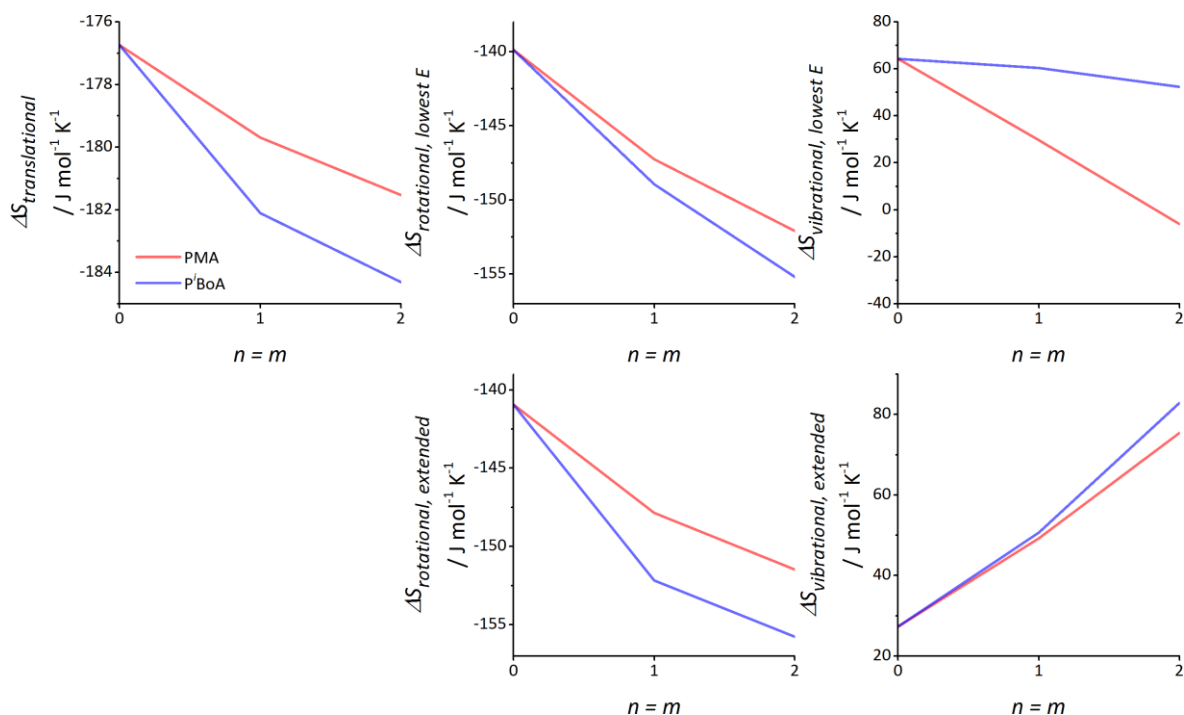


Figure 3-2 Calculated changes in the entropy (ΔS in $\text{J mol}^{-1} \text{K}^{-1}$) of model DA reactions for different n, m (chain lengths) of poly(methyl acrylate) (PMA) or poly(isobornyl acrylate) (PⁱBoA) macromonomers in their lowest energy or extended chain conformation. In these figures, the more negative ΔS , the lower the Gibbs free energy of bonding, or the greater the extent of debonding, at a given temperature. Adapted from Ref.¹⁴² – Published by The Royal Society of Chemistry.

As the translational entropy ΔS_{trans} only depends on the (molecular) mass, there are no individual calculations for the different conformations necessary. Consequently and similar to previous findings, ΔS_{trans} decreases to reach more negative values with increasing chain length or mass of the side-chain substituents ($\text{PMA} < \text{P}^i\text{BoA}$), thus leading to a more favored debonding alias a less favored bonding process or, in other words, a decreased retro reaction temperature for heavier and longer ligated chain species.⁸³ In contrast to ΔS_{trans} , the rotational entropy ΔS_{rot} is not only dependent on the mass of the involved species, but also its distribution in space, leading to a dependence on molecular geometry and conformation. Despite such a complex interplay, the same trends as observed for ΔS_{trans} also emerge for ΔS_{rot} , leading to a further reinforcing of debonding events for longer and heavier chains. A detailed analysis of the effect of chain stiffness on reaction properties will

be conducted in the next part of the thesis (Section 3.3). However, a first look into the vibrational entropy ΔS_{vib} – being related to the phenomenon of chain stiffness – leads to very dissimilar results for the lowest energy and extended chain conformers, as the complex interplay of vibrational modes for newly formed inter- as well as intramolecular covalent and non-covalent interactions is highly dependent on the respective conformation. These observations are hinting at a possibly changed relative behavior of short vs. extended chain pairings of PMA and PⁱBoA, as – especially for the lowest energy PⁱBoA conformer – the vibrational contributions to entropy may counteract the previously expected effect of its higher molecular mass and bulkiness on the Gibbs free energy via the translational and rotational parts of reaction entropy. The combination of the calculated entropic values with reaction enthalpy as well as solvation energy can be utilized to determine a qualitative temperature dependent degree of bonding or debonding (%_{debond}) for the different employed conformers (Figure 3-3).

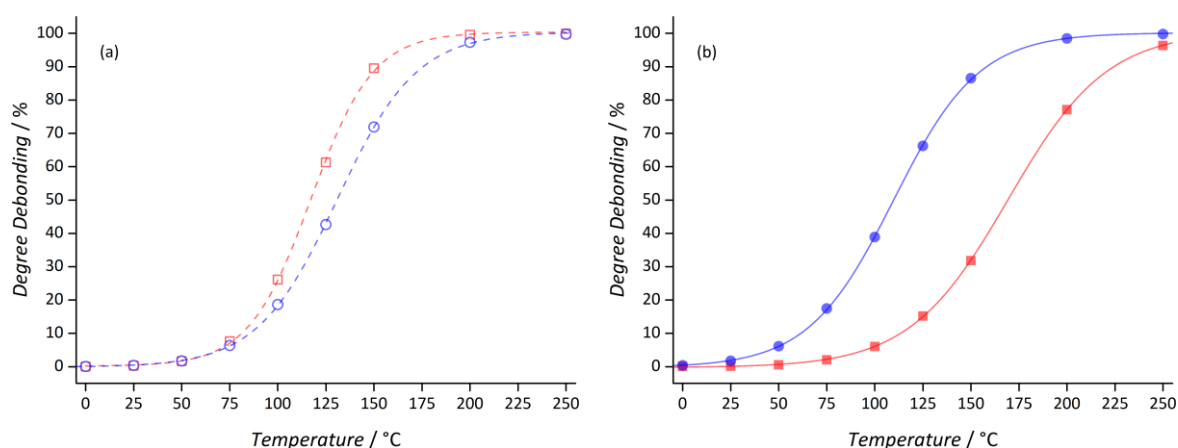
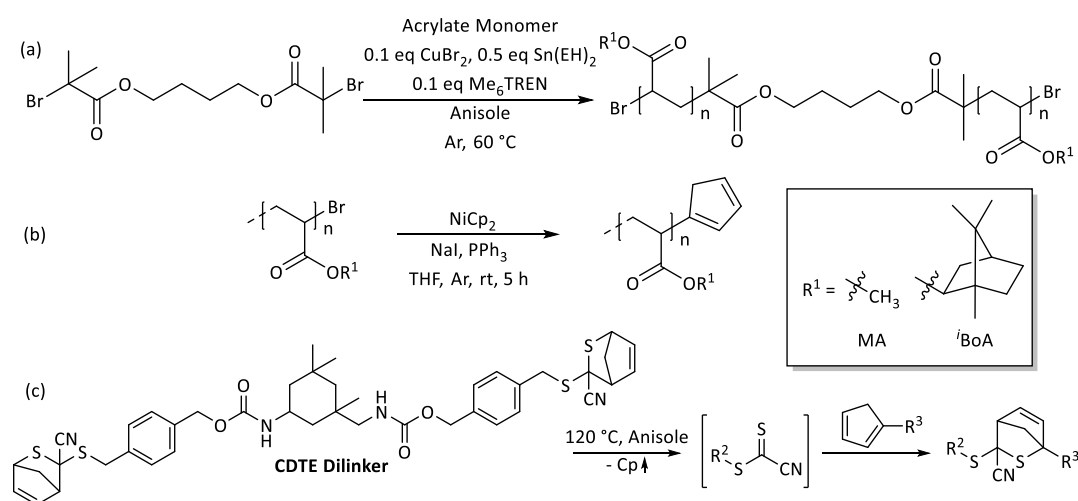


Figure 3-3 Degree of debonding (determined from the calculated reaction energies for $n = m = 2$ chain lengths) vs. temperature for (a) lowest energy and (b) extended chain conformers of PMA (■) or PⁱBoA (●). Adapted from Ref.¹⁴² – Published by The Royal Society of Chemistry.

Interestingly, as expected above, the calculated %_{debond} for the different conformers – modeling short or extended longer chains – actually reflect the altered influence of ΔS_{vib} : For short and globular chain conformations (Figure 3-3 (a)), the increased impact of ΔS_{trans} and ΔS_{rot} of heavier and bulkier chains which should lead to a lower debonding temperature is counteracted, while for extended systems (Figure 3-3 (b)), the previously established effect of increased chain masses leading to lower debonding temperatures is reproduced.⁸³ To test and verify these theoretical and qualitative results, the computationally assessed systems were experimentally investigated in the following sections.

3.2.3 High Temperature NMR

Diene difunctional building blocks were synthesized via ARGET ATRP with the help of a bromo difunctional initiator to enable a high end-group fidelity (Scheme 3-4 (a), refer to Figure 3-4 for the SEC chromatograms of the molecular weight distributions) and a subsequent substitution of the resulting bromo end-groups with a cyclopentadiene function via nickelocene (Scheme 3-4 (b), refer to Figure 3-4 for the SEC chromatograms).



Scheme 3-4 Reaction scheme for the generation of thermoreversibly connected macromolecules of different building block sizes via (a) ARGET ATRP of acrylate monomers with a bromo difunctional initiator, (b) subsequent substitution of the bromo end-groups via nickelocene and (c) Diels–Alder step-growth of diene and dienophile difunctional blocks. Adapted from Ref.¹⁴² – Published by The Royal Society of Chemistry.

Analogous to the computational calculations of model systems for small and extended chains, shorter and longer polymer blocks of both PMA and PⁱBoA of either 10 or 50 repeating units were prepared (Table 3-1). Step-growth polymers, formed from cyclopentadiene α,ω -difunctional polyacrylate building blocks, were assembled via a cyanodithioester (CDTE) dilinker (Scheme 3-4 (c), refer to Figure 3-4 for SEC chromatograms). A DA reaction of linker and diene functional polymer is readily occurring upon heating of the concentrated reaction mixture in anisole to 120 °C – at the same time enabling an evaporation of the released Cp as well as a dynamic protection of the re-activated dithioester in its equilibrium with the newly formed DA adduct – and subsequent cooling to ambient temperature. Note that the employed catalyst-free DA reaction of a cyanodithioester with dienes is not stereoselective, but such a characteristic is also not necessary for its envisaged application in thermoreversible polymer ligation.

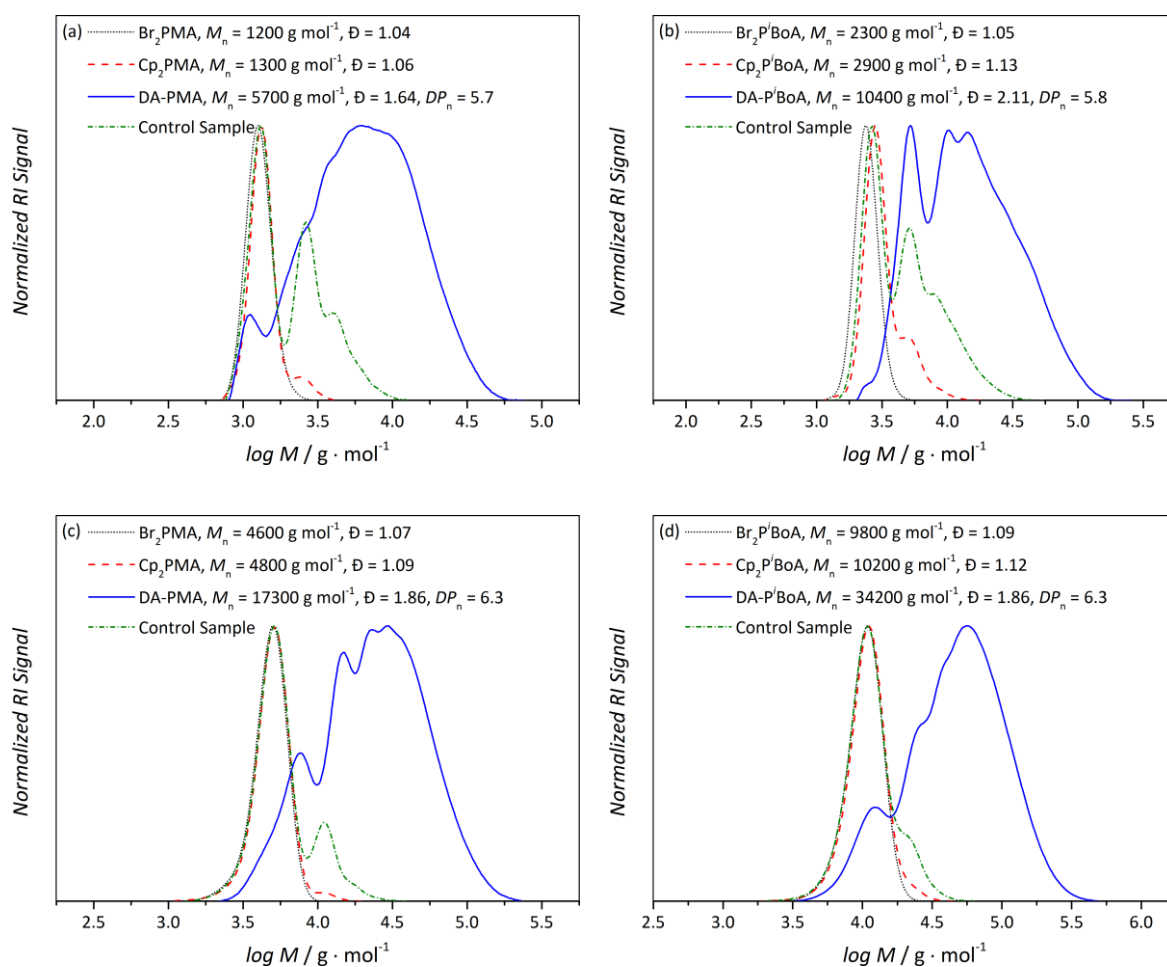


Figure 3-4 SEC chromatograms of the dibromo precursor polymer (····), Cp functional building block (----), Diels–Alder polymer (—) and control sample of heated Cp difunctional macromonomer without CDTE dilinker (— · —) for 10 (a) methyl acrylate and (b) isobornyl acrylate repeating units or for 50 (c) methyl acrylate and (d) isobornyl acrylate repeating units per building block, measured in THF at 35 °C. Adapted from Ref.¹⁴² – Published by The Royal Society of Chemistry.

Table 3-1 List of the synthesized bromo and Cp difunctional polyacrylates, their number average molecular weight M_n , dispersity \mathcal{D} and average number of repeating units n .

Polymer	$M_n / \text{g} \cdot \text{mol}^{-1}$	\mathcal{D}	n
$\text{Br}_2\text{PMA}_{\text{small}}$	1200	1.04	9
$\text{Br}_2\text{P}^i\text{BoA}_{\text{small}}$	2300	1.05	9
$\text{Br}_2\text{PMA}_{\text{large}}$	4600	1.07	49
$\text{Br}_2\text{P}^i\text{BoA}_{\text{large}}$	9800	1.09	45
$\text{Cp}_2\text{PMA}_{\text{small}}$	1300	1.06	11
$\text{Cp}_2\text{P}^i\text{BoA}_{\text{small}}$	2900	1.13	12
$\text{Cp}_2\text{PMA}_{\text{large}}$	4800	1.09	52
$\text{Cp}_2\text{P}^i\text{BoA}_{\text{large}}$	10200	1.12	47

Step-growth adducts ought to allow for a good demonstration of entropic effects due to their relatively large size and the availability of multiple dynamic bonding sites within one molecule. An average degree of (Diels–Alder) polymerization (DP_n) of approximately 6 was envisaged for the step-growth adducts to enable comparable and reproducible results for the subsequent HT NMR evaluation. Suitable Mark-Houwink parameters for the SEC evaluation of macromolecular samples were employed (refer to Experimental Section, Methods and Instruments). Additional control samples of the Cp difunctional macromolecules without linker, but under the same heating conditions as employed for the step-growth formation, assured a significantly slower occurrence of the unwanted DA dimerization of Cp groups in comparison with the desired DA reaction channel of CDTE with Cp (Figure 3-4, control samples). The gained DA step-growth specimen underwent HT NMR measurements from 25 to 140 °C to allow for a quantification of the degree of (r)DA reaction for different backbone materials and lengths. In contrast to previous studies where the degree of bonding could be evaluated via offline SEC characterization of polymeric DA adducts with slow (r)DA properties, the DA reaction of cyanodithioesters with Cp exhibits very fast reaction rates and thus an online analysis via (concentration controlled) HT NMR is not only possible, but mandatory.^{83, 132}

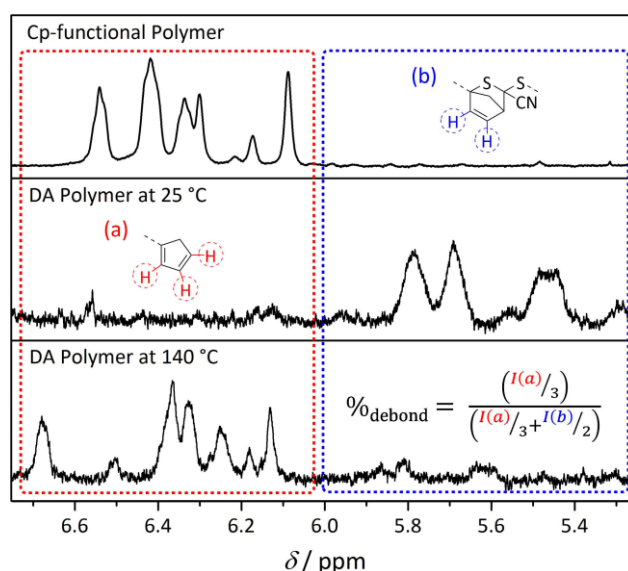


Figure 3-5 Calculation of the temperature dependent degree of debonding $\%_{\text{debond}}$ via the ^1H NMR signal ratios of (a) free Cp chain end groups and (b) closed HDA adducts. Adapted from Ref.¹⁴² – Published by The Royal Society of Chemistry.

The temperature dependent degree of debonding ($\%_{\text{debond}}$) was calculated via the ratio of free Cp group vs. DA adduct ^1H NMR signals (Figure 3-5), with the employed integration

limits being determined via measurements of isolated Cp functional chains or DA adducts. Repeated measurements allowed for the determination of an error of $\pm 2\%$ $\%_{\text{debond}}$. When plotting the determined temperature dependent $\%_{\text{debond}}$ for all four specimen (Figure 3-6), clear trends in accordance with the theoretical results were deduced.

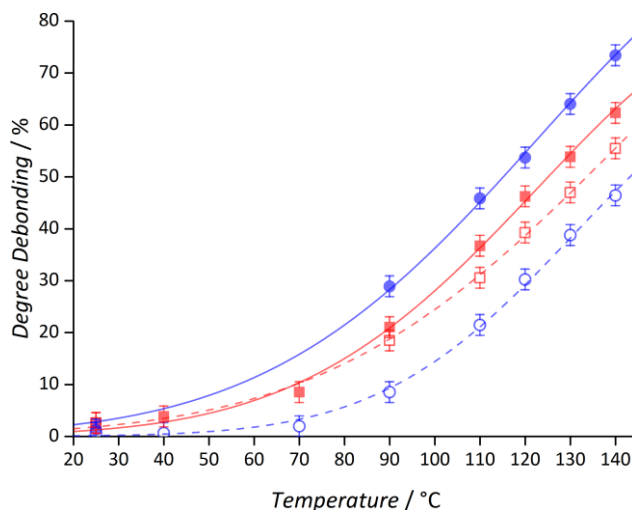


Figure 3-6 Temperature dependent degree of debonding for Diels–Alder polymers consisting of Cp difunctional PMA_{large} (■, 50 repeating units), P'BoA_{large} (●, 50 repeating units), PMA_{small} (□, 10 repeating units) or P'BoA_{small} (○, 10 repeating units) building blocks and CDTE dilinker assessed by HT NMR spectroscopy. Adapted from Ref.¹⁴² – Published by The Royal Society of Chemistry.

First of all, in a comparison of only similar backbone materials with different chain lengths (i.e., PMA_{small} vs. PMA_{large} or P'BoA_{small} vs. P'BoA_{large}, Figure 3-6), a clear mass effect on entropy and thus the reaction equilibrium and the resulting degree of (de-)bonding is demonstrated, as longer and heavier building blocks of the same monomer lead to an – in the case of P'BoA drastic – increase of the $\%_{\text{debond}}$ of up to ca. 30 percentage points. Then again, for the adducts formed from short chains with ca. 10 repeating units with differing backbone materials (PMA_{small} vs. P'BoA_{small}, Figure 3-6), the – theoretically foreshadowed (Section 3.2.2) – significantly increased influence of vibrational entropy with decreased chain length is reflected (refer to Figure 3-2 and Figure 3-3 (a)): Despite incorporating heavier building blocks, the P'BoA_{small} specimen undergoes nearly 10 percentage points less debonding at the same temperature than the PMA_{small} one. Such a behavior hints at the parallel occurrence of a stiffness effect on reaction equilibria which levels off for longer and thus also more mobile chains, but a definitive conclusion can only be achieved via specified experiments of isomeric systems comprising similar chain lengths and masses while incorporating sterically different side-chains as performed in Section 3.3. Finally, for the

samples of differing backbones with increased building block chain lengths of ca. 50 repeating units (PMA_{large} vs. PⁱBoA_{large}, Figure 3-6), the increased influence of ΔS_{vib} is again counteracted by the dominating mass effect, as was predicted via the quantum chemical calculations (Figure 3-3 (b)), leading to a preferred cleavage of long and heavy building blocks with debonding values increased by 10 percentage points in comparison to lighter ones of the same length.

3.2.4 Temperature Dependent SEC

In an approach to further experimentally verify these results, temperature dependent size exclusion chromatography (TD SEC) was conducted for the specimen comprising the longer building blocks PMA_{large} and PⁱBoA_{large}. An additional advantage of the employed step-growth polymers – at least for said larger building blocks, as in the cases of the specimen containing smaller building blocks, the relatively similar adduct, linker and building block signals cannot be isolated sufficiently well for a reliable assessment of the obtained data – is their significant difference in weight between building blocks and formed adduct, leading to a possible evaluation via TD SEC. As a consequence, the evolution of the molar mass distributions can be monitored while they undergo a rDA reaction, leading to more information on the debonding process in total. With increasing reaction time at elevated temperatures, the detected peak signal shifts from higher adduct masses to lower ones for the cleavage products, until it converges with the chromatogram of the isolated building block. Unfortunately, a facile data evaluation of average molar masses determined via a calibration with polymer standards is not possible due to the mixed composition of the samples and the variable temperature in TD SEC. Hence, via monitoring the decrease of DA polymer concentration throughout the rDA reaction, another methodology was utilized (Figure 3-7, refer to the original publication¹⁴² for a detailed description of the employed TD SEC technique). Such values cannot be directly related to the previously via HT NMR determined degree of debonding, as the sensitivity of the employed TD SEC techniques towards small molecular cleavage, i.e., the scission of single linker molecules from macromolecules, is not as high as in NMR measurements due to the small mass and elution time differences and the associated overlapping of signals, thus leading to an exaggeration of debonding.

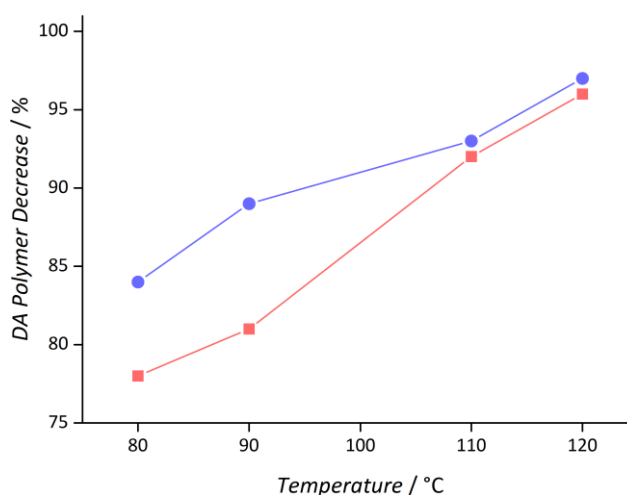


Figure 3-7 TD SEC results: decrease of concentration of DA polymer due to rDA reaction of the DA polymers consisting of Cp difunctional PMA_{large} (■, 50 repeating units) and P'BoA_{large} (●, 50 repeating units) building blocks and CDTE dilinker. Adapted from Ref.¹⁴² – Published by The Royal Society of Chemistry.

Nevertheless, valuable qualitative insights into the validity of the previously observed characteristics of entropic effects on dynamic reactions can be obtained. In accordance with the theoretical calculations and the HT NMR measurements, the TD SEC measurements also evidence the highest decrease of DA polymer concentration at a given temperature for the DA step-growth adduct formed from heavier P'BoA building blocks (Figure 3-7). Accordingly, the counteracting influence of ΔS_{vib} resulting in increased retro reaction temperatures for short P'BoA chains (compare Section 3.2.2 and 3.2.3) is again overcompensated by the increasing mass effect in elongated chains, demonstrating the impact of chain mass and length also via SEC techniques.

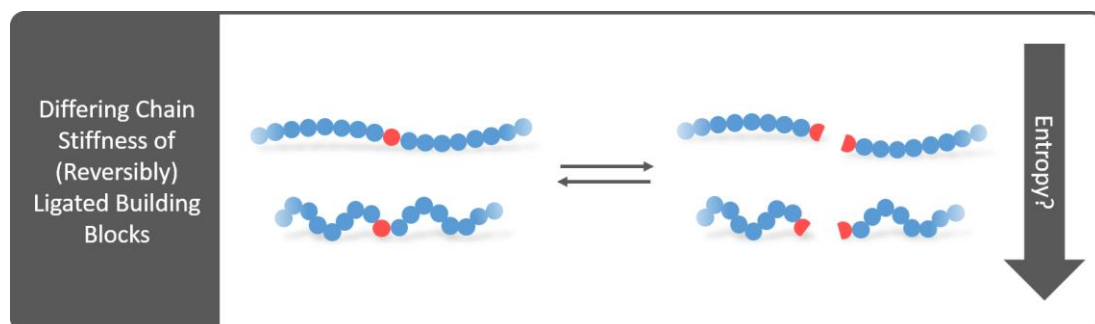
3.2.5 Summary

The principle of an entropic mass effect on dynamic reaction equilibria, previously only established for one specific catalyzed DA reaction, was expanded to and clearly reproduced for another catalyst-free DA reaction of a CDTE linker with Cp moieties comprising rapid reaction rates.⁸³ In the course of these studies, quantum chemical *ab initio* calculations isolated characteristic trends for different building block lengths, masses or substituents and provided for detailed insights into the entropic causes of the observed effects. Subsequently, the computationally assessed reversible bonding systems were synthesized and experimentally characterized via HT NMR and TD SEC, yielding results in good accordance with the theoretic outcomes. For reversibly ligated polymer blocks of the same

backbone material, longer and thus also heavier blocks lead to a significantly decreased retro reaction temperature, with higher degrees of debonding of up to 30 percentage points at a given temperature being observed for the employed chemistry. Clearly, such effects can be harnessed to shift reaction equilibria and thus material properties as, for example, the temperature dependent cross-linking of different backbone materials via dynamic chemistries or the reversible ligation of (bio-)molecules. At the same time, the influence of entropy must be considered when defined bonding properties are envisaged while transferring known parameters from small-molecular to macromolecular reactions. Also, the herein observed effect of chain mass and length was shown to be counteracted by the vibrational entropy in short and bulky chains, leading to a possibly lower degree of debonding for short and stiff chains of higher mass vs. more mobile chains of lower mass and hence the assumption of an impact of chain stiffness on entropy as well as the connected dynamic equilibrium. To assess the question of a possible chain stiffness effect, additional more specified studies with a focus on the reversible bonding behavior of chain species of varying intramolecular mobility while excluding different masses and thus an overlapping mass effect were carried out in the next section (Section 3.3).

3.3 Chain Stiffness Effect on Reaction Equilibria

Not only length and mass of a molecule define its degrees of freedom and thus entropic properties, but also the chain mobility alias its stiffness. In addition to the promising findings regarding the differently pronounced influence of vibrational entropy for different chain lengths in the preceding section, more specialized experiments for an isolation of the impact of molecular stiffness (Scheme 3-5) on dynamic bonding properties were designed.[†]



Scheme 3-5 Reversibly ligated building blocks of differing backbone stiffness.

3.3.1 Experimental Design

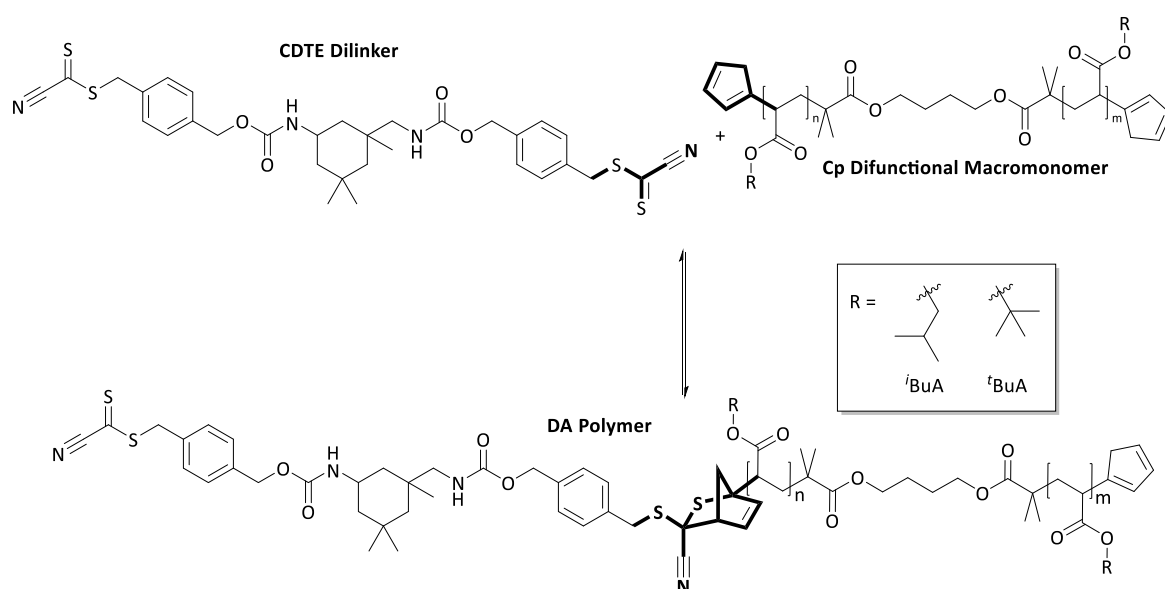
Similar to the experimental setup in Section 3.2, diverse thermoreversible DA adducts of macromolecular building blocks – now comprising different backbone stiffness while keeping the same chain length and in the cases of the butyl isomers also weight – were synthesized and assessed (Scheme 3-7).⁷³ In addition to the aforementioned step-growth polymers from diene difunctional building blocks comprising different backbones and a CDTE dienophile dilinker, also A,A'-diblock polymers were synthesized via the ligation of Cp monofunctional polymethacrylate chains and characterized via HT NMR and TD SEC. Polymethacrylate blocks with similar numbers of repeating units and thus length, but different side-chain substituents were chosen due to their better precipitation abilities in comparison to polyacrylates. In employing also diene monofunctional species, the specificity of entropic effects in molecules with decreased a number of dynamic ligation

[†] Parts of the current section are reproduced or adapted from K. Pahnke, J. Brandt, G. Gryn'ova, P. Lindner, R. Schweins, F. G. Schmidt, A. Lederer, M. L. Coote, C. Barner-Kowollik, *Chem. Sci.* **2015**, *6*, 1061-1074, with permission from The Royal Society of Chemistry. J. Brandt carried out the TD SEC and SANS measurements. G. Gryn'ova conducted the quantum chemical calculations. P. Lindner and R. Schweins helped with the SANS measurements. F. G. Schmidt, A. Lederer and M. L. Coote helped with discussions. C. Barner-Kowollik motivated and supervised the project and contributed to the scientific discussions.

sites or predetermined cleavage points should be investigated and a possible influence of Cp-Cp dimerization should be decreased, as here – in contrast to Cp difunctional materials – an under the given conditions irreversible dimerization leads to non-functional material and thus no falsification of the measurements via elongated block sizes. On the other hand, polyacrylates allowed for lower dispersity values below $\bar{D} = 1.1$ and hence a lower broadening of effects, so analogous step-growth systems from Cp difunctional polyacrylates as employed in Section 3.2 were also investigated, now comprising three differently substituted isomeric butyl acrylates of the same chain length. Again, the experimental studies were guided and substantiated via quantum chemical *ab initio* calculations.

3.3.2 Computational Studies

First, to computationally investigate the influence of different side-chain substituents with their inherently different impact on chain stiffness via their altered steric properties while keeping the same molecular weight, poly(*tert*-butyl acrylate) ($P^t\text{BuA}$) and poly(*iso*-butyl acrylate) ($P^i\text{BuA}$) building blocks and their reversible ligation to a CDTE linker was assessed as model systems via *ab initio* calculations in the Gaussian 09 software package, conducted by collaboration partners at the Australian National University (Canberra).



Scheme 3-6 Model DA reaction of isomeric polyacrylates of differing chain stiffness with a CDTE linker studied using quantum chemistry. Fragments in bold correspond to the core layer (reaction center) in the ONIOM-like approximation. Adapted from Ref.¹⁴² – Published by The Royal Society of Chemistry.

In this way, due to their isomeric structure, the previously investigated effect of molecular mass on entropy and thus the Gibbs free energy of a reaction can be excluded and a possible effect of chain stiffness on such parameters can be isolated. Similar to the previous calculations, rotational (ΔS_{rot}) and vibrational (ΔS_{vib}) entropy of the DA reaction between oligomeric building block species ($n = m = 0-2$) of said differing backbone materials with a CDTE linker (Scheme 3-6) was each calculated for the optimized lowest energy conformer and an optimized extended chain version of these initial structures (refer to Figure 3-1) to resemble short or longer chains and their respective altered entropic characteristics (Figure 3-8).

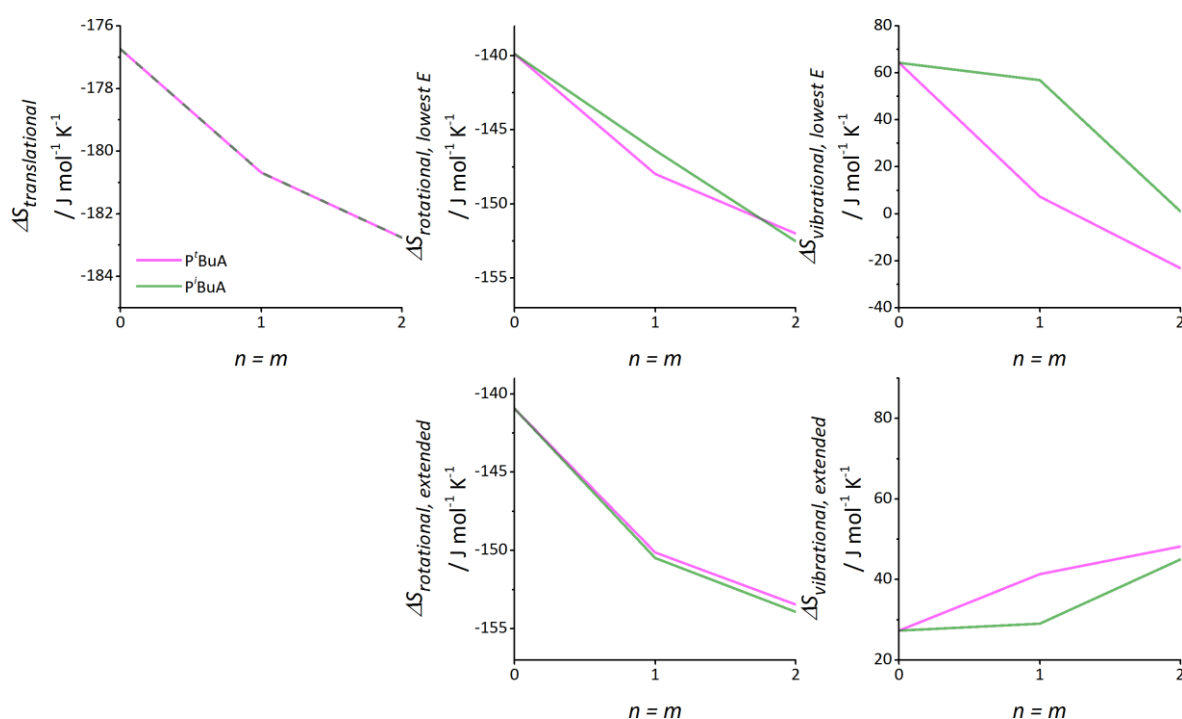


Figure 3-8 Calculated changes in the entropy (ΔS in $\text{J mol}^{-1} \text{K}^{-1}$) of model DA reactions for different n, m (chain lengths) of poly(*iso*-butyl acrylate) or poly(*tert*-butyl acrylate) macromonomers in their lowest energy or extended chain conformation. In these figures, the more negative ΔS , the lower the Gibbs free energy of bonding, or the greater the extent of debonding, at a given temperature. Adapted from Ref.¹⁴² – Published by The Royal Society of Chemistry.

With the translational entropy (ΔS_{trans}) being only dependent on the mass of the employed molecule and not its mass distribution in space, no different conformers had to be analyzed and naturally, the calculations for both isomers of similar molecular weight led to the same result (Figure 3-8, top left). With increasing length of the oligomeric species, the previously obtained trend of heavier and longer species leading to a more favored debonding via ΔS_{trans} and ΔS_{rot} is reproduced. The differences in ΔS_{rot} between either the different

conformers or the different isomers are not sufficiently large for clear conclusions on the debonding behavior of actual polymeric species, but a slight trend of the longest calculated oligomer ($n = m = 2$) to lower values for the *iso*-butyl derivative may indicate its more favored debonding for longer species. Due to its high dependency on conformation, the data obtained for ΔS_{vib} again differs strongly for the globular vs. the extended chain models. While for very short, globular chains modelled via the lowest energy conformer, the supposedly less stiff *iso*-butyl moiety – which nevertheless leads to a more spread mass distribution in very short chains – may undergo less debonding due to its higher ΔS_{vib} values, the trend is reversed for the long-chain model of optimized extended geometries. A similar behavior was already attributed to short vs. long chains of PⁱBoA vs. PMA (Section 3.2.2) and is also reflected in the calculated degree of (de-)bonding vs. temperature in Figure 3-9 with DA adducts of short PⁱBuA chains with the CDTE linker undergoing rDA reactions at higher temperatures than the adducts comprising short P^tBuA chains, while the extended chain models result in lower debonding temperatures for the more mobile PⁱBuA species in comparison with the stiffer P^tBuA one.

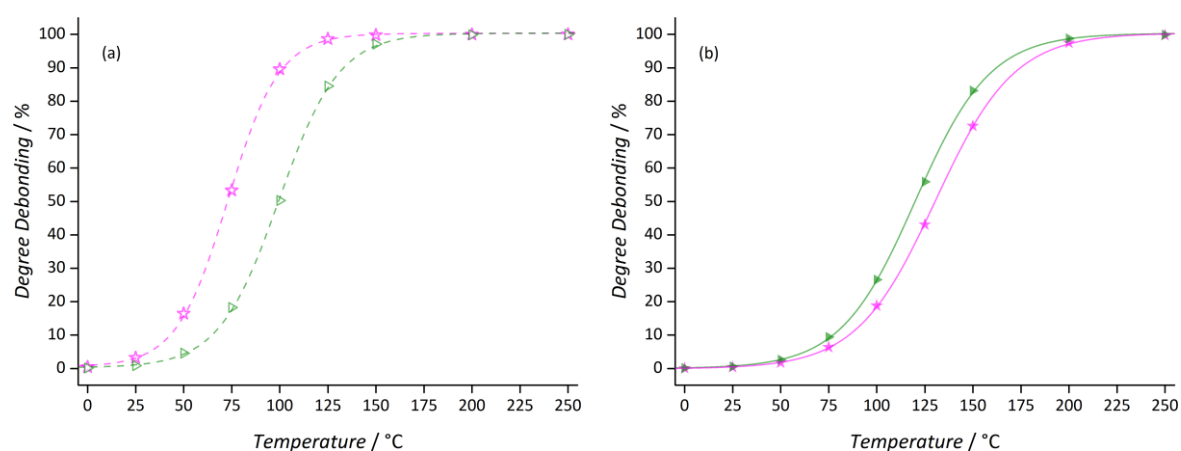
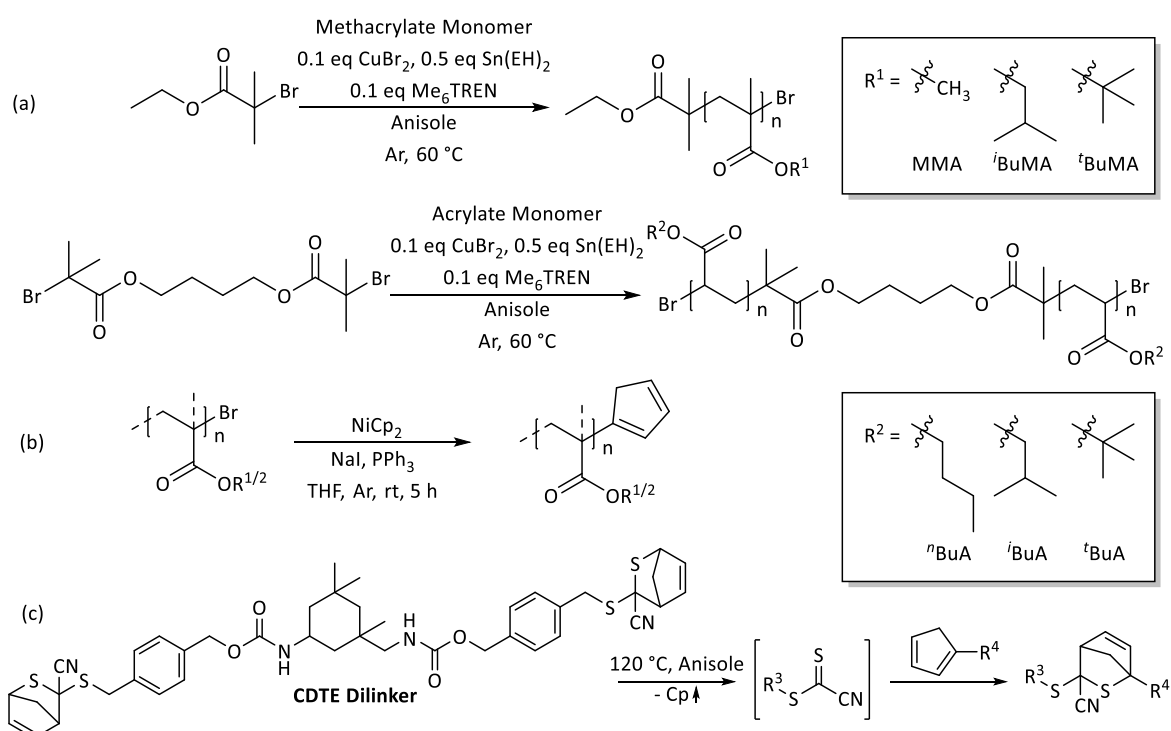


Figure 3-9 Degree of debonding (determined from the calculated reaction energies for $n = m = 2$ chain lengths) vs. temperature for (a) lowest energy and (b) extended chain conformers of PⁱBuA (►) or P^tBuA (★). Adapted from Ref.¹⁴² – Published by The Royal Society of Chemistry.

Although these general trends allow for the anticipation of an impact of chain stiffness on association equilibria, due to the limited validity of these results for significantly larger polymer systems, experimental studies are necessary to quantify the obtained results. The final computational data is provided in the Experimental Section, yet for full details, refer to the original publication.¹⁴²

3.3.3 High Temperature NMR

Samples for HT NMR measurements were prepared in a similar way as described in Section 3.2.3 from – in the case of the DA step-growth polymers close to – equimolar amounts of Cp (di-)functional blocks and CDTE dilinker (Scheme 3-7 (c)). The building blocks were synthesized via ARGET ATRP (Scheme 3-7 (a)) with a subsequent quantitative substitution of the bromo end-groups via NiCP₂ (Scheme 3-7 (b)) to ensure a near to quantitative Cp end-group fidelity (refer to Figure 3-10 for SEC chromatograms).^{90, 229}



Scheme 3-7 Reaction scheme for the generation of thermoreversibly connected macromolecules of different building block sizes via (a) ARGET ATRP of (meth-) acrylate monomers with a bromo (di-) functional initiator, (b) subsequent substitution of the bromo end-groups via nickelocene and (c) Diels–Alder step-growth or diblock formation of dienophile difunctional and diene mono- or difunctional blocks. Adapted from Ref.¹⁴² – Published by The Royal Society of Chemistry.

Chain lengths of all blocks were adjusted to approximately 50 repeating units (Table 3-2) to enable an investigation of the influence of the chain stiffness of extended polymer species without the complicating effects of a globular conformation of very short chain species (refer to ΔS_{vib} in Section 3.3.2 and 3.2.2). The diblock DA adducts were composed from blocks of isomeric poly(*iso*-butyl methacrylate) (ⁱBuMA) or poly(*tert*-butyl-methacrylate) (^tBuMA) chains and were in addition compared to an adduct of similarly long, but lighter poly(methyl methacrylate) (PMMA) blocks to allow for a classification of stiffness vs. mass

effect. DA step-growth adducts with a DP_n of approximately 6 in each case for good comparability were formed from the reaction of the CDTE linker with isomeric Cp α,ω -difunctional poly(*n*-, *iso*-, or *tert*-butyl acrylates) (PBuAs).

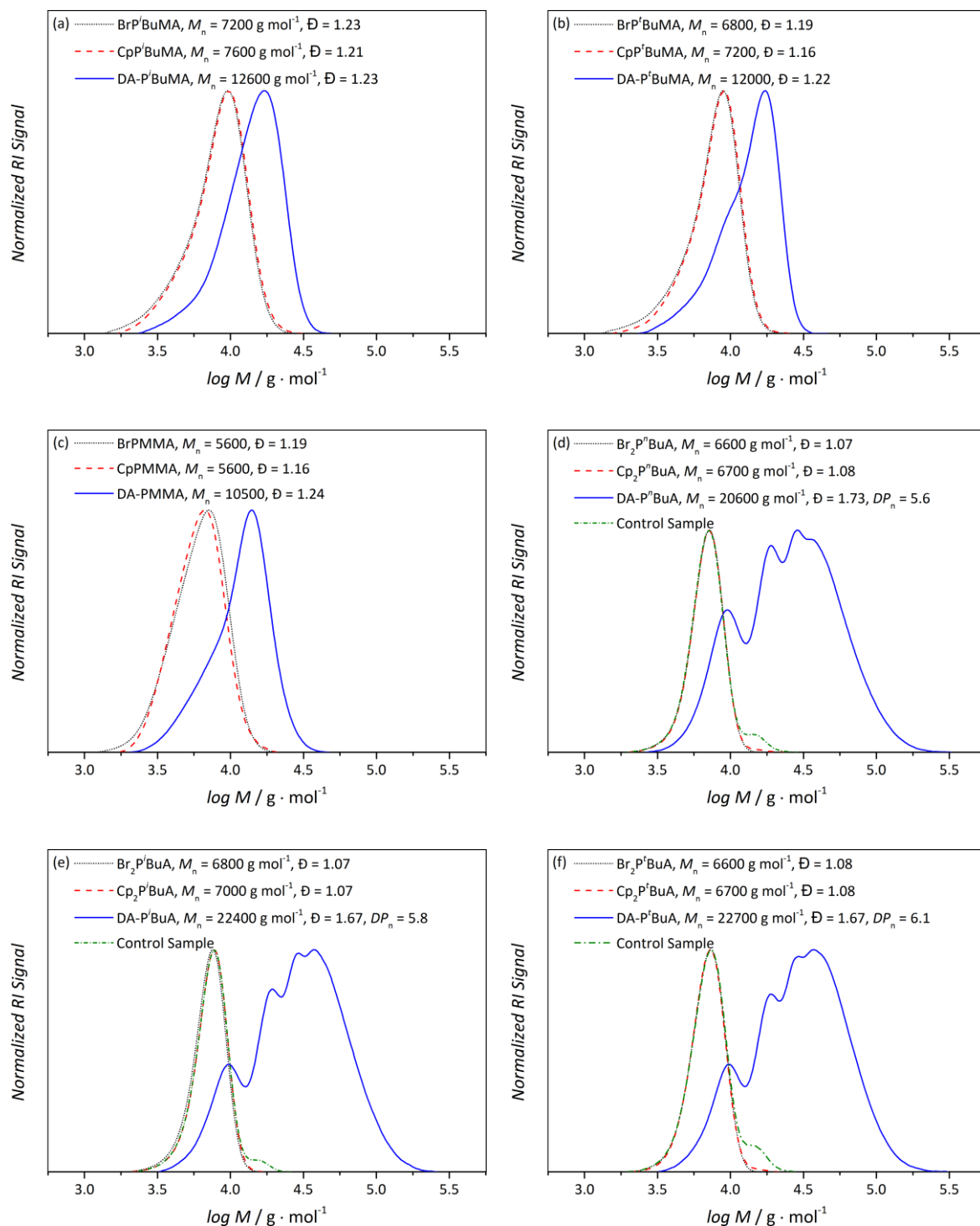


Figure 3-10 SEC elugrams of the (di-) bromo precursor polymer (····), Cp functional building block (----), Diels–Alder diblock or step-growth polymer (—) and control sample of heated Cp difunctional acrylate macromonomer without CDTE dilinker (---) for 50 (a) ^tBuMA, (b) ⁱBuMA, (c) MMA, (d) ⁿBuA, (e) ⁱBuA and (f) ^tBuA repeating units per building block, measured in THF at 35 °C. Adapted from Ref.¹⁴² – Published by The Royal Society of Chemistry.

The efficient coupling of all block types as well as the negligibility of unwanted Cp-Cp coupling of the polyacrylates during heating of control samples without linker was monitored via SEC, employing appropriate Mark-Houwink parameters (Figure 3-10).

Table 3-2 List of the synthesized bromo and Cp (di-)functional polymers, their number average molecular weight M_n , dispersity \mathcal{D} and average number of repeating units n .

Polymer	$M_n / \text{g} \cdot \text{mol}^{-1}$	\mathcal{D}	n
BrPMMA	5600	1.19	52
BrP ⁱ BuMA	7200	1.23	48
BrP ^t BuMA	6800	1.19	45
Br ₂ P ⁿ BuA	6600	1.07	49
Br ₂ P ⁱ BuA	6800	1.07	50
Br ₂ P ^t BuA	6600	1.08	49
CpPMMA	5600	1.16	52
CpP ⁱ BuMA	7600	1.21	51
CpP ^t BuMA	7200	1.16	48
Cp ₂ P ⁿ BuA	6700	1.08	49
Cp ₂ P ⁱ BuA	7000	1.07	52
Cp ₂ P ^t BuA	6700	1.08	49

All samples of similar concentration underwent HT NMR measurements up to 140 °C in toluene- d_8 in a pressure tube and the degree of debonding of the DA adduct was calculated via the ratio of Cp to DA adduct signal as described in Section 3.2.3. The evaluation of the data obtained from the HT NMR measurements of the poly(butyl methacrylate) (PBuMA) DA A,A'-diblock specimen clearly demonstrates the variable effect of differing side-chain substituents on reaction equilibria (Figure 3-11). The previously established chain-mass effect on dynamic reactions is reproduced in the comparison of the lighter PMMA vs. the heavier PBuMA samples, the latter both exhibiting lower rDA temperatures or higher degrees of debonding at a given temperature. Remarkably, as anticipated via the computational *ab initio* calculations of oligomeric model systems in Section 3.3.2, the employment of isomeric side-chain substituents of differing steric properties effectively results in altered bonding properties of the individual blocks with a similar specificity as

observed for the blocks of different masses: Both the difference in the degree of debonding between samples with PMMA or P^tBuMA as well as P^tBuMA or PⁱBuMA amounts to approximately 7 percentage points.

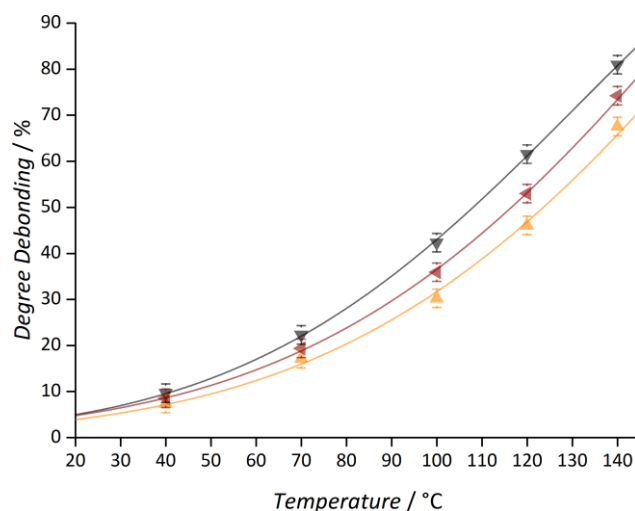


Figure 3-11 Temperature dependent degree of debonding for Diels–Alder A,A'-type diblockcopolymers consisting of PMMA (▲), PⁱBuMA (▼) or P^tBuMA (◄) building blocks with a length of 50 repeating units assessed by HT NMR spectroscopy. Adapted from Ref.¹⁴² – Published by The Royal Society of Chemistry.

Analogous to the mass effect, the causes of such a substituent effect can be ascribed to the entropic parameters via theoretical calculations (Section 3.3.2). The dissimilar chain mobility values as a consequence of the different steric demands of the side chains is an obvious reason: In chain scission events, the rotational and vibrational degrees of freedom are being decreased, as the resulting smaller chain segment lengths are closer to their stiffness-defining persistence length and thus possess less flexibility.^{58, 230, 231} When keeping all other parameters such as segment weight and cleavage position similar, the difference in entropic potential of differently mobile backbone materials should in fact lead to differences in the debonding behaviour with more mobile (i.e., less stiff) chains underlying less entropic constraints and thus cleave more facile. As a rough approximation for chain mobility, the glass transition temperature T_g of the respective polymers were examined. Although T_g values are clearly an inadequate measure for polymer stiffness in solution, as these temperatures are properties of bulk polymer melts, for similar backbones with altered side-chain substituents of differing steric demand they should approximately reflect their relative molecular mobility without the possibility of solvent interactions leading to deviations.^{232, 233} With a distinctive difference in reported T_g values of 70 K ($T_{g,P^tBuMA} = 118$ °C, $T_{g,P^iBuMA} = 48$ °C), it can be assumed that PⁱBuMA should essentially be a

significantly less rigid polymer species than P^tBuMA and thus exhibit lower cleavage temperatures, as was indicated by the computational calculation of ΔS_{rot} as well as ΔS_{vib} of extended acrylate chain species with *iso*- or *tert*-butyl substituents (Figure 3-8) and actually observed in experiment, thus supporting the hypothesis of the presumed chain stiffness effect.²³⁴⁻²³⁶ On a side note, although a PMMA backbone ($T_{\text{g,PMMA}} = 105$ °C) may be more mobile than a P^tBuMA one, its lower mass and thus also less significant translational as well as rotational entropy seems to overcompensate the effect of chain stiffness on the Gibbs free energy, hence leading to lower debonding values in experiment.^{237, 238} As the difference in T_{g} is not as substantial for PMMA vs. P^tBuMA and a quantification of chain stiffness would be desirable to allow for a clear assignment of causality, small angle neutron scattering (SANS) measurements of building block persistence lengths (l_p) as well as additional HT NMR measurements of isomeric DA step-growth polymers formed from PBuA macromonomers were conducted to verify the previously obtained results. During SANS measurements, the same solvent as utilized later on in the HT NMR measurements (toluene-d₈) was employed. The obtained data was evaluated via a procedure by Casassa and Holtzer, resulting in quantitative persistence lengths for the three PBuA isomers in toluene-d₈ (Table 3-3).^{239, 240}

Table 3-3 The different poly(butyl acrylates) investigated in the current section and the corresponding literature values for their glass transition temperatures T_{g} as well as measured persistence lengths (l_p) in toluene-d₈.

Polymer	$T_{\text{g}} / ^\circ\text{C}$	Ref.	l_p / nm
poly(<i>n</i> -butyl acrylate)	-54	238	2.0
poly(<i>iso</i> -butyl acrylate)	-24	241	1.8
poly(<i>tert</i> -butyl acrylate)	43	242	2.3

The obtained persistence lengths allow for the conclusion that the effect of the solvent on chain conformation and stiffness should not be underestimated: Although the T_{g} value of PⁿBuA is 30 K lower than for PⁱBuA, its persistence length in the employed solvent is actually longer and thus the chain is more rigid in the employed solvent. As solvents in general are well known to be crucial for polymer conformation, it is not surprising that also in other solvents as for example tetrahydrofuran, PⁱBuA is reported to be less stiff than PⁿBuA,

therefore demonstrating the importance of the careful evaluation of molecular parameters for the given conditions.²⁴³ The characterization of the experimental reversible bonding behavior of the DA step-growth polymers formed from the three different isomeric Cp difunctional P*Bu*A building blocks and a CDTE dienophile dilinker (refer to Scheme 3-7 for the synthesis route and Figure 3-10 (d)-(f) for SEC chromatograms) via HT NMR measurements at 25 to 140 °C (Figure 3-12) clearly substantiates the previous experimental results and validates the hypothesis of a chain stiffness dependent effect on ligation equilibria via the differences in reaction entropy: In good accordance with the computational calculations of extended chain conformers (Figure 3-8 and Figure 3-9) and the findings for thermoreversibly connected P*Bu*MA A,A'-diblock polymers (Figure 3-11), the bonding of the investigated isomeric P*Bu*A step-growth polymers is proportional to their respective persistence lengths (Table 3-3), as the least rigid P^{*i*}*Bu*A blocks lead to a lower *r*DA temperature than P^{*n*}*Bu*A ones, finally followed by the most rigid P^{*t*}*Bu*A macromonomers (Figure 3-12).

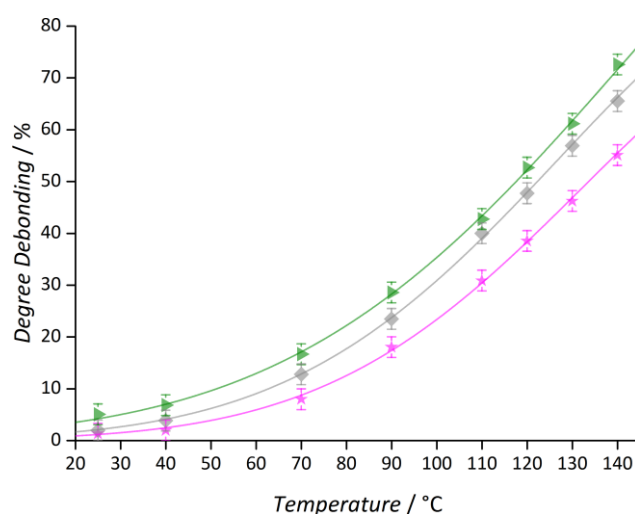


Figure 3-12 Temperature dependent degree of debonding for Diels–Alder polymers consisting of Cp difunctional P^{*i*}BuA (▲), P^{*n*}BuA (◆) or P^{*t*}BuA (★) building blocks with a length of 50 repeating units and CDTE dilinker assessed by HT NMR spectroscopy. Adapted from Ref.¹⁴² – Published by The Royal Society of Chemistry.

The obtainable %_{debond} of specimen containing *n*-butyl side chains lies ca. 11 percentage points above the isomeric samples comprising *tert*-butyl substituents, while it is approximately 7 percentage points lower than for similar samples with *iso*-butyl groups. In conclusion, the degree of debonding was altered by nearly 20 percentage points via the simple substitution of isomeric side-chain substituents of similar mass, but different steric

properties, resulting in altered chain stiffness and thus also conformation and reaction entropy.

3.3.4 Temperature Dependent SEC

As previously noted, the employed DA step-growth adducts of relatively long macromonomers allow for an evaluation via TD SEC experiments, because their molecular mass is drastically reduced during chain cleavage, leading to a reliable separation and detection of masses via such chromatographic methods. Figure 3-13 shows an exemplary chromatogram of the DA step-growth polymer formed from Cp difunctional P^tBuA building blocks and CDTE and its thermally induced cleavage at 80 °C.

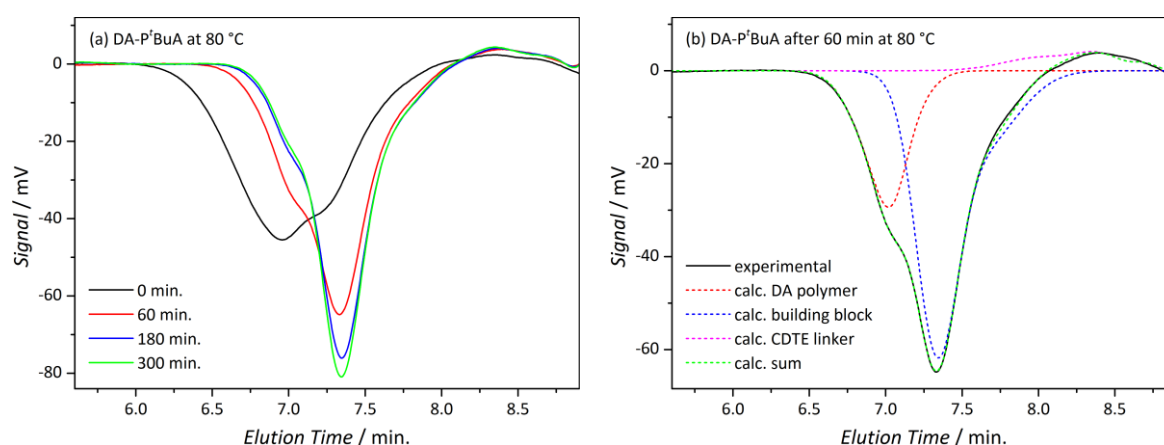


Figure 3-13 TD SEC chromatograms, (a) DA-P^tBuA after different rDA times at 80 °C in 60 % TCB and 40 % DMF, (b) DA-P^tBuA after 60 min. rDA at 80 °C and distributions calculated by peak deconvolution of the individual components. Adapted from Ref.¹⁴² – Published by The Royal Society of Chemistry.

Similar to Section 3.2.4, the analysis of such temperature dependent chromatograms enabled the determination of a concentration decrease of the initially present DA polymer at elevated temperatures, performed in a mixture of 60 % 1,2,4-trichlorobenzene (TCB) with 40 % *N,N*-Dimethylformamide (DMF) (Figure 3-14). Again, the obtained values cannot be directly compared to the %_{debond} values as calculated via HT NMR measurements due to the limited sensitivity of the employed SEC method towards the release of a small molecular linker, thus accompanied by an overestimation of debonding, yet they provide for a convenient visualization of the debonding process and its qualitative trends. Interestingly, while the *tert*-butyl derivative again features the lowest decrease of DA polymer and is thus in perfect agreement with the HT NMR measurements (Figure 3-12), the specimen containing *n*- or *iso*-butyl side-chain substituents interchange their respective

debonding characteristics in TD SEC experiments with *n*-butyl residues leading to the highest decrease of DA polymer at a given temperature, now reproducing the trends as expected via the order of T_g values (Table 3-3).

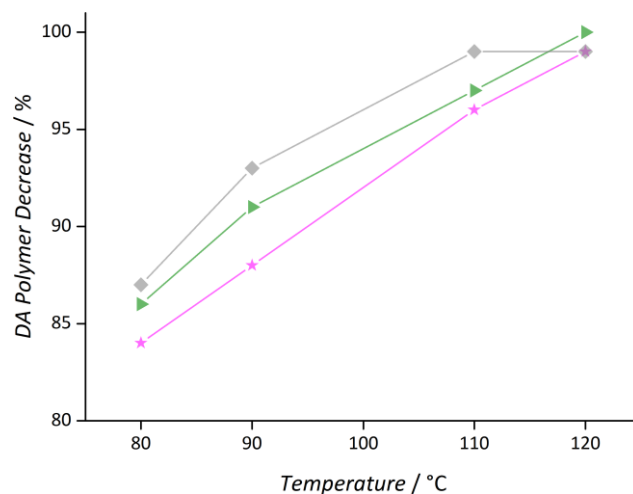


Figure 3-14 TD SEC results: decrease of concentration of DA polymers due to rDA reactions of the DA polymers consisting of Cp difunctional PⁱBuA (▲), PⁿBuA (◆) or P^tBuA (★) building blocks with a length of 50 repeating units and CDTE dilinker. Adapted from Ref.¹⁴² – Published by The Royal Society of Chemistry.

Most probably, these deviating results can be traced back to the altered solvent necessary for the employed TD SEC method with its substantially changed influence on chain conformation. Still, the significant effect of different side-chain substituents, their steric properties and thus the inherent chain stiffness was again demonstrated, at the same time highlighting the vital impact of the solvent in reactions of polymeric species.

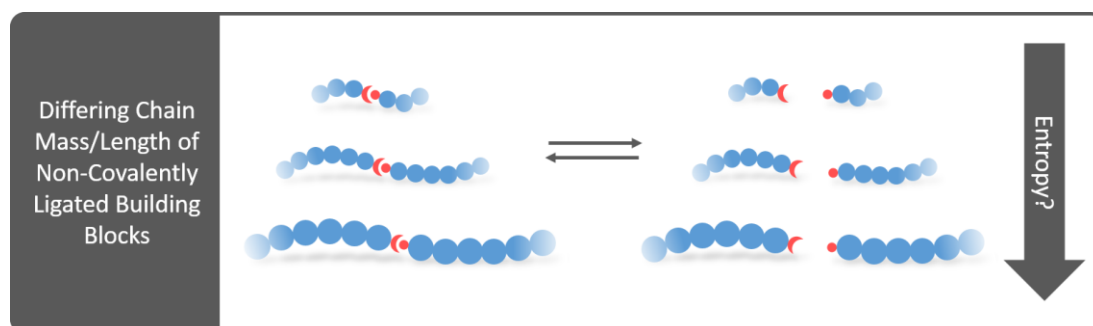
3.3.5 Summary

The role of physical molecular parameters influencing reaction entropy and thus leading to altered reaction equilibria was expanded to the steric properties of side-chain substituents and the associated chain stiffness of thermoreversibly ligated isomeric poly(butyl methacrylates) and poly(butyl acrylates). The computationally backed evaluation of A,A'-diblock or step-growth polymers, bonded via the thermoreversible reaction of a cyanodithioester dienophile linker with cyclopentadiene end-group functionalities of polymers, by HT NMR and TD SEC led to the conclusion of a more favored release of more mobile (i.e., less stiff) chains in a cleavage process. Such a behavior can be explained via the less constrained rotational and vibrational entropy of less rigid species in connection with the increasing rigidity of cleaved and thus shortened chain species. In addition, the

crucial importance of solvent, solvation properties and resulting conformational properties of chain molecules were pointed out via the altered reactivity of similar specimen in different solvent mixtures. These findings once again emphasize the importance of entropic effects while evaluating especially reversible bonding processes, as – besides the previously explored effect of molecular mass and length – also less obvious molecular characteristics such as their stiffness or mobility are revealed to alter ligation properties.

3.4 Entropic Effects on Non-Covalent Ligation

After establishing entropic effects on dynamic covalent chemistries, the question arose if the general principle – which in theory should apply to all kinds of association – can be transferred to supramolecular chemistries as for example a mass effect on hydrogen bonding (Scheme 3-8) to corroborate its universal applicability.[‡] Effects of entropy on non-covalent interactions such as enthalpy-entropy compensation, the characteristics of phase transition or aggregation of supramolecularly associated block polymers have been described previously, highlighting the importance of entropy in supramolecular chemistry and indicating a likely presence of other entropic effects on association equilibria which formerly may not have been investigated.^{220-222, 244-247} As supramolecular chemistries are increasingly being employed for the generation of reversibly ligated substrates with applications such as self-healing or -assembling materials and structures, selective recognition or first approaches towards the synthesis of artificial proteins and enzymes, an in-depth understanding of the different underlying factors with an impact on bonding parameters is essential.^{9, 23, 29, 31, 46, 70, 110, 162, 169, 182, 193, 215, 248-253}



Scheme 3-8 Supramolecularly ligated building blocks of differing length or mass.

Not only can entropic effects be potentially harnessed to achieve an adjustment of ligation properties, but they also have to be taken into account when standard chemistries are transferred to macromolecular species, e.g., when mimicking protein self-folding behavior with reversible recognition units along a chain molecule, as the entropic properties of the

[‡] Parts of the current section are reproduced or adapted with permission from K. Pahnke, O. Altintas, F. G. Schmidt, C. Barner-Kowollik, *ACS Macro Lett.* **2015**, *4*, 774-777. Copyright 2015 American Chemical Society. O. Altintas helped with the synthesis of RAFT agents, small molecular binding motifs and medium-sized PⁿBuA polymer samples. F. G. Schmidt helped with discussions. C. Barner-Kowollik supervised the project and contributed to the scientific discussions.

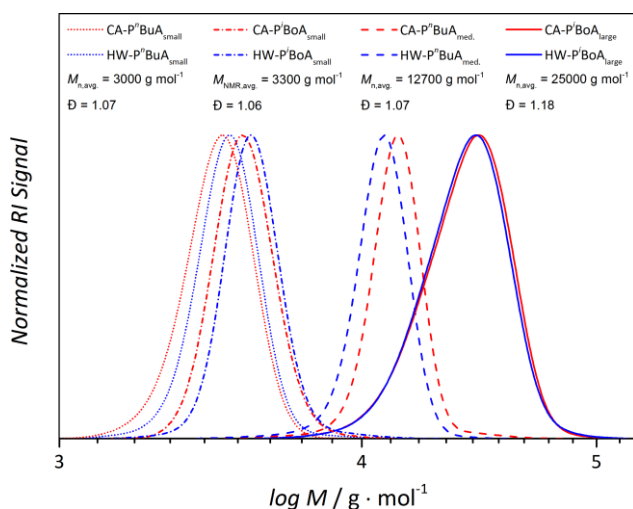
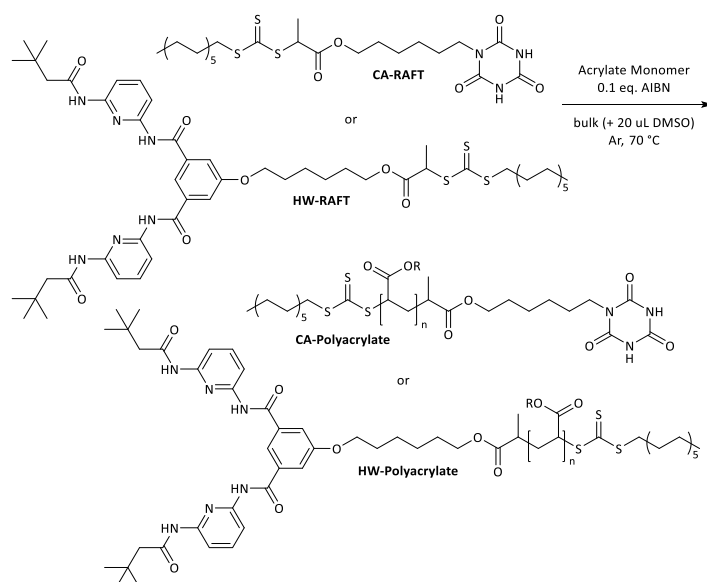


Figure 3-16 SEC chromatograms of the employed CA- and HW-functional polymer building blocks, measured in THF at 35 °C. Adapted with permission from Reference²⁵⁴. Copyright 2015 American Chemical Society.



Scheme 3-9 Reaction scheme of the employed RAFT polymerizations to obtain CA- and HW-functional polymers of defined chain lengths.

Unwanted intramolecular interactions of acrylate backbones with the binding motifs was inhibited via an aliphatic spacer comprising six carbon atoms.²⁵⁶ Water impurities and thus a falsification of measurements due to hydrogen bonding of water to the recognition units was excluded via drying of the specimen over sodium sulfate as well as under reduced pressure for 24 h and storage in a desiccator over silica gel. Qualitative evidence regarding the degree of association of the investigated hydrogen bonding pairing can be given via the association dependent shift of the cyanuric acid imide proton signal in ¹H NMR measurements, while quantitative conclusions in terms of association constants can be gained via NMR titration methods.

3.4.2 NMR Measurements

To be able to observe hydrogen bonding, an aprotic solvent with good solvation qualities for polyacrylates, tetrachloroethane- d_2 ($C_2D_2Cl_4$), was chosen for the NMR measurements of the supramolecular diblocks.⁷³ During sample preparation for the NMR measurements, diblock formation was achieved via dissolution of equimolar amounts of cyanuric acid as well as Hamilton wedge functional small molecular or polymeric species. An end-group concentration of 6 mmol L^{-1} was employed for all samples to circumvent different degrees of association due to differing concentrations and thus a shifted equilibrium. The samples were left for 6 h to guarantee full equilibration. In addition, intermolecular interaction of the employed polyacrylate backbones with the recognition units was excluded via test measurements of the small molecular recognition unit pairing and equimolar amounts of non-functional $P^n\text{BuA}$ or $P^i\text{BoA}$ samples, leading to the conclusion of an unaltered behavior in comparison with similar samples without polyacrylate content (refer to the Experimental Section). In order to enable consistent spectra evaluation, all measurements were normalized on tetramethylsilane (TMS) as internal standard ($\delta = 0 \text{ ppm}$). All diblock samples underwent HT ^1H NMR measurements at 25 to 140 °C to examine the temperature-dependent association via the association-dependent shift of the imide proton signal of the cyanuric acid species (Figure 3-17).

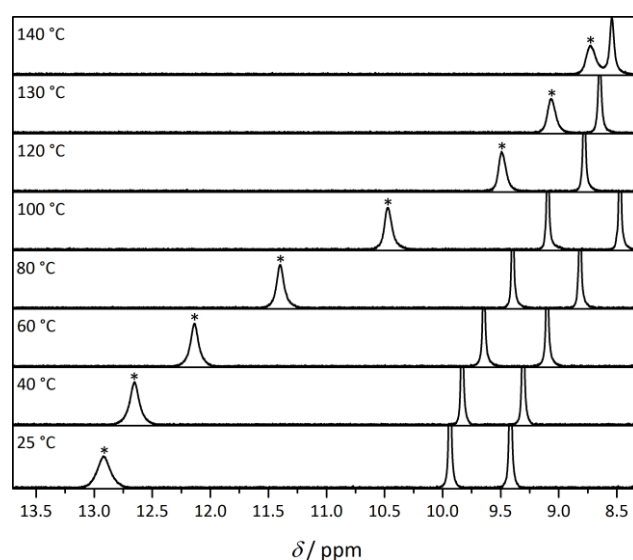


Figure 3-17 Exemplary temperature dependent ^1H NMR spectra of the CA- and HW-functional small molecule pairing (refer to Figure 3-15) in $C_2D_2Cl_4$ (6 mmol L^{-1} , each) with the association dependent shift of the CA imide proton resonance (*). Adapted with permission from Reference²⁵⁴. Copyright 2015 American Chemical Society.

The higher the observed downfield shift, the higher is the underlying degree of association and vice versa while heating of the sample leads to higher degrees of dissociation.^{32, 257} Repeated measurements allowed for the assumption of an experimental error of ± 0.01 ppm. The chemical shift values obtained via these measurements were then plotted vs. the respective measurement temperature (Figure 3-18), demonstrating the differences in imide proton resonances for hydrogen bonding motifs with chain substituents of different lengths and masses. Evidently, these qualitative measurements visualize a dependence of the association equilibrium on the respective chain substituent.

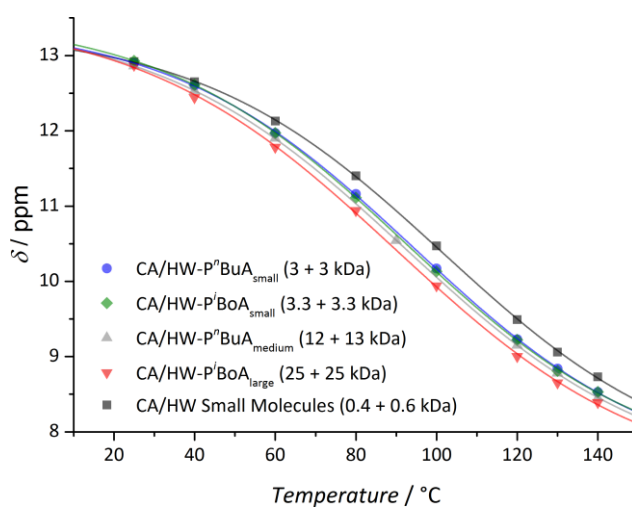


Figure 3-18 Temperature dependent chemical shift values of the CA imide proton resonance for CA and HW functional building block pairings of different lengths and masses in $C_2D_2Cl_4$. Adapted with permission from Reference²⁵⁴. Copyright 2015 American Chemical Society.

In accordance with the previously discussed findings for dynamic covalent species (Section 3.2), longer chains or higher chain masses presumably result in an increased degree of dissociation due to their increased translational and rotational entropic values and thus in a decreased downfield shift of the imide resonance in question.¹⁴² To exclude other possible causes for the observed phenomena, e.g., dissimilar polarities or solubilities of the different investigated species leading to potentially altered self-aggregation characteristics, and to quantify the observed differences in association, the dissociation constants K_{diss} were evaluated for all diblock pairings via NMR titration experiments (refer to the Experimental Section for details) of different ratios of Hamilton wedge to cyanuric acid end-groups from 0 to 3 at a fixed concentration of the CA end-group functional species of 2 mmol L^{-1} .²⁵⁸ Due to unfavourable exchange rates at ambient temperature which lead to an insufficient signal resolution, while at $140 \text{ }^\circ\text{C}$ the imide proton resonance was

overlapping with other signals for some end-group ratios, a temperature of 100 °C was chosen to bypass problems of signal isolation. The obtained dissociation constants were plotted against the averaged molar mass $M_{n,avg.}$ of ligated species (Figure 3-19), demonstrating a clear correlation of molecular mass of associated building blocks and their degree of dissociation at a given temperature. Before an off-levelling of the entropic effect can be observed for block masses above approximately 13 kDa, the determined K_{diss} values double from small molecular adduct ($1.78 \cdot 10^5$) to large polymeric systems ($3.71 \cdot 10^5$).

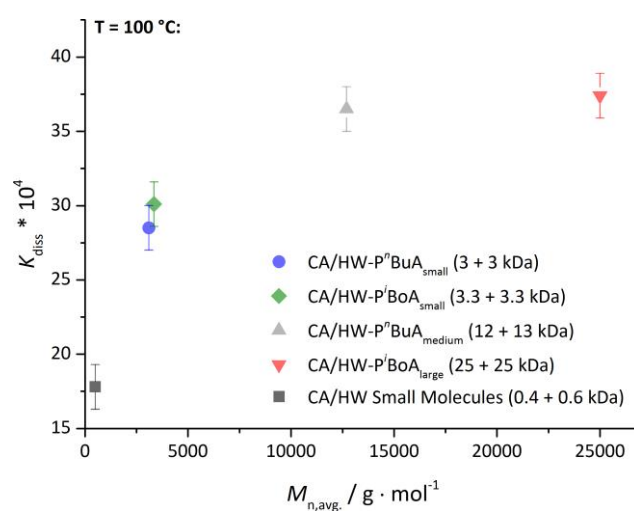


Figure 3-19 Dissociation constant values K_{diss} at 100 °C of differently sized CA and HW functional building block pairings, associated *via* hydrogen bonding in $C_2D_2Cl_4$. Adapted with permission from Reference²⁵⁴. Copyright 2015 American Chemical Society.

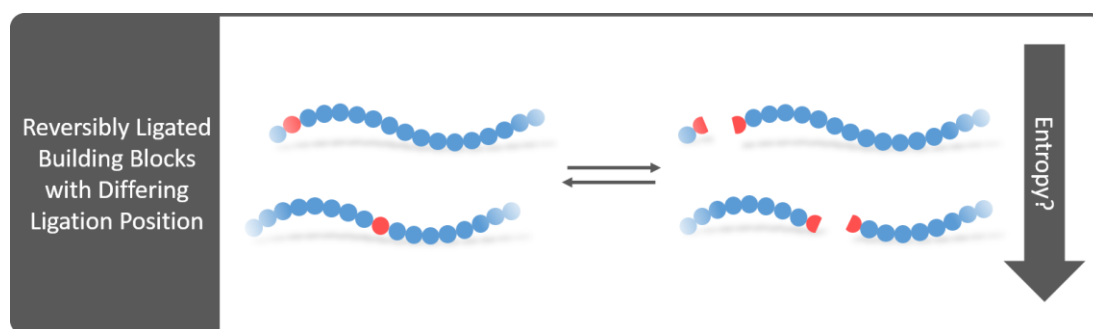
3.4.3 Summary

Following the establishment of an entropic mass and chain-length effect on dynamic covalent ligation, the principle was transferred to a system associated via supramolecular hydrogen bonding. Particularly for elevated temperatures, these findings highlight the necessity to not only consider data obtained for small molecules when employing similar recognition units in large, e.g., macromolecular and thus entropically altered systems, but also physical parameters such as chain-length or -weight of the desired target system. A coherence between such parameters, which clearly have an influence on the entropic contributions of a molecule, and the degree of association is evidenced with a doubling of dissociation constants for small molecular vs. macromolecular associates. As a result, it is highly likely that differences in the dissociation constants and thus the temperature dependent degree of association are connected to similar entropic causes as demonstrated

for covalently bonded systems, validating the general applicability of entropic effects on diverse – covalent as well as non-covalent – ligation methods.

3.5 Effect of the Ligation Position on Reactions

Finally, the previously explored effects of physical molecular parameters on the reaction entropy and thus reaction or association equilibria posed the question if also the position of a ligation site or scission of a chemical bond inside a molecule may affect the reversible formation or cleavage of adducts (Scheme 3-10).[§] The supposedly grave differences in entropy for a cleavage of a molecule in the middle vs. a cleavage of a terminal section provided for a promising initial position for further computational as well as experimental studies of mathematical models, covalent and supramolecular adducts. Thereby, not only deeper insights into the specificity of reversible bonding processes, but also into degradation mechanisms should be generated.

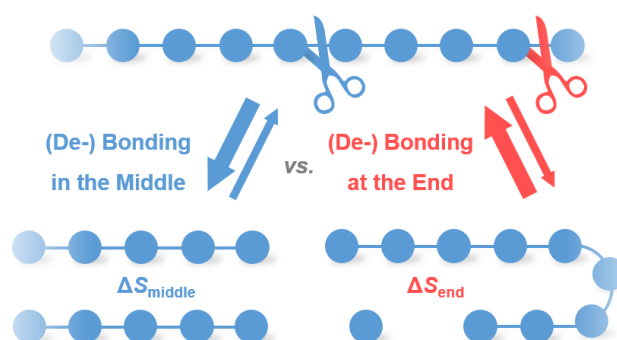


Scheme 3-10 Reversibly ligated building blocks with differing ligation positions inside a molecule.

3.5.1 Experimental Design

As foreshadowed previously, the studies of entropic chain length and mass effects as well as general knowledge led to the assumption of different bonding characteristics at different positions inside a molecule. To test this hypothesis, the two extremes – a ligation position at the end vs. one in the middle of a molecule – should undergo computational as well as experimental assessment. Thus, a series of theoretical as well as chemical experiments investigating these specific linkage or chain scission positions (Scheme 3-11) was considered.

[§] Parts of the current section are reproduced or adapted from K. Pahnke, J. Brandt, G. Gryn'ova, C. Y. Lin, O. Altintas, F. G. Schmidt, A. Lederer, M. L. Coote, C. Barner-Kowollik, *Angew. Chem.* **2016**, *128*, 1537-1541, with permission from Wiley-VCH. Josef Brandt carried out the TD SEC measurements. G. Gryn'ova and C. Y. Lin conducted the quantum chemical calculations. O. Altintas synthesized the RAFT agents. F. G. Schmidt and A. Lederer helped with discussions. C. Barner-Kowollik and M. L. Coote motivated and supervised this project as well as contributed to the scientific discussions.



Scheme 3-11 Schematic view of the theoretical and experimental setup to determine characteristic differences between bond cleavage (a) in the middle and (b) at the end of a molecule. Adapted with permission from Reference²⁵⁹. © 2016 WILEY-VCH Verlag GmbH & Co. KGaA, Weinheim.

Although naturally a plethora of other positions inside a molecule are possible, by focusing on the two extremes, the most significantly different positions are covered. To begin with, a simplified mathematical model of chemical cleavage of chains was employed for first insights into and to isolate the entropic causes of a position dependent cleavage of chains. In the experiments, supramolecular diblock adducts with their reversible association site located either in the middle or at the end of a chain molecule of similar length were compared. Finally, covalent step-growth adducts were analyzed via TD SEC to investigate, if small-molecular, terminal linker molecules are cleaved-off as readily as the macromolecular adducts they are connecting.

3.5.2 Computational Studies

In an attempt to theoretically verify the hypothesis of differing entropic bonding attributes at different positions inside a (macro-)molecule, a universally applicable mathematical model of bonding chemistries was examined by our cooperation partners at the Australian National University (Canberra). Polymers were modeled as linear chains of point masses of arbitrarily chosen, but realistic proportions. Via standard textbook equations, a determination of translational (ΔS_{trans}) and rotational (ΔS_{rot}) measures of the entropy released upon chain cleavage was conducted (Table 3-4), with additional calculations of increased weight or length based on the initial arbitrary system for further information on the impact of physical molecular parameters and their alteration on the association or binding characteristics. For full details on the employed mathematical model, refer to the original publication.²⁵⁹

Table 3-4 Values for the translational and rotational entropy^a for de-bonding of simple geometric models determined via statistical thermodynamics methods.

Cleavage in/at the middle:		... end:	
	ΔS_{trans}	ΔS_{rot}	ΔS_{trans}	ΔS_{rot}
initial	148.9	82.4	136.1	-2.6
longer	148.9	87.6	136.1	-0.7
heavier	157.5	99.3	137.4	-0.3

^a ΔS in J mol⁻¹ K⁻¹ at 298 K.

Although simplified, the model should allow for qualitative insights into the occurrence of entropy-caused effects leading to a general preference or discrimination of molecular cleavage at specific positions and at the same time enable the investigation of significantly larger systems in comparison to the very complex and time consuming calculation of actual chemical structures, especially for computationally non-feasible polymer dimensions. The employed method disregards enthalpic contributions as well as vibrational entropy – two factors mainly controlled by the local chemistry of the utilized reactive groups, but quite unaffected by chain-length and thus negligible in the current study – to allow for the isolation of the chain-length dependent causes in question without further complexation of computation and interpretation of the obtained data.¹⁴² Clearly, the data displayed in Table 3-4 leads to the assumption of an entropically favored – i.e., increased positive values for ΔS – chain cleavage in the middle vs. at the end of a chain molecule, as both translational as well as rotational entropy are significantly larger for the central cleavage position. An additional conclusion provided by the computational data is an increased specificity of the observed preference of a chain cleavage in the middle of molecules with increasing weight or length of the analyzed chain species, leading to more distinctive and presumably more slowly converging chain length or mass effects observable for mid-chain cleavage. These promising theoretical results represent a substantial basis for further experimental work and enable a more facile tracing of the underlying entropic causes of macroscopic effects.

3.5.3 NMR Titration of Hydrogen-Bonding Specimen

In a next step, the theoretical findings should be transferred to and verified via actual chemical systems to provide for a confirmation of the simplified model calculations.

Moreover, experimental work should allow for not only qualitative trends, but also a quantification of observable effects. A promising method to gain more insights into position-dependent bonding characteristics is the investigation of differently sized diblock polymer building blocks, e.g., associated via hydrogen bonding. As demonstrated in Section 3.4.2, temperature dependent ^1H NMR measurements can be utilized for both qualitative visualization of the association of specific hydrogen bonding pairings as well as the quantitative determination of association or dissociation constants via titration experiments and thus provide for a suitable characterization technique in this context. Analogous to the specimen in Section 3.3, associates assembled from cyanuric acid or Hamilton wedge functional polymers, synthesized via reversible addition-fragmentation chain transfer (RAFT) polymerization (refer to Section 2.1.5), were also used for the present study.

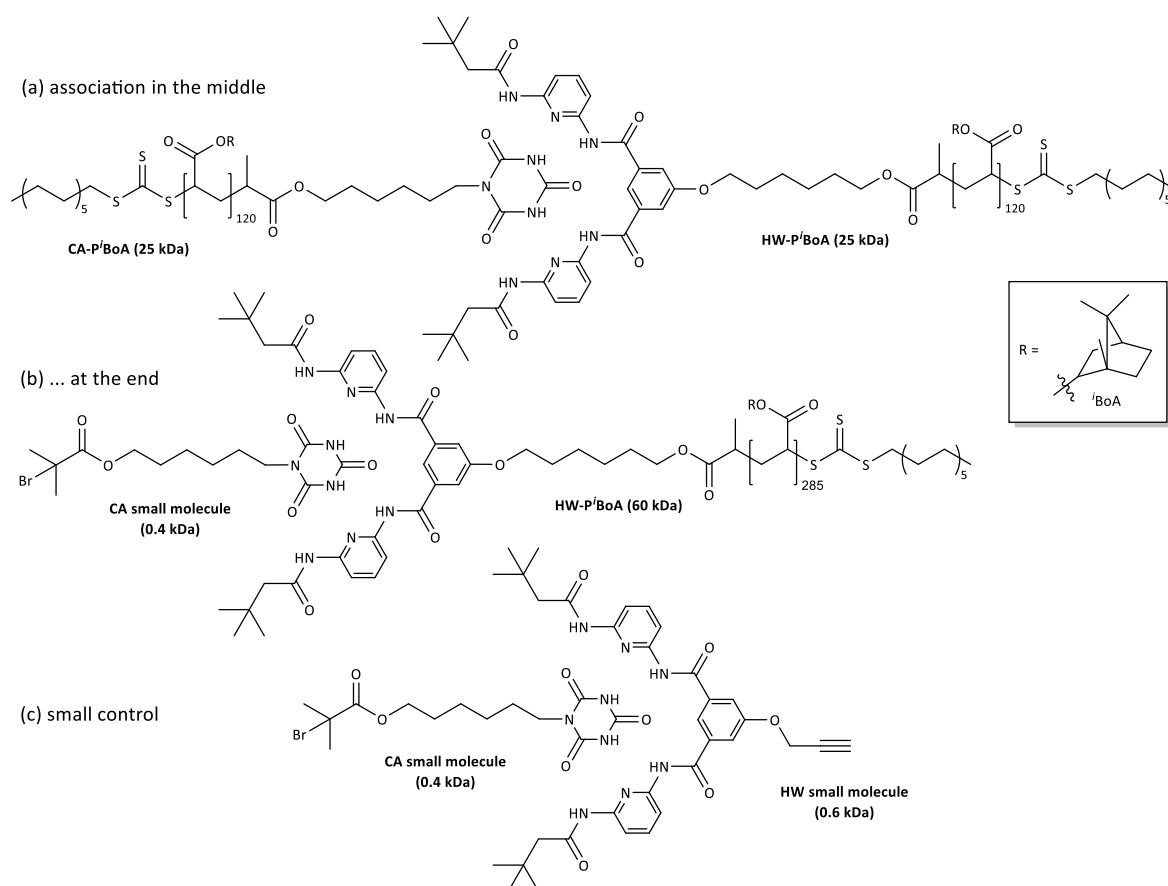


Figure 3-20 The supramolecular building block pairings with (a) poly(isobornyl acrylate) moieties of $M_{n,SEC/NMR} = 25$ kDa on both sides of the ligation site, (b) one small molecular CA unit in combination with a HW functional poly(isobornyl acrylate) of $M_{NMR} = 60$ kDa and (c) the small molecular control test. Adapted with permission from Reference²⁵⁹. © 2016 WILEY-VCH Verlag GmbH & Co. KGaA, Weinheim.

Two supramolecular diblocks of similar molar concentration and total length – one assembled from two blocks of the same size to model association in the middle (Figure 3-20 (a)), the other comprising one large chain of essentially the envisaged total length plus an associated small molecular binding motif (Figure 3-20 (b)) – were compared to the association characteristics of a small molecular sample of similar recognition units (Figure 3-20 (c)). The samples were self-assembled in tetrachloroethane- d_2 ($C_2D_2Cl_4$, $c = 6 \text{ mmol L}^{-1}$), an aprotic and good solvent for polyacrylates allowing for the observation of hydrogen bonding between the employed specific binding motifs.^{32, 73} As stated above in Section 3.4.2, unwanted intra- and intermolecular interactions were excluded via an aliphatic spacer between binding motif and polymer backbone as well as measurements of CA and HW species with and without non-functional polyacrylate samples.^{254, 256} Again, the 1H NMR resonance of the CA imide proton can be utilized to visualize the temperature dependent degree of association – a higher downfield shift being linked to increased degrees of association – of the specimen with differing ligation positions in HT NMR experiments (Figure 3-21).^{32, 254, 257}

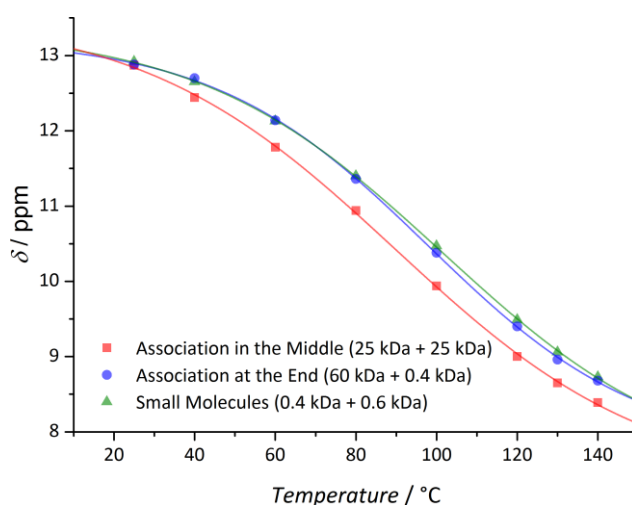


Figure 3-21 Temperature dependent CA imide proton resonance in $C_2D_2Cl_4$ for building blocks associated via CA and HW recognition units in the middle (■) or at the end (●) of macromolecules as well as for small molecular adducts (▲), indicating higher degrees of association for higher downfield shift values. Adapted with permission from Reference²⁵⁹. © 2016 WILEY-VCH Verlag GmbH & Co. KGaA, Weinheim.

As theoretically predicted, the qualitative evaluation of the respective degrees of association via Figure 3-21 underpins the occurrence of a preferred cleavage of – here supramolecular – adducts in the middle rather than at the end of a chain molecule, indicating a comparably unfavorable dissociation of terminal association sites as in small

molecules. Similar NMR titration experiments as seen in Section 3.4.2 – also conducted at 100 °C for reasons of signal isolation – yielded quantitative dissociation constants K_{diss} , confirming the previously obtained theoretical and qualitative experimental trends: It was shown that – under the employed conditions – dissociation in the middle ($K_{\text{diss,middle}} = (3.7 \pm 0.15) \cdot 10^{-3}$) is two times more favorable than dissociation of small molecules at terminal ligation sites ($K_{\text{diss,end}} = (1.9 \pm 0.15) \cdot 10^{-3}$), the latter thus being as (un-)favorable as the dissociation of small molecular samples ($K_{\text{diss,small}} = (1.8 \pm 0.15) \cdot 10^{-3}$, refer to Section 3.4.2). As a result, the impact of the ligation position and the hereby resulting entropic differences were demonstrated for supramolecular association. At the same time, the computationally estimated greater effect of physical molecular properties on cleavage events in the center of a macromolecule (refer to Section 3.5.2) was fortified, as – in spite of the highly extended dimensions of the employed polymers – a possibly occurring mass effect with supposedly higher degrees of dissociation for heavier cleavage products as present for the system seen in Figure 3-20 (b) could not counteract the effect of the association position and thus increased dissociation of central binding motifs.

3.5.4 Temperature Dependent SEC of Covalently Bonded Materials

Lastly, temperature dependent SEC measurements allowed for insights into the position dependent cleavage of reversible covalent adducts. Similar step-growth polymers from a cyanodithioester dilinker and Cp α,ω -functional macromolecular building blocks as employed in previous studies (refer to Section 3.2 and 3.3) – for this study comprising poly(methyl acrylate) (PMA), poly(isobornyl acrylate) (PⁱBoA) as well as polystyrene (PS) backbones – underwent TD SEC measurements to reveal the degree of depolymerization vs. the degree of released small molecular CDTE linker species. In doing so, the statistical or non-statistical nature of the debonding of building blocks and linker molecules should be investigated. The thermoreversibly connected step-growth polymers formed from different macromolecular building blocks underwent TD SEC measurements at 90 °C after different heating intervals to guarantee a good equilibration of the temperature dependent DA reaction. During an initial measurement of the exemplary PMA system, as anticipated, a fairly broad mass distribution is observed (Figure 3-22 (a)), but the inseting retro reaction is evidenced via the loss of high molecular weight material (compare Figure 3-4 (c) for an initial chromatogram of the starting material, measured in THF at 35 °C).

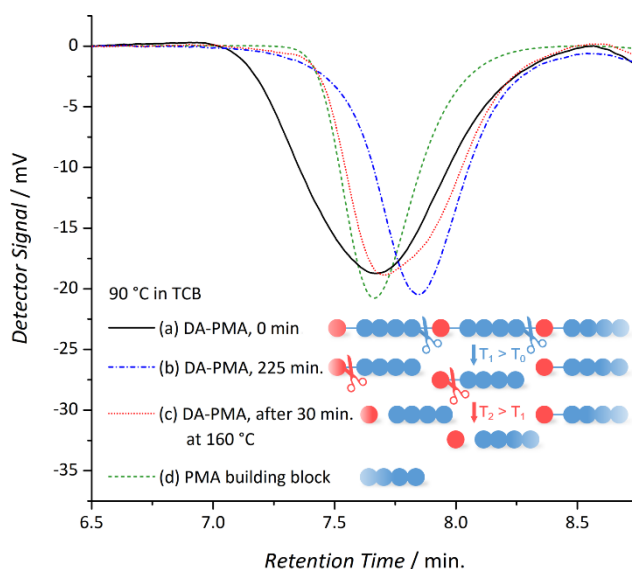


Figure 3-22 TD SEC chromatogram of a thermoreversible DA-PMA at 90 °C and 160 °C and its corresponding building block in 1,3,5-trichlorobenzene (TCB) as well as a schematic view of the degradation process of such DA step-growth polymers, consisting of macromonomers (blue) and a small molecular dilinker (red), at increasing temperatures, here T_0 = ambient temperature, T_1 = 90 °C, T_2 = 160 °C. Adapted with permission from Reference²⁵⁹. © 2016 WILEY-VCH Verlag GmbH & Co. KGaA, Weinheim.

It has to be noted that the TD SEC setup has a limited resolution in comparison to standard SEC devices due to a smaller number of chromatography columns, nevertheless the trends of cleavage processes can clearly be observed. To allow for the highest achievable degree of debonding for the employed temperature, the next measurement was conducted after 225 min. (Figure 3-22 (b)), illustrating the expected shift to higher elution times and thus lower molecular weights as well as a more narrow distribution as a consequence of the rDA reaction and therefore chain cleavage of the step-growth adduct taking place. Naturally, as a thermal degradation of the employed polymers in solution was excluded via additional measurements of the isolated polymer block species at the respective temperatures, the lowest feasible weight of released macromolecules in such a cleavage process should match the one of the incorporated building blocks and thus their initial chromatogram (Figure 3-22 (d)). Yet, the obtained chromatogram after prolonged heating times at 90 °C shows a distinctive shift of the chromatogram to unreasonably high elution times and thus lower molecular weights as should be possible in the retro DA cleavage process. A possible cause for such behavior in liquid chromatography is an enthalpic interaction of a polar analyte with the column material, resulting in a prolonged retention of the examined molecule and thus leading to the assumption of a lower molecular weight. Due to the highly polar groups of the employed CDTE linker, the observed behavior can be ascribed to

polymer building blocks which are still ligated to one or two linker molecules, leading to an altered retention despite their weight being quite similar to non-ligated polymer blocks. Accordingly, further heating of such specimen to higher temperatures should lead to a more distinctive cleavage of the terminal linker species and thus a shift of the signal of released, non-ligated polymer blocks to resemble its primordial chromatogram without polar linker content. Actually, upon heating the very same sample to 160 °C for 30 min. and then immediately measuring it at 90 °C to achieve similar conditions (Figure 3-22 (c)), the anticipated signal shift back to lower elution volumes can be detected, indicating the cleavage of polar linker molecules and the merging of released block with the initial building block weight distribution signal. In doing so, the enthalpic interactions of the polar CDTE linker was intentionally harnessed to investigate the cleavage behavior of ligation sites, supporting the hypothesis of a less favorable cleavage of terminal small molecules, as their scission can only be observed upon drastically elevated temperatures, while the central bonding positions between macromolecules cleave at significantly lower temperatures. Similar observations were made for an analogous system comprising PS building blocks (refer to the original publication²⁵⁹ for details).

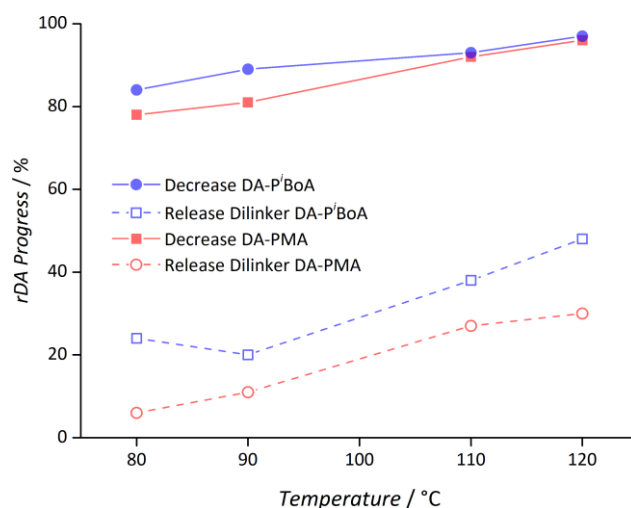


Figure 3-23 Temperature dependent decrease of DA-P'BoA or DA-PMA in comparison with the release of the DA dilinker. Adapted with permission from Reference²⁵⁹. © 2016 WILEY-VCH Verlag GmbH & Co. KGaA, Weinheim.

Further experiments with the DA-P'BoA or DA-PMA step-growth adducts formed from the larger building blocks as stated in Section 3.2.3 and 3.2.4 (refer to Figure 3-4 (c) and (d) for initial SEC chromatograms at 35 °C in THF), now employing modified solvent mixtures (60 % TCB with 40 % dimethylformamide (DMF)) to circumvent solvent signal overlap and

suppress the observed enthalpic interactions of polar CDTE molecules with the column material, allowed for the isolation and thus quantitative measurement of the temperature dependent degrees of released linker vs. polymer signals (Figure 3-23, refer to the original publication²⁵⁹ for details). The overall increased degree of depolymerization for the PⁱBoA sample in comparison with the PMA specimen, the latter being synthesized from building blocks with lower molecular weight, can again be ascribed to a mass effect as discussed in Section 3.2. But more importantly, no pure statistical chain scission with a proportional release of CDTE linker and degree of depolymerization is proceeding for both samples: After a rapid depolymerization of the step-growth adduct into pieces of approximately the size of the employed macromolecular building blocks, considerably elevated temperatures are necessary to cleave off significant fractions of the linker, again proving the disfavored cleavage of terminally bound small molecules.

3.5.5 Summary

In conclusion, after the establishment of entropic mass, chain-length and -stiffness effects in the previous sections, also a favored debonding or dissociation of covalently or supramolecularly connected molecules in the middle vs. at terminal ligation sites was demonstrated. The reported behavior could again be ascribed to entropic causes via computational calculations and experimentally assessed for hydrogen bonded diblock polymers as well as covalent Diels–Alder step-growth adducts. Such a position-dependent effect can not only be utilized to alter reaction or association equilibria and explain dissimilar binding attributes of similar ligation sites at different positions within a molecule, but could also lead to drastic consequences regarding all reactions which include macromolecules. As the observed effects arise due to the physical molecular attributes of the employed chains – and not due to the chemical parameters of the ligation site – they are not exclusive to self-healing or other dynamic materials, but are a universal principle of bonding. As such, moreover, these chain effects on equilibria do not have to be limited to diffusion controlled reactions, thus also have a likely impact on chemically-controlled bimolecular reactions of macromolecules. Consequently, a position dependence of reactivity in terms of bonding or debonding should also have an impact on, for example, the degradation of polymers, a control agent addition during controlled radical polymerizations or chain transfer events between smaller or larger (chain) species. In fact,

polymer degradation via shearing or, more specifically, ultrasonication is known to result in favored mid-chain cleavage.^{260, 261} On the other hand, thermal or oxidative degradation of polymers is more prone to various side reactions, e.g, via the diverse possibilities of radical formation in such a process, leading to, for example, an exceeding impact of terminal unsaturated initiation sites in comparison to an entropically favored homolysis in the middle of a chain, rendering an isolation of reaction channels challenging.²⁶² Thus, only the impact of molecular mass with an accelerated degradation of longer polymer chains was known from literature until now.^{223, 263, 264} Continuing with the example of controlled radical polymerizations such as RAFT processes, a lower reactivity of macromolecular control agents proportional to the conversion and thus chain length of the propagating polymer chain in comparison to their small molecular analogues is suggested by the outcomes of the present section. In other words, the addition of a growing radical polymer species to a RAFT agent attached to a polymer chain should be thermodynamically as well as kinetically disfavored in comparison to otherwise chemically similar small molecules. Consequently, the discussed entropic effects could lead to a better understanding and explanation of inconsistencies when transferring measured or calculated thermodynamic or kinetic properties from small molecules to macromolecular systems.^{98, 265, 266}

3.6 Conclusions

In the preceding chapter, diverse previously unforeseen entropic effects of physical molecular parameters such as chain length and mass or stiffness as well as the ligation position within a molecule on dynamic chemistries were demonstrated and investigated in experiment and via quantum chemical calculations. The principle of a mass effect on macromolecular ligation leading to a more favored chain scission of heavier and longer chains due to entropic causes such as increased translational and rotational terms of entropy – hardly investigated in previous works – was expanded and transferred to more diverse covalent as well as supramolecular and thus more universal association methods, corroborating the versatility and general applicability of the observed effects. In addition, the – until now unexpected – impact of chain stiffness or intramolecular mobility on cleavage events was assessed via thermoreversibly linked isomeric polymer systems of similar weight – excluding any overlapping effect of molecular mass – but differing steric properties of the side-chain substituents and hence chain flexibility. In the course of these studies, a stiffness effect on reversible bonding sites due to the differences in rotational and vibrational entropy was established, with more stiff chains being less easily cleaved due to their more pronounced restrictions in terms of entropy. That is to say, in other words, that lower retro reaction temperatures can be observed for more mobile adducts as a result of their less decreased degrees of freedom upon chain scission events. Finally, the explored principles were further combined to look into the question of a possibly altered bonding behavior in the middle vs. at the end of a chain molecule due to the established differences in entropy. In fact, for block systems of similar total size, but differently positioned reversible ligation sites either in the middle or at terminal binding spots, a significantly altered bonding character was observed with debonding being strongly favored in the middle of a chain molecule in comparison to terminal bonding sites. Again, such an outcome was verified for both covalent and supramolecular association mechanisms and the underlying entropic causes were identified via a computational model of chain scission. All mentioned effects are presumed to have a substantial impact on dynamic bonding in numerous applications such as, for example, self-healing or stimuli responsive materials, re-shapeable organic sheets or thermoreversible networks, the mimicking of proteins via supramolecular folding of synthetic polymer chains or, in general,

the transfer of small molecular chemistries to macromolecular or otherwise extended and thus entropically very different systems. Accordingly, bond attributes can not only be chemically altered, but also entropy can be harnessed for a more universal tuning of parameters without the need to change the actual binding motifs. In addition, these newly described effects can also be consulted to generate a better understanding of ligation chemistry and explain differences in reported bonding characteristics of similar ligation sites in altered molecular environments or when comparing experiments or computationally assessed predictions of isolated small molecular sections of macromolecules with experimental results of the actual extended chain systems.

4

EXCURSION: DITHIOOXALATES AS THERMOREVERSIBLE LINKERS

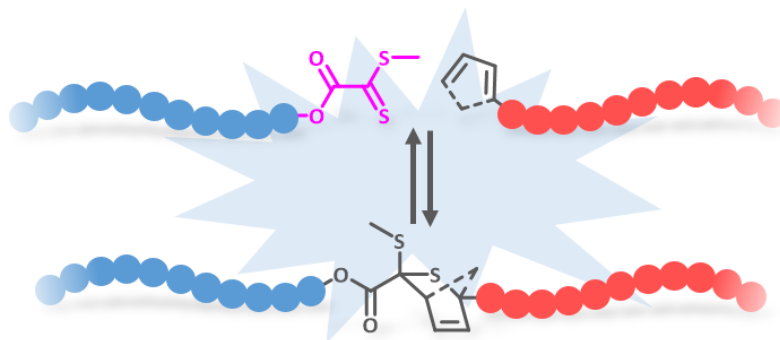
4.1 Motivation

While the preceding chapter of the present thesis pointed out the influence and versatility of entropic effects on reaction or association equilibria of established ligation pairings, the current chapter addresses the enthalpic part of a dynamic reaction via establishing a novel, efficient and thermoreversible Diels–Alder dienophile dilinker.** Although the previously explored entropic effects allow for a significant adjustment of the (de-)bonding parameters of assembly equilibria, the necessary substitution of macromolecular backbones or their

** Parts of the current chapter are adapted or reproduced from K. Pahnke, N. L. Haworth, J. Brandt, U. Paulmann, C. Richter, F. G. Schmidt, A. Lederer, M. L. Coote, C. Barner-Kowollik, *Polym. Chem.* **2016**, *7*, 3244-3250 with permission from The Royal Society of Chemistry. N. L. Haworth carried out the quantum chemical calculations. J. Brandt conducted the TD SEC measurements. U. Paulmann and C. Richter synthesized the MTTA dilinker. F. G. Schmidt and A. Lederer helped with discussions. C. Barner-Kowollik and M. L. Coote supervised this project and contributed to the scientific discussions.

side-chains might not always be feasible. Moreover, different reactive groups may have different advantages or restrictions as for example differing kinetics, the need for a protecting group or catalyst and more or less suitable debonding temperatures for small molecular ligation. In general, dynamic linkers can be characterized via key features, e.g., their capability to undergo a (retro) reaction with specific reaction rates, and the bond strengths of the formed adducts. Based on the plentiful possibilities to form dynamically switchable adducts via covalent or supramolecular association of building blocks, due to its efficiency and flexibility in many cases, the Diels–Alder [4+2] cycloaddition (also refer to Section 2.2.1) of dienes with dienophiles is one of the most renown and employed possibilities to generate self-healing or other thermoreversibly ligated materials as for instance organic sheets, re-codeable surfaces or self-reporting debonding on-demand adhesives.^{22, 27, 135, 267} The presently available Diels–Alder systems allow for a manifold of bonding conditions, yet still there are individual limitations to their applicability in academic or industrial processes. For example, while the reaction of furan dienes with maleimide dienophiles is very popular due to the facile integration of such functional groups in chemical systems and their readily occurring addition, with long forward and retro reaction times and rather high retro reaction temperatures it also possesses limitations. Accordingly, numerous efforts have been undertaken to discover, explore and generate more convenient reaction conditions, including the aforementioned entropic effects, supporting hybrid networks and – importantly – hetero Diels–Alder (HDA) reactions.^{5, 83, 120, 142, 145, 206, 259} The latter allow for adjusted HOMO-LUMO interactions which can enable straightforward reactions under ambient conditions, but may require a catalyst or lead to side reactions. As an example, many thiocarbonyls, available, e.g., after RAFT polymerizations as an end-group, or nitrosocarbonyls readily undergo cycloaddition with diverse dienes, but require elevated temperatures or alternatively a catalyst to allow for ambient reaction conditions.^{50, 126, 130, 145} There also exist dienophiles with even higher reactivity as for instance cyanodithioesters, thus enabling a catalyst-free reaction, but the reactivity comes at a price: To prevent dimerization and other degradation reactions of the reactant, it has to be handled in a trapped state where the dienophile is protected by the addition of a cleavable diene, e.g., cyclopentadiene.^{22, 132} Such an approach not only results in lower atom- and cost-efficiency, but it also requires elevated temperatures for an *in situ* re-activation of the dienophile, thus potentially supporting unwanted degradation

mechanisms of the reactants. As a result, possible Diels–Alder pairings and their reaction conditions undergo a constant process of optimization. With all the advantages and disadvantages mentioned above in mind, literature-known dithiooxalates seem to be promising with respect to their applicability in mild, straightforward, efficient as well as catalyst-free cycloadditions with diverse diene species (Scheme 4-1).

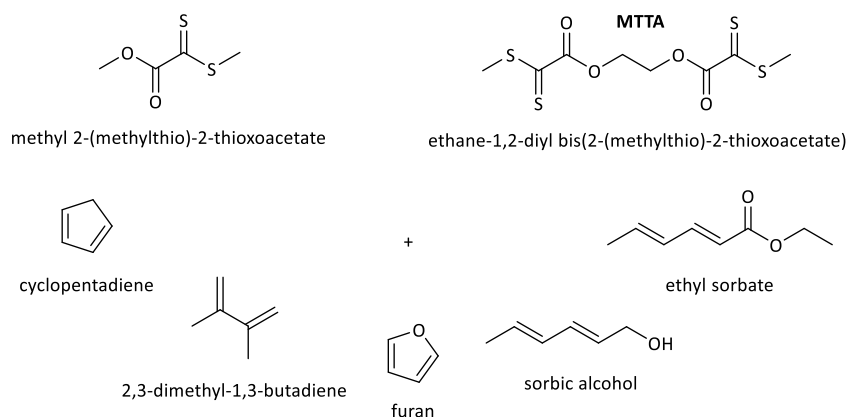


Scheme 4-1 General approach of the thermoreversible ligation of diene-functional (macro-) molecules via dithiooxalates. Adapted from Ref.¹²³ with permission from The Royal Society of Chemistry.

A limited set of previous investigations demonstrated readily and sometimes rapidly occurring small molecular reactions under ambient conditions with and without catalyst, for example in studies of stereoselective formations of heterocycles.²⁶⁸⁻²⁷¹ Nevertheless, no multifunctional linker species or studies of a potential thermoreversibility of the Diels–Alder adducts of dithiooxalates with dienes have been explored yet, so more detailed insights should be gained in the subsequent sections.

4.2 Computational Guidance

Due to the limited information available in the literature, the Gaussian 09 software package was employed by cooperation partners at the Australian National University (Canberra) to carry out *ab initio* quantum chemical calculations, determining the Gibbs free energies and the respective associated thermodynamic parameters of the forward and retro Diels–Alder (DA and rDA) reactions of a dithiooxalate monofunctional small molecular model system (methyl 2-(methylthio)-2-thioacetate) with diverse dienes (Scheme 4-2) as a guidance for the experimental selection of possible reactants and a first classification of reactivity.²²⁷ For such an investigation, common and readily available small molecular dienes were chosen: cyclopentadiene (Cp), 2,3-dimethyl-1,3-butadiene (DMBD), furan as well as the two sorbic derivatives sorbic alcohol and ethyl sorbate.



Scheme 4-2 Schematic view of the computationally investigated reaction of a small molecular model dithiooxalate with different diene species as well as the difunctional dithiooxalate.

The calculations of reactants and products in their optimized minimum energy conformation were conducted in an acetonitrile (MeCN) solvent field to represent realistic experimental conditions as employed later on in UV/Vis measurements (refer to Section 4.4). To allow for a facile comparison and classification of the results, the temperature at which the equilibrium constant corresponds to 20 % debonding (i.e., 80 % of diene species bound to a dithiooxalate) was determined, as such degrees of open reversible ligation points are known to enable self-healing behavior in dynamic materials (Table 4-1).^{27, 132}

Table 4-1 List of computationally determined temperatures for DA reaction equilibrium constants of a dithiooxalate with different diene species in MeCN corresponding to a degree of debonding of 20 %.^a

Methyl 2-(methylthio)-2-thioacetate + ...	$T_{20\% \text{ debonding, theo.}} / ^\circ\text{C}$
furan	-169
cyclopentadiene	166
ethyl sorbate	225
sorbic alcohol	240
2,3-dimethyl-1,3-butadiene	427

^a All calculations were based on a single ligation equilibrium for a small (monofunctional) model of MTTA, for a concentration of reactive groups of 0.05 M. Refer to the experimental part or the original publication for more information.¹²³

Evidently, some first assumptions can be deduced from the quantum chemical calculations. First of all, a reaction of furan with a dithiooxalate species seems to be thermodynamically very unlikely at ambient temperature, whereas all other investigated pairings should allow

for a straightforward product formation of a Diels–Alder adduct between dithiooxalate dienophile and the respective diene. Moreover, a thermoreversible character of the cycloadducts formed from dithiooxalates and Cp or – at fairly more elevated temperatures – probably also the sorbic derivatives should be possible, whereas the ligation of DMBD via dithiooxalates should lead to a very stable product in regard to its theoretical retro reaction temperature. As a difunctional linking agent is envisaged in the experimental studies, the calculations of a small monofunctional dienophile species can only account for a coarse classification of relative reaction parameters. In doing so, the entropic contributions to the debonding process are highly underestimated when directly transferring these results to a larger difunctional dithiooxalate species. For such longer and heavier molecules, it should be expected to observe lower debonding temperatures than for the monofunctional model system analogue due to the stated entropic effects (see also Section 3.2). To verify this assumption and calculate realistic theoretical debonding temperatures for comparison with experimental ones, additional calculations of the two-step reaction of a full, difunctional ethane-1,2-diyl bis(2-(methylthio)-2-thioacetate) (MTTA, Scheme 4-2) dilinker with Cp or sorbic alcohol was quantum chemically assessed (Table 4-2).

Table 4-2 List of computationally determined temperatures for DA reaction equilibrium constants of full MTTA with different diene species in MeCN corresponding to a degree of debonding of 20 %.^a

MTTA + ...	$T_{20\% \text{ debonding, theo.}} / ^\circ\text{C}$
cyclopentadiene (2-step)	105
sorbic alcohol (2-step)	240

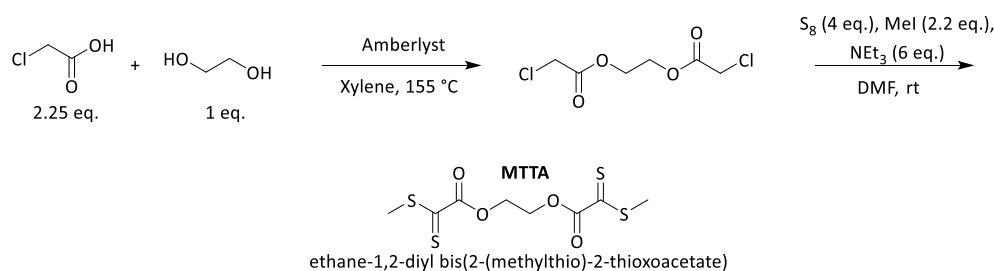
^a Concentration of reactive groups: 0.05 M. Refer to the experimental part or the original publication for more information.¹²³

As anticipated, the debonding temperature decreases for the Diels–Alder reaction of Cp with the full MTTA dilinker molecule, resulting in a temperature of 105 °C for 20 % debonding which is in very good agreement with the experimentally determined value (ca. 100 °C according to HT NMR, refer to Section 4.5.2). In contrast, the debonding temperature of sorbic alcohol is unaltered in comparison with its small molecular model system, as hydrogen bonding of both ends of the fully ligated linker compensate for the entropically more favored cleavage of heavier and longer molecules due to a stabilization of the adduct. Nevertheless, incorporating sorbic alcohol type dienes – or, in an attempt to

circumvent hydrogen bonding and besides enable a facile linkage, its esterified derivatives – in polymeric systems should again lead to an increasing influence of the entropy which is released upon product cleavage and thus decreased debonding temperatures, indicating a possible application of sorbic derivatives in thermoreversible linkage at temperatures between 150-200 °C. The computational data is provided in the experimental part, for full details on the employed procedure refer to the original publication.¹²³

4.3 Design of a Novel Diels–Alder Linker

Due to the encouraging outcomes of the computational studies, a synthesis route – later on performed by collaboration partners at Evonik Industries – of an easily accessible dithiooxalate difunctional linker was designed via adopting a literature procedure, while focusing on cheap and readily available starting materials (Scheme 4-3).^{272, 273}



Scheme 4-3 Reaction scheme of the two-step synthesis route employed for the generation of a dithiooxalate difunctional HDA dilinker. Adapted from Ref.¹²³ with permission from The Royal Society of Chemistry.

Ethylene glycol was chosen as a difunctional core molecule which can readily undergo an esterification with chloroacetic acid. The resulting chloro difunctional species can then be employed in a one-pot oxidation with elemental sulphur with a subsequent methylation via methyl iodide. A total product yield of 60-70 % deep purple, oily-solid ethane-1,2-diyl bis(2-(methylthio)-2-thioacetate) (Scheme 4-3) could be isolated in a 100 g scale synthesis, demonstrating the straightforward synthesis route. Successful product formation could be evidenced via ¹H and ¹³C NMR (Figure 4-1) as well as quadrupole mass spectrometry (ESI-MS (M+Na)⁺ C₈H₁₀O₄S₄+Na⁺ $m/z_{\text{theo}} = 320.9360$, $m/z_{\text{exp}} = 320.9370$, $\Delta m/z = 0.0010$). More information on the employed reaction conditions can be found in the experimental part (Synthetic Procedures, Section 6.3).

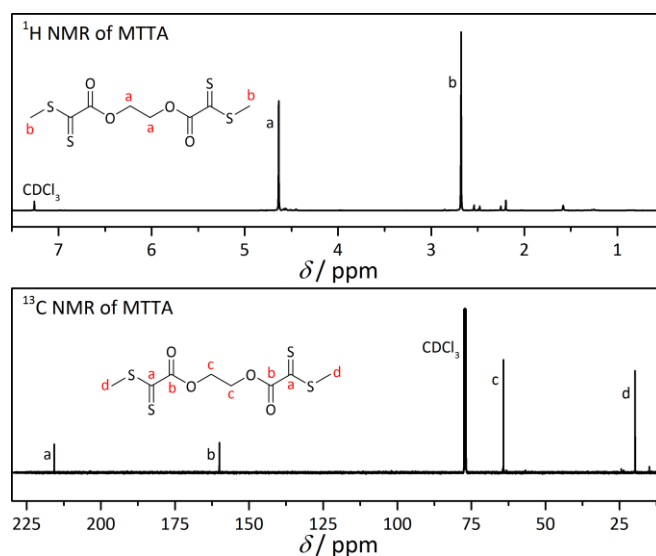
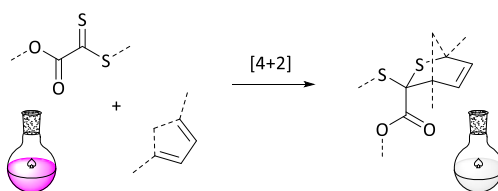


Figure 4-1 ^1H and ^{13}C NMR spectra of MTTA in CDCl_3 . Adapted from Ref.¹²³ with permission from The Royal Society of Chemistry.

4.4 UV/Vis Kinetics Studies

With its deep purple color as a consequence of the absorbance of the C=S thiocarbonyl double bond at 500 nm (Figure 4-2), the Diels–Alder reaction and conversion of MTTA in a [4+2] cycloaddition – resulting in the C=S double bond being converted to a C-S single bond and thus leading to the discoloration and a self-reporting character of the DA reaction of dithiooxalates – can easily be monitored via UV/Vis spectrometry.



Scheme 4-4 Diels–Alder reaction of a deep purple dithiooxalate species with a diene, leading to the conversion of a C=S double bond to a C-S single bond and an accompanying discoloration of the dienophile species. Adapted from Ref.¹²³ with permission from The Royal Society of Chemistry.

Such a behavior can be harnessed to gain access to more insights into the reactivity of the newly formed MTTA HDA dilinker in combination with, e.g., the theoretically assessed dienes (Section 4.2) in a facile way, enabling a quantification of reaction rates for different reactant combinations, ratios and reaction conditions.

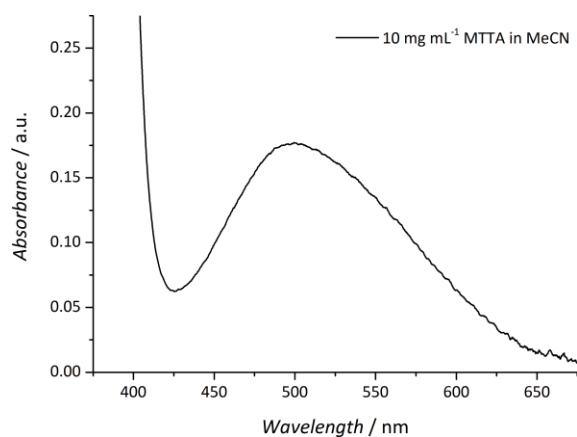


Figure 4-2 UV/Vis spectrum of the characteristic C=S double bond absorbance of MTTA (10 mg mL⁻¹, 33.5 mmol L⁻¹ in MeCN) at 500 nm. Adapted from Ref.¹²³ with permission from The Royal Society of Chemistry.

Consequently, a set of experiments with differing ratios of diene to dienophile as well as reaction temperatures was considered. In an attempt to demonstrate the efficiency of the cycloaddition at near to equimolar reaction conditions while still guaranteeing full conversion of the dithiooxalate species and thus its full discoloration, 1.2 eq. of diene species regarding dithiooxalate end-groups were employed at both ambient conditions (25 °C) or slightly elevated temperatures (50 °C). In addition, also 5 eq. of diene were employed under ambient conditions to exhibit other possibilities to accelerate the reaction via the excess of one reactant. To guarantee good comparability of the results, if possible, all UV/Vis measurements were performed with a concentration of 20 mg mL⁻¹ (67.0 mmol L⁻¹) of MTTA dilinker in MeCN as solvent due to its suitable UV/Vis characteristics as well as boiling point, allowing also for measurements at elevated temperatures. Nevertheless, test reactions were also carried out in dichloromethane to enable a more facile solvent evaporation, yielding similar results as observed for MeCN. Not surprisingly, no discoloration can be observed for a reaction mixture of furan with MTTA, confirming the theoretical calculations of a very low retro temperature for such a pairing. In contrast to furan, mixtures of MTTA with all other investigated dienes resulted in a more or less rapid discoloration and thus conversion of the reactants: as one could expect, Cp undergoes the fastest reaction with MTTA in only minutes due to its *cis*-configuration, followed by DMBD, where the methyl substituents are forcing a higher degree of *cis*-configuration than for the other open-chain dienes, sorbic alcohol and ethyl sorbate (Figure 4-3).

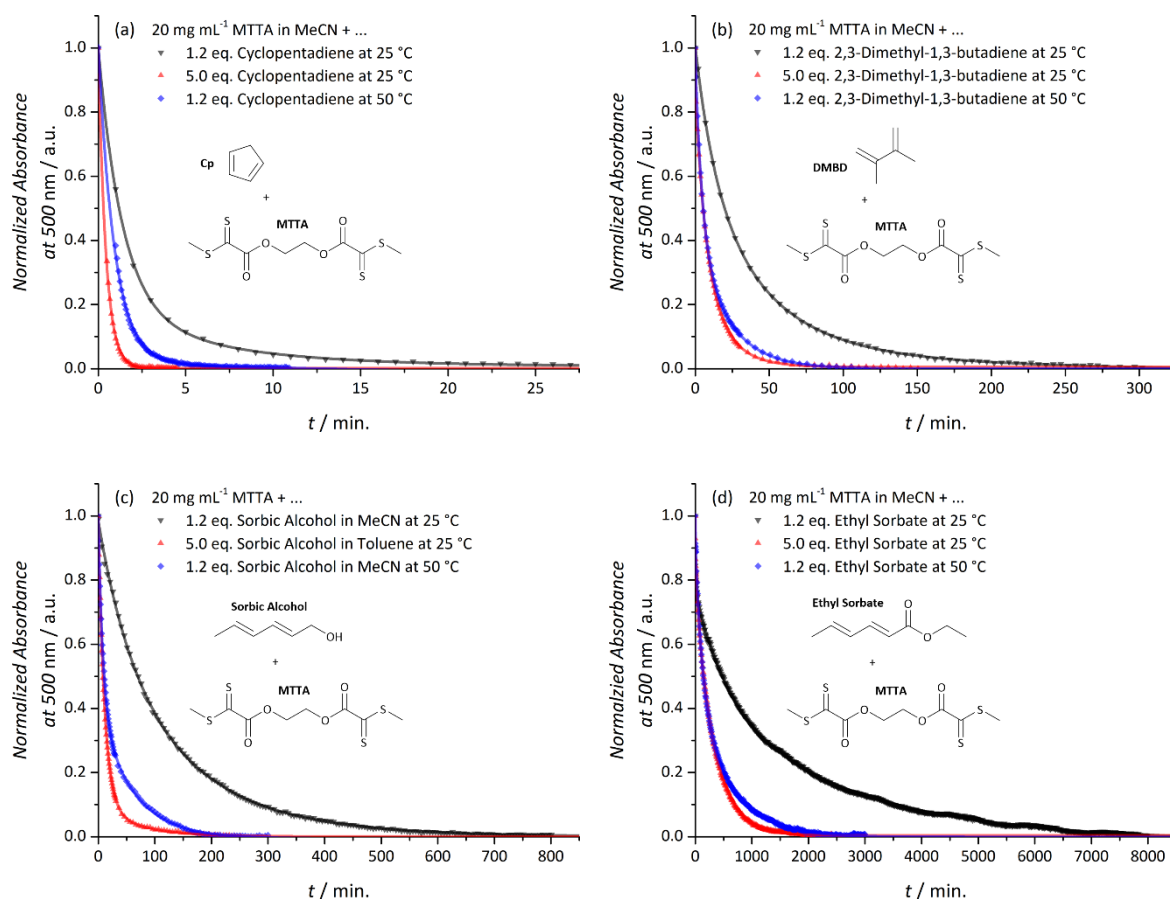


Figure 4-3 Kinetic plot of the C=S double bond absorbance at 500 nm of a reaction mixture of 20 mg mL⁻¹ (67 mmol L⁻¹) MTTA in acetonitrile or toluene and several dienes vs. time with different equivalents of diene species as well as reaction temperatures. Adapted from Ref.¹²³ with permission from The Royal Society of Chemistry.

The fast reaction kinetics – especially for Cp – emphasize the efficient and straightforward process of the investigated ligation. Therefore, the use of dithiooxalates is also promising for methods such as polymer ligation, cross-linking or step-growth processes where very great demands are made concerning efficiency while having limited purification possibilities.²²⁶ As a result of the obtained UV/Vis kinetics, a quantification of rate coefficients is readily possible by normalizing the reactant concentrations to the observed absorbance values. Via judiciously assuming a 2nd order reaction kinetic due to the negligible degree of retro reaction at the employed reaction temperatures and repeated measurements, rate coefficients with an error of approximately $\pm 15\%$ were obtained (Table 4-3).¹⁸³ A good consistency of rate coefficients determined for the same diene at different concentrations and – reasonably – an approximate doubling of reaction rates for a temperature increase of 10 K can be observed. The rate coefficients for similar reactant

ratios at different temperatures allow for the determination of an average activation energy of $52 \text{ kJ mol}^{-1} \text{ K}^{-1}$ via the Arrhenius equation.¹⁸³

Table 4-3 List of rate coefficients ($\pm 15\%$) for the DA reaction of MTTA with different equivalents of dienes in MeCN at ambient or elevated ($50\text{ }^\circ\text{C}$) temperature.

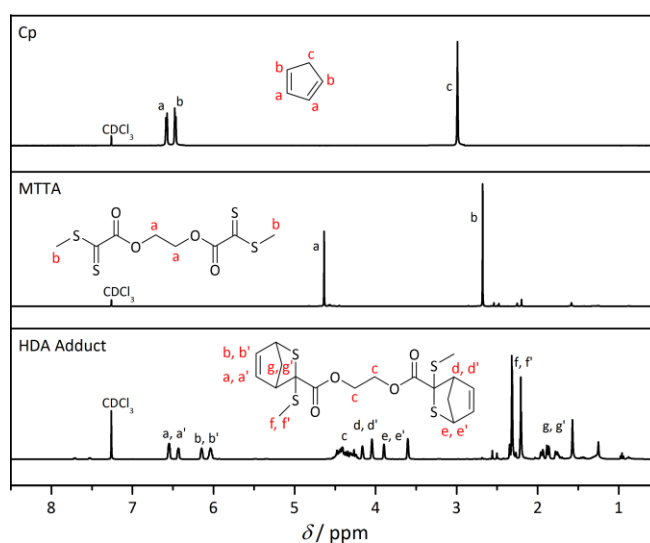
20 mg mL ⁻¹ MTTA in MeCN + ...	$k / \text{L mol}^{-1} \text{s}^{-1}$
1.2 eq. furan at $25\text{ }^\circ\text{C}$	–
1.2 eq. Cp at $25\text{ }^\circ\text{C}$	$7.1 \cdot 10^{-2}$
5.0 eq. Cp at $25\text{ }^\circ\text{C}$	$7.3 \cdot 10^{-2}$
1.2 eq. Cp at $50\text{ }^\circ\text{C}$	$3.6 \cdot 10^{-1}$
1.0 eq. Cp ₂ P ^t BuA	$4 \cdot 10^{-1}$
1.2 eq. DMBD at $25\text{ }^\circ\text{C}$	$3.4 \cdot 10^{-3}$
5.0 eq. DMBD at $25\text{ }^\circ\text{C}$	$2.5 \cdot 10^{-3}$
1.2 eq. DMBD at $50\text{ }^\circ\text{C}$	$1.8 \cdot 10^{-2}$
1.2 eq. sorbic alcohol at $25\text{ }^\circ\text{C}$	$1.7 \cdot 10^{-3}$
5.0 eq. sorbic alcohol at $25\text{ }^\circ\text{C}^*$	$1.9 \cdot 10^{-3}$
1.2 eq. sorbic alcohol at $50\text{ }^\circ\text{C}$	$8.4 \cdot 10^{-3}$
1.0 eq. IPDI-SA	$7 \cdot 10^{-3}$
1.2 eq. ethyl sorbate at $25\text{ }^\circ\text{C}$	$1.2 \cdot 10^{-4}$
5.0 eq. ethyl sorbate at $25\text{ }^\circ\text{C}$	$0.9 \cdot 10^{-4}$
1.2 eq. ethyl sorbate at $50\text{ }^\circ\text{C}$	$6.4 \cdot 10^{-4}$

*measured in toluene due to poor solubility in MeCN.

To assure the desired product formation, the solvent of the reaction mixture as well as – if volatile – the excess of diene was evaporated after completion of the UV/Vis measurements and the products were characterized without further purification via ¹H NMR (refer to Figure 4-4 for an exemplary data set, depicting spectra of reactants and product of the reaction of MTTA plus Cp) as well as quadrupole mass spectrometry (Table 4-4), clearly verifying the straightforward generation of the anticipated Diels–Alder adduct.

Table 4-4 Sum formulae and experimental as well as theoretical m/z ratios of reaction products of MTTA + diverse small molecular dienes in ESI-MS.

MTTA + ...	Sum formula	m/z_{exp}	m/z_{theo}	$\Delta m/z$
Cp	$\text{C}_{18}\text{H}_{22}\text{O}_4\text{S}_4+\text{Na}^+$	453.0315	453.0299	0.0016
DMBD	$\text{C}_{20}\text{H}_{30}\text{O}_4\text{S}_4+\text{Na}^+$	485.0941	485.0925	0.0016
sorbic alcohol	$\text{C}_{20}\text{H}_{30}\text{O}_6\text{S}_4+\text{Na}^+$	517.0843	517.0823	0.0020
ethyl sorbate	$\text{C}_{24}\text{H}_{34}\text{O}_8\text{S}_4+\text{Na}^+$	601.1062	601.1034	0.0028

**Figure 4-4** ^1H NMR spectra of (top) Cp, (middle) MTTA and (bottom) the resulting HDA adduct in a reaction of both reactants, measured in CDCl_3 . An endo/exo ratio of approximately 60:40 can be calculated via the integral ratios of signals of different stereoisomers. Adapted from Ref.¹²³ with permission from The Royal Society of Chemistry.

4.5 Transfer to Reversible Polymer Ligation

4.5.1 Step-Growth Polymerization of Difunctional Dienes

As indicated before, with its efficient characteristics in Diels–Alder reactions, dithiooxalates hold great promise for polymer ligation and related applications such as step-growth polymerization or cross-linking of macromolecules. In a first approach, to clarify if the MTTA dilinker can measure up to such expectations, it was tested in its ability to form step-growth polymers in combination with Cp α,ω -difunctional macromolecular poly(*tert*-butyl acrylate) building blocks ($\text{Cp}_2\text{P}^t\text{BuA}$, 6000 g mol^{-1} , Figure 4-5 (a)) – simultaneously mimicking linear “cross-linking” of polymer chains – or a small molecular open-chain diene difunctional isophorone bis(sorbic carbamate) (IPDI-SA, Figure 4-5 (b)).

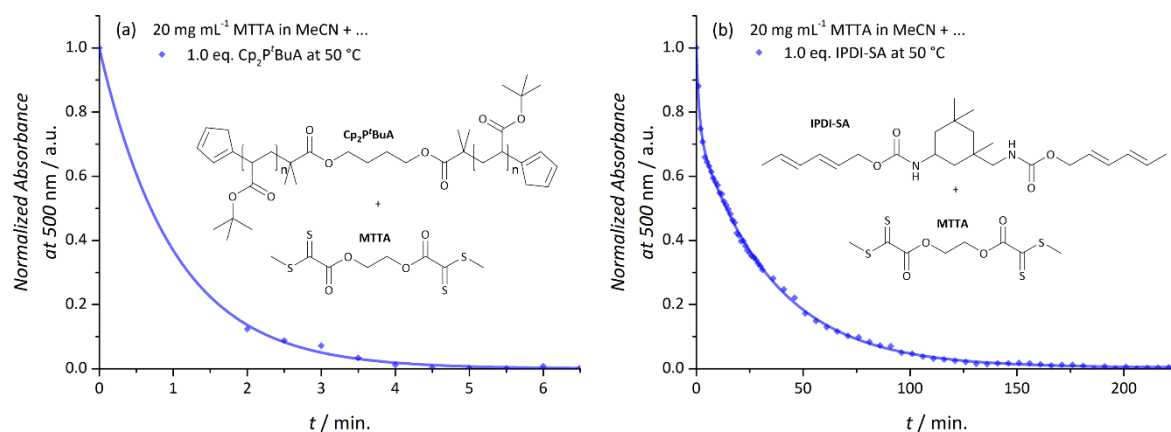


Figure 4-5 Kinetic plot of the C=S double bond absorbance at 500 nm of a reaction mixture of 20 mg mL⁻¹ MTTA in acetonitrile with equimolar amounts of (a) Cp difunctional poly(*tert*-butyl acrylate) (Cp₂P^tBuA) or (b) isophorone bis(sorbic carbamate) (IPDI-SA) at 50 °C. Adapted from Ref.¹²³ with permission from The Royal Society of Chemistry.

The reaction was again monitored via UV/Vis spectroscopy under similar conditions as tested for the small molecules (20 mg mL⁻¹ MTTA in MeCN, 50 °C), as they led to rapid product formation in ca. 5 minutes for MTTA plus Cp or 2-3 h for sorbic alcohol, but to enable a step-growth character, equimolar amounts of linker and difunctional diene were employed now. During the evaluation of the UV/Vis kinetics of – especially Cp₂P^tBuA, but also to some degree for IPDI-SA plus MTTA – the color of the (polymeric) diene difunctional building block, its time-consuming solvation process – and thus an ongoing reaction and loss of data points before starting the actual measurement – as well as the high viscosity of the reaction mixture have to be considered. As a result, increased error margins should be assumed due to a less dependable analysis. Still, the determined reaction rate coefficient of 0.4 L mol⁻¹ s⁻¹ for the Diels–Alder reactions of Cp₂P^tBuA plus MTTA or 7 · 10⁻³ L mol⁻¹ s⁻¹ for IPDI-SA plus MTTA are in accordance with the values determined for the small molecular model systems (compare Table 4-3). Subsequent characterization via SEC confirms an efficiently proceeding step-growth behavior for both systems (Figure 4-6) and thus the applicability of MTTA in polymer ligation, step-growth processes and – probably – also cross-linking of polymer species. While for the P^tBuA-system, appropriate MHKS parameters could be employed, no calibration for the IPDI-SA species is available, thus rendering the use of a calibration via polystyrene standards most probably inadequate. Nevertheless, the step-growth behavior of both samples can readily be visualized by SEC measurements.

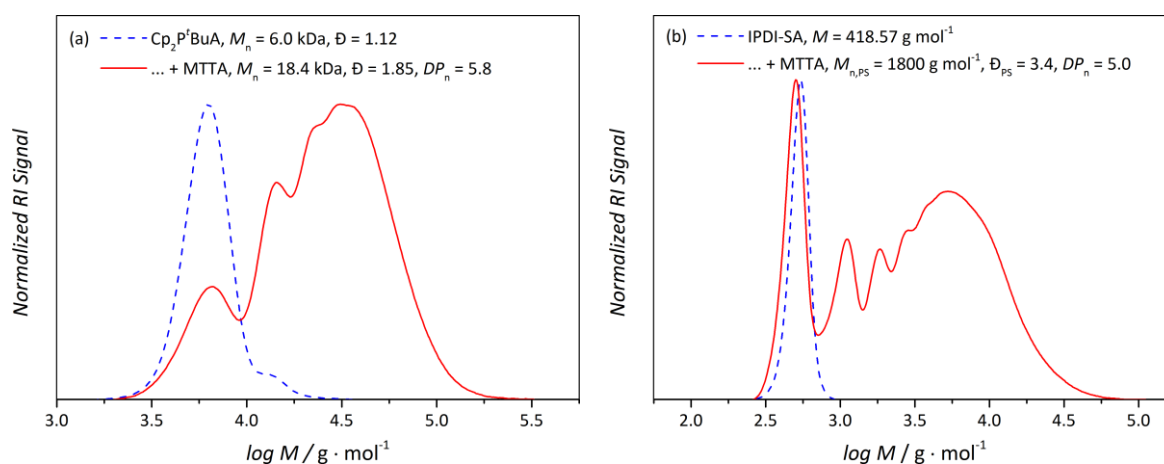


Figure 4-6 SEC trace of (a) $\text{Cp}_2\text{P}^t\text{BuA}$ (---) or (b) IPDI-SA and their DA step-growth adduct (—) with equimolar amounts of MTTA (20 mg mL^{-1} in MeCN), measured in THF at 35°C . Adapted from Ref.¹²³ with permission from The Royal Society of Chemistry.

The relatively large amount of starting material in the IPDI-sample likely arises due to unfunctionalized IPDI-species, as in ^1H NMR measurements of the adduct no free dienes can be detected anymore (refer to Experimental Section).

4.5.2 Demonstration of Thermoreversible Bonding Character

In a next step, the thermoreversible character of the adduct formation should be experimentally proven and investigated. As a result of their in theory most convenient retro reaction temperature range (refer to Table 4-1 and Table 4-2) and rapid conversion rates (see Table 4-3, Figure 4-3 (a) and Figure 4-5 (a)), adducts of MTTA with Cp functional groups were chosen for this study. High temperature (HT) ^1H NMR measurements should allow for a facile quantification of free to ligated diene ratios while temperature dependent size exclusion chromatography (TD SEC) enables a good visualization of de- and re-bonding of thermoreversibly connected macromolecular building blocks.^{132, 142, 274} During HT NMR experiments, a sample is heated inside the NMR instrument to directly observe the cleavage of diene species from the DA adduct via their characteristic signals, while subsequent cooling should lead to recurring adduct formation. Both the adducts of small molecular Cp as well as the step-growth polymer of $\text{Cp}_2\text{P}^t\text{BuA}$ with MTTA underwent such treatment (Figure 4-7).

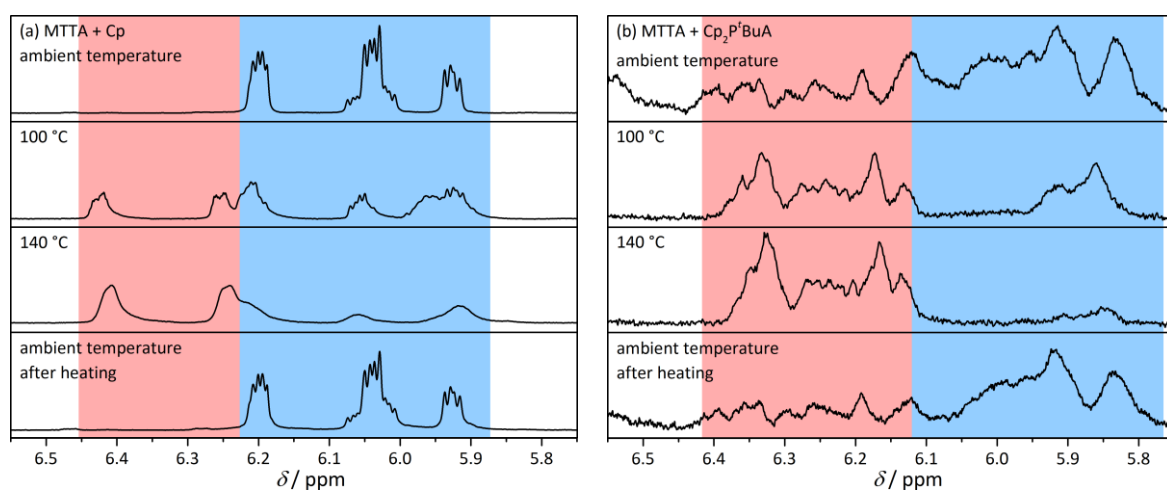


Figure 4-7 Demonstration of the thermoreversibility of the DA adduct of (a) MTTA and Cp or (b) MTTA and Cp α,ω -difunctional poly(*tert*-butyl acrylate) via ^1H HT NMR measurements in toluene- d_8 . Adapted from Ref. ¹²³ with permission from The Royal Society of Chemistry.

The signal ratio of free Cp to DA adduct signal allows for an estimation of approximately 20 % debonding at 100 °C for the small molecular adduct (Figure 4-7 (a)), being in good agreement with the theoretical results obtained via quantum chemical calculations (20 % debonding at 105 °C, refer to Table 4-2) despite a difficult ^1H NMR signal isolation due to overlapping adduct and diene signals and the use of a different solvent, toluene- d_8 , due to its higher boiling point in comparison with MeCN used for UV/Vis measurements and the computational calculations. In the case of the thermoreversibly joint step-growth adduct of MTTA with $\text{Cp}_2\text{P}^t\text{BuA}$, higher degrees of free Cp end-groups and thus debonding values of ca. 50 % at 100 °C are observed (Figure 4-7 (b)). Such behavior most probably arises due to entropic effects as discussed in Section 3.2, but could also be a consequence of lower end-group concentrations in the macromolecular specimen or a slight excess of Cp end-groups during product formation as a consequence of the relative mass determination of the polymeric building block via SEC, although fitting Mark-Houwink parameters were employed, and thus a possible resulting error during the composition of an equimolar reaction mixture. For both the small molecular as well as the polymeric step-growth adduct, a good thermocyclability was evidenced, as the initial signal ratios are recurring upon cooling the specimen to ambient conditions (Figure 4-7 (a) and (b)).

Finally, TD SEC experiments enabled the visualization of the thermoreversible product formation or cleavage for the macromolecular step-growth sample. A solution of the specimen in a suitable solvent for TD SEC, dimethylacetamide (DMAc), underwent multiple

temperature cycles between ambient temperature and 100 or 120 °C. As the employed sample concentration – necessary for a rapid re-polymerization of the building blocks at lower temperatures – is too high for a direct measurement via SEC methods, small volumes of the sample solution were further diluted and measured via TD SEC (Figure 4-8) at 70 °C to achieve readily comparable measurement conditions.

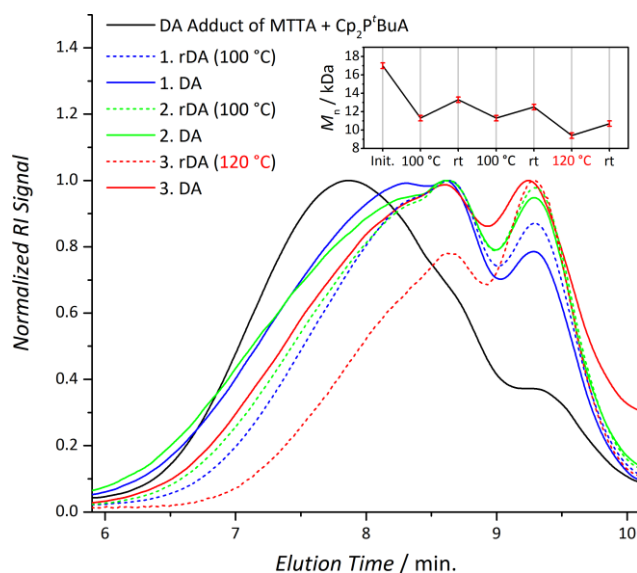


Figure 4-8 SEC trace of the step-growth polymer formed from equimolar amounts of MTTA and Cp₂P^tBuA after multiple thermocycles. The rDA reactions were induced by heating the sample to 100-120 °C, the re-emerging DA reactions were achieved upon cooling to ambient temperature. Inset: fluctuation of the molar mass of the DA step-growth adduct as a function of the bonding/debonding cycles. Adapted from Ref.¹²³ with permission from The Royal Society of Chemistry.

As the explored reaction is occurring rapidly, measurements at ambient temperatures are not reasonable to observe possible debonding. Unfortunately, also moderately elevated temperatures lead to cleavage of the step-growth adduct as indicated by the HT NMR measurements (Figure 4-7) and thus the degree of re-bonding is also falsified if the measurements are conducted at elevated temperatures. The employed measurement temperature is a good compromise between an occurring adduct formation or cleavage temperature to enable qualitative insights into the thermocycling behavior of the DA reaction. Clearly, it can be observed that with increasing temperatures the elution times are increased and thus the observed molecular masses decreased, indicating a cleavage of the step-growth polymer into smaller blocks via a rDA reaction while decreased temperatures lead to a reversion of the effect, corroborating a recurring adduct formation. Accordingly, a clear correlation between (r)DA conversion and temperature and thus the

thermoreversible character of the DA ligation of dithiooxalates and dienes is again evidenced.

4.6 Conclusions

With a dithiooxalate difunctional species, a novel and promising candidate for thermoreversible, rapid, mild and catalyst-free ligation, e.g., in small molecular or polymer systems, was designed and evaluated. A synthesis route to ethane-1,2-diyl bis(2-(methylthio)-2-thioacetate) from cheap and readily available starting materials with a total yield of 60-70 % was established jointly with the industrial collaborator. The experimental studies were supported by quantum chemical calculations of the thermodynamics of small molecular model reactions, allowing for a straightforward selection of reaction pairings and conditions. It was further demonstrated that even for equimolar reaction mixtures rapid reaction times and full conversion of some dienes with the novel dienophile dilinker can be reached within minutes while still employing mild and catalyst-free reaction conditions. Furthermore, the thermoreversible character of the formed DA adducts was confirmed via HT NMR as well as TD SEC measurements, establishing valuable possibilities for materials applications. While the reaction of Cp with MTTA results in adducts with debonding characteristics suitable for self-healing materials (ca. 20 % debonding at 100 °C), the employment of sorbic derivatives with their open-chain diene functionality may lead to the formation of high temperature reversible cross-linking for applications such as organic sheets or re-mendable networks. In addition, the combination of dithiooxalates with open-chain dienes comprising no heteroatom substituents as for example DMBD can be harnessed to enable rapid ligation without retro reaction for a presumably very wide temperature range, rendering it virtually irreversible and thus very stable. With these reported diverse and versatile characteristics, dithiooxalates and multifunctional derivatives could lead to further developments of self-healing or other stimuli-responsive materials as well as applications in rapid ligation of sensitive substrates under mild conditions, reversible or irreversible cross-linking or the generation of complex macromolecular structures.

5

CONCLUDING REMARKS AND OUTLOOK

The increasing use of dynamic chemistries in diverse applications such as self-healing materials, re-shapeable networks, the mimicking of protein folding in synthetic macromolecules and many more leads to an increased accompanying demand for tunable bonding and association characteristics of the utilized binding motifs to enable more and more novel materials with tailor-made active and stimuli-responsive properties. While the ever-growing database of available functional groups allows for very versatile chemical pathways of incorporating altered dynamic ligation attributes, the potentially complex synthetic efforts to achieve such an aim may discourage necessary investigations, rendering more physical methods of altering bonding attributes desirable. In addition, differences in reported bonding behavior of similar binding groups, incorporated in dissimilar molecules, raised the question for more detailed insights into the implications of altered physical molecular parameters for similar chemistries.

Consequently, the present thesis aims at the exploration and establishment of entropic effects on dynamic ligation chemistries, arising from different physical molecular parameters while keeping the actual chemical linkage unaltered. Polymer chemistry with its easily adaptable chain lengths via, e.g., reversible-deactivation radical polymerization methods and the countless available monomers, in addition enabling the facile modification of steric chain properties, served as an ideal model platform. Furthermore, a novel thermoreversible linker could be realized to achieve yet another promising building block in modular ligation.

Chapter 3 contains the different approaches taken to investigate the influence of physical molecular parameters on bonding equilibria via altering the entropy of involved molecules. First of all, Section 3.2 addresses the previously only marginally established effect of molecular mass and chain length on reversible covalent bonding by investigating the temperature-dependent degree of bonding for Diels–Alder adducts formed from polymer chains with differing chain lengths or side-chain substituents of different masses via high temperature NMR and temperature dependent SEC. A clear correlation – backed by quantum chemical calculations – of increasing chain mass and length with an increasing degree of debonding due to the altered entropy values was established. Thereby, previous reports could be expanded to other ligation chemistries as well as characterization techniques.

In Section 3.3, a further physical property of chain molecules, namely their stiffness, could be shown to have a similar impact on bonding properties as observed for their masses. Isomeric Diels–Alder adducts comprising chains of similar length and thus also mass, but side-chain substituents of differing steric hindrance – resulting in altered intramolecular mobility and thus stiffness – were investigated via the high temperature NMR and temperature dependent SEC methods established in the preceding section. The experimental results in combination with further *ab initio* calculations of model systems demonstrated a more facile chain cleavage of less stiff macromolecules due to the less pronounced loss of entropy in comparison to rigid chain molecules.

To verify the general applicability of the findings from Section 3.2 and 3.3 not only in covalent bonding mechanisms, Section 3.4 explores entropic effects on supramolecular association. Therefore, the dissociation constants of diblock polymers, associated via a

selective hydrogen bonding pairing, were determined for different block lengths and masses via NMR titration methods. Again, a distinctive correlation between the mass of associated molecules and their bonding characteristics was evidenced, with heavier blocks comprising up to doubled dissociation constants than small molecular recognition units, thus undergoing a significantly more favored dissociation.

In a last study of entropic effects, Section 3.5 considers the entropic difference of reversible covalent as well as supramolecular bonding in the middle of a chain molecule vs. similar ligation at terminal binding sites. Again, model calculations suggested substantial differences between the translational and rotational entropy terms for such different bonding positions. Temperature dependent SEC of reversible covalent Diels–Alder step-growth systems as well as NMR titration experiments of supramolecular block systems verified these results and demonstrated a comparably unfavorable debonding of terminally bound groups as observed for small molecules.

All these explored effects of entropy and thus the connected physical properties of (macro-)molecules have a substantial impact on diverse fields of chemistry, for example when specific binding attributes are necessary for desired materials characteristics, during the degradation of macromolecules, when small molecular reactions or theoretical calculations of fragments are transferred to macromolecular species or when investigating the reactivity of growing polymer chains. Thus, the consideration of entropic effects while planning and executing chemical reactions or processing – especially polymeric – materials are of high importance.

In addition to the studies of entropic reaction parameters, Chapter 4 addressed the investigation of a novel hetero Diels–Alder linker comprising dithiooxalate dienophile groups to enable rapid, mild, efficient, catalyst-free and thermoreversible or irreversible linkage of different diene species. Its efficiency was shown to enable facile small molecular or polymer ligation as well as step-growth polymerizations of diene difunctional building blocks under ambient conditions. The versatility and efficiency of the established linker promises a multitude of possible future applications such as self-healing materials, mendable organic sheets, cross-linkable filaments for rapid prototyping, ligation of substrates which are sensitive to heat or catalyst species as well as the construction of complex molecular architectures, amongst others.

In summary, diverse possibilities to influence (reversible) bonding characteristics were explored, establishing the previously essentially unforeseen impact of physical molecular attributes such as molecular mass, length, stiffness or the bonding position inside a molecule on otherwise similar ligation sites via altering the reaction entropy of the involved molecules. In addition, a favorable new candidate in thermoreversible hetero Diels–Alder linkage was established via the incorporation of dithiooxalates in a multifunctional species.

The novel findings of a substantial impact of diverse physical (macro-)molecular parameters may lead to a paradigm shift in the approaches taken to control and tune specific reaction equilibria in the pursuit of very defined bonding attributes. Certainly, the explored effects allow for an expanded, non-enthalpic tool box and thus new strategies to alter dynamic reaction properties to introduce new design paradigms in the very important and emerging field of adaptable materials. Likewise, with their general applicability, many other fields such as, for example, processing technologies, product lifetime assessments or biotechnology may benefit from the obtained insights into differing material properties of apparently similar chemical constitution. A challenging, but important and interesting field of future research could be the exploration of entropic effects in dynamically cross-linked species such as dissociative thermoreversible networks or associatively bond-exchanging vitrimers with applications in self-healing or re-processible networks, composite materials, organic sheets etc. Due to the much more pronounced restriction of entropy in networks, its role in (de-)bonding events may play a more important role than previously expected. The newly established dithiooxalate hetero Diels–Alder linker could also be of high value for such network studies – besides all its other mentioned application possibilities – due to its beneficial bonding characteristics, facile handling and readily observable reaction parameters via, e.g., NMR or UV/Vis techniques. On the other hand, the variable cross-link density in networks could lead to an enthalpic control over retro reactions, thus resulting in a very complex interplay of different factors. Therefore, a very careful selection and adjustment of molecular parameters is certainly necessary to achieve conclusive results. Nevertheless, the present thesis provides a first step towards an advanced understanding of bonding and debonding mechanisms in a variety of non-cross-linked dynamic systems, the underlying entropic effects and towards advanced functional and active materials.

6

EXPERIMENTAL SECTION

6.1 Materials

Stabilized methyl acrylate, *iso*-butyl acrylate (Alfa Aesar, 99 %), isobornyl acrylate (ABCR, 85 %), *tert*-butyl methacrylate (Sigma-Aldrich, 98 %), *iso*-butyl methacrylate, methyl methacrylate (ABCR, 99 %), *tert*-butyl acrylate, butyl acrylate (Sigma-Aldrich, 99 %) and styrene (99 %, VWR) were deinhibited *via* a short column of basic aluminum oxide.

Cyclopentadiene was freshly cracked at 180 °C from dicyclopentadiene (Sigma-Aldrich, stab. with BHT).

2,2'-Azobis(2-methylpropionitrile) (AIBN, 98 %, Sigma-Aldrich) was recrystallized from methanol.

Copper(I) bromide (Sigma-Aldrich, ≥ 98 %), tin(II) 2-ethylhexanoate (Sigma-Aldrich, 95 %), tris[2-(dimethylamino)ethyl]amine (Sigma-Aldrich, 97 %), butylene bis(2-bromoisobutyrate) (Evonik Industries), ethyl α -bromoisobutyrate (Sigma Aldrich, 98 %), sodium sulphate (Na_2SO_4 , ≥ 99 %, Roth), triphenylphosphine, sodium iodide (ABCR, 99 %),

dimethylaminopyridine (DMAP, 99 %, Acros), *N,N'*-dicyclohexylcarbodiimide (DCC, 99 %, Acros), 2-((dodecylsulfanyl)carbonothioyl)sulfanyl propanoic acid (DoPAT, Orica Pty. Ltd., Melbourne, Australia) and tetramethylsilane (99 %, Merck) were used as received.

Tetrahydrofuran (Sigma-Aldrich, anhydrous, ≥ 99.9 %) and nickelocene (ABCR, 99 %) were used as received and handled in a glovebox.

Anisole (Acros, 99 %), methanol (VWR, p.a.), dimethylsulfoxide (DMSO, ≥ 99.7 %, extra dry, Acros), ethyl acetate (p.a., VWR), dichloromethane (p.a., VWR), dichloromethane (99.8 %, dry, Acros) and tetrachloroethane- d_2 ($C_2D_2Cl_4$, 99.6 % D, < 0.02 % H_2O , Euriso-top) were used as received.

6.2 Methods and Instruments

Offline size exclusion chromatography of polymeric samples was carried out on a Polymer Laboratories/Varian PL-GPC 50 Plus system, comprising an autosampler, a Polymer Laboratories 5.0 μm bead-size guard column (50 x 7.5 mm²), followed by three PL columns and a differential refractive index detector. Measurements were performed in THF at 35 °C with a flow rate of 1 ml·min⁻¹. The SEC system was calibrated using linear poly(methyl methacrylate) standards ranging from 800 g·mol⁻¹ to 1.6·10⁶ g·mol⁻¹ (MHKS parameters: $K = 12.8 \cdot 10^{-5} \text{ dL g}^{-1}$, $\alpha = 0.69$)²⁷⁵ or polystyrene standards ranging from 500 g·mol⁻¹ to 2.5·10⁶ g·mol⁻¹ ($K = 14.1 \cdot 10^{-5} \text{ dL g}^{-1}$, $\alpha = 0.70$).²⁷⁶

Table 6-1 Applied Mark-Houwink-Kuhn-Sakurada parameters:

<i>Polymer</i>	<i>K / 10⁻³ mL·g⁻¹</i>	<i>α</i>	<i>Ref.</i>
PMA	19.50	0.66	277
P ⁱ BoA	5.00	0.745	278
PMMA	12.80	0.72	279
P ^t BuMA	5.84	0.76	280
P ⁱ BuMA	9.70	0.705	281
P ^t BuA	19.70	0.66	278
P ⁿ BuA	12.20	0.70	282
P ⁱ BuA	12.70	0.71	283
PS	14.1	0.70	276

¹H NMR spectra were measured on a Bruker Avance III 400 spectrometer with a CryoProbe at 400 MHz in CDCl₃ for standard measurements and toluene-d₈ or C₂D₂Cl₄ in a pressure tube for measurements at elevated temperatures (HT NMR). A baseline correction was applied.

For the **HT NMR** measurements conducted in Section 3.2, 3.3 and 4.5, after the stabilization of an adjusted temperature within minutes, the establishment of the equilibrium was ensured by repeated additional measurements with 16 scans before and after the actual measurement with 128 scans until (typically immediately) no difference could be determined in the measured data anymore. To compensate the varying shift of the signals

at different measurement temperatures, the signals were adjusted to a polymer backbone signal. The recyclability of the samples was checked after cooling to ambient temperature overnight. A typical measurement and data processing error of on average $\pm 2\%$ was determined *via* the two-fold measurement of DA material from the same batch at different days. A similar methodology was employed for the measurements in Section 3.4. A sample concentration of 6 mmol L^{-1} was employed. Each sample underwent HT NMR measurements at all the desired temperatures from lower to higher ones, consecutively. After the stabilization of an adjusted temperature, the establishment of the equilibrium was ensured by similar means as described before. The recyclability of the samples was checked after cooling to ambient temperature and an experimental error of $\pm 0.01 \text{ ppm}$ was determined via repeated measurements. To compensate the varying shift of the signals at different measurement temperatures, the signals were adjusted to TMS ($\delta = 0 \text{ ppm}$).

During **NMR titration**, typically a concentration of $c = 2 \text{ mmol L}^{-1}$ CA species in $\text{C}_2\text{D}_2\text{Cl}_4$ was employed (Section 3.5: $c = 1 \text{ mmol L}^{-1}$ CA species). Samples with a HW/CA ratio of approximately 0, 0.5, 0.75, 1.0, 1.5, 2.0 and 3.0 were prepared *via* stock solutions of the respective species and measured at 100°C . NMR titration and data evaluation for the determination of K_{ass} and K_{diss} was conducted according to literature.²⁵⁸ A standard fitting error for the determination of K_{ass} of ± 10 was determined.

Mass spectra were recorded on a Q-Exactive (Orbitrap) mass spectrometer (Thermo Fisher Scientific, San Jose, CA, USA) equipped with a HESI II probe. The instrument was calibrated in the m/z range of 74-1822 via premixed calibration solutions (Thermo Scientific). A constant spray voltage of 4.7 kV and a dimensionless sheath gas of 5 were applied. The capillary temperature and the S-lens RF level were set to 320°C and 62.0, respectively. The samples were dissolved with a concentration of $0.05 \text{ mg}\cdot\text{mL}^{-1}$ in a mixture of THF and MeOH (3:2) containing $100 \mu\text{mol}$ of sodium triflate and infused with a flow of $5 \mu\text{L}\cdot\text{min}^{-1}$.

UV/Vis measurements were carried out on a Varian Cary 50 Bio spectrophotometer. Spectra were recorded between 300 and 800 nm and kinetics were measured at 500 nm in acetonitrile or toluene in a 10 mm path length cell with a baseline correction regarding the solvent. For an evaluation of the reaction rates, the time dependent reactant concentrations were calculated via the known starting concentrations and the normalized time dependent absorbance of the C=S double bond at 500 nm, which decreases with

ongoing hetero Diels–Alder reaction of the thiocarbonyl species with dienes. Via the time dependent reactant concentrations and the assumption of a 2nd order reaction ($A + B \rightarrow C$) without retro reaction at the given reaction temperatures (as computationally predicted), reaction rate coefficients k are accessible via standard textbook equations:¹⁸³ for $[A]_0 \neq [B]_0$, k is the slope of $\ln\left(\frac{[B]/[B]_0}{[A]/[A]_0}\right) \cdot \frac{1}{([B]_0 - [A]_0)}$ vs. t , whereas for $[A]_0 = [B]_0$, k is the slope of $\frac{1}{[A]} - \frac{1}{[A]_0}$ vs. t . A typical graph can be seen in Figure 6-1.

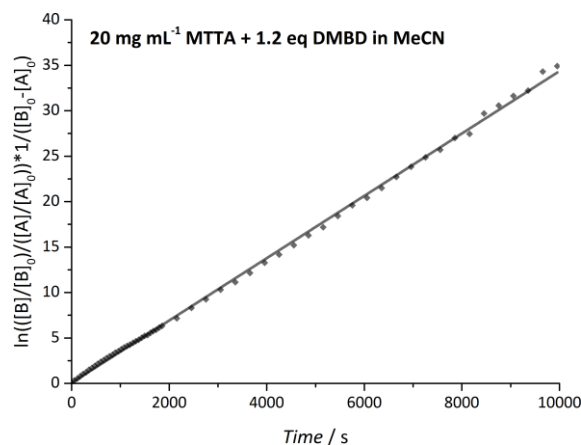


Figure 6-1 Linear fit to determine k as the slope of $\ln\left(\frac{[B]/[B]_0}{[A]/[A]_0}\right) \cdot \frac{1}{([B]_0 - [A]_0)}$ vs. t for the Diels–Alder reaction of 1.2 eq. DMBD with MTTA (20 mg mL⁻¹ in MeCN).

The activation energies (E_a) were determined via the subtraction of the two logarithmic forms of the Arrhenius equations $E_a = R \cdot \ln\left(\frac{k_1}{k_2}\right) \cdot \frac{T_1 \cdot T_2}{T_1 - T_2}$ for the rate coefficients as determined for 25 °C (298.15 K) and 50 °C (323.15 K) with R being the universal gas constant.¹⁸³

Additional UV/Vis measurements of single spectra under similar conditions were carried out on an OceanOptics USB4000 spectrometer with a USB-ISS-UV-Vis detecting unit.

The **temperature dependent SEC** (TD SEC) experiments were carried out by Josef Brandt (IPF, Dresden) on a PL GPC 220 high temperature chromatograph (Agilent Technologies, US), featuring a temperature controlled autosampler, column oven and dRI as well as viscosity and UV detection. For the measurements performed in Section 3.2 and 3.3, separation was achieved through one PL ResiPore column (3 μm bead-size). A mixture of 60 % 1,2,4-trichlorobenzene (TCB) in *N,N*-dimethylformamide (DMF) was employed as a solvent at a flow rate of 1 mL min⁻¹. Details regarding the evaluation of the chromatograms

can be found in the original publication.¹⁴² In Section 3.5, 1,2,4-trichlorobenzene (TCB) or a mixture of 40 % *N,N*-dimethylformamide (DMF) in 60 % TCB was employed as a solvent at a flow rate of 1 mL min⁻¹. Details regarding the evaluation of the chromatograms can be found in the original publication.²⁵⁹ In Section 4.5, DMAc (+ 3 g/L LiCl) was used as a solvent at a flow rate of 1 mL/min on an ABOA DMAc-phil column (AppliChrom, Germany). Details regarding the evaluation of the chromatograms can be found in the original publication.¹²³

Small-angle neutron scattering (SANS) measurements were carried out by Josef Brandt (IPF, Dresden) at the instrument D11 of the ILL in Grenoble with a wavelength of 6 Å and at two sample-detector distances of 8 m and 1.2 m, covering a broad *q*-range from 0.0083-0.0824 Å⁻¹ (at 8 m) and 0.06-0.514 Å⁻¹ (at 1.2 m) with a good overlap of the two *q*-regimes. The samples were measured at concentrations of approximately 1, 2, 3, 4 and 5 wt%. The solvent toluene-d₈ was also measured, normalized and then subtracted from the solution data. Data analysis was performed according to the procedure proposed by Casassa and Holtzer.^{239, 240} For more details on the methodology refer to the original publication.¹⁴²

For details on the **computational methods** – performed by collaboration partners at the Australian National University (Canberra) under the supervision from Prof. Michelle Coote – for the quantum chemical assessment of entropic effects as described in Chapter 3 or for the evaluation of promising reactants as performed in Chapter 4, refer to the original publications.^{123, 142, 259}

6.3 Synthetic Procedures

6.3.1 Syntheses from Section 3.2 and 3.3

Synthesis of a Cyanodithioester (CDTE) Dilinker. The synthesis was conducted according to literature.¹³² The cyanodithioester (CDTE) dilinker was obtained as a yellow solid. Overall yield: 5 %. ¹H NMR (400 MHz, CDCl₃) δ [ppm]: 7.41-7.29 (m, 8H, ArH), 7.22-7.20 (m, 1H, NH), 6.65-6.63 (dd, J = 5.4, 2.8 Hz, 1H, C=CH), 6.45-6.43 (dd, J = 5.1, 2.8 Hz, 1H, C=CH), 6.10-6.08 (dd, 5.2, 3.3 Hz, 1H, C=CH), 5.80-5.78 (dd, 5.2, 3.3 Hz, 1H, C=CH), 5.12-5.04 (m, 4H, NCOOCH₂), 4.82 (s, 1H, CHSC), 4.54 (s, 1H, CHSC), 4.30-4.071 (m, 4H, SCH₂Ar), 4.01-3.98 (m, 2H, CHCCN), 3.81 (br, 1H, OCONHCH), 2.97-2.87 (br, 2H, OCONHCH₂), 2.15-1.82 (m, 4H, CHCH₂CH), 1.75-1.69 (br, 2H, CH₂), 1.23-0.80 (m, 13H, CH₃, CH₂).

Synthesis of Bromo (Di-)Functional Polymers. Activators regenerated by electron transfer atom transfer radical polymerization (ARGET ATRP) protocols were adapted from the literature.⁹⁰ In a typical procedure, copper(I) bromide (13.6 mg, 0.09 mmol), tris[2-(dimethylamino)ethyl]amine (0.095 mmol, 278 μ L, 0.34 mmol mL⁻¹ in anisole) and isobornyl acrylate (20 mL, 94.7 mmol) were dissolved in anisole (5 mL) in a flame dried Schlenk flask and degassed *via* nitrogen purging for 45 minutes. In two additional Schlenk flasks, butylene bis(2-bromoisobutyrate) (183.7 mg, 0.95 mmol) and tin(II) 2-ethylhexanoate (153 μ L, 0.47 mmol) were dissolved in anisole (7.5 mL each) and degassed. Subsequently, the solutions were transferred into the first Schlenk flask *via* a cannula and stirred at 60 °C for 35 minutes. The polymerization was stopped in an ice bath and quenched with air at low conversion values (~25 %) in order to control for unwanted chain termination before filtration over neutral aluminum oxide and precipitation in cold methanol. The white polymer powder was dried *in vacuo* and characterized *via* SEC and ¹H NMR, evidencing a high bromo end group fidelity of consistently between 98-99 % for each synthesized polymer system *via* the comparison of initiator to end group signals (refer to Table 3-1 and Table 3-2 for the full list of synthesized polymers, Figure 3-4 and Figure 3-10 for the SEC characterization, Figure 6-2 to Figure 6-5 for NMR characterization and Table 6-2 for the synthetic details of bromo monofunctional poly(methacrylates) as well as Table 6-3 for the ones of bromo difunctional polyacrylates).

Experimental Section

Table 6-2 List of ARGET ATRP synthetic conditions for the generation of bromo functional polymethacrylates.

Polymer	m_{CuBr} / mg	V_{Me6TREN^*} / μL	V_{Monomer} / mL	$V_{\text{EBIB}^{**}}$ / μL	$V_{\text{Sn(EH)2}}$ / μL	V_{Anisole} / mL	t / min.	Precip. in cold
BrPMMA	9.4	192.0	15.0	95.7	106	15.0	35	Hex./Et ₂ O 1:1
BrP ⁱ BuMA	6.2	127.8	15.0	63.8	70	15.0	45	MeOH/ H ₂ O 4:1
BrP ^t BuMA	6.2	126.2	15.0	63.0	70	15.0	56	MeOH/ H ₂ O 4:1

*c = 0.34 mmol mL⁻¹; **ethyl α -bromoisobutyrate

Table 6-3 List of ARGET ATRP synthetic conditions for the generation of bromo difunctional polyacrylates.

Polymer	m_{CuBr} / mg	V_{Me6TREN^*} / μL	V_{Monomer} / mL	$m_{\text{BDBIB}^{**}}$ / mg	$V_{\text{Sn(EH)2}}$ / μL	V_{Anisole} / mL	t / min.	Precip. in cold
Br ₂ P ⁿ BuA	272.5	412.9	20.0	272.5	227.4	20.0	55	MeOH/H ₂ O 4:1
Br ₂ P ⁱ BuA	19.9	408.0	20.0	269.5	225.0	20.0	45	MeOH/H ₂ O 4:1
Br ₂ P ^t BuA	21.4	439.0	20.0	289.5	242.0	20.0	40	MeOH/H ₂ O 4:1
Br ₂ PMA large	31.9	653.0	20.0	431.0	359.6	20.0	35	MeOH/H ₂ O 7:3
Br ₂ P ⁱ BoA large	13.6	278.4	20.0	183.7	153.0	20.0	35	MeOH
Br ₂ PMA small	95.6	1959	12.0	2586	1079	20.0	55	MeOH/H ₂ O 7:3
Br ₂ P ⁱ BoA small	4.1	460.0	12.0	1102	575.0	20.0	55	MeOH

*c = 0.34 mmol mL⁻¹; **butylene bis(2-bromoisobutyrate)

Synthesis of Cp (Di-)Functional Polymers. The synthetic procedure was adapted from the literature.²²⁹ In a typical procedure, bromo difunctional poly(isobornyl acrylate) (3.0 g, 0.30 mmol), sodium iodide (545 mg, 3.63 mmol) and triphenylphosphine (318 mg,

1.21 mmol) were dissolved in anhydrous THF (6.0 mL). Nickelocene (229 mg, 1.21 mmol) was added and the reaction mixture was stirred under argon at ambient temperature for 5 hours. The reaction was subsequently purged with air, filtered over basic aluminum oxide and the polymer was repeatedly precipitated in cold methanol. The off-white polymer was characterized *via* SEC and ^1H NMR to ensure quantitative conversion (refer to Table 3-1 and Table 3-2 for the full list of synthesized polymers, Figure 6-2 to Figure 6-5 for NMR characterization and Table 6-4 for the synthetic details).

Table 6-4 List of reaction conditions for the Cp functionalization reactions of the bromo (di-) functional poly(meth-)acrylates.

Polymer	$m_{\text{Br(2)Polym.}}$ / g	m_{NaI} / mg	m_{PPh_3} / mg	V_{THF} / mL	m_{NiCp_2} / mg	t / h
CpPMMA	0.86	138.1	80.6	4.0	58.0	12
CpP ⁱ BuMA	2.00	264.5	154.3	6.0	111.1	12
CpP ^t BuMA	1.37	170.7	99.6	5.0	71.8	12
Cp ₂ P ⁿ BuA	2.68	149.9	262.3	8.0	306.8	5
Cp ₂ P ⁱ BuA	2.45	648.0	378.0	7.0	275.0	5
Cp ₂ P ^t BuA	3.4	927.0	541.0	10.0	389.0	5
Cp ₂ PMA _{large}	3.23	1336	779.0	15.0	561.0	5
Cp ₂ P ⁱ BoA _{large}	2.99	549.0	320.0	6.0	231.0	5
Cp ₂ PMA _{small}	2.02	3050	1779	17.0	1281	5
Cp ₂ P ⁱ BoA _{small}	1.00	785.0	458.0	4.5	330.0	5

Synthesis of CDTE Diels–Alder Polymers/Diblock Adducts. In a typical procedure, cyclopentadiene difunctional poly(isobornyl acrylate) (50.0 mg, 0.005 mmol) and close to equimolar amounts of CDTE dilinker (around 4.0 mg, 0.005 mmol) were dissolved in anisole (200 μL) and heated to 120 °C for 10 minutes. The reaction was then slowly cooled to ambient temperature within 1 hour to achieve the DA step growth polymer with the desired amount of repeating units. The product was characterized *via* SEC, temperature dependent SEC and temperature dependent ^1H NMR (refer to Figure 3-4 and Figure 3-10 for the SEC characterization, Table 6-5 for the synthetic details for all DA polymers, Figure 6-6 to Figure 6-10 for HT NMR spectra and Table 6-6 for a list of debonding values).

Table 6-5 List of synthetic conditions for the DA linkage reactions.

Polymer	$m_{\text{Cp(2)Polymer}} / \text{mg}$	$m_{\text{CDTE}} / \text{mg}$	$V_{\text{Anisole}} / \mu\text{L}$
b-PMMA	50.0	5.4	200.0
b-P ⁱ BuMA	50.0	3.3	200.0
b-P ^t BuMA	50.0	4.5	200.0
DA-P ⁿ BuA	50.0	8.5	200.0
DA-P ⁱ BuA	50.0	8.2	200.0
DA-P ^t BuA	50.0	11.5	200.0
DA-PMA _{large}	50.0	12.7	200.0
DA-P ⁱ BoA _{large}	50.0	4.0	200.0
DA-PMA _{small}	50.0	35.0	200.0
DA-P ⁱ BoA _{small}	49.0	29.0	200.0

Table 6-6 List of experimental debonding values determined via HT NMR.

Polymer	Degree of Debonding / %								
	25 °C	40 °C	70 °C	90 °C	100 °C	110 °C	120 °C	130 °C	140 °C
PMMA	n.d.	7.4	17.1	n.d.	30.2	n.d.	46.0	n.d.	67.5
P ⁱ BuMA	n.d.	9.6	22.3	n.d.	42.3	n.d.	61.5	n.d.	81.0
P ^t BuMA	n.d.	8.5	19.3	n.d.	35.9	n.d.	53.0	n.d.	74.2
P ⁿ BuA	2.0	3.9	12.8	23.5	n.d.	40.0	47.7	56.9	65.5
P ⁱ BuA	5.1	6.8	16.7	28.6	n.d.	42.7	52.7	61.1	72.6
P ^t BuA	1.3	2.0	8.0	18.0	n.d.	30.9	38.5	46.2	55.1
PMA _{large}	2.6	3.9	8.5	21.1	n.d.	36.7	46.2	53.9	62.3
P ⁱ BoA _{large}	1.3	n.d.	n.d.	28.9	n.d.	45.9	53.7	64.0	73.4
PMA _{small}	2.6	n.d.	n.d.	18.5	n.d.	30.6	39.3	47.0	55.5
P ⁱ BoA _{small}	0.6	0.7	2.0	8.5	n.d.	21.5	30.2	38.8	46.4

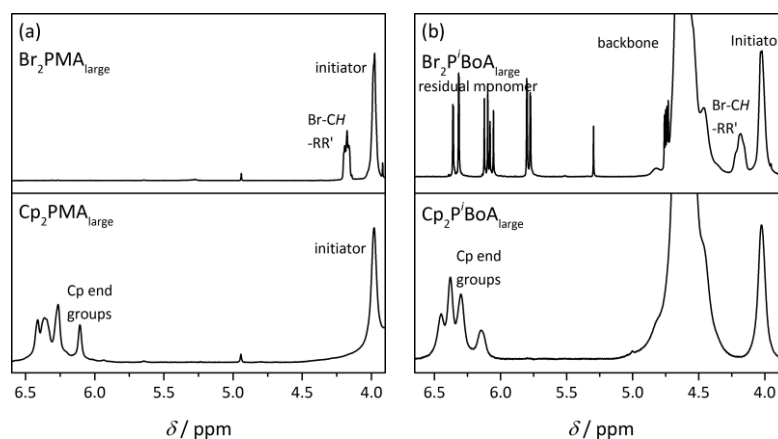


Figure 6-2 ^1H NMR spectra of the dibromo precursor and Cp difunctionalized polymer building blocks with 50 (a) methyl acrylate or (b) isobornyl butyl acrylate repeating units in CDCl_3 .

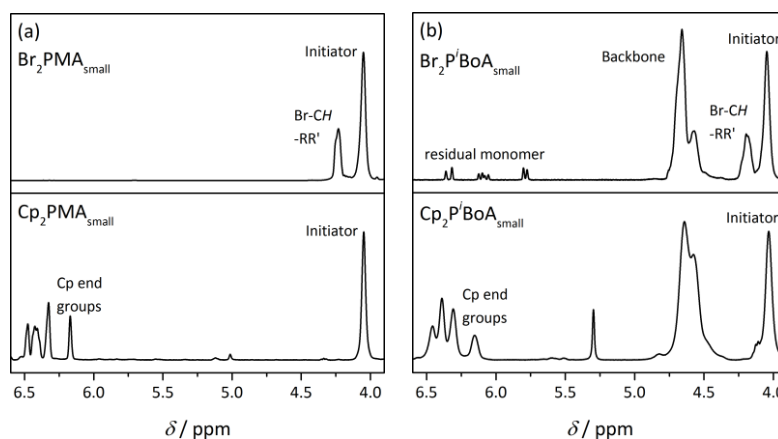


Figure 6-3 ^1H NMR spectra of the dibromo precursor and Cp difunctionalized polymer building blocks with 10 (a) methyl acrylate or (b) isobornyl butyl acrylate repeating units in CDCl_3 .

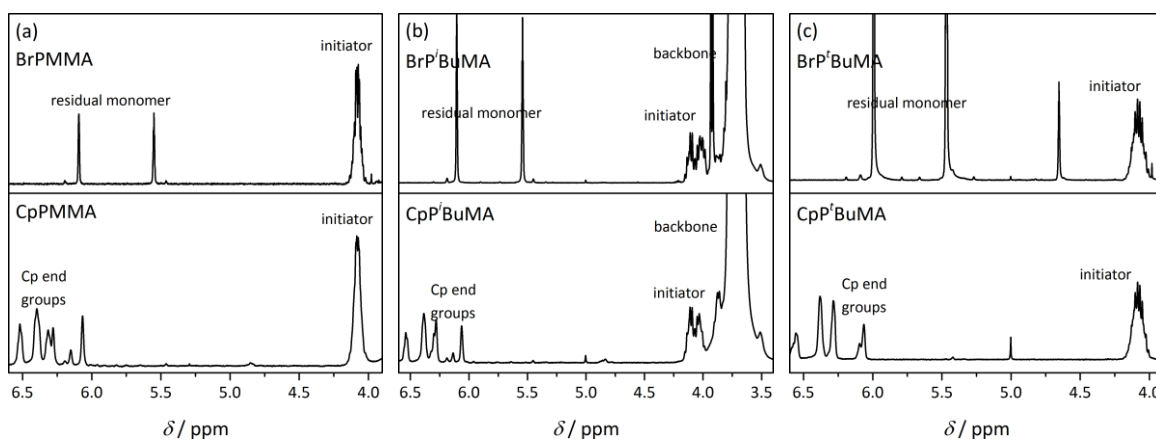


Figure 6-4 ^1H NMR spectra of the bromo precursor and Cp functionalized polymer building blocks with 50 (a) methyl methacrylate, (b) *iso*-butyl methacrylate or (c) *tert*-butyl methacrylate repeating units in CDCl_3 .

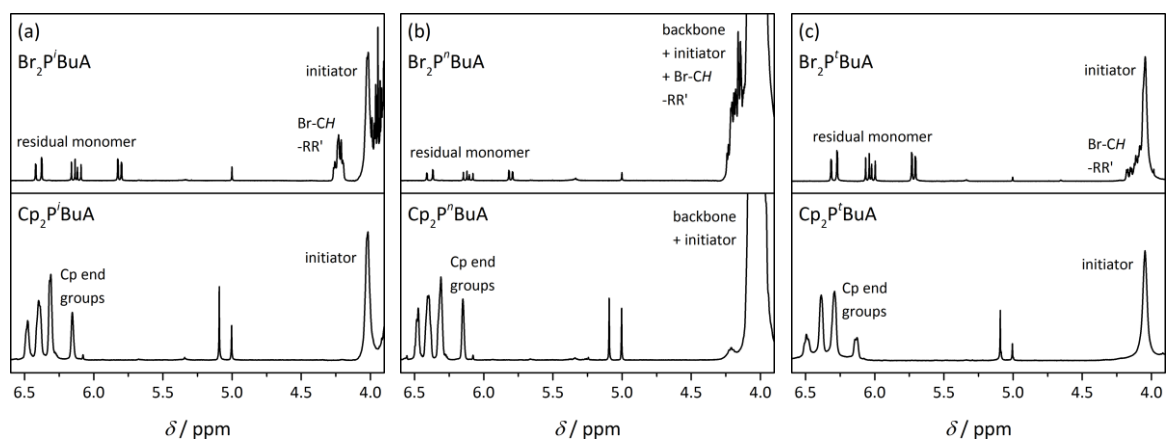


Figure 6-5 ^1H NMR spectra of the dibromo precursor and Cp difunctionalized polymer building blocks with 50 (a) *iso*-butyl acrylate, (b) *n*-butyl acrylate or (c) *tert*-butyl acrylate repeating units in CDCl_3 .

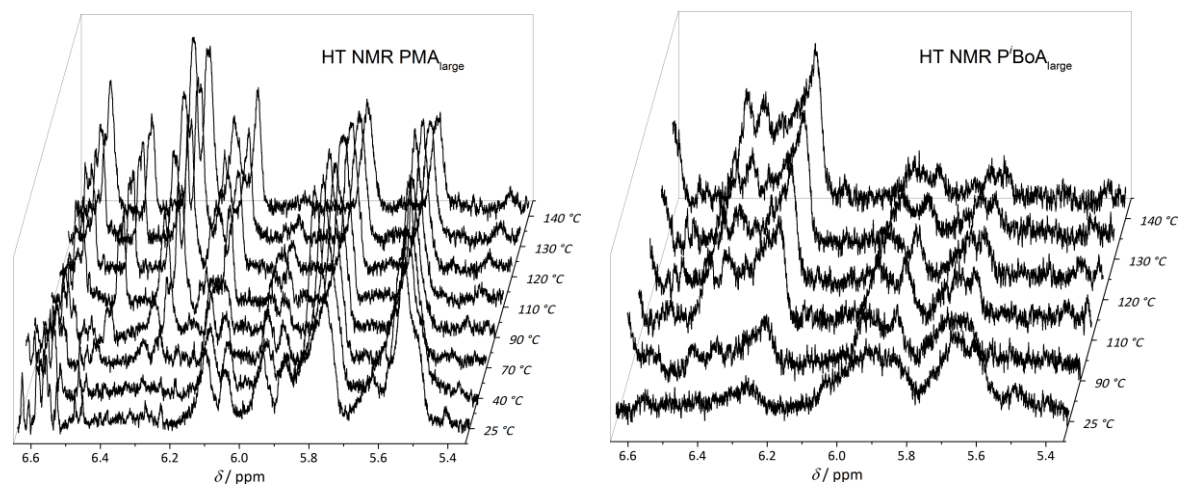


Figure 6-6 ^1H HT NMR spectra of the DA polymer formed from (left) $\text{PMA}_{\text{large}}$ or (right) $\text{P}^i\text{BoA}_{\text{large}}$ building blocks.

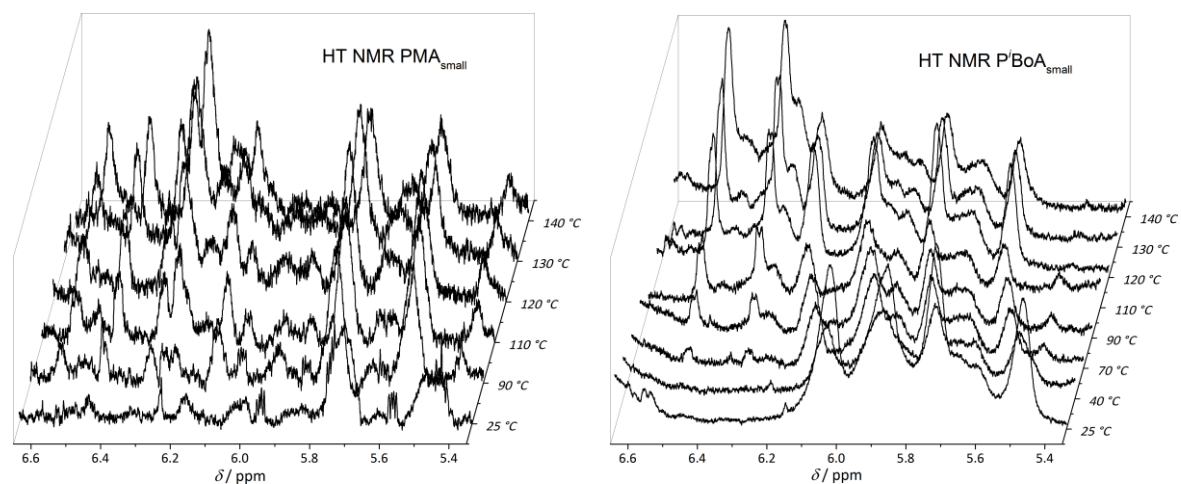


Figure 6-7 ^1H HT NMR spectra of the DA polymer formed from (left) $\text{PMA}_{\text{small}}$ or (right) $\text{P}^i\text{BoA}_{\text{small}}$ building blocks.

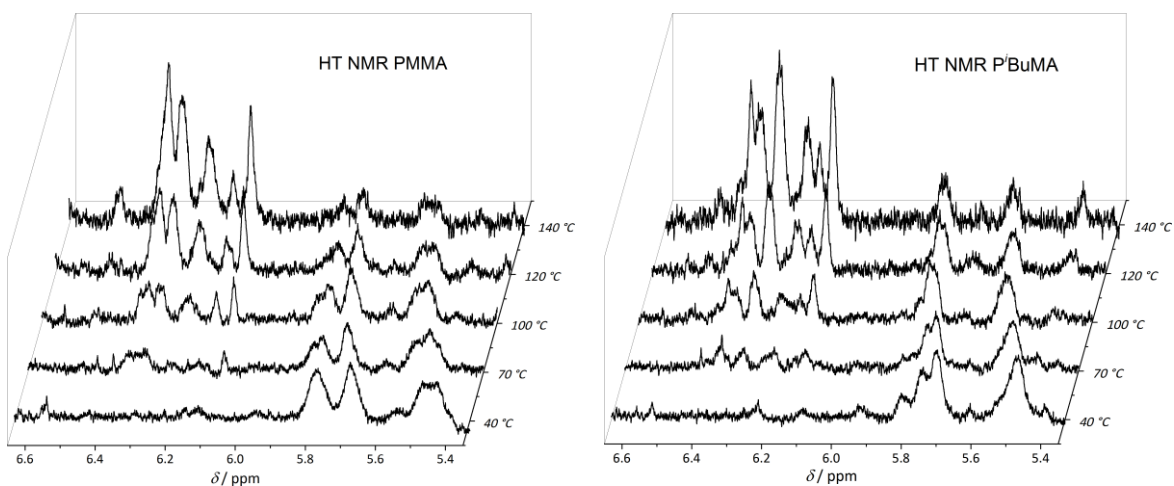


Figure 6-8 ^1H HT NMR spectra of the DA diblock polymer formed from PMMA or PⁱBuMA building blocks.

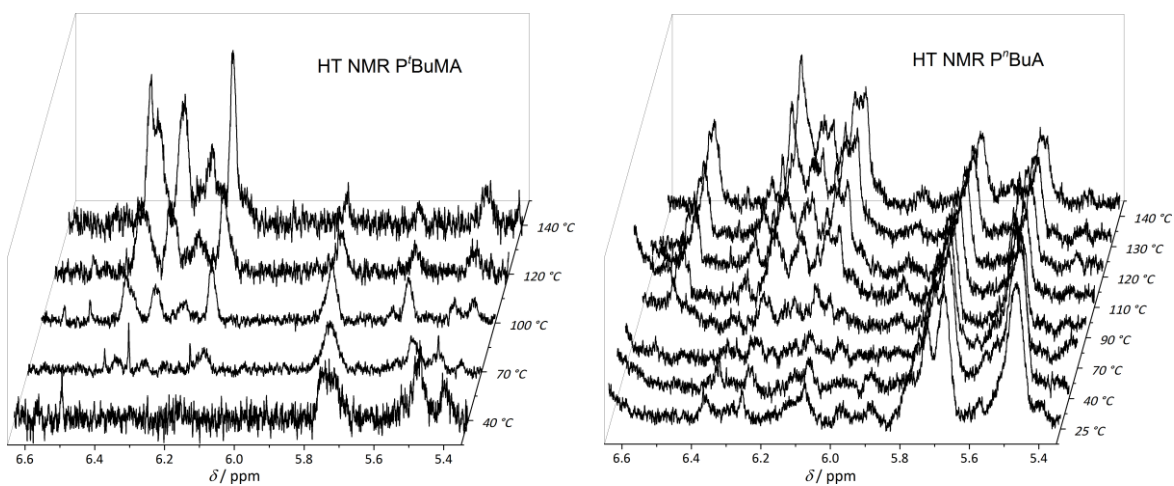


Figure 6-9 ^1H HT NMR spectra of the DA diblock polymer formed from (left) PⁱBuMA or (right) PⁿBuA building blocks.

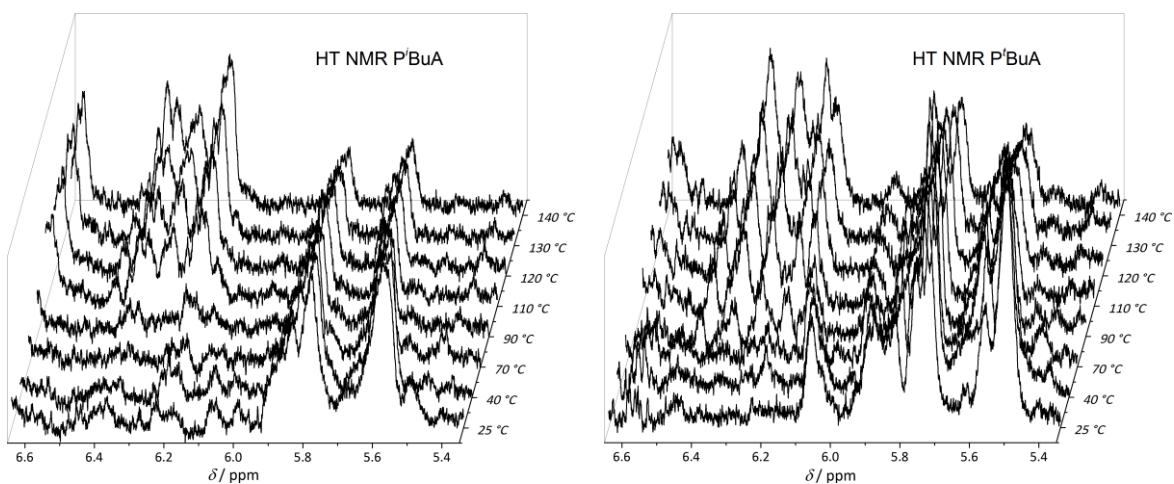


Figure 6-10 ^1H HT NMR spectra of the DA polymer formed from (left) PⁱBuA or (right) P^tBuA building blocks.

6.3.2 Syntheses from Section 3.4

Syntheses of CA-/HW-RAFT and CA/HW Small Molecules were performed by Özcan Altintas, refer to the original publication for details.²⁵⁴

RAFT Polymerization of CA-Polyacrylates. The RAFT polymerization protocol was adapted from literature.³² In a typical procedure, **CA-RAFT** (87.0 mg, 0.15 mmol) and AIBN (0.5 mg, 0.003 mmol) were dissolved in *n*-butyl acrylate (0.55 mL, 3.84 mmol) and DMSO (90 μ L) in a Schlenk tube, which was deoxygenated by three freeze–pump–thaw cycles. The Schlenk tube was immersed in an oil bath at 70 °C for 50 min. The reaction was stopped by immersing the tube into liquid nitrogen. The polymer was precipitated four times into cold methanol/water (4:1) for PⁿBuAs or cold methanol for PⁱBoAs, dried over Na₂SO₄ and the solvent was evaporated *in vacuo* for 24 h.

CA-PⁿBuA_{small}: $M_{n,SEC} = 3000 \text{ g mol}^{-1}$, $PDI = 1.07$

CA-PⁿBuA_{med.}: $M_{n,SEC} = 13800 \text{ g mol}^{-1}$, $PDI = 1.07$.

¹H NMR (400 MHz, CDCl₃) δ (ppm) = 8.70 (bs, 2H, H¹), 4.75 (m, 1H, H²), 4.03 (bm, backbone, H³), 3.83 (s, 2H, H⁴), 3.33 (t, 2H, H⁵), 2.60–0.70 (aliphatic protons of PⁿBuA).

CA-PⁱBoA_{small}: $M_{NMR} = 3350 \text{ g mol}^{-1}$, $\bar{D} = 1.06$.

CA-PⁱBoA_{large}: $M_{n,SEC} = 25000 \text{ g mol}^{-1}$, $\bar{D} = 1.18$

¹H NMR (400 MHz, CDCl₃) δ (ppm) = 8.32 (bs, 2H, H¹), 4.62 (bm, backbone, H²), 4.04 (s, 2H, H³), 3.83 (s, 2H, H⁴), 3.33 (t, 2H, H⁵), 2.60–0.70 (aliphatic protons of PⁱBoA).

RAFT Polymerization of HW-Polyacrylates. The RAFT polymerization protocol was adapted from literature.³² In a typical procedure, **HW-RAFT** (154.2 mg, 0.16 mmol) and AIBN (0.5 mg, 0.003 mmol) were dissolved in *n*-butyl acrylate (0.55 mL, 3.84 mmol) and DMSO (150 μ L) in a Schlenk tube, which was deoxygenated by three freeze–pump–thaw cycles. The Schlenk tube was immersed in an oil bath at 70 °C for 50 min. The reaction was stopped by immersing the tube into liquid nitrogen. The polymer was precipitated four times into

cold methanol/water (4:1) for PⁿBuAs or cold methanol for PⁱBoAs, dried over Na₂SO₄ and the solvent was evaporated *in vacuo* for 24 h.

HW-PⁿBuA_{small}: $M_{n,SEC} = 3200 \text{ g mol}^{-1}$, $\mathcal{D} = 1.07$

HW-PⁿBuA_{med.}: $M_{n,SEC} = 11800 \text{ g mol}^{-1}$, $\mathcal{D} = 1.07$.

¹H NMR (400 MHz, CDCl₃) δ (ppm) = 8.50 (bs, 4H, H¹), 8.04-7.63 (m, 9H, H²), 4.75 (m, 1H, H³), 4.03 (bm, backbone, H⁴), 3.32 (t, 2H, H⁵), 2.60–0.70 (aliphatic protons of PⁿBuA).

HW-PⁱBoA_{small}: $M_{n,SEC} = 3300 \text{ g mol}^{-1}$, $\mathcal{D} = 1.06$.

HW-PⁱBoA_{large}: $M_{n,SEC} = 24700 \text{ g mol}^{-1}$, $\mathcal{D} = 1.18$

¹H NMR (400 MHz, CDCl₃) δ (ppm) = 8.38 (bs, 2H, H¹), 8.04-7.63 (m, 9H, H²), 4.62 (bm, backbone, H³), 4.10 (m, 2H, H⁴), 3.33 (t, 2H, H⁵), 2.60–0.70 (aliphatic protons of PⁱBoA).

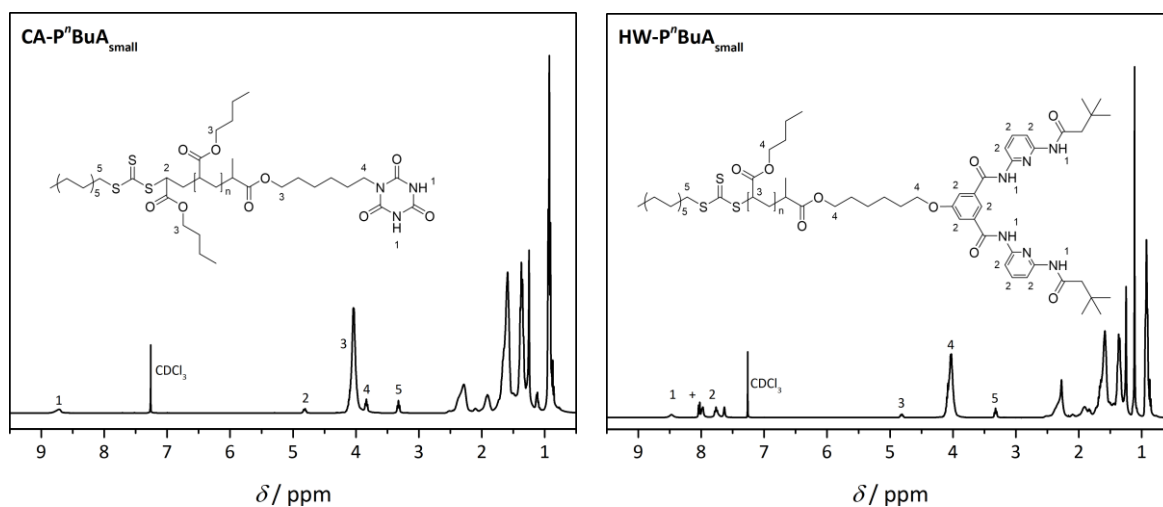


Figure 6-11 Left: ¹H NMR (400 MHz, CDCl₃) of CA-PⁿBuA_{small}. The ratio of the integral values of the signals H¹ and H² allow for the determination of the CA end-group fidelity as ~98 %. Right: ¹H NMR (400 MHz, CDCl₃) of HW-PⁿBuA_{small}. The ratio of the integral values of the signals H¹⁺² and H³ allow for the determination of the CA end-group fidelity as ~99 %.

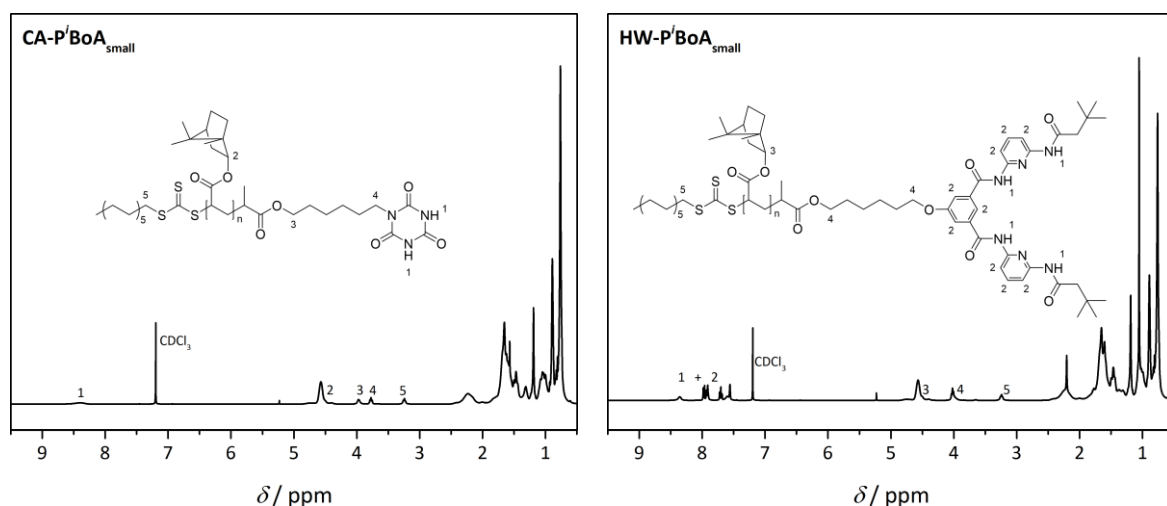


Figure 6-12 Left: ^1H NMR (400 MHz, CDCl_3) of $\text{CA-P}'\text{BoA}_{\text{small}}$. The ratio of the integral values of the signals H^1 and H^5 allow for the determination of the CA end-group fidelity as $\sim 99\%$. Right: ^1H NMR (400 MHz, CDCl_3) of $\text{HW-P}'\text{BoA}_{\text{small}}$. The ratio of the integral values of the signals H^{1+2} and H^5 allow for the determination of the CA end-group fidelity as $\sim 99\%$.

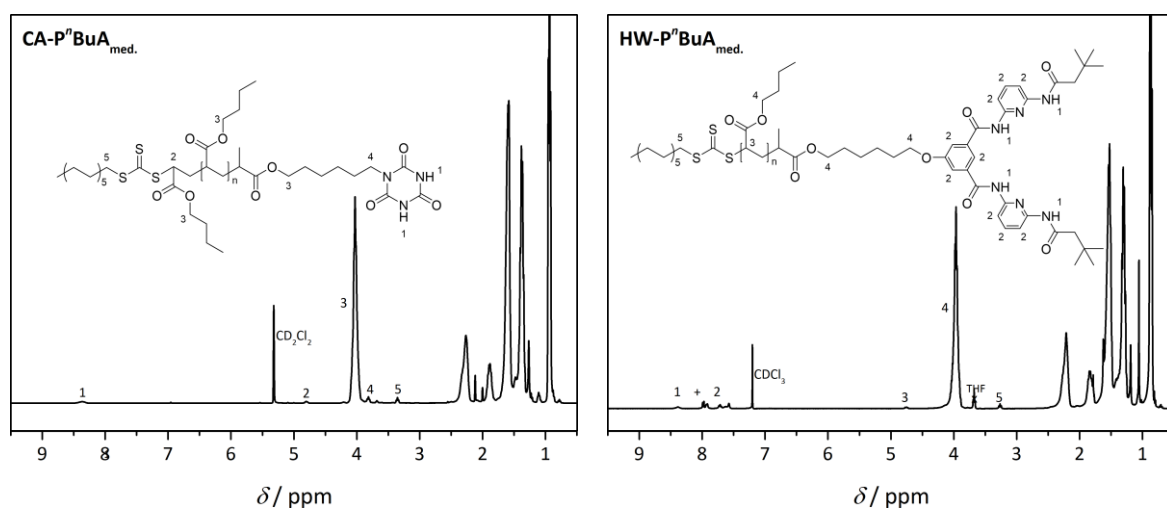


Figure 6-13 Left: ^1H NMR (400 MHz, CD_2Cl_2) of $\text{CA-P}^n\text{BuA}_{\text{med}}$. The ratio of the integral values of the signals H^1 and H^2 allow for the determination of the CA end-group fidelity as $\sim 99\%$. Right: ^1H NMR (400 MHz, CDCl_3) of $\text{HW-P}^n\text{BuA}_{\text{med}}$. The ratio of the integral values of the signals H^{1+2} and H^3 allow for the determination of the CA end-group fidelity as $\sim 99\%$.

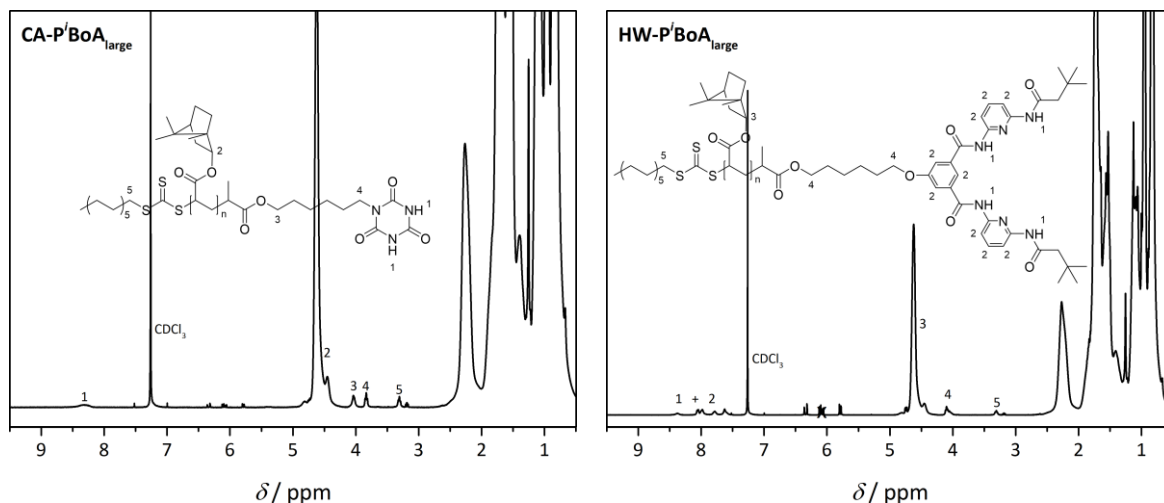


Figure 6-14 Left: ^1H NMR (400 MHz, CDCl_3) of $\text{CA-P}^i\text{BoA}_{\text{large}}$. The ratio of the integral values of the signals H^1 and H^5 allow for the determination of the CA end-group fidelity as $\sim 99\%$. Right: ^1H NMR (400 MHz, CDCl_3) of $\text{HW-P}^i\text{BoA}_{\text{large}}$. The ratio of the integral values of the signals H^{1+2} and H^5 allow for the determination of the CA end-group fidelity as $\sim 99\%$ (x: residual monomer).

HT NMR Samples. All materials were dried over Na_2SO_4 as well as under reduced pressure for 24 h and stored in a desiccator over silica gel to avoid falsified measurements due to residual water. An end-group concentration of 6 mmol L^{-1} was adjusted.

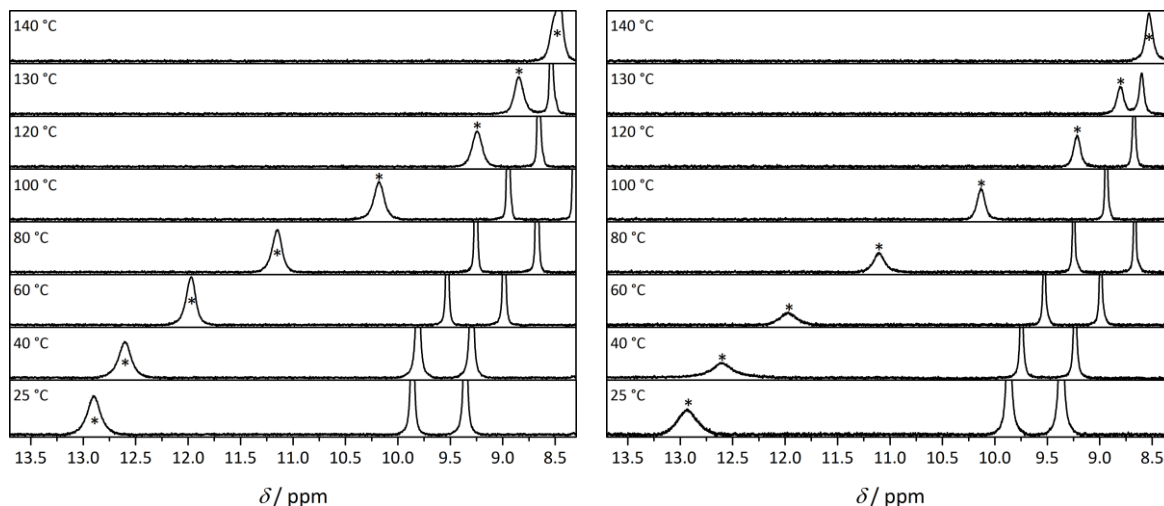


Figure 6-15 Expanded temperature dependent ^1H NMR spectra ($n_s = 128$) of equimolar amounts of left: HW- and $\text{CA-P}^n\text{BuA}_{\text{small}}$ or right: HW- and $\text{CA-P}^i\text{BoA}_{\text{small}}$ in $\text{C}_2\text{D}_2\text{Cl}_4$ ($c = 6 \text{ mmol L}^{-1}$), showing the debonding dependent shift of the CA imide proton resonance (*).

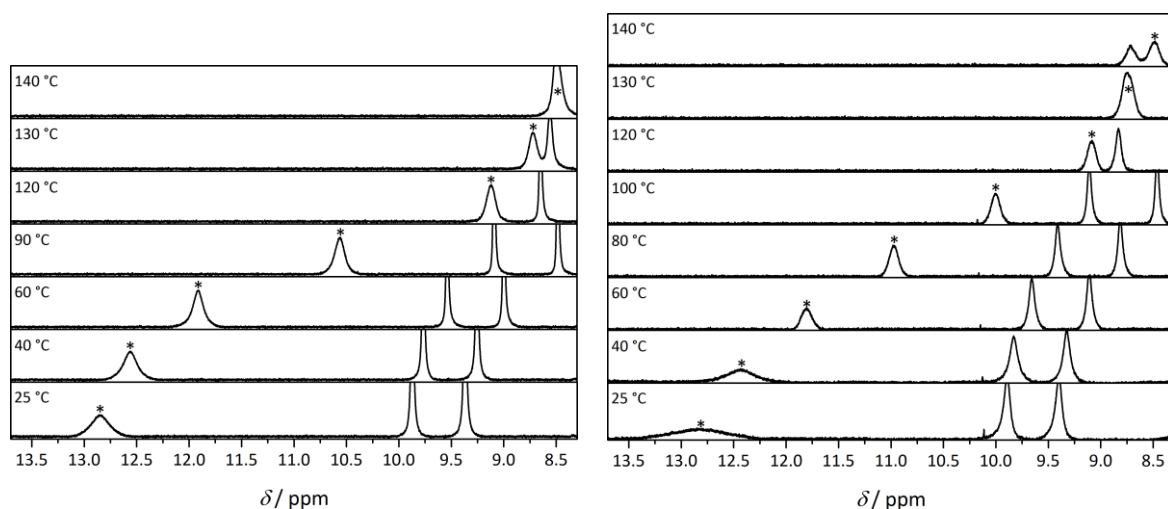


Figure 6-16 Expanded temperature dependent ^1H NMR spectra ($n_s = 128$) of equimolar amounts of left: HW- and CA- $\text{P}^{\text{B}}\text{BuA}_{\text{med}}$. or right: HW- and CA- $\text{P}^{\text{B}}\text{BoA}_{\text{large}}$ in $\text{C}_2\text{D}_2\text{Cl}_4$ ($c = 6 \text{ mmol L}^{-1}$), showing the debonding dependent shift of the CA imide proton resonance (*).

To ensure that no competing interactions of polyacrylate backbone with the hydrogen bonding motif under investigation lead to the observed effects, temperature dependent ^1H NMR measurements of **CA** and **HW Small Molecule** plus a readily available non-functional $\text{P}^{\text{B}}\text{BoA}$ (50 kDa; each $c = 6 \text{ mmol L}^{-1}$) were conducted, yielding no significant signal shifts (Figure 6-17 left).

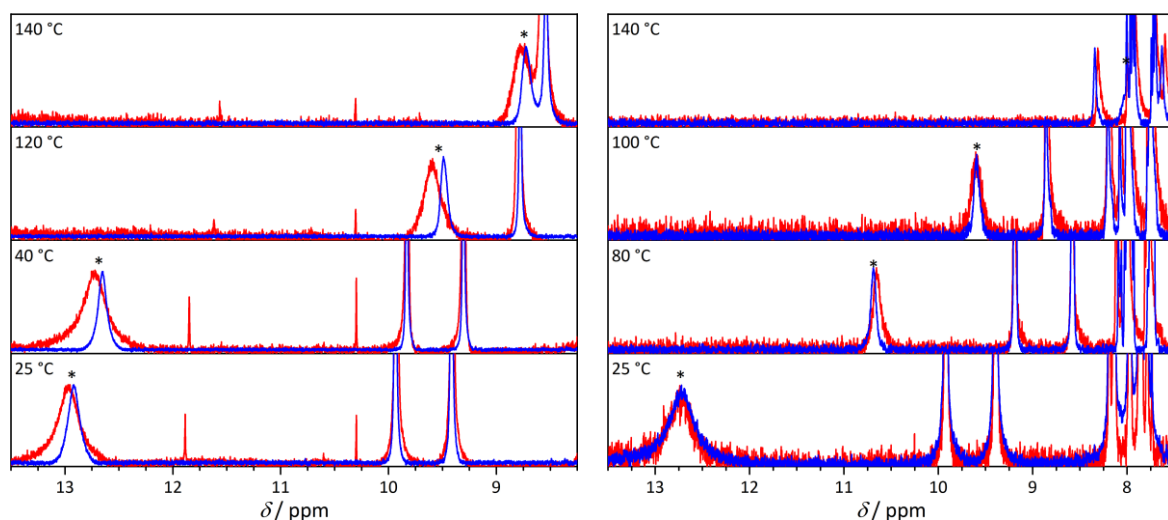


Figure 6-17 Left: Expanded ^1H NMR spectra of CA plus HW Small Molecule (6 mM) without (blue) and with (red) additional non-functional $\text{P}^{\text{B}}\text{BoA}$ (50 kDa) in $\text{C}_2\text{D}_2\text{Cl}_4$ (6 mM), showing the CA imide proton signal (*). Right: Expanded ^1H NMR spectra of CA plus HW Small Molecule (2 mM) without (blue) and with (red) additional non-functional $\text{P}^{\text{B}}\text{BoA}$ (7 kDa) in $\text{C}_2\text{D}_2\text{Cl}_4$ (2 mM), showing the CA imide proton signal (*).

In addition, the negligible shifts point in the other direction as the ones observed for the investigated entropic effects and thus even further support the occurrence of chain mass and length effects. To also exclude a steric shielding of the acrylate backbone by the bulky

isobornyl substituents, analogous measurements were conducted with **CA** and **HW Small Molecule** plus a readily available non-functional PⁿBoA (7 kDa; each c = 2 mmol L⁻¹), again yielding no significant signal shifts (Figure 6-17 right).

NMR titration experiments (Figure 6-18) for the determination of the association/dissociation constants were conducted as indicated in the methods and instruments section above. The determined values for K_{ass} and K_{diss} are listed in Table 6-7:

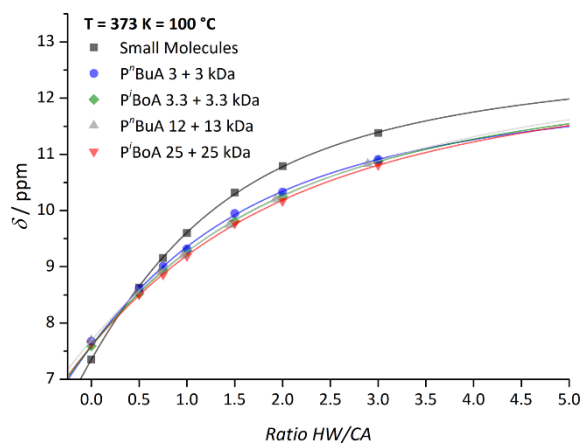


Figure 6-18 Chemical shifts observed for different ratios of HW/CA species of different molecular weights at 100 °C ($c_{\text{CA}} = 2 \text{ mmol L}^{-1}$).

Table 6-7 Experimental equilibrium constant values for association (K_{ass}) and dissociation (K_{diss}) of differently sized hydrogen bonding diblocks determined via ¹H HT NMR titration ($c_{\text{CA}} = 2 \text{ mmol L}^{-1}$).

Sample	K_{ass}	$K_{\text{diss}} * 10^4$
CA + HW Small Molecule	562.3	17.8
CA- + HW-P ⁿ BuA _{small}	350.9	28.5
CA- + HW-P ⁱ BoA _{small}	332.1	30.1
CA- + HW-P ⁿ BuA _{med.}	274.3	36.5
CA- + HW-P ⁱ BoA _{large}	269.8	37.1

6.3.3 Syntheses from Section 3.5

Synthesis of the Cyanodithioester HDA Dilinker. The employed CDTE dilinker was readily available from Section 3.2 and 3.3, synthesized according to literature.¹³²

Synthesis of Cp Bifunctional Polymers. Readily available Cp difunctional poly(methyl acrylate) and poly(isobornyl acrylate) as employed in Section 3.2 and 3.3 were used. Similarly, a Cp difunctional polystyrene macromonomer (Figure 6-19) was synthesized according to literature via ARGET ATRP of styrene with a bromo difunctional initiator and a subsequent substitution of the bromine end-groups with Cp units via nickelocene.^{46, 90, 142} End-group fidelity was determined via ¹H NMR as ~99 %, $n \approx 25$.

Cp₂PMA: $M_{n,SEC} = 4800 \text{ g mol}^{-1}$, $\mathcal{D} = 1.09$

Cp₂PⁱBoA: $M_{n,SEC} = 10200 \text{ g mol}^{-1}$, $\mathcal{D} = 1.12$

Cp₂PS: $M_{n,SEC} = 5500 \text{ g mol}^{-1}$, $\mathcal{D} = 1.08$

Synthesis of Diels–Alder step-growth polymers. DA step-growth polymers (Figure 6-19) were synthesized according to Section 3.2 and 3.3.¹⁴² To achieve comparable results, it was aimed for a degree of polymerization $DP_n = \frac{M(\text{Adduct})}{(M(\text{Building Block})+M(\text{Dilinker}))/2}$ of 6-7.

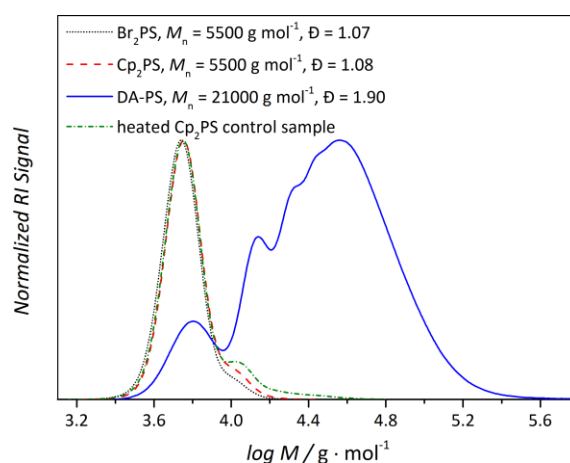


Figure 6-19 Exemplary SEC chromatograms of the dibromo precursor polystyrene (····), Cp difunctional polystyrene (----), Diels–Alder polystyrene (—) and control sample of heated Cp difunctional polystyrene without CDTE dilinker (-·-·) in THF at 35 °C.

Synthesis of HW-RAFT, CA + HW Small Molecule, CA-/HW-PⁱBoA (25 kDa). The materials and their association data were readily available from Section 3.4.

RAFT Polymerization of HW-Polyacrylates. The RAFT polymerization protocol of **HW-PⁱBoA (60 kDa)** was adapted from literature.³² **HW-RAFT** (17.9 mg, 0.018 mmol) and AIBN (0.3 mg, 0.002 mmol) were dissolved in isobornyl acrylate (1.9 mL, 8.99 mmol) and DMSO (25 μ L) in a Schlenk tube, which was deoxygenated by three freeze–pump–thaw cycles. The Schlenk tube was immersed in an oil bath at 70 °C for 22 min. The reaction was stopped by immersing the tube into liquid nitrogen. The polymer was precipitated five times into cold methanol, dried over Na₂SO₄ and the solvent was evaporated *in vacuo* for 24 h.

$$M_{n,SEC} = 50000 \text{ g mol}^{-1}, \bar{D} = 1.21, M_{NMR} = 60000 \text{ g mol}^{-1}$$

¹H NMR (400 MHz, CDCl₃) δ (ppm) = 8.38 (bs, 2H, H¹), 8.04-7.63 (m, 9H, H²), 4.62 (bm, backbone, H³), 4.10 (m, 2H, H⁴), 3.33 (t, 2H, H⁵), 2.60-0.70 (aliphatic protons of PⁱBoA).

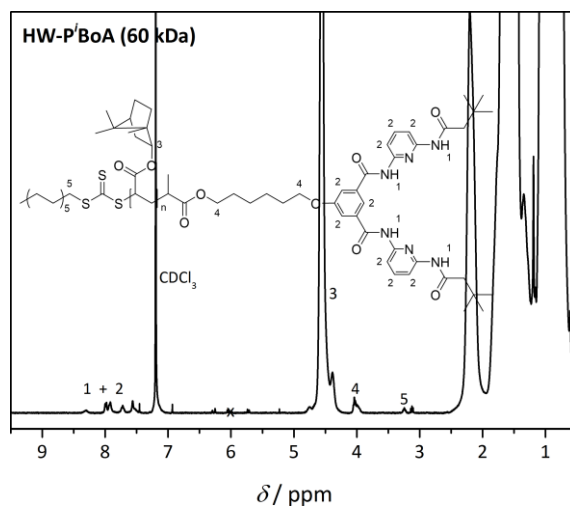


Figure 6-20 ¹H NMR (400 MHz, CDCl₃) of HW-PⁱBoA (60 kDa). The ratio of the integral values of the signals H¹⁺² and H⁵ allow for the determination of the CA end-group fidelity as ~99 % (x: residual monomer).

HT NMR Samples. All materials were dried over Na₂SO₄ as well as under reduced pressure for 24 h and stored in a desiccator over silica gel to avoid falsified measurements due to residual water. An end-group concentration of 6 mmol L⁻¹ was adjusted.

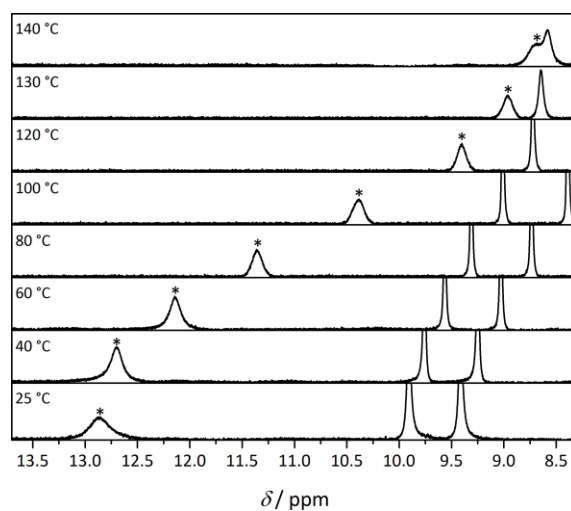


Figure 6-21 Expanded temperature dependent ^1H NMR spectra of equimolar amounts ($c = 6 \text{ mmol L}^{-1}$) of $\text{CA}_{\text{small molecule}}$ and HW- P^iBoA (60 kDa) in $\text{C}_2\text{D}_2\text{Cl}_4$ ($n_s = 128$) showing the debonding dependent shift of the CA imide proton resonance (*).

Competing interactions of polyacrylate backbones with the hydrogen bonding motifs were excluded via control measurements in Section 3.4. NMR titration was done according to literature,²⁵⁸ see Methods and Instruments for details.

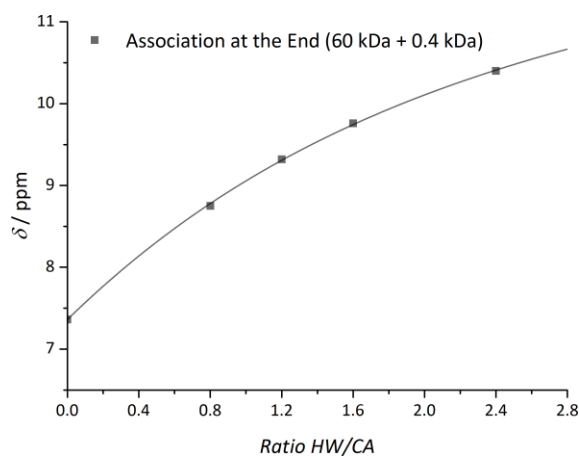
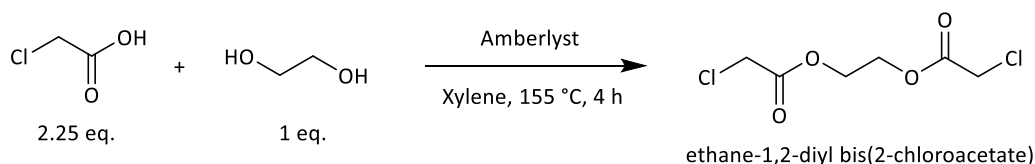


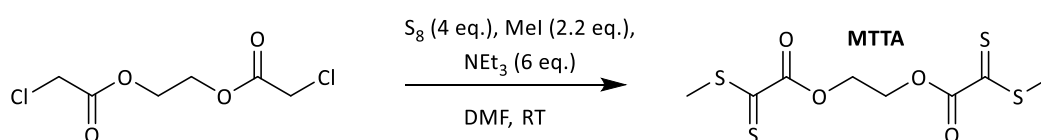
Figure 6-22 Chemical shifts observed for different ratios of $\text{CA}_{\text{small molecule}}$ + HW- P^iBoA (60 kDa) at $100 \text{ }^\circ\text{C}$ ($c_{\text{CA}} = 1 \text{ mmol L}^{-1}$ in $\text{C}_2\text{D}_2\text{Cl}_4$).

6.3.4 Syntheses from Chapter 4

Synthesis of MTTA. The synthetic procedure for the formation of MTTA was planned and designed at the KIT and performed by Uwe Paulmann and Christian Richter at Evonik Industries.



A literature procedure was adopted and refined to generate the desired dithiooxalate dilinker.^{272, 273} Ethylene glycol (124.1 g, 2.0 mol) and chloroacetic acid (472.5 g, 5.0 mol) were dissolved in 1 L xylol, Amberlyst-15 (16.0 g) was added and the reaction mixture was heated to 165 °C under reflux in a Dean-Stark apparatus for 4 h. After cooling, Amberlyst was separated via decantation and the reaction mixture was washed three times with saturated sodium carbonate solution (2x250 mL, 1x70 mL) and two times with brine (250 mL). The organic phase was dried over magnesium sulfate and the solvent was removed under reduced pressure. The product was further purified via vacuum distillation at 170 °C, yielding crystalline ethane-1,2-diyl bis(2-chloroacetate) (357.1 g, 83 %).



Subsequently, triethylamine (282 g, 2.79 mol) was added to a suspension of sulphur (60 g, 1.86 mol) in DMF (1.1 L) under nitrogen. Slowly, a solution of ethane-1,2-diyl bis(2-chloroacetate) (100 g, 0.47 mol) in 100 mL DMF (dry) was added dropwise over 1 h to allow the reaction mixture to reach 40 °C. The mixture was stirred for an additional 3 h at ambient temperature and then cooled to 10 °C. Methyl iodide (145 g, 64 mL, 1.02 mol) was added dropwise within 1 h while keeping the temperature of the reaction mixture ≤ 10 °C, whereafter the mixture was stirred for an additional 2 h at 10 °C. The crude mixture was diluted with methyl *tert*-butyl ether (5 L) and the emerging yellow-orange precipitate was filtered-off via a short column of silica. The filtrate was washed two times each with 0.5 M sulphuric acid (1.6 L), water (1.6 L) and a 4:1 mixture of brine and saturated sodium

hydrogen carbonate solution (1.2 L). The organic phase was dried over magnesium sulfate and the solvent was removed under reduced pressure to yield the dark violet oily solid product (119.7 g, 83 %). Further purification can be achieved via flash chromatography (cyclohexane/ethylacetate 8:1, silica, $R_f = 0.38$). Although the product seems to be stable under ambient conditions and also – at least for limited time scales – at elevated temperatures, a storage in the freezer is recommended due to its reactivity and literature reports of smaller, fully liquid dithiooxalate species.²⁶⁹

ESI-MS (M+Na)⁺ C₈H₁₀O₄S₄+Na⁺ theoretical: 320.9360 Da, experimental: 320.9370 Da

¹H NMR (400 MHz, CDCl₃) δ (ppm) = 4.64 (s, 4H, -O-CH₂-), 2.68 (s, 6H, -S-CH₃).

¹³C NMR (100 MHz, CDCl₃) δ (ppm) = 215.75 (-C=S), 160.02 (-C=O), 64.20 (-O-CH₂-), 19.75 (-CH₃).

Synthesis of Cp₂P^tBuA. Synthesis of Cp₂P^tBuA was carried out similar to Section 3.3, according to a literature procedure earlier established by us.^{142, 229} $M_n = 6000 \text{ g mol}^{-1}$, $D = 1.12$

Synthesis of Diels–Alder adducts of MTTA with diverse Dienes:

MTTA + Cp. In a typical procedure, MTTA (20 mg, 0.67 mmol \cong 0.13 mmol dithiooxalate end-groups) was dissolved in 1 mL acetonitrile, transferred into a UV/Vis cuvette and heated to the desired reaction temperature (25 or 50 °C). Cyclopentadiene (depending on the desired reaction conditions 1.2 eq., 13.3 μL , 0.16 mmol or 5.0 eq., 55.4 μL , 0.67 mmol) was added and the reaction mixture was shaken to guarantee good intermixture. The reaction process was tracked immediately in a UV/Vis spectrometer via the decreasing C=S double bond absorbance at 500 nm. Subsequently, the solvent and the excess of cyclopentadiene was evaporated and the slightly yellow product was characterized without further purification.

ESI-MS (M+Na)⁺ C₁₈H₂₂O₄S₄+Na⁺ theoretical: 453.0299 Da, experimental: 453.0315 Da

^1H NMR (400 MHz, CDCl_3) δ (ppm) = 6.54 (dd, 1 H, H^{a}), 6.43 (dd, 1 H, $\text{H}^{\text{a}'}$), 6.15 (dd, 1 H, H^{b}), 6.04 (dd, 1 H, $\text{H}^{\text{b}'}$), 4.53-4.20 (m, 4 H, H^{c}), 4.16 (s, 1 H, H^{d}), 4.05 (s, 1 H, $\text{H}^{\text{d}'}$), 3.90 (s, 1 H, H^{c}), 3.60 (s, 1 H, $\text{H}^{\text{c}'}$), 2.33-2.19 (m, 6 H, $\text{H}^{\text{f,f}'}$), 2.01-1.68 (m, 3 H, H^{g}), 1.58-1.22 (m, 3 H, $\text{H}^{\text{g}'}$).

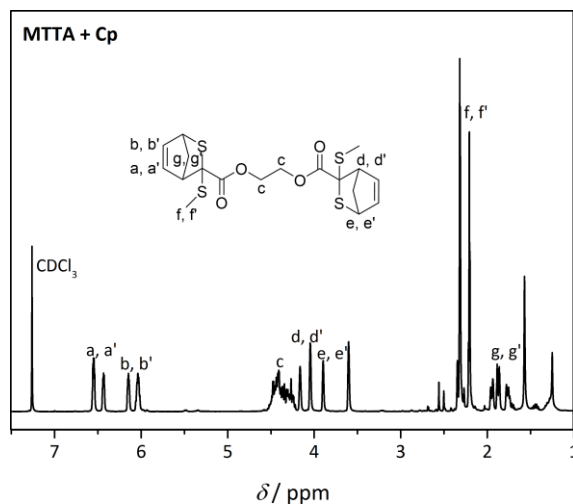


Figure 6-23 ^1H NMR (400 MHz, CDCl_3) of the DA adduct of MTTA and cyclopentadiene.

MTTA + 2,3-Dimethyl-1,3-butadiene

ESI-MS ($\text{M}+\text{Na}$) $^+$ $\text{C}_{20}\text{H}_{30}\text{O}_4\text{S}_4+\text{Na}^+$ theoretical: 485.0925 Da, experimental: 485.0941 Da

^1H NMR (400 MHz, CDCl_3) δ (ppm) = 4.50-4.31 (m, 4H, H^{a}), 3.28+2.84 (ABX, 2H, H^{b}), 2.88+2.44 (ABX, 2H, H^{c}), 2.18 (s, 6 H, H^{d}), 1.72 (s, 6 H, H^{e}), 1.69 (s, 6 H, $\text{H}^{\text{e}'}$).

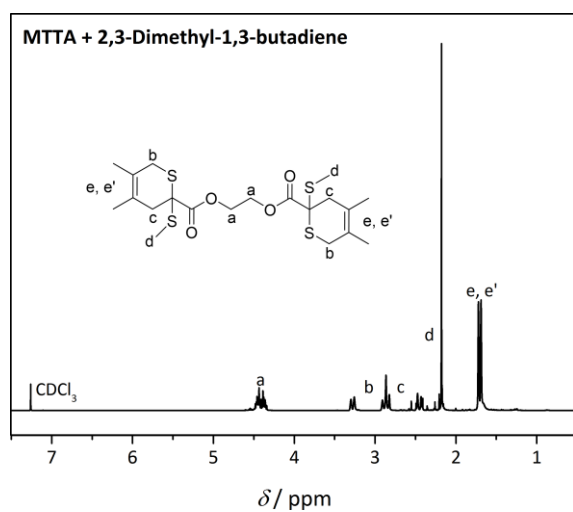


Figure 6-24 ^1H NMR (400 MHz, CDCl_3) of the DA adduct of MTTA and 2,3-dimethyl-1,3-butadiene.

MTTA + Sorbic Alcohol

ESI-MS (M+Na)⁺ C₂₀H₃₀O₆S₄+Na⁺ theoretical: 517.0823 D Da, experimental: 517.0843 Da

¹H NMR (400 MHz, CDCl₃) δ (ppm) = 5.92-5.59 (m, 4 H, H^a), 4.53-4.29 (m, 4 H, H^b), 4.11-3.53 (m, 6 H, H^{c,c',d,d'}), 3.22-2.68 (m, 2 H, H^{e,e'}), 2.24-2.16 (m, 6 H, H^{f,f'}), 1.39-1.12 (m, 6 H, H^{g,g'}).

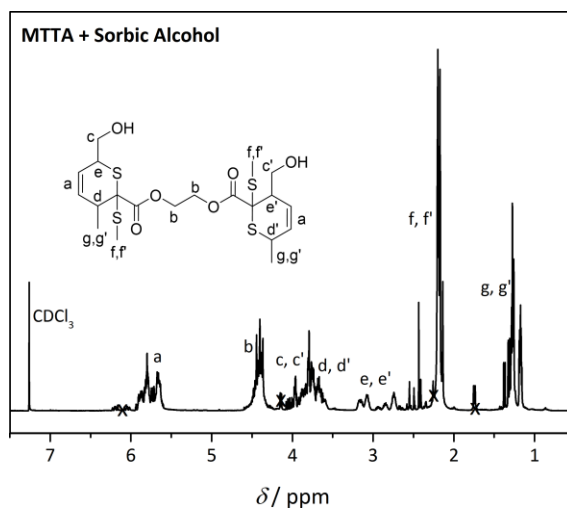


Figure 6-25 ¹H NMR (400 MHz, CDCl₃) of the DA adduct of MTTA and sorbic alcohol; x: residual sorbic alcohol.

MTTA + Ethyl Sorbate

ESI-MS (M+Na)⁺ C₂₄H₃₄O₈S₄+Na⁺ theoretical: 601.1034 Da, experimental: 601.1062 Da

¹H NMR (400 MHz, CDCl₃) δ (ppm) = 5.97-5.76 (m, 4 H, H^a), 4.48-4.35 (m, 4 H, H^b), 4.25-4.10 (m, 4 H, H^{c,c'}), 4.13-3.95 (m, 2 H, H^{d,d'}), 3.71-3.52 (m, 2 H, H^{e,e'}), 2.19+2.16 (s, 6 H, H^{f,f'}), 1.39-1.19 (m, 12 H, H^{g,g',h}).

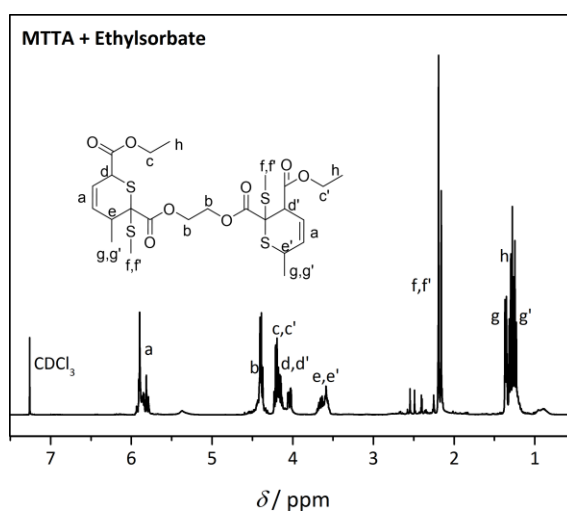


Figure 6-26 ¹H NMR (400 MHz, CDCl₃) of the DA adduct of MTTA and ethyl sorbate.

MTTA + IPDI-SA

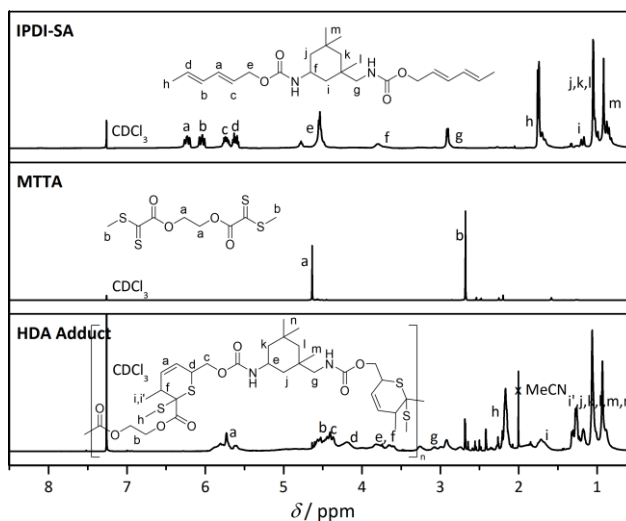


Figure 6-27 ^1H NMR (400 MHz, CDCl_3) of IPDI-SA (top), MTTA (middle) and their step-growth adduct (bottom). Isophorone bis(sorbic carbamate) (IPDI-SA) was provided by Evonik Industries. From Figure 6-27, it can be seen that all diene groups of the IPDI-SA have reacted in a Diels–Alder reaction with the MTTA dilinker. The implied step-growth behavior is evidenced via SEC in Figure 4-6 (b). The degree of polymerization is calculated as:

$$DP_n = \frac{M(\text{Adduct})}{(M(\text{Building Block}) + M(\text{Dilinker}))/2}$$

Although the employed SEC calibration via polystyrene standards is likely inadequate for the material at hand, the method allows for a convenient visualization of the step-growth. The assumedly low DP_n as well as the residual starting material visible in the SEC trace (Figure 4-6 (b)) are probably a result of a non-functional IPDI species and is not arising due to limited reactivity, as no dienes can be identified via NMR anymore (Figure 6-27).

6.4 Computational Data

The quantum chemical calculations were performed by collaboration partners under the supervision from Prof. Michelle Coote at the Australian National University (Canberra). Thus, only the most important and final results are summarized here. For details on the employed methodology as well as the optimized geometries in the form of Gaussian archive entries refer to the original publications.^{123, 142, 259}

6.4.1 Computational Data from Section 3.2 and 3.3

The quantum chemically calculated thermodynamic data for the investigation of a chain mass, length and stiffness effect – exemplified via the hetero Diels–Alder model reaction of a cyanodithioester linker and Cp functional polymer blocks of differing length, mass or chain mobility – can be found below.

Table 6-8 Calculated entropies, enthalpies and free energies of DA reactions in the gas phase and in toluene solution at 25 °C.

<i>n=m=</i>	<i>R</i>	ΔS_{trans}	ΔS_{rot}	ΔS_{vib}	ΔS_{tot}	$-T\Delta S$	ΔE_{DFT}	ΔE_{ONIOM}	ΔH^{0K}	ΔH^{298K}	ΔG_{gas}	ΔG_{soln}
		$\text{J mol}^{-1} \text{K}^{-1}$		kJ mol^{-1}								
Extended chain conformers												
0	n/a	-176.7	-140.9	27.3	-290.4	86.6	-119.4	-119.3	-106.8	-112.2	-25.6	-27.0
1	MA	-179.7	-147.9	49.2	-278.4	83.0	-118.4	-118.3	-106.3	-111.3	-28.3	-29.9
	^t BuA	-180.7	-150.1	41.3	-289.6	86.3	-125.1	-125.0	-112.3	-117.8	-31.4	-30.8
	ⁱ BuA	-180.7	-150.5	29.0	-302.2	90.1	-120.8	-120.7	-107.4	-113.0	-22.9	-24.9
	ⁱ BoA	-182.1	-152.2	50.6	-283.7	84.6	-119.8	-119.6	-106.9	-111.9	-27.4	-29.1
2	MA	-181.5	-151.5	75.4	-257.6	76.8	-109.8	-109.7	-98.4	-102.7	-25.9	-29.9
	^t BuA	-182.8	-153.5	48.2	-288.1	85.9	-115.0	-114.9	-102.4	-107.2	-21.3	-24.7
	ⁱ BuA	-182.8	-153.9	44.9	-291.8	87.0	-116.9	-116.8	-103.8	-109.5	-22.5	-22.5
	ⁱ BoA	-184.3	-155.8	82.8	-257.2	76.7	-104.7	-104.6	-91.3	-94.0	-17.4	-16.9
Lowest energy conformers												
0	n/a	-176.7	-139.9	64.3	-252.4	75.2	-119.8	-119.7	-106.8	-109.9	-34.6	-32.1
1	MA	-179.7	-147.3	29.6	-297.4	88.7	-172.4	-172.3	-157.0	-162.0	-73.3	-63.9
	^t BuA	-180.7	-148.0	7.3	-321.4	95.8	-173.5	-173.4	-156.6	-163.0	-67.1	-54.8
	ⁱ BuA	-180.7	-146.4	56.9	-270.2	80.6	-137.7	-137.6	-122.3	-126.3	-45.7	-45.9
	ⁱ BoA	-182.1	-149.0	60.4	-270.7	80.7	-137.3	-137.2	-122.0	-126.4	-45.7	-48.8
2	MA	-181.5	-152.1	-6.1	-339.7	101.3	-159.4	-159.3	-143.8	-150.5	-49.2	-26.2
	^t BuA	-182.8	-152.0	-23.2	-358.0	106.7	-150.6	-150.5	-132.4	-140.2	-33.5	-13.9
	ⁱ BuA	-182.8	-152.5	1.0	-334.3	99.7	-153.0	-152.9	-132.4	-139.3	-39.7	-20.5
	ⁱ BoA	-184.3	-155.2	52.3	-287.2	85.6	-151.8	-151.7	-136.7	-140.3	-54.7	-24.6

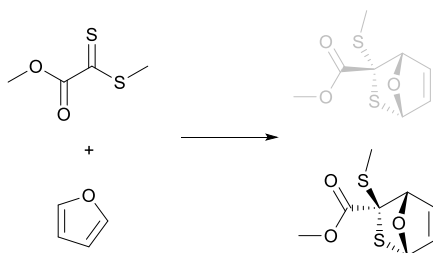
Table 6-9 Contributions to the free energies of all species at 25 °C. ^a

<i>n=m=</i>	<i>R</i>	<i>Species</i>	<i>ZPVE</i> / kJ mol ⁻¹	<i>TC</i> ^{298K} / kJ mol ⁻¹	ΔS_{trans} / J mol ⁻¹ K ⁻¹	ΔS_{rot} / J mol ⁻¹ K ⁻¹	ΔS_{vib} / J mol ⁻¹ K ⁻¹	<i>E</i> _{DFT} / Hartree	ΔG_{solv} / kcal mol ⁻¹
Extended chain conformers									
		CDTE	1631.6414	125.6937	189.8686	172.6474	899.7482	-3352.88164	-25.18
0	n/a	Cp ₂ R _{nm}	1230.4532	77.0501	182.0938	153.5117	493.9101	-1156.76869	-15.65
		DA	2874.6165	197.3387	195.2222	185.2170	1420.9089	-4509.69581	-39.27
1	MA	Cp ₂ R _{nm}	1747.3673	114.3286	186.9863	164.5139	773.3666	-1769.51907	-21.11
		DA	3391.0211	234.9987	197.1553	189.2908	1722.2989	-5122.44581	-44.77
	^t BuA	Cp ₂ R _{nm}	2175.9329	136.0542	188.8221	168.3404	929.3106	-2005.30301	-23.54
		DA	3820.2958	256.2532	198.0010	190.8449	1870.3272	-5358.23231	-46.66
	ⁱ BuA	Cp ₂ R _{nm}	2182.0835	135.7107	188.8221	168.1402	942.5430	-2005.29037	-24.07
		DA	3827.0276	255.8036	198.0010	190.2962	1871.2812	-5358.21803	-47.83
	ⁱ BoA	Cp ₂ R _{nm}	2836.8834	161.2541	191.7106	173.1194	1107.3776	-2472.01821	-28.11
		DA	4481.2816	281.9043	199.4683	193.5855	2057.7479	-5824.94546	-51.82
2	MA	Cp ₂ R _{nm}	2263.1802	151.0864	190.4912	172.2773	1055.7870	-2382.27614	-26.77
		DA	3906.1582	272.4673	198.8285	193.4364	2030.9266	-5735.19961	-51.01
	^t BuA	Cp ₂ R _{nm}	3121.4899	194.0171	193.1686	177.3284	1349.2083	-2853.83932	-30.43
		DA	4765.5947	314.9215	200.2721	196.5071	2297.1203	-6206.76474	-54.53
	ⁱ BuA	Cp ₂ R _{nm}	3134.6214	193.8876	193.1686	177.9135	1379.6645	-2853.81577	-32.31
		DA	4779.2142	313.9018	200.2721	196.6235	2324.3575	-6206.74192	-55.60
	ⁱ BoA	Cp ₂ R _{nm}	4446.5582	243.7436	197.0754	184.8147	1685.5159	-3787.26716	-39.37
		DA	6091.4842	366.6700	202.6302	201.6869	2668.1104	-7140.18867	-62.55

Lowest energy conformers									
0	n/a	Cp ₂ R _{nm}	1636.4399	122.4521	189.8686	164.7263	789.9214	-3352.90249	-22.08
		DA	1232.5235	74.6264	182.0938	147.3629	425.6339	-1156.77903	-13.28
1	MA	Cp ₂ R _{nm}	2881.8795	193.9691	195.2222	172.2027	1279.8073	-4509.72714	-32.86
		DA	1750.1724	111.3840	186.9863	157.4583	704.1694	-1769.53529	-17.95
	^t BuA	Cp ₂ R _{nm}	3401.9044	228.8460	197.1553	174.9131	1523.6806	-5122.50343	-35.90
		DA	2179.5628	132.8813	188.8221	159.6643	839.2074	-2005.32394	-18.52
	ⁱ BuA	Cp ₂ R _{nm}	3832.7661	249.0228	198.0010	176.4008	1636.3850	-5358.29251	-35.77
		DA	2186.0904	131.2480	188.8221	158.5328	812.4027	-2005.32110	-17.28
	ⁱ BoA	Cp ₂ R _{nm}	3837.8255	249.6885	198.0010	176.8598	1659.1784	-5358.27603	-37.50
		DA	2843.0628	156.1613	191.7106	163.9197	962.2787	-2472.05114	-20.08
2	MA	Cp ₂ R _{nm}	4494.7328	274.2276	199.4683	179.6939	1812.5741	-5825.00594	-41.01
		DA	2267.1863	147.5858	190.4912	163.6835	948.0688	-2382.29937	-21.09
	^t BuA	Cp ₂ R _{nm}	3919.1827	263.3122	198.8285	176.3090	1731.8758	-5735.26258	-35.78
		DA	3126.0584	190.6702	193.1686	167.1302	1244.5727	-2853.87288	-23.41
	ⁱ BuA	Cp ₂ R _{nm}	4780.5524	305.3181	200.2721	179.8408	2011.3248	-6206.83272	-38.90
		DA	3136.2416	190.2279	193.1686	167.9530	1257.8938	-2853.84793	-27.24
	ⁱ BoA	Cp ₂ R _{nm}	4793.1644	305.7227	200.2721	180.1388	2048.8095	-6206.80868	-42.85
		DA	6102.3206	357.6053	202.6302	183.5647	2369.4788	-7140.27142	-42.82

^a ONIOM electronic energy correction from the core-layer reaction is equal to 0.111 kJ mol⁻¹.

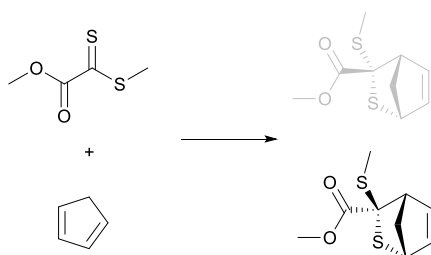
6.4.2 Computational Data from Chapter 4

Furan + MTTA_{half} ($T_{\log K=2.6} = -169\text{ }^{\circ}\text{C}$)

Key thermodynamic parameters and equilibrium constants in acetonitrile as a function of temperature, using M05-2X/6-31G* geometries and frequencies.

T	$\log K$	ΔG^*_{soln}	$\Delta H(g)$	$\Delta S(g)$	$\Delta\Delta G^*_{\text{solv}}$
$^{\circ}\text{C}$		kJ mol^{-1}	kJ mol^{-1}	$\text{J mol}^{-1}\text{K}^{-1}$	kJ mol^{-1}
-250	31.1	-13.8	-25.8	-164.8	7.1
-225	12.8	-11.8	-26.5	-185.4	5.1
-200	7.2	-10.1	-27.0	-193.8	3.5
-150	1.3	-3.0	-27.6	-200.3	1.1
-100	-1.1	3.7	-27.9	-202.1	-0.8
-50	-2.5	10.8	-27.9	-202.3	-2.3
0	-3.5	18.1	-27.8	-201.7	-3.5
25	-3.8	21.8	-27.7	-201.3	-3.9
50	-4.1	25.5	-27.5	-200.8	-4.4
100	-4.6	33.0	-27.1	-199.8	-5.1
150	-5.0	40.5	-26.7	-198.6	-5.7
200	-5.3	48.0	-26.1	-197.4	-6.2
250	-5.5	55.5	-25.6	-196.2	-6.6

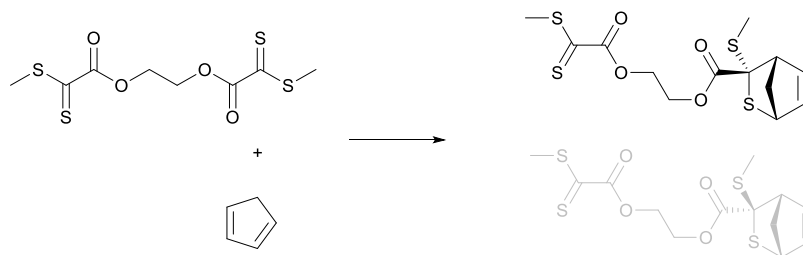
Cp + MTTA_{half} ($T_{\log K=2.6} = 166 \text{ }^{\circ}\text{C}$)



Key thermodynamic parameters and equilibrium constants in acetonitrile as a function of temperature, using M05-2X/6-31G* geometries and frequencies.

<i>T</i>	<i>log K</i>	ΔG^*_{soln}	$\Delta H(g)$	$\Delta S(g)$	$\Delta\Delta G^*_{\text{soln}}$
$^{\circ}\text{C}$		kJ mol^{-1}	kJ mol^{-1}	$\text{J mol}^{-1} \text{K}^{-1}$	kJ mol^{-1}
0	9.1	-47.6	-98.5	-206.6	1.7
25	7.7	-43.8	-98.5	-206.6	1.2
50	6.5	-40.0	-98.5	-206.4	0.7
100	4.5	-32.4	-98.3	-205.9	-0.2
150	3.0	-24.7	-98.0	-205.2	-0.9
200	1.9	-17.0	-97.6	-204.4	-1.5
250	0.9	-9.3	-97.2	-203.5	-2.1

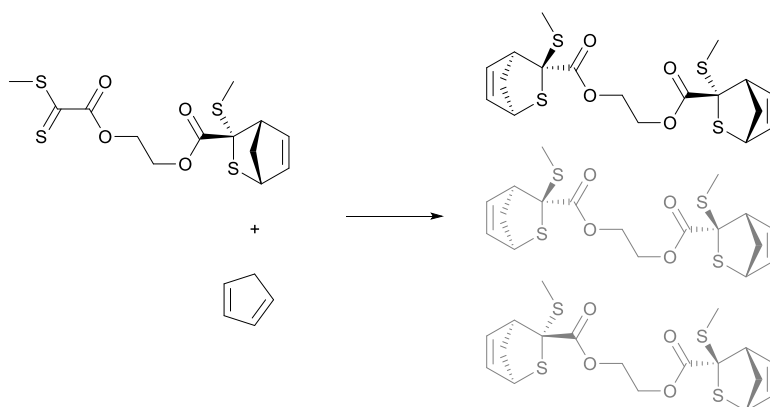
Cp + MTTA_{full} ($T_{\log K=2.6} = 113 \text{ }^\circ\text{C}$)



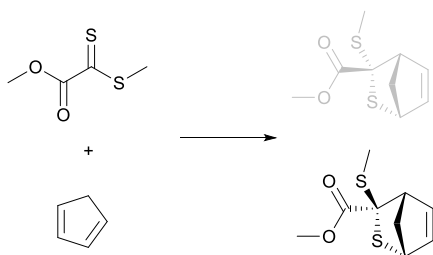
Key thermodynamic parameters and equilibrium constants in acetonitrile as a function of temperature, using M05-2X/6-31G* geometries and frequencies.

T	$\log K$	ΔG^*_{soln}	$\Delta H(g)$	$\Delta S(g)$	$\Delta\Delta G^*_{\text{solv}}$
$^\circ\text{C}$		kJ mol^{-1}	kJ mol^{-1}	$\text{J mol}^{-1} \text{K}^{-1}$	kJ mol^{-1}
0	9.0	-46.9	-108.7	-214.5	10.0
25	7.2	-41.3	-106.9	-214.6	9.3
50	5.7	-35.4	-104.9	-214.6	8.7
100	3.2	-22.9	-100.1	-214.3	7.6
150	1.2	-9.5	-94.4	-213.7	6.7
200	-0.5	4.7	-88.0	-212.9	6.0
250	-1.9	19.5	-80.8	-212.1	5.3

Cp + Cp-MTTA_{full} ($T_{\log K=2.6} = 87\text{ °C}$)



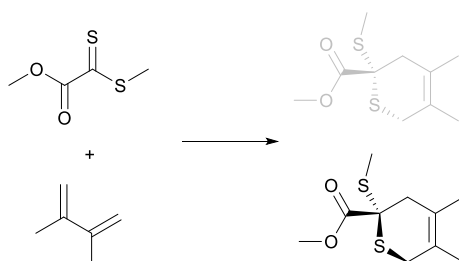
ONIOM Core (Cp-MTTA_{half}):



Key thermodynamic parameters and equilibrium constants in acetonitrile as a function of temperature, using M05-2X/6-31G* geometries and frequencies.

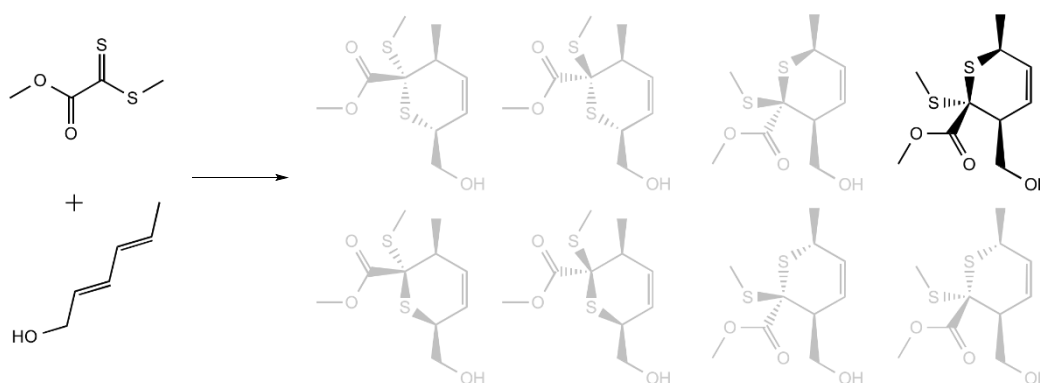
T	$\log K$	ΔG^*_{soln}	$\Delta H(g)$	$\Delta S(g)$	$\Delta\Delta G^*_{\text{solv}}$
°C		kJ mol ⁻¹	kJ mol ⁻¹	J mol ⁻¹ K ⁻¹	kJ mol ⁻¹
0	7.4	-38.5	-93.5	-209.1	4.8
25	5.8	-32.9	-91.6	-209.1	4.1
50	4.4	-27.1	-89.5	-209.0	3.6
100	2.1	-14.8	-84.7	-208.5	2.6
150	0.2	-1.6	-78.9	-207.9	1.7
200	-1.4	12.3	-72.4	-207.1	1.0
250	-2.7	26.8	-65.2	-206.2	0.4

DMBD + MTTA_{half} ($T_{\log K=2.6} = 427\text{ °C}$)



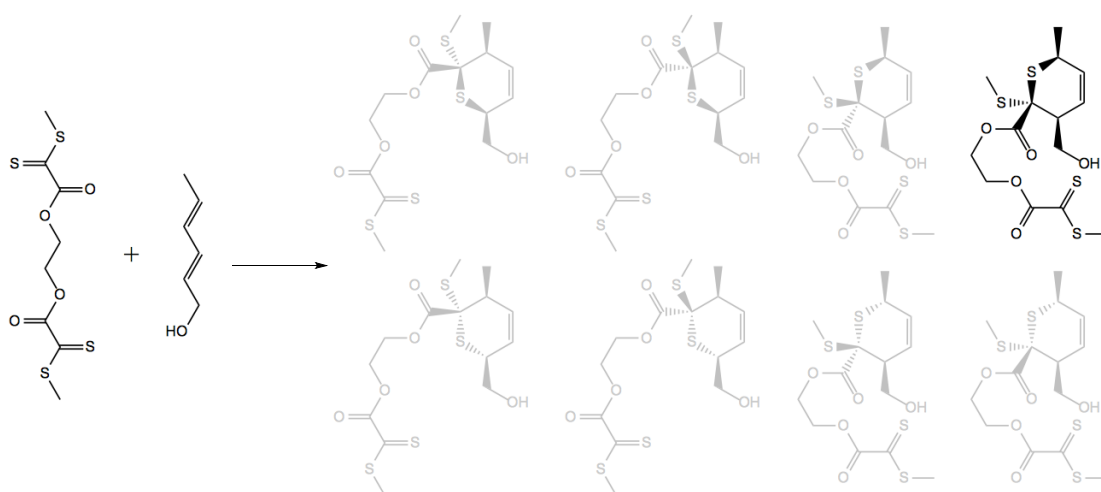
Key thermodynamic parameters and equilibrium constants in acetonitrile as a function of temperature, using M05-2X/6-31G* geometries and frequencies.

<i>T</i>	<i>log K</i>	ΔG^*_{soln}	$\Delta H(g)$	$\Delta S(g)$	$\Delta\Delta G^*_{solv}$
°C		kJ mol^{-1}	kJ mol^{-1}	$\text{J mol}^{-1} \text{K}^{-1}$	kJ mol^{-1}
0	17.5	-91.3	-133.2	-188.4	-3.4
25	15.4	-88.1	-133.1	-188.2	-4.0
50	13.7	-84.8	-133.1	-188.0	-4.5
100	10.9	-78.2	-132.9	-187.6	-5.5
150	8.8	-71.4	-132.7	-187.0	-6.2
200	7.1	-64.7	-132.4	-186.4	-6.9
250	5.8	-57.9	-132.1	-185.7	-7.4
300	4.7	-51.1	-131.7	-184.9	-7.9
350	3.7	-44.3	-131.2	-184.1	-8.3

Sorbic Alcohol + MTTA_{half} ($T_{\log K=2.6} = 240\text{ }^{\circ}\text{C}$)


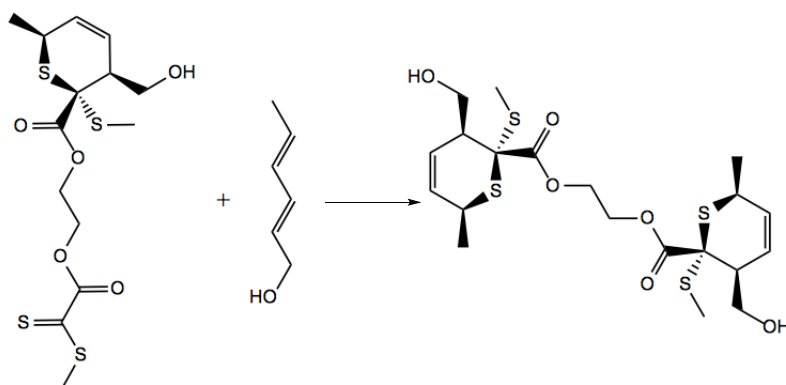
Key thermodynamic parameters and equilibrium constants in acetonitrile as a function of temperature, using M05-2X/6-31G* geometries and frequencies.

<i>T</i>	<i>log K</i>	ΔG^*_{soln}	$\Delta H(g)$	$\Delta S(g)$	$\Delta\Delta G^*_{\text{soln}}$
$^{\circ}\text{C}$		kJ mol^{-1}	kJ mol^{-1}	$\text{J mol}^{-1} \text{K}^{-1}$	kJ mol^{-1}
0	12.0	-62.9	-134.0	-234.9	10.8
25	10.4	-59.6	-134.1	-235.2	9.1
50	9.1	-56.0	-134.1	-235.3	7.6
100	6.8	-48.5	-134.1	-235.1	5.2
150	5.0	-40.4	-133.9	-234.6	3.4
200	3.5	-31.9	-133.6	-233.9	2.1
250	2.3	-23.3	-133.2	-233.1	1.0
300	1.3	-14.5	-132.7	-232.3	0.1
350	0.5	-5.7	-132.2	-231.4	-0.6
400	-0.2	3.1	-131.7	-230.6	-1.2

Sorbic Alcohol + MTTA_{full} ($T_{\log K=2.6} = 340\text{ °C}$)


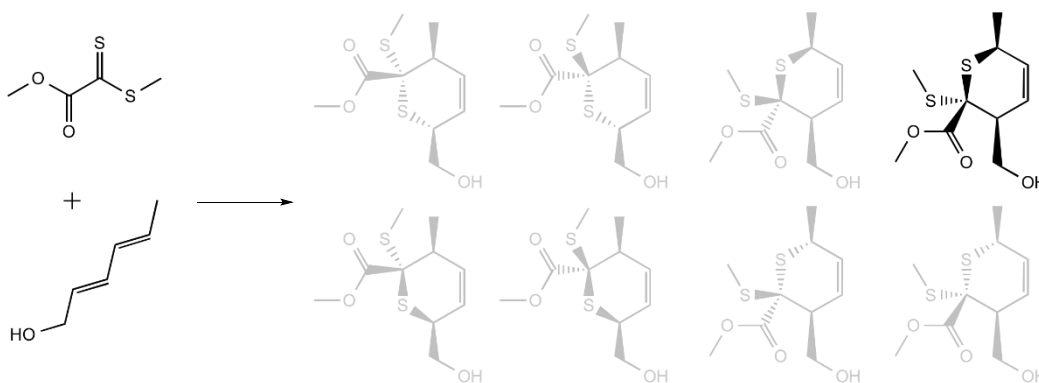
Key thermodynamic parameters and equilibrium constants in acetonitrile as a function of temperature, using M05-2X/6-31G* geometries and frequencies.

T	$\log K$	ΔG^*_{soln}	$\Delta H(g)$	$\Delta S(g)$	$\Delta \Delta G^*_{\text{solv}}$
°C		kJ mol^{-1}	kJ mol^{-1}	$\text{J mol}^{-1} \text{K}^{-1}$	kJ mol^{-1}
0	16.8	-87.6	-162.5	-243.0	15.3
25	14.8	-84.2	-162.6	-243.3	13.5
50	13.0	-80.6	-162.6	-243.3	11.9
100	10.2	-72.9	-162.5	-243.1	9.3
150	8.0	-64.5	-162.3	-242.6	7.4
200	6.2	-55.8	-162.0	-241.8	5.9
250	4.7	-46.8	-161.6	-241.0	4.8
300	3.4	-37.7	-161.1	-240.1	3.9
350	2.4	-28.5	-160.6	-239.2	3.1
400	1.5	-19.3	-160.0	-238.3	2.4

Sorbic Alcohol + Sorbic Alcohol-MTTA_{full} ($T_{\log K=2.6} = 114\text{ }^{\circ}\text{C}$)


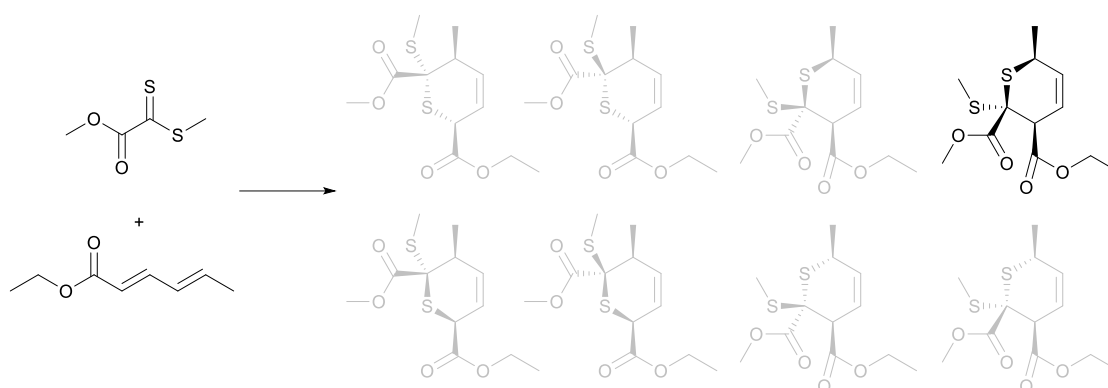
Conformational/isomer searching not performed – isomer and conformation chosen based on the strong preference of SA-MTTA_{half} and SA-MTTA_{full} for the given structure.

The debonding temperature of the first sorbic alcohol from the SA-MTTA_{full}–SA adduct is much lower than for the cleavage of the second sorbic alcohol as the SA-MTTA_{full} adduct is stabilized via strong hydrogen bonding interactions.

ONIOM Core (Sorbic Alcohol-MTTA_{half}):


Key thermodynamic parameters and equilibrium constants in acetonitrile as a function of temperature, using M05-2X/6-31G* geometries and frequencies.

<i>T</i>	<i>log K</i>	ΔG^{*soln}	$\Delta H(g)$	$\Delta S(g)$	$\Delta\Delta G^{*solv}$
°C		kJ mol ⁻¹	kJ mol ⁻¹	J mol ⁻¹ K ⁻¹	kJ mol ⁻¹
0	7.2	-37.5	-116.1	-242.8	8.2
25	5.9	-33.9	-116.2	-243.0	6.6
50	4.9	-30.0	-116.2	-243.1	5.3
100	3.1	-21.9	-116.1	-242.9	3.0
150	1.6	-13.3	-115.9	-242.3	1.4
200	0.5	-4.4	-115.6	-241.6	0.1
250	-0.5	4.7	-115.2	-240.8	-0.9
300	-1.3	13.9	-114.7	-239.9	-1.7
350	-1.9	23.2	-114.2	-239.0	-2.4
400	-2.5	32.4	-113.6	-238.2	-3.0

Ethyl sorbate + MTTA_{half} ($T_{\log K=2.6} = 225\text{ °C}$)

Key thermodynamic parameters and equilibrium constants in acetonitrile as a function of temperature, using M05-2X/6-31G* geometries and frequencies.

T	$\log K$	ΔG^*_{soln}	$\Delta H(g)$	$\Delta S(g)$	$\Delta\Delta G^*_{\text{solv}}$
°C		kJ mol ⁻¹	kJ mol ⁻¹	J mol ⁻¹ K ⁻¹	kJ mol ⁻¹
0	12.2	-63.8	-122.5	-231.1	2.6
25	10.4	-59.6	-122.5	-231.1	1.9
50	8.9	-55.2	-122.4	-231.0	1.3
100	6.5	-46.5	-122.2	-230.5	0.3
150	4.7	-37.7	-121.9	-229.7	-0.5
200	3.2	-28.9	-121.5	-228.8	-1.2
250	2.0	-20.1	-121.1	-227.8	-1.8

Furan + MTTA_{half}, components of Solution Free Energy Calculations– values in E_h unless otherwise specified

Species	Entropy (298K) / J mol ⁻¹ K ⁻¹	$H^{298} - H^0$	ZPVE	HLC	$E[\text{M05-2X}/$ 6-31G* SMD, gas geom]	$E[\text{M05-2X}/$ 31G* SMD, sol geom]	$E[\text{MP2}/$ 6-31G*]	$E[\text{MP2}/$ G3MP2Large]	$E[\text{CCSD(T)}/$ 6-31G*]
Furan	273.3	0.004733	0.068875	-0.122369	-229.998527	-229.998551	-229.309880	-229.561891	-229.363438
MTTA _{half}	402.6	0.010476	0.097745	-0.216499	-1102.771496	-1102.771707	-1100.815553	-1101.328463	-1100.911710
Furan – MTTA _{half}	474.6	0.014218	0.170380	-0.338868	-1332.783794	-1332.784513	-1330.137845	-1330.903460	-1330.287758

Species	E^0 [G3MP2,CC]	H^{298} [G3MP2,CC]	G_{gas} (298K) [G3MP2,CC]	$\Delta G_{\text{sol}} (298\text{K})$ [COSMO(RS)]	E_{relax} [M06-2X/ 6-31G*, SMD]	G°_{sol} (298K) [G3MP2,CC]
Furan	-229.668943	-229.664210	-229.695248	-0.006368	-0.000024	-229.698573
MTTA _{half}	-1101.543374	-1101.532898	-1101.578621	-0.012714	-0.000211	-1101.588105
Furan – MTTA _{half}	-1331.221861	-1331.207643	-1331.261541	-0.020586	-0.000718	-1331.278390

Cp + MTTA, components of Solution Free Energy Calculations– values in E_h unless otherwise specified

Species	Entropy (298K) / J mol ⁻¹ K ⁻¹	$H^{298} - H^0$	ZPVE	HLC	E[M05-2X/ 6-31G* SMD, gas geom]	E[M05-2X/ 6-31G* SMD, sol geom]	E[MP2/ 6-31G*]	E[MP2/ G3MP2Large]	E[CCSD(T)/ 6-31G*]
Cp	280.9	0.005225	0.090763	-0.122369	-194.080257	-194.080278	-193.425083	-193.647864	-193.494232
MTTA _{half}	402.6	0.010476	0.097745	-0.216499	-1102.771496	-1102.771707	-1100.815553	-1101.328463	-1100.911710
MTTA	576.2	0.019177	0.177408	-0.423585	-2204.360345	-2204.360849	-2200.474347	-2201.480435	-2200.659468
Cp – MTTA _{half}	477.0	0.014411	0.194153	-0.338868	-1296.894881	-1296.895043	-1294.288452	-1295.024835	-1294.447126
Cp – MTTA (as product)	636.9	0.022724	0.274385	-0.545954	-2398.487115	-2398.487761	-2393.954324	-2395.184495	
Cp – MTTA (as reactant)	636.9	0.022724	0.274385	-0.545954	-2398.487115	-2398.487761	-2393.954324	-2395.184495	
Cp – MTTA – Cp	703.2	0.026632	0.370795	-0.668323	-2592.609090	-2592.609820	-2587.428620	-2588.882540	

Experimental Section

Species	E^0 [G3MP2,CC]	H^{298} [G3MP2,CC]	G_{gas} (298K) [G3MP2,CC]	ΔG_{solv} (298K) [COSMO(RS)]	E_{relax} [M06-2X/ 6-31G*, SMD]	G°_{sol} (298K) [G3MP2,CC]
Cp	-193.748619	-193.743394	-193.775294	-0.005554	-0.000021	-193.777808
MTTA _{half}	-1101.543374	-1101.532898	-1101.578621	-0.012714	-0.000211	-1101.588105
MTTA	-2201.310414	-2201.291237	-2201.356670	-0.026363	-0.000504	-2201.379510
Cp – MTTA _{half}	-1295.328224	-1295.313813	-1295.367977	-0.017812	-0.000162	-1295.382607
Cp – MTTA (as product)	-2395.098225	-2395.075501	-2395.147830	-0.028377	-0.000646	-2395.172542
Cp – MTTA (as reactant)	-2394.812236	-2394.789511	-2394.861841	-0.028377	-0.000646	-2394.886553
Cp – MTTA – Cp	-2588.594573	-2588.567941	-2588.647796	-0.032355	-0.000730	-2588.676402

DMBD + MTTA_{half}, components of Solution Free Energy Calculations– values in E_h unless otherwise specified

Species	Entropy (298K) / J mol ⁻¹ K ⁻¹	$H^{298} - H^0$	ZPVE	HLC	$E[\text{M05-2X}/$ 6-31G* SMD, gas geom]	$E[\text{M05-2X}/$ 6-31G* SMD, sol geom]	$E[\text{MP2}/$ 6-31G*]	$E[\text{MP2}/$ G3MP2Large]	$E[\text{CCSD(T)}/$ 6-31G*]
DMBD	332.3	0.008107	0.139527	-0.160021	-234.586554	-234.586578	-233.762827	-234.059894	-233.857046
MTTA _{half}	402.6	0.010476	0.097745	-0.216499	-1102.771496	-1102.771707	-1100.815553	-1101.328463	-1100.911710
DMBD – MTTA _{half}	546.7	0.018040	0.241647	-0.376520	-1337.419616	-1337.420174	-1334.639905	-1335.449314	-1334.823870

Species	E^0 [G3MP2,CC]	H^{298} [G3MP2,CC]	G_{gas} (298K) [G3MP2,CC]	G_{solv} (298K) [COSMO(RS)]	E_{relax} [M06-2X/ 6-31G*, SMD]	G°_{sol} (298K) [G3MP2,CC]
DMBD	-234.174607	-234.166501	-234.204230	-0.004580	-0.000023	-234.205768
MTTA _{half}	-1101.543374	-1101.532898	-1101.578621	-0.012714	-0.000211	-1101.588105
DMBD – MTTA _{half}	-1335.768151	-1335.750112	-1335.812190	-0.018814	-0.000559	-1335.827427

Sorbic alcohol + MTTA, components of Solution Free Energy Calculations– values in E_h unless otherwise specified

Species	Entropy (298K) / J mol ⁻¹ K ⁻¹	$H^{298} - H^0$	ZPVE	HLC	E [M05-2X/ 6-31G* SMD, gas geom]	E [M05-2X/ 6-31G* SMD, sol geom]	E [MP2/ 6-31G*]	E [MP2/ G3MP2Large]	E [CCSD(T)/ 6-31G*]
SA	376.8	0.009635	0.143924	-0.188260	-309.792225	-309.792439	-308.786687	-309.169559	-308.886143
MTTA _{half}	403.9	0.010523	0.097640	-0.216499	-1102.770887	-1102.771697	-1100.815552	-1101.328457	-1100.911714
MTTA	576.2	0.019177	0.177408	-0.423585	-2204.360345	-2204.360849	-2200.474347	-2201.480435	-2200.659468
SA – MTTA _{half}	545.5	0.018238	0.247853	-0.404759	-1412.616091	-1412.618356	-1409.660602	-1410.560199	-1409.849476
SA - MTTA	709.7	0.026826	0.327454	-0.611845	-2514.216669	-2514.217497	-2509.331850	-2510.724004	-2509.608480
SA - MTTA - SA	843.4	0.034651	0.477532	-0.800105	-2824.049170	-2824.054470	-2818.167199	-2819.948908	

Species	E^0 [G3MP2,CC]	H^{298} [G3MP2,CC]	G_{gas} (298K) [G3MP2,CC]	G_{solv} (298K) [COSMO(RS)]	E_{relax} [M06-2X/ 6-31G*, SMD]	G^o_{sol} (298K) [G3MP2,CC]
SA	-309.313351	-309.303716	-309.346501	-0.010945	-0.000215	-309.354212
MTTA _{half}	-1101.543478	-1101.532955	-1101.578818	-0.012773	-0.000810	-1101.587762
MTTA	-2201.911733	-2201.892556	-2201.957988	-0.026363	-0.000504	-2201.980829
SA - MTTA _{half}	-1410.905979	-1410.887741	-1410.949685	-0.020259	-0.002265	-1410.964660
SA - MTTA	-2511.285025	-2511.258199	-2511.338789	-0.032184	-0.000828	-2511.367127
SA - MTTA - SA	-2820.065009	-2820.030359	-2820.126136	-0.040603	-0.005300	-2820.158420

Ethyl sorbate + MTTA, components of Solution Free Energy Calculations– values in E_h unless otherwise specified

Species	Entropy (298K) / J mol ⁻¹ K ⁻¹	$H^{298} - H^0$	ZPVE	HLC	$E[\text{M05-2X}/$ 6-31G* SMD, gas geom]	$E[\text{M05-2X}/$ 6-31G* SMD, sol geom]	$E[\text{MP2}/$ 6-31G*]	$E[\text{MP2}/$ G3MP2Large]	$E[\text{CCSD(T)}/$ 6-31G*]
Ethylsorbate	442.2	0.012656	0.182196	-0.263564	-462.450496	-462.450663	-461.017407	-461.555792	-461.146024
MTTA _{half}	402.6	0.010476	0.097745	-0.216499	-1102.771496	-1102.771707	-1100.815553	-1101.328463	-1100.911710
Ethsorb. – MTTA _{half}	613.7	0.021663	0.285046	-0.480063	-1565.271285	-1565.271840	-1561.886457	-1562.941204	-1562.104558

Species	E^0 [G3MP2,CC]	H^{298} [G3MP2,CC]	G_{gas} (298K) [G3MP2,CC]	G_{solv} (298K) [COSMO(RS)]	E_{relax} [M06-2X/ 6-31G*, SMD]	G^o_{sol} (298K) [G3MP2,CC]
Ethylsorbate	-461.765776	-461.753121	-461.803335	-0.011957	-0.000167	-461.812273
MTTA _{half}	-1101.543374	-1101.532898	-1101.578621	-0.012714	-0.000211	-1101.588316
Ethsorb. – MTTA _{half}	-1563.354322	-1563.332659	-1563.402348	-0.023942	-0.000555	-1563.423272

BIBLIOGRAPHY

- 1 N. Roy, B. Bruchmann and J.-M. Lehn, *Chem. Soc. Rev.*, 2015, **44**, 3786-3807.
- 2 M. A. C. Stuart, W. T. S. Huck, J. Genzer, M. Muller, C. Ober, M. Stamm, G. B. Sukhorukov, I. Szleifer, V. V. Tsukruk, M. Urban, F. Winnik, S. Zauscher, I. Luzinov and S. Minko, *Nat. Mater.*, 2010, **9**, 101-113.
- 3 H. Meng and J. L. Hu, *J. Intell. Mater. Syst. Struct.*, 2010, **21**, 859-885.
- 4 C. J. Kloxin and C. N. Bowman, *Chem. Soc. Rev.*, 2013, **42**, 7161-7173.
- 5 N. K. Guimard, K. K. Oehlenschlaeger, J. Zhou, S. Hilf, F. G. Schmidt and C. Barner-Kowollik, *Macromol. Chem. Phys.*, 2012, **213**, 131-143.
- 6 W. Denissen, J. M. Winne and F. E. Du Prez, *Chem. Sci.*, 2016, **7**, 30-38.
- 7 D. Klinger and K. Landfester, *Polymer*, 2012, **53**, 5209-5231.
- 8 T. P. Huynh and H. Haick, *Adv. Mater.*, 2016, **28**, 138-143.
- 9 J. T. Auletta, G. J. LeDonne, K. C. Gronborg, C. D. Ladd, H. Liu, W. W. Clark and T. Y. Meyer, *Macromolecules*, 2015, **48**, 1736-1747.
- 10 S. Stefani, S. Hönzke, J. L. Cuellar Camacho, F. Neumann, A. K. Prasad, S. Hedtrich, R. Haag and P. Servin, *Polymer*, 2016, **96**, 156-166.
- 11 M. Langer, J. Brandt, A. Lederer, A. S. Goldmann, F. H. Schacher and C. Barner-Kowollik, *Polym. Chem.*, 2014, **5**, 5330-5338.
- 12 H. Qi, T. Zhou, S. Mei, X. Chen and C. Y. Li, *ACS Macro Lett.*, 2016, DOI: 10.1021/acsmacrolett.6b00251, 651-655.
- 13 E. Borre, J. F. Stumbe, S. Bellemin-Laponnaz and M. Mauro, *Angew. Chem. Int. Ed.*, 2016, **55**, 1313-1317.
- 14 W. P. J. Appel, M. M. L. Nieuwenhuizen, M. Lutz, B. F. M. de Waal, A. R. A. Palmans and E. W. Meijer, *Chem. Sci.*, 2014, **5**, 3735-3745.
- 15 T. Ueki, R. Usui, Y. Kitazawa, T. P. Lodge and M. Watanabe, *Macromolecules*, 2015, **48**, 5928-5933.
- 16 J. Ling, M. Z. Rong and M. Q. Zhang, *J. Mater. Chem.*, 2011, **21**, 18373-18380.
- 17 L. P. Zhou, J. X. Li, Q. Luo, J. Y. Zhu, H. X. Zou, Y. Z. Gao, L. Wang, J. Y. Xu, Z. Y. Dong and J. Q. Liu, *Soft Matter*, 2013, **9**, 4635-4641.
- 18 N. Hohlbein, A. Shaaban and A. M. Schmidt, *Polymer*, 2015, **69**, 301-309.
- 19 A. C. Aragonès, N. L. Haworth, N. Darwish, S. Ciampi, N. J. Bloomfield, G. G. Wallace, I. Diez-Perez and M. L. Coote, *Nature*, 2016, **531**, 88-91.

- 20 H. Meng and G. Li, *Polymer*, 2013, **54**, 2199-2221.
- 21 X. Q. Feng, G. Z. Zhang, Q. M. Bai, H. Y. Jiang, B. Xu and H. J. Li, *Macromol. Mater. Eng.*, 2016, **301**, 125-132.
- 22 K. K. Oehlenschlaeger, J. O. Mueller, J. Brandt, S. Hilf, A. Lederer, M. Wilhelm, R. Graf, M. L. Coote, F. G. Schmidt and C. Barner-Kowollik, *Adv. Mater.*, 2014, **26**, 3561-3566.
- 23 T. Aida, E. W. Meijer and S. I. Stupp, *Science*, 2012, **335**, 813-817.
- 24 M. D. Hager, S. Bode, C. Weber and U. S. Schubert, *Prog. Polym. Sci.*, 2015, **49-50**, 3-33.
- 25 Q. Wei, C. Schlaich, S. Prévost, A. Schulz, C. Böttcher, M. Gradzielski, Z. Qi, R. Haag and C. A. Schalley, *Adv. Mater.*, 2014, **26**, 7358-7364.
- 26 L. M. de Espinosa, G. L. Fiore, C. Weder, E. Johan Foster and Y. C. Simon, *Prog. Polym. Sci.*, 2015, **49-50**, 60-78.
- 27 X. Chen, M. A. Dam, K. Ono, A. Mal, H. Shen, S. R. Nutt, K. Sheran and F. Wudl, *Science*, 2002, **295**, 1698-1702.
- 28 I. S. Choi, X. Li, E. E. Simanek, R. Akaba and G. M. Whitesides, *Chem. Mater.*, 1999, **11**, 684-690.
- 29 P. Cordier, F. Tournilhac, C. Soulie-Ziakovic and L. Leibler, *Nature*, 2008, **451**, 977-980.
- 30 G. I. Peterson, M. B. Larsen and A. J. Boydston, *Macromolecules*, 2012, **45**, 7317-7328.
- 31 N. Hosono, M. A. J. Gillissen, Y. Li, S. S. Sheiko, A. R. A. Palmans and E. W. Meijer, *J. Am. Chem. Soc.*, 2013, **135**, 501-510.
- 32 O. Altintas, D. Schulze-Suenninghausen, B. Luy and C. Barner-Kowollik, *Eur. Polym. J.*, 2015, **62**, 409-417.
- 33 R. A. McBride and E. R. Gillies, *Macromolecules*, 2013, **46**, 5157-5166.
- 34 M. A. Azagarsamy, D. D. McKinnon, D. L. Alge and K. S. Anseth, *ACS Macro Lett.*, 2014, **3**, 515-519.
- 35 W. H. Binder, *Self-Healing Polymers*, Wiley-VCH, Weinheim, Germany, 2013.
- 36 X. K. D. Hillewaere and F. E. Du Prez, *Prog. Polym. Sci.*, 2015, **49-50**, 121-153.
- 37 J. Oh, S. Y. An, D. Arunbabu, S. M. Noh and Y. K. Song, *Chem. Commun.*, 2015, **51**, 13058-13070.
- 38 J. R. McElhanon and D. R. Wheeler, *Org. Lett.*, 2001, **3**, 2681-2683.
- 39 M. A. Tasdelen, *Polym. Chem.*, 2011, **2**, 2133-2145.
- 40 S. Telitel, Y. Amamoto, J. Poly, F. Morlet-Savary, O. Soppera, J. Lalevee and K. Matyjaszewski, *Polym. Chem.*, 2014, **5**, 921-930.
- 41 J. Canadell, H. Goossens and B. Klumperman, *Macromolecules*, 2011, **44**, 2536-2541.
- 42 L. Imbernon, E. Oikonomou, S. Norvez and L. Leibler, *Polym. Chem.*, 2015, **6**, 4271-4278.
- 43 S. Y. An, S. M. Noh, J. H. Nam and J. K. Oh, *Macromol. Rapid Commun.*, 2015, **36**, 1255-1260.

- 44 H. Wang, P. Wang, H. Xing, N. Li and X. Ji, *J. Polym. Sci., Part A: Polym. Chem.*, 2015, **53**, 2079-2084.
- 45 D. Montarnal, M. Capelot, F. Tournilhac and L. Leibler, *Science*, 2011, **334**, 965-968.
- 46 J. Willenbacher, O. Altintas, P. W. Roesky and C. Barner-Kowollik, *Macromol. Rapid Commun.*, 2014, **35**, 45-51.
- 47 L. R. Hart, N. A. Nguyen, J. L. Harries, M. E. Mackay, H. M. Colquhoun and W. Hayes, *Polymer*, 2015, **69**, 293-300.
- 48 H. C. Kolb, M. G. Finn and K. B. Sharpless, *Angew. Chem. Int. Ed.*, 2001, **40**, 2004-2021.
- 49 C. Barner-Kowollik and A. J. Inglis, *Macromol. Chem. Phys.*, 2009, **210**, 987-992.
- 50 A. J. Inglis, M. H. Stenzel and C. Barner-Kowollik, *Macromol. Rapid Commun.*, 2009, **30**, 1792-1798.
- 51 J. Zhou, N. K. Guimard, A. J. Inglis, M. Namazian, C. Y. Lin, M. L. Coote, E. Spyrou, S. Hilf, F. G. Schmidt and C. Barner-Kowollik, *Polym. Chem.*, 2012, **3**, 628-639.
- 52 C. Goodyear, *Polytechnisches Journal*, 1838, **69**, 382-384.
- 53 C. Goodyear, US3633, 1844.
- 54 R. J. Young and P. A. Lovell, *Introduction to Polymers*, CRC Press, Boca Raton, 3rd edn., 2011.
- 55 J. W. Hyatt, US105338, 1870.
- 56 A. v. Baeyer, *Ber. Dtsch. Chem. Ges.*, 1872, **5**, 1094-1100.
- 57 L. H. Baekeland, US942699, 1907.
- 58 M. D. Lechner, E. H. Nordmeier and K. Gehrke, *Makromolekulare Chemie*, Birkhäuser, Basel, 4th edn., 2010.
- 59 G. Patterson, *A Prehistory of Polymer Science*, Springer, Heidelberg, 2012.
- 60 B. Tieke, *Makromolekulare Chemie*, Wiley-VCH, Weinheim, 2nd edn., 2005.
- 61 T. Graham, *Philos. Trans. R. Soc. London*, 1861, **151**, 183-224.
- 62 R. Mülhaupt, *Angew. Chem. Int. Ed.*, 2004, **43**, 1054-1063.
- 63 K. Ziegler, E. Holzkamp, H. Breil and H. Martin, *Angew. Chem.*, 1955, **67**, 541-547.
- 64 G. Natta, *Angew. Chem.*, 1964, **76**, 553-566.
- 65 *Plastics – the Facts 2012*, PlasticsEurope, Brussels, 2012.
- 66 K. Matyjaszewski and J. Spanswick, *Mater. Today*, 2005, **8**, 26-33.
- 67 C. A. Blencowe, A. T. Russell, F. Greco, W. Hayes and D. W. Thornthwaite, *Polym. Chem.*, 2011, **2**, 773-790.
- 68 K. Matyjaszewski, *Prog. Polym. Sci.*, 2005, **30**, 858-875.
- 69 S. Sinnwell, M. Lammens, M. H. Stenzel, F. E. Du Prez and C. Barner-Kowollik, *J. Polym. Sci., Part A: Polym. Chem.*, 2009, **47**, 2207-2213.
- 70 A. V. Ambade, S. K. Yang and M. Weck, *Angew. Chem. Int. Ed.*, 2009, **48**, 2894-2898.

- 71 J. K. Sprafke, J. M. Spruell, K. M. Mattson, D. Montarnal, A. J. McGrath, R. Pötzsch, D. Miyajima, J. Hu, A. A. Latimer, B. I. Voit, T. Aida and C. J. Hawker, *J. Polym. Sci., Part A: Polym. Chem.*, 2014, **53**, 319-326.
- 72 L. Chang and E. M. Woo, *Polym. Chem.*, 2010, **1**, 198-202.
- 73 J. Brandrup and E.-H. Immergut, *Polymer Handbook*, Wiley, Chichester, UK, 3rd edn., 1989.
- 74 P. J. Flory, *Principles of Polymer Chemistry*, Cornell University Press, 1953.
- 75 A. P. Haehnel, M. Schneider-Baumann, L. Arens, A. M. Misske, F. Fleischhaker and C. Barner-Kowollik, *Macromolecules*, 2014, **47**, 3483-3496.
- 76 O. Olabisi and K. Adewale, *Handbook of Thermoplastics*, CRC Press, Boca Raton, 2nd edn., 2016.
- 77 C. Barner-Kowollik and G. T. Russell, *Prog. Polym. Sci.*, 2009, **34**, 1211-1259.
- 78 G. Moad and D. H. Solomon, *The Chemistry of Radical Polymerization*, Elsevier Science, 2005.
- 79 N. V. Tsarevsky and B. S. Sumerlin, *Fundamentals of Controlled/Living Radical Polymerization*, Royal Society of Chemistry, 2012.
- 80 K. Matyjaszewski and T. P. Davis, *Handbook of Radical Polymerization*, Wiley, 2002.
- 81 A. Postma, T. P. Davis, G. Li, G. Moad and M. S. O'Shea, *Macromolecules*, 2006, **39**, 5307-5318.
- 82 S. Liu, S. Srinivasan, M. C. Grady, M. Soroush and A. M. Rappe, *Int. J. Quantum Chem.*, 2014, **114**, 345-360.
- 83 N. K. Guimard, J. Ho, J. Brandt, C. Y. Lin, M. Namazian, J. O. Mueller, K. K. Oehlenschlaeger, S. Hilf, A. Lederer, F. G. Schmidt, M. L. Coote and C. Barner-Kowollik, *Chem. Sci.*, 2013, **4**, 2752-2759.
- 84 W. A. Braunecker and K. Matyjaszewski, *Prog. Polym. Sci.*, 2007, **32**, 93-146.
- 85 B. Klumperman, in *Encyclopedia of Polymer Science and Technology*, John Wiley & Sons, Inc., 2002.
- 86 J.-S. Wang and K. Matyjaszewski, *J. Am. Chem. Soc.*, 1995, **117**, 5614-5615.
- 87 M. Kato, M. Kamigaito, M. Sawamoto and T. Higashimura, *Macromolecules*, 1995, **28**, 1721-1723.
- 88 K. Matyjaszewski, *Macromolecules*, 2012, **45**, 4015-4039.
- 89 C. Scholz and K. Matyjaszewski, *Polym. Int.*, 2014, **63**, 801-802.
- 90 W. Jakubowski and K. Matyjaszewski, *Angew. Chem. Int. Ed.*, 2006, **45**, 4482-4486.
- 91 B. P. Fors and C. J. Hawker, *Angew. Chem. Int. Ed.*, 2012, **51**, 8850-8853.
- 92 E. Frick, A. Anastasaki, D. M. Haddleton and C. Barner-Kowollik, *J. Am. Chem. Soc.*, 2015, **137**, 6889-6896.

- 93 M. A. Tasdelen, M. Uygun and Y. Yagci, *Macromol. Chem. Phys.*, 2011, **212**, 2036-2042.
- 94 N. J. Treat, H. Sprafke, J. W. Kramer, P. G. Clark, B. E. Barton, J. Read de Alaniz, B. P. Fors and C. J. Hawker, *J. Am. Chem. Soc.*, 2014, **136**, 16096-16101.
- 95 G. Moad, E. Rizzardo and S. H. Thang, *Acc. Chem. Res.*, 2008, **41**, 1133-1142.
- 96 G. Moad, E. Rizzardo and S. H. Thang, *Aust. J. Chem.*, 2012, **65**, 985-1076.
- 97 P. Corpart, D. Charmot, T. Biadatti, S. Z. Zard and D. Michelet, WO 9858974, 1998.
- 98 C. Barner-Kowollik, *Handbook of RAFT Polymerization*, Wiley-VCH, Weinheim, Germany, 2008.
- 99 M. Glassner, J. P. Blinco and C. Barner-Kowollik, *Polym. Chem.*, 2011, **2**, 83-87.
- 100 D. J. Keddie, G. Moad, E. Rizzardo and S. H. Thang, *Macromolecules*, 2012, **45**, 5321-5342.
- 101 S. D. Bergman and F. Wudl, *J. Mater. Chem.*, 2008, **18**, 41-62.
- 102 J. Willenbacher, B. V. K. J. Schmidt, D. Schulze-Suenninghausen, O. Altintas, B. Luy, G. Delaittre and C. Barner-Kowollik, *Chem. Commun.*, 2014, **50**, 7056-7059.
- 103 S. Tamesue, Y. Takashima, H. Yamaguchi, S. Shinkai and A. Harada, *Angew. Chem. Int. Ed.*, 2010, **49**, 7461-7464.
- 104 B. V. K. J. Schmidt, M. Hetzer, H. Ritter and C. Barner-Kowollik, *Macromolecules*, 2013, **46**, 1054-1065.
- 105 Y. Chujo, K. Sada, A. Naka, R. Nomura and T. Saegusa, *Macromolecules*, 1993, **26**, 883-887.
- 106 M. A. R. Meier, B. G. G. Lohmeijer and U. S. Schubert, *Macromol. Rapid Commun.*, 2003, **24**, 852-857.
- 107 M. A. R. Meier and U. S. Schubert, *J. Polym. Sci., Part A: Polym. Chem.*, 2003, **41**, 2964-2973.
- 108 M. Watanabe and N. Yoshie, *Polymer*, 2006, **47**, 4946-4952.
- 109 E. Krieg, H. Weissman, E. Shirman, E. Shimoni and B. Rybtchinski, *Nat. Nanotechnol.*, 2011, **6**, 141-146.
- 110 M. Guo, L. M. Pitet, H. M. Wyss, M. Vos, P. Y. Dankers and E. W. Meijer, *J. Am. Chem. Soc.*, 2014, **136**, 6969-6977.
- 111 O. Diels and K. Alder, *Liebigs Ann. Chem.*, 1928, **460**, 98-122.
- 112 R. Brückner, *Reaktionsmechanismen*, Spektrum Akademischer Verlag, Munich, 3rd edn., 2004.
- 113 I. Fleming, *Pericyclic Reactions*, Oxford University Press, Oxford, Repr. edn., 2007.
- 114 K. P. C. Vollhardt and N. E. Schore, *Organische Chemie*, Wiley-VCH, Weinheim, 5th edn., 2011.
- 115 R. Hoffmann and R. B. Woodward, *J. Am. Chem. Soc.*, 1965, **87**, 2046-2048.
- 116 R. B. Woodward and R. Hoffmann, *Angew. Chem. Int. Ed.*, 1969, **8**, 781-853.

- 117 I. Fleming, *Molecular orbitals and organic chemical reactions*, Wiley, Chichester, Reference edn., 2010.
- 118 J. Sauer, D. K. Heldmann, J. Hetzenegger, J. Krauthan, H. Sichert and J. Schuster, *Eur. J. Org. Chem.*, 1998, **1998**, 2885-2896.
- 119 R. Hoffmann and R. B. Woodward, *J. Am. Chem. Soc.*, 1965, **87**, 4388-4389.
- 120 V. Eschenbrenner-Lux, K. Kumar and H. Waldmann, *Angew. Chem. Int. Ed.*, 2014, **53**, 11146-11157.
- 121 J. Sauer and R. Sustmann, *Angewandte Chemie International Edition in English*, 1980, **19**, 779-807.
- 122 D. Craig, J. J. Shipman and R. B. Fowler, *J. Am. Chem. Soc.*, 1961, **83**, 2885-2891.
- 123 K. Pahnke, N. L. Haworth, J. Brandt, U. Paulmann, C. Richter, F. G. Schmidt, A. Lederer, M. L. Coote and C. Barner-Kowollik, *Polym. Chem.*, 2016, **7**, 3244-3250.
- 124 R. Breslow, *Acc. Chem. Res.*, 1991, **24**, 159-164.
- 125 M. Glassner, G. Delaittre, M. Kaupp, J. P. Blinco and C. Barner-Kowollik, *J. Am. Chem. Soc.*, 2012, **134**, 7274-7277.
- 126 S. Sinnwell, A. J. Inglis, T. P. Davis, M. H. Stenzel and C. Barner-Kowollik, *Chem. Commun.*, 2008, 2052-2054.
- 127 D. L. Boger and S. M. Weinreb, *Hetero Diels-Alder Methodology in Organic Synthesis*, Academic Press, Inc., San Diego, 2012.
- 128 K.-i. Takao, R. Munakata and K.-i. Tadano, *Chem. Rev.*, 2005, **105**, 4779-4807.
- 129 J. Barluenga, J. Joglar, F. J. González and S. Fustero, *Synlett*, 1990, **1990**, 129-138.
- 130 A. J. Inglis, S. Sinnwell, M. H. Stenzel and C. Barner-Kowollik, *Angew. Chem. Int. Ed.*, 2009, **48**, 2411-2414.
- 131 Z. Wang, Z. Ma, Z. Zhang, F. Wu, H. Jiang and X. Jia, *Polym. Chem.*, 2014, **5**, 6893-6897.
- 132 K. K. Oehlenschlaeger, N. K. Guimard, J. Brandt, J. O. Mueller, C. Y. Lin, S. Hilf, A. Lederer, M. L. Coote, F. G. Schmidt and C. Barner-Kowollik, *Polym. Chem.*, 2013, **4**, 4348-4355.
- 133 S. Sinnwell, C. V. Synatschke, T. Junkers, M. H. Stenzel and C. Barner-Kowollik, *Macromolecules*, 2008, **41**, 7904-7912.
- 134 T. N. Gevrek, T. Bilgic, H. A. Klok and A. Sanyal, *Macromolecules*, 2014, **47**, 7842-7851.
- 135 A. M. Schenzel, C. Klein, K. Rist, N. Moszner and C. Barner-Kowollik, *Adv. Sci.*, 2016, **3**, 1500361.
- 136 A. Gandini, *Prog. Polym. Sci.*, 2013, **38**, 1-29.
- 137 W. M. McGregor and D. C. Sherrington, *Chem. Soc. Rev.*, 1993, **22**, 199-204.
- 138 M. Glassner, K. K. Oehlenschlaeger, A. Welle, M. Bruns and C. Barner-Kowollik, *Chem. Commun.*, 2013, **49**, 633-635.

- 139 G. Bähr and G. Schleitzer, *Chem. Ber.*, 1955, **88**, 1771-1777.
- 140 G. Bähr and G. Schleitzer, *Chem. Ber.*, 1957, **90**, 438-443.
- 141 H. E. Simmons, D. C. Blomstrom and R. D. Vest, *J. Am. Chem. Soc.*, 1962, **84**, 4756-4771.
- 142 K. Pahnke, J. Brandt, G. Gryn'ova, P. Lindner, R. Schweins, F. G. Schmidt, A. Lederer, M. L. Coote and C. Barner-Kowollik, *Chem. Sci.*, 2015, **6**, 1061-1074.
- 143 A. J. Inglis and C. Barner-Kowollik, *Macromol. Rapid Commun.*, 2010, **31**, 1247-1266.
- 144 A. J. Inglis, L. Nebhani, O. Altintas, F. G. Schmidt and C. Barner-Kowollik, *Macromolecules*, 2010, **43**, 5515-5520.
- 145 A. V. Samoshin, C. J. Hawker and J. Read de Alaniz, *ACS Macro Lett.*, 2014, **3**, 753-757.
- 146 S. Billiet, K. De Bruycker, F. Driessen, H. Goossens, V. Van Speybroeck, J. M. Winne and F. E. Du Prez, *Nat. Chem.*, 2014, **6**, 815-821.
- 147 T. Tischer, T. K. Claus, M. Bruns, V. Trouillet, K. Linkert, C. Rodriguez-Emmenegger, A. S. Goldmann, S. Perrier, H. G. Börner and C. Barner-Kowollik, *Biomacromolecules*, 2013, **14**, 4340-4350.
- 148 K. Hildebrandt, T. Pauloehrl, J. P. Blinco, K. Linkert, H. G. Börner and C. Barner-Kowollik, *Angew. Chem. Int. Ed.*, 2015, **54**, 2838-2843.
- 149 P. G. Sammes, *Tetrahedron*, 1976, **32**, 405-422.
- 150 J. L. Charlton and M. M. Alauddin, *Tetrahedron*, 1987, **43**, 2873-2889.
- 151 J. L. Segura and N. Martin, *Chem. Rev.*, 1999, **99**, 3199-3246.
- 152 L. Dell'Amico, A. Vega-Peñaloza, S. Cuadros and P. Melchiorre, *Angew. Chem. Int. Ed.*, 2016, **55**, 3313-3317.
- 153 T. Gründling, K. K. Öhlenschläger, E. Frick, M. Glassner, C. Schmid and C. Barner-Kowollik, *Macromol. Rapid Commun.*, 2011, **32**, 807-812.
- 154 M. Winkler, J. O. Mueller, K. K. Oehlenschlaeger, L. Montero de Espinosa, M. A. R. Meier and C. Barner-Kowollik, *Macromolecules*, 2012, **45**, 5012-5019.
- 155 T. Pauloehrl, A. Welle, K. K. Oehlenschlaeger and C. Barner-Kowollik, *Chem. Sci.*, 2013, **4**, 3503-3507.
- 156 M. Kaupp, A. S. Quick, C. Rodriguez-Emmenegger, A. Welle, V. Trouillet, O. Pop-Georgievski, M. Wegener and C. Barner-Kowollik, *Adv. Funct. Mater.*, 2014, **24**, 5649-5661.
- 157 T. K. Claus, B. Richter, V. Hahn, A. Welle, S. Kayser, M. Wegener, M. Bastmeyer, G. Delaittre and C. Barner-Kowollik, *Angew. Chem. Int. Ed.*, 2016, **55**, 3817-3822.
- 158 X. K. D. Hillewaere and F. E. Du Prez, *Prog. Polym. Sci.*, 2015, **49-50**, 121-153.
- 159 S. K. Yang and S. C. Zimmerman, *Isr. J. Chem.*, 2013, **53**, 511-520.
- 160 J.-M. Lehn, *Science*, 2002, **295**, 2400-2403.
- 161 J. M. Lehn, *Science*, 1993, **260**, 1762-1763.

- 162 D. J. Cram, *Angew. Chem. Int. Ed.*, 1988, **27**, 1009-1020.
- 163 M. Kotera, J.-M. Lehn and J.-P. Vigneron, *Tetrahedron*, 1995, **51**, 1953-1972.
- 164 T. F. A. De Greef, M. M. J. Smulders, M. Wolffs, A. P. H. J. Schenning, R. P. Sijbesma and E. W. Meijer, *Chem. Rev.*, 2009, **109**, 5687-5754.
- 165 L. C. Gilday, S. W. Robinson, T. A. Barendt, M. J. Langton, B. R. Mullaney and P. D. Beer, *Chem. Rev.*, 2015, **115**, 7118-7195.
- 166 Y. Chen and Z. Guan, *Chem. Commun.*, 2014, **50**, 10868-10870.
- 167 B. Zhang, Z. Digby, J. Flum, E. Foster, J. Sparks and D. Konkolewicz, *Polym. Chem.*, 2015, **6**, 7368-7372.
- 168 A. R. Ramesh and K. G. Thomas, *Chem. Commun.*, 2010, **46**, 3457-3459.
- 169 O. Altintas, E. Lejeune, P. Gerstel and C. Barner-Kowollik, *Polym. Chem.*, 2012, **3**, 640-651.
- 170 D. C. Sherrington and K. A. Taskinen, *Chem. Soc. Rev.*, 2001, **30**, 83-93.
- 171 W. H. Binder and R. Zirbs, in *Hydrogen Bonded Polymers*, Springer, Berlin, 2007.
- 172 E. Riedel and C. Janiak, *Anorganische Chemie*, de Gruyter, Berlin, 7th edn., 2007.
- 173 R. P. Sijbesma, F. H. Beijer, L. Brunsveld, B. J. B. Folmer, J. H. K. K. Hirschberg, R. F. M. Lange, J. K. L. Lowe and E. W. Meijer, *Science*, 1997, **278**, 1601-1604.
- 174 S. K. Chang and A. D. Hamilton, *J. Am. Chem. Soc.*, 1988, **110**, 1318-1319.
- 175 V. Berl, M. Schmutz, M. J. Krische, R. G. Khoury and J.-M. Lehn, *Chem. Eur. J.*, 2002, **8**, 1227-1244.
- 176 O. Altintas, P. Krolla-Sidenstein, H. Gliemann and C. Barner-Kowollik, *Macromolecules*, 2014, **47**, 5877-5888.
- 177 B. Gong, *Polym. Int.*, 2007, **56**, 436-443.
- 178 D. Montarnal, N. Delbosc, C. Chamignon, M.-A. Virolleaud, Y. Luo, C. J. Hawker, E. Drockenmuller and J. Bernard, *Angew. Chem. Int. Ed.*, 2015, **54**, 11117-11121.
- 179 J. M. McGrath and M. D. Pluth, *J. Org. Chem.*, 2014, **79**, 711-719.
- 180 S. Chen, N. Mahmood, M. Beiner and W. H. Binder, *Angew. Chem. Int. Ed.*, 2015, **54**, 10188-10192.
- 181 O. Altintas, P. Gerstel, N. Dingenouts and C. Barner-Kowollik, *Chem. Commun.*, 2010, **46**, 6291-6293.
- 182 O. Altintas, U. Tunca and C. Barner-Kowollik, *Polym. Chem.*, 2011, **2**, 1146-1155.
- 183 P. W. Atkins, *Physikalische Chemie*, Wiley-VCH, Weinheim, 2006.
- 184 H. Weingärtner, *Chemische Thermodynamik*, Teubner, Wiesbaden, 1st edn., 2003.
- 185 W. Göpel and H.-D. Wiemhöfer, *Statistische Thermodynamik*, Spektrum, Akad. Verl., Heidelberg, 2000.

- 186 T. L. Hill, *An Introduction to Statistical Thermodynamics*, Dover Publications, Inc., New York, 1986.
- 187 J. B. Foresman and A. Frisch, *Exploring Chemistry with Electronic Structure Models*, Gaussian, Inc., Pittsburgh, PA, 2nd edn., 1996.
- 188 S. M. Bachrach, *Computational Organic Chemistry*, Wiley, Hoboken, New Jersey, 2014.
- 189 P. Echenique and J. L. Alonso, *Mol. Phys.*, 2007, **105**, 3057-3098.
- 190 A. D. Becke, *The Journal of Chemical Physics*, 1993, **98**, 5648-5652.
- 191 D. Cremer and Z. He, *J. Phys. Chem.*, 1996, **100**, 6173-6188.
- 192 M. Lee, D. V. Schoonover, A. P. Gies, D. M. Hercules and H. W. Gibson, *Macromolecules*, 2009, **42**, 6483-6494.
- 193 B. V. K. J. Schmidt, T. Rudolph, M. Hetzer, H. Ritter, F. H. Schacher and C. Barner-Kowollik, *Polym. Chem.*, 2012, **3**, 3139-3145.
- 194 M. Yonekawa, Y. Furusho, T. Takata and T. Endo, *J. Polym. Sci., Part A: Polym. Chem.*, 2014, **52**, 921-928.
- 195 P. F. Du, M. Y. Wu, X. X. Liu, Z. Zheng, X. L. Wang, T. Joncheray and Y. F. Zhang, *J. Appl. Polym. Sci.*, 2014, **131**, 40234.
- 196 P. Taynton, K. Yu, R. K. Shoemaker, Y. Jin, H. J. Qi and W. Zhang, *Adv Mater*, 2014, **26**, 3938-3942.
- 197 E. Trovatti, T. M. Lacerda, A. J. Carvalho and A. Gandini, *Adv Mater*, 2015, **27**, 2242-2245.
- 198 X. Kuang, G. Liu, X. Dong, X. Liu, J. Xu and D. Wang, *J. Polym. Sci., Part A: Polym. Chem.*, 2015, **53**, 2094-2103.
- 199 A. Duval, H. Lange, M. Lawoko and C. Crestini, *Green Chem.*, 2015, **17**, 4991-5000.
- 200 T. A. Plaisted and S. Nemat-Nasser, *Acta Mater.*, 2007, **55**, 5684-5696.
- 201 G. Scheltjens, M. M. Diaz, J. Brancart, G. Van Assche and B. Van Mele, *React. Funct. Polym.*, 2013, **73**, 413-420.
- 202 S. Chen, F. Wang, Y. Peng, T. Chen, Q. Wu and P. Sun, *Macromol. Rapid Commun.*, 2015, **36**, 1687-1692.
- 203 L. M. Polgar, M. van Duin, A. A. Broekhuis and F. Picchioni, *Macromolecules*, 2015, **48**, 7096-7105.
- 204 D. H. Turkenburg and H. R. Fischer, *Polymer*, 2015, **79**, 187-194.
- 205 T. Defize, J.-M. Thomassin, M. Alexandre, B. Gilbert, R. Riva and C. Jérôme, *Polymer*, 2016, **84**, 234-242.
- 206 G. B. Lyon, A. Baranek and C. N. Bowman, *Adv. Funct. Mater.*, 2016, **26**, 1477-1485.
- 207 J. J. Cash, T. Kubo, A. P. Bapat and B. S. Sumerlin, *Macromolecules*, 2015, **48**, 2098-2106.
- 208 O. R. Cromwell, J. Chung and Z. Guan, *J. Am. Chem. Soc.*, 2015, **137**, 6492-6495.

- 209 J. Su, Y. Amamoto, T. Sato, M. Kume, T. Inada, T. Ohishi, Y. Higaki, A. Takahara and H. Otsuka, *Polymer*, 2014, **55**, 1474-1480.
- 210 C. E. Yuan, M. Z. Rong and M. Q. Zhang, *Polymer*, 2014, **55**, 1782-1791.
- 211 Z. P. Zhang, M. Z. Rong and M. Q. Zhang, *Polymer*, 2014, **55**, 3936-3943.
- 212 S. Mukherjee, M. R. Hill and B. S. Sumerlin, *Soft Matter*, 2015, **11**, 6152-6161.
- 213 J. Collins, Z. Xiao, A. Espinosa-Gomez, B. P. Fors and L. A. Connal, *Polym. Chem.*, 2016, **7**, 2581-2588.
- 214 R. J. Wojtecki, M. A. Meador and S. J. Rowan, *Nat. Mater.*, 2011, **10**, 14-27.
- 215 U. S. Schubert and M. Heller, *Chem. Eur. J.*, 2001, **7**, 5252-5259.
- 216 A. Noro, S. Matsushima, X. He, M. Hayashi and Y. Matsushita, *Macromolecules*, 2013, **46**, 8304-8310.
- 217 S. Basak, J. Nanda and A. Banerjee, *Chem. Commun.*, 2014, **50**, 2356-2359.
- 218 D. Mozhdzhi, S. Ayala, O. R. Cromwell and Z. Guan, *J. Am. Chem. Soc.*, 2014, **136**, 16128-16131.
- 219 Z. Sun, F. Lv, L. Cao, L. Liu, Y. Zhang and Z. Lu, *Angew. Chem. Int. Ed.*, 2015, **54**, 7944-7948.
- 220 P. Gilli, V. Ferretti, G. Gilli and P. A. Borea, *J. Phys. Chem.*, 1994, **98**, 1515-1518.
- 221 J. D. Dunitz, *Chem. Biol.*, 1995, **2**, 709-712.
- 222 V. M. Krishnamurthy, B. R. Bohall, V. Semetey and G. M. Whitesides, *J. Am. Chem. Soc.*, 2006, **128**, 5802-5812.
- 223 O. Altintas, K. Riaz, R. Lee, C. Y. Lin, M. L. Coote, M. Wilhelm and C. Barner-Kowollik, *Macromolecules*, 2013, **46**, 8079-8091.
- 224 H. Gao, G. Louche, B. S. Sumerlin, N. Jahed, P. Golas and K. Matyjaszewski, *Macromolecules*, 2005, **38**, 8979-8982.
- 225 K. C. Nicolaou, S. A. Snyder, T. Montagnon and G. Vassilikogiannakis, *Angew. Chem. Int. Ed.*, 2002, **41**, 1668-1698.
- 226 C. Barner-Kowollik, F. E. Du Prez, P. Espeel, C. J. Hawker, T. Junkers, H. Schlaad and W. Van Camp, *Angew. Chem. Int. Ed.*, 2011, **50**, 60-62.
- 227 G. W. T. M. J. Frisch, H. B. Schlegel, G. E. Scuseria, M. A. Robb, J. R. Cheeseman, G. Scalmani, V. Barone, B. Mennucci, G. A. Petersson, H. Nakatsuji, M. Caricato, X. Li, H. P. Hratchian, A. F. Izmaylov, J. Bloino, G. Zheng, J. L. Sonnenberg, M. Hada, M. Ehara, K. Toyota, R. Fukuda, J. Hasegawa, M. Ishida, T. Nakajima, Y. Honda, O. Kitao, H. Nakai, T. Vreven, J. A. Montgomery Jr., J. E. Peralta, F. Ogliaro, M. Bearpark, J. J. Heyd, E. Brothers, K. N. Kudin, V. N. Staroverov, R. Kobayashi, J. Normand, K. Raghavachari, A. Rendell, J. C. Burant, S. S. Iyengar, J. Tomasi, M. Cossi, N. Rega, M. J. Millam, M. Klene, J. E. Knox, J. B. Cross, V. Bakken, C. Adamo, J. Jaramillo, R. Gomperts, R. E. Stratmann, O. Yazyev, A. J. Austin, R. Cammi, C.

- Pomelli, J. W. Ochterski, R. L. Martin, K. Morokuma, V. G. Zakrzewski, G. A. Voth, P. Salvador, J. J. Dannenberg, S. Dapprich, A. D. Daniels, Ö. Farkas, J. B. Foresman, J. V. Ortiz, J. Cioslowski, D. J. Fox, *Gaussian 09 (Revision D.01)*, Gaussian Inc., Wallingford CT, 2009.
- 228 E. Espinosa, M. Glassner, C. Boisson, C. Barner-Kowollik and F. D'Agosto, *Macromol. Rapid Commun.*, 2011, **32**, 1447-1453.
- 229 A. J. Inglis, T. Paulöhr and C. Barner-Kowollik, *Macromolecules*, 2009, **43**, 33-36.
- 230 L. H. Sperling, *Introduction to Physical Polymer Science*, Wiley-VCH, Weinheim, 2006.
- 231 T. P. Lodge and M. Muthukumar, *J. Phys. Chem.*, 1996, **100**, 13275-13292.
- 232 X. Lu and B. Jiang, *Polymer*, 1991, **32**, 471-478.
- 233 C. C. Cypcar, P. Camelio, V. Lazzeri, L. J. Mathias and B. Waegell, *Macromolecules*, 1996, **29**, 8954-8959.
- 234 S. Krause, J. J. Gormley, N. Roman, J. A. Shetter and W. H. Watanabe, *J. Polym. Sci. Part A*, 1965, **3**, 3573-3586.
- 235 J. Heijboer, *Proc. Intern. Conf. on Physics of Non-Crystalline Solids*, North Holland Publishing, Amsterdam, 1965.
- 236 Z. A. Azimov, S. P. Mitsengendler and A. A. Korotkov, *Polym. Sci. USSR*, 1965, **7**, 929-933.
- 237 G. M. Martin, S. S. Rogers and L. Mandelkern, *J. Polym. Sci.*, 1956, **20**, 579-581.
- 238 L. J. Hughes and G. L. Brown, *J. Appl. Polym. Sci.*, 1961, **5**, 580-588.
- 239 E. F. Casassa, *J. Chem. Phys.*, 1955, **23**, 596-597.
- 240 A. Holtzer, *J. Polym. Sci.*, 1955, **17**, 432-434.
- 241 C. E. Rehberg, W. A. Faucette and C. H. Fisher, *J. Am. Chem. Soc.*, 1944, **66**, 1723-1724.
- 242 J. A. Shetter, *J. Polym. Sci., Part B: Polym. Lett.*, 1963, **1**, 209-213.
- 243 J. F. J. Coelho, E. Y. Carvalho, D. S. Marques, A. V. Popov, V. Percec and M. H. Gil, *J. Polym. Sci., Part A: Polym. Chem.*, 2008, **46**, 6542-6551.
- 244 A. Al-Mulla, *Int. J. Chem. Eng.*, 2012, **2012**, 782346.
- 245 O. Colombani and L. Bouteiller, *New J. Chem.*, 2004, **28**, 1373-1382.
- 246 E. H. Feng, W. B. Lee and G. H. Fredrickson, *Macromolecules*, 2007, **40**, 693-702.
- 247 R. Stadler, *Macromolecules*, 1988, **21**, 121-126.
- 248 J.-M. Lehn, *Makromol. Chem. Macromol. Symp.*, 1993, **69**, 1-17.
- 249 L. Brunsveld, B. J. B. Folmer, E. W. Meijer and R. P. Sijbesma, *Chem. Rev.*, 2001, **101**, 4071-4098.
- 250 F. Huang, D. S. Nagvekar, C. Slebodnick and H. W. Gibson, *J. Am. Chem. Soc.*, 2005, **127**, 484-485.
- 251 W. H. Binder, M. J. Kunz, C. Kluger, G. Hayn and R. Saf, *Macromolecules*, 2004, **37**, 1749-1759.

- 252 S. Chen, A. Bertrand, X. Chang, P. Alcouffe, C. Ladavière, J.-F. Gérard, F. Lortie and J. Bernard, *Macromolecules*, 2010, **43**, 5981-5988.
- 253 P. Y. W. Dankers, M. C. Harmsen, L. A. Brouwer, M. J. A. Van Luyn and E. W. Meijer, *Nat. Mater.*, 2005, **4**, 568-574.
- 254 K. Pahnke, O. Altintas, F. G. Schmidt and C. Barner-Kowollik, *ACS Macro Lett.*, 2015, **4**, 774-777.
- 255 Z. S. Yang, Y. G. Shi, W. Chen and F. Wang, *Polym. Chem.*, 2015, **6**, 5540-5544.
- 256 T. F. A. De Greef, M. J. Kade, K. E. Feldman, E. J. Kramer, C. J. Hawker and E. W. Meijer, *J. Polym. Sci., Part A: Polym. Chem.*, 2011, **49**, 4253-4260.
- 257 S. K. Yang, A. V. Ambade and M. Weck, *J. Am. Chem. Soc.*, 2010, **132**, 1637-1645.
- 258 R. S. Macomber, *J. Chem. Educ.*, 1992, **69**, 375-378.
- 259 K. Pahnke, J. Brandt, G. Gryn'ova, C. Y. Lin, O. Altintas, F. G. Schmidt, A. Lederer, M. L. Coote and C. Barner-Kowollik, *Angew. Chem. Int. Ed.*, 2015, **55**, 1514-1518.
- 260 B. M. E. van der Hoff and C. E. Gall, *J. Macromol. Sci. Part A Pure Appl. Chem.*, 1977, **11**, 1739-1758.
- 261 G. J. Price and P. F. Smith, *Polym. Int.*, 1991, **24**, 159-164.
- 262 R. Lee and M. L. Coote, *PCCP*, 2013, **15**, 16428-16431.
- 263 Roestamsjah, L. A. Wall, R. E. Florin, M. H. Aldridge and L. J. Fetters, *J. Res. Nat. Bur. Stand.*, 1978, **83**, 371-380.
- 264 J. Ulbricht, R. Jordan and R. Luxenhofer, *Biomaterials*, 2014, **35**, 4848-4861.
- 265 C. Barner-Kowollik, M. Buback, B. Charleux, M. L. Coote, M. Drache, T. Fukuda, A. Goto, B. Klumperman, A. B. Lowe, J. B. McLeary, G. Moad, M. J. Monteiro, R. D. Sanderson, M. P. Tonge and P. Vana, *J. Polym. Sci., Part A: Polym. Chem.*, 2006, **44**, 5809-5831.
- 266 T. Junkers, C. Barner-Kowollik and M. L. Coote, *Macromol. Rapid Commun.*, 2011, **32**, 1891-1898.
- 267 T. N. Gevrek, T. Bilgic, H.-A. Klok and A. Sanyal, *Macromolecules*, 2014, **47**, 7842-7851.
- 268 W. Thiel and R. Mayer, *Z. Chem.*, 1986, **26**, 433-434.
- 269 H. Dentel, I. Chataigner, F. Le Cavalier and M. Gulea, *Tetrahedron Lett.*, 2010, **51**, 6014-6017.
- 270 H. Dentel, I. Chataigner, J.-F. Lohier and M. Gulea, *Tetrahedron*, 2012, **68**, 2326-2335.
- 271 H. Jiang, D. C. Cruz, Y. Li, V. H. Lauridsen and K. A. Jørgensen, *J. Am. Chem. Soc.*, 2013, **135**, 5200-5207.
- 272 W. Thiel, H. Viola and R. Mayer, *Z. Chem.*, 1977, **17**, 366-367.
- 273 W. Thiel and R. Mayer, *J. Prakt. Chem.*, 1989, **331**, 243-262.

- 274 J. Brandt, N. Guimard, C. Barner-Kowollik, F. Schmidt and A. Lederer, *Anal. Bioanal. Chem.*, 2013, **405**, 8981-8993.
- 275 A. Rudin and H. L. W. Hoegy, *J. Polym. Sci., Part A: Polym. Chem.*, 1972, **10**, 217-235.
- 276 C. Strazielle, H. Benoit and O. Vogl, *Eur. Polym. J.*, 1978, **14**, 331-334.
- 277 D. A. P. R. A. Hutchinson, Jr, J. H. McMinn, S. Beuermann, R. E. Fuller, C. Jackson, *DECHEMA Monogr.*, 1995, **131**, 467-492.
- 278 B. Dervaux, T. Junkers, M. Schneider-Baumann, F. E. Du Prez and C. Barner-Kowollik, *J. Polym. Sci., Part A: Polym. Chem.*, 2009, **47**, 6641-6654.
- 279 H. L. Wagner, *J. Phys. Chem. Ref. Data*, 1985, **14**, 1101-1106.
- 280 G. E. Roberts, T. P. Davis, J. P. A. Heuts and G. E. Ball, *Macromolecules*, 2002, **35**, 9954-9963.
- 281 R. A. Hutchinson, S. Beuermann, D. A. Paquet and J. H. McMinn, *Macromolecules*, 1997, **30**, 3490-3493.
- 282 S. Beuermann, D. A. Paquet, J. H. McMinn and R. A. Hutchinson, *Macromolecules*, 1996, **29**, 4206-4215.
- 283 E. Penzel and N. Goetz, *Angew. Makromol. Chem.*, 1990, **178**, 191-200.

LIST OF SCHEMES, FIGURES AND TABLES

Schemes

Scheme 1-1 Overview of the investigated possibilities to adjust the reaction entropy and thus equilibrium of (reversible) covalent or non-covalent ligation sites via altering (a) chain mass or length, (b) chain stiffness or (c) the ligation position of adducts as well as a schematic depiction of the novel self-reporting dithiooxalate hetero Diels–Alder linker (d) with valuable ligation properties.....	3
Scheme 2-1 Two-step initiation process in free radical polymerization, top: initial radical formation via homolysis of an initiator, bottom: addition of the monomer to the initiator radical.	11
Scheme 2-2 Propagation of a (macro-)radical species with monomer molecules in a radical polymerization.....	11
Scheme 2-3 Termination reactions in radical polymerization, top: recombination of radical species, bottom: disproportionation of two macroradicals.	12
Scheme 2-4 Chain transfer of an active center from a propagating chain to another molecule.	13
Scheme 2-5 Schematic depiction of the step-growth polymerization of A-A- plus B-B-type (top) or of A-B-type monomers (bottom).	14
Scheme 2-6 General mechanism for ATRP techniques enabling a reversible deactivation of a (propagating) radical species. Mt: transition metal activator with oxidation number m, L: ligand, R-X: organic halide, M: monomer.....	17
Scheme 2-7 Mechanistic scheme of the RAFT polymerization process with (a) initiation, (b) pre-equilibrium, (c) re-initiation, (d) main equilibrium and (e) termination.	19
Scheme 2-8 Schematic depiction of appropriately chosen R- and Z-groups for RAFT polymerizations of controlled (—) or limited controlled (---) character, employing various	

monomers (MMA: methyl methacrylate, HPMAM: N-(2-hydroxypropyl)methacrylamide, VAc: vinyl acetate, NVP: N-vinylpyrrolidone, St: styrene, MA: methyl acrylate, AM: acrylamide, AN: acrylonitrile). Adapted with permission from Reference ¹⁰⁰ . Copyright 2012 American Chemical Society.	20
Scheme 2-9 Examples for dynamic covalent and non-covalent chemical linkage methods such as thermo-, redox- or photoresponsive (a) Diels–Alder reactions, (b) disulfide bridges, (c) alkoxyamines, (d) coumarine photodimerization, (e) hydrogen bonding, (f) metal-ligand complexation or (g) host-guest interactions.	21
Scheme 2-10 Formal scheme of a pericyclic [4+2] Diels–Alder cycloaddition of a diene with a dienophile resulting in the formation of cyclohexene-analogue six-membered rings.	22
Scheme 2-11 Correlation diagram of the [4+2] cycloaddition of 1,3-butadiene and ethylene.	22
Scheme 2-12 Diels–Alder reaction of cyclopentadiene and maleic anhydride and the kinetically preferred <i>endo</i> product.	23
Scheme 2-13 Diels–Alder Reaction of furan and maleimides functional species.	25
Scheme 2-14 Examples of thiocarbonyl compounds as dienophiles: (a) thioaldehydes, (b) thioketones, (c) activated dithioesters as well as (d) pyridinyl- or (e) phosphoryl-substituted dithioesters suitable for Lewis acid activation.	25
Scheme 2-15 Hetero Diels–Alder reactions via (a) nitrosocarbonyl or (b) triazolinedione hetero dienophiles.	26
Scheme 2-16 Light-triggered photoenol-formation from <i>o</i> -methylphenyl ketones and subsequent Diels–Alder reaction with a maleimide species.	27
Scheme 2-17 Photo-induced formation of thioaldehydes from phenacyl sulfides and their Diels–Alder reaction with dienes.	27
Scheme 2-18 Examples for (a) single, (b) two-centered, (c) triple, (d) quadruple and (e) multiple hydrogen-bonding interactions.	29
Scheme 2-19 Schematic depiction of (a) hydrogen bonding, (b) attractive and (c) repulsive secondary interactions between donor (D) and acceptor (A) species.	30
Scheme 3-1 General scheme of entropic influences on dynamic reaction equilibria via physical molecular parameters such as (a) molecular weight and length, (b) chain stiffness or (c) the ligation position inside a molecule.	42
Scheme 3-2 Reversibly ligated building blocks of differing length or mass.	45

Scheme 3-3 Model DA reaction of CDTE linkers plus Cp functional polymers with side-chain substituents of different masses studied using quantum chemistry. Fragments in bold correspond to the reaction center in the ONIOM-like approximation. Adapted from Ref. ¹⁴² – Published by The Royal Society of Chemistry.....	47
Scheme 3-4 Reaction scheme for the generation of thermoreversibly connected macromolecules of different building block sizes via (a) ARGET ATRP of acrylate monomers with a bromo difunctional initiator, (b) subsequent substitution of the bromo end-groups via nickelocene and (c) Diels–Alder step-growth of diene and dienophile difunctional blocks. Adapted from Ref. ¹⁴² – Published by The Royal Society of Chemistry.....	50
Scheme 3-5 Reversibly ligated building blocks of differing backbone stiffness.	57
Scheme 3-6 Model DA reaction of isomeric polyacrylates of differing chain stiffness with a CDTE linker studied using quantum chemistry. Fragments in bold correspond to the core layer (reaction center) in the ONIOM-like approximation. Adapted from Ref. ¹⁴² – Published by The Royal Society of Chemistry.	58
Scheme 3-7 Reaction scheme for the generation of thermoreversibly connected macromolecules of different building block sizes via (a) ARGET ATRP of (meth-) acrylate monomers with a bromo (di-) functional initiator, (b) subsequent substitution of the bromo end-groups via nickelocene and (c) Diels–Alder step-growth or diblock formation of dienophile difunctional and diene mono- or difunctional blocks. Adapted from Ref. ¹⁴² – Published by The Royal Society of Chemistry.....	61
Scheme 3-8 Supramolecularly ligated building blocks of differing length or mass.	71
Scheme 3-9 Reaction scheme of the employed RAFT polymerizations to obtain CA- and HW-functional polymers of defined chain lengths.....	73
Scheme 3-10 Reversibly ligated building blocks with differing ligation positions inside a molecule.	79
Scheme 3-11 Schematic view of the theoretical and experimental setup to determine characteristic differences between bond cleavage (a) in the middle and (b) at the end of a molecule. Adapted with permission from Reference ²⁵⁹ . © 2016 WILEY-VCH Verlag GmbH & Co. KGaA, Weinheim.	80
Scheme 4-1 General approach of the thermoreversible ligation of diene-functional (macro-) molecules via dithiooxalates. Adapted from Ref. ¹²³ with permission from The Royal Society of Chemistry.	93

Scheme 4-2 Schematic view of the computationally investigated reaction of a small molecular model dithiooxalate with different diene species as well as the difunctional dithiooxalate.	94
Scheme 4-3 Reaction scheme of the two-step synthesis route employed for the generation of a dithiooxalate difunctional HDA dilinker. Adapted from Ref. ¹²³ with permission from The Royal Society of Chemistry.....	96
Scheme 4-4 Diels–Alder reaction of a deep purple dithiooxalate species with a diene, leading to the conversion of a C=S double bond to a C-S single bond and an accompanying discoloration of the dienophile species. Adapted from Ref. ¹²³ with permission from The Royal Society of Chemistry.....	97

Figures

Figure 2-1 Degree of polymerization DP_n vs. conversion p in a step-growth polymerization.	15
Figure 3-1 Optimized geometries of the DA adducts of CDTE and Cp difunctional poly(methyl acrylate) (with $n = m = 2$) corresponding to (a) the lowest energy conformation and (b) the extended chain conformation. Reproduced from Ref. ¹⁴² – Published by The Royal Society of Chemistry.	47
Figure 3-2 Calculated changes in the entropy (ΔS in $J mol^{-1} K^{-1}$) of model DA reactions for different n, m (chain lengths) of poly(methyl acrylate) (PMA) or poly(isobornyl acrylate) (P ⁱ BoA) macromonomers in their lowest energy or extended chain conformation. In these figures, the more negative ΔS , the lower the Gibbs free energy of bonding, or the greater the extent of debonding, at a given temperature. Adapted from Ref. ¹⁴² – Published by The Royal Society of Chemistry.	48
Figure 3-3 Degree of debonding (determined from the calculated reaction energies for $n = m = 2$ chain lengths) vs. temperature for (a) lowest energy and (b) extended chain conformers of PMA (■) or P ⁱ BoA (●). Adapted from Ref. ¹⁴² – Published by The Royal Society of Chemistry.	49
Figure 3-4 SEC chromatograms of the dibromo precursor polymer (····), Cp functional building block (----), Diels–Alder polymer (—) and control sample of heated Cp difunctional macromonomer without CDTE dilinker (---) for 10 (a) methyl acrylate and (b) isobornyl acrylate repeating units or for 50 (c) methyl acrylate and (d) isobornyl acrylate repeating units per building block, measured in THF at 35 °C. Adapted from Ref. ¹⁴² – Published by The Royal Society of Chemistry.....	51
Figure 3-5 Calculation of the temperature dependent degree of debonding $\%_{\text{debond}}$ via the ¹ H NMR signal ratios of (a) free Cp chain end groups and (b) closed HDA adducts. Adapted from Ref. ¹⁴² – Published by The Royal Society of Chemistry.	52
Figure 3-6 Temperature dependent degree of debonding for Diels–Alder polymers consisting of Cp difunctional PMA _{large} (■, 50 repeating units), P ⁱ BoA _{large} (●, 50 repeating units), PMA _{small} (□, 10 repeating units) or P ⁱ BoA _{small} (○, 10 repeating units) building blocks and CDTE dilinker assessed by HT NMR spectroscopy. Adapted from Ref. ¹⁴² – Published by The Royal Society of Chemistry.	53

- Figure 3-7** TD SEC results: decrease of concentration of DA polymer due to rDA reaction of the DA polymers consisting of Cp difunctional PMA_{large} (■, 50 repeating units) and PⁱBoA_{large} (●, 50 repeating units) building blocks and CDTE dilinker. Adapted from Ref.¹⁴² – Published by The Royal Society of Chemistry. 55
- Figure 3-8** Calculated changes in the entropy (ΔS in J mol⁻¹ K⁻¹) of model DA reactions for different n , m (chain lengths) of poly(*iso*-butyl acrylate) or poly(*tert*-butyl acrylate) macromonomers in their lowest energy or extended chain conformation. In these figures, the more negative ΔS , the lower the Gibbs free energy of bonding, or the greater the extent of debonding, at a given temperature. Adapted from Ref.¹⁴² – Published by The Royal Society of Chemistry. 59
- Figure 3-9** Degree of debonding (determined from the calculated reaction energies for $n = m = 2$ chain lengths) vs. temperature for (a) lowest energy and (b) extended chain conformers of PⁱBuA (►) or P^tBuA (★). Adapted from Ref.¹⁴² – Published by The Royal Society of Chemistry. 60
- Figure 3-10** SEC elugrams of the (di-) bromo precursor polymer (⋯), Cp functional building block (----), Diels–Alder diblock or step-growth polymer (—) and control sample of heated Cp difunctional acrylate macromonomer without CDTE dilinker (·-·-) for 50 (a) ⁱBuMA, (b) ^tBuMA, (c) MMA, (d) ⁿBuA, (e) ⁱBuA and (f) ^tBuA repeating units per building block, measured in THF at 35 °C. Adapted from Ref.¹⁴² – Published by The Royal Society of Chemistry. 62
- Figure 3-11** Temperature dependent degree of debonding for Diels–Alder A,A'-type diblockcopolymers consisting of PMMA (▲), PⁱBuMA (▼) or P^tBuMA (◄) building blocks with a length of 50 repeating units assessed by HT NMR spectroscopy. Adapted from Ref.¹⁴² – Published by The Royal Society of Chemistry. 64
- Figure 3-12** Temperature dependent degree of debonding for Diels–Alder polymers consisting of Cp difunctional PⁱBuA (►), PⁿBuA (◆) or P^tBuA (★) building blocks with a length of 50 repeating units and CDTE dilinker assessed by HT NMR spectroscopy. Adapted from Ref.¹⁴² – Published by The Royal Society of Chemistry. 66
- Figure 3-13** TD SEC chromatograms, (a) DA-P^tBuA after different rDA times at 80 °C in 60 % TCB and 40 % DMF, (b) DA-P^tBuA after 60 min. rDA at 80 °C and distributions calculated by

peak deconvolution of the individual components. Adapted from Ref. ¹⁴² – Published by The Royal Society of Chemistry.	67
Figure 3-14 TD SEC results: decrease of concentration of DA polymers due to rDA reactions of the DA polymers consisting of Cp difunctional P ⁱ BuA (▶), P ⁿ BuA (◆) or P ^t BuA (★) building blocks with a length of 50 repeating units and CDTE dilinker. Adapted from Ref. ¹⁴² – Published by The Royal Society of Chemistry.....	68
Figure 3-15 Set of experiments with the applied (macro-)molecules of different functionality, chain length and their corresponding average molecular mass: CA small molecule (378.22 g mol ⁻¹), HW small molecule (598.69 g mol ⁻¹), CA- and HW-functional P ⁿ BuA _{small} ($M_{n,avg.} = 3000$ g mol ⁻¹), P ⁱ BoA _{small} ($M_{NMR,avg.} = 3300$ g mol ⁻¹), P ⁿ BuA _{medium} ($M_{n,avg.} = 12700$ g mol ⁻¹) as well as P ⁱ BoA _{large} ($M_{n,avg.} = 25000$ g mol ⁻¹). Adapted with permission from Reference ²⁵⁴ . Copyright 2015 American Chemical Society.	72
Figure 3-16 SEC chromatograms of the employed CA- and HW-functional polymer building blocks, measured in THF at 35 °C. Adapted with permission from Reference ²⁵⁴ . Copyright 2015 American Chemical Society.	73
Figure 3-17 Exemplary temperature dependent ¹ H NMR spectra of the CA- and HW-functional small molecule pairing (refer to Figure 3-15) in C ₂ D ₂ Cl ₄ (6 mmol L ⁻¹ , each) with the association dependent shift of the CA imide proton resonance (*). Adapted with permission from Reference ²⁵⁴ . Copyright 2015 American Chemical Society.	74
Figure 3-18 Temperature dependent chemical shift values of the CA imide proton resonance for CA and HW functional building block pairings of different lengths and masses in C ₂ D ₂ Cl ₄ . Adapted with permission from Reference ²⁵⁴ . Copyright 2015 American Chemical Society.	75
Figure 3-19 Dissociation constant values K_{diss} at 100 °C of differently sized CA and HW functional building block pairings, associated <i>via</i> hydrogen bonding in C ₂ D ₂ Cl ₄ . Adapted with permission from Reference ²⁵⁴ . Copyright 2015 American Chemical Society.	76
Figure 3-20 The supramolecular building block pairings with (a) poly(isobornyl acrylate) moieties of $M_{n,SEC/NMR} = 25$ kDa on both sides of the ligation site, (b) one small molecular CA unit in combination with a HW functional poly(isobornyl acrylate) of $M_{NMR} = 60$ kDa and (c) the small molecular control test. Adapted with permission from Reference ²⁵⁹ . © 2016 WILEY-VCH Verlag GmbH & Co. KGaA, Weinheim.	82

- Figure 3-21** Temperature dependent CA imide proton resonance in $C_2D_2Cl_4$ for building blocks associated via CA and HW recognition units in the middle (■) or at the end (●) of macromolecules as well as for small molecular adducts (▲), indicating higher degrees of association for higher downfield shift values. Adapted with permission from Reference²⁵⁹. © 2016 WILEY-VCH Verlag GmbH & Co. KGaA, Weinheim..... 83
- Figure 3-22** TD SEC chromatogram of a thermoreversible DA-PMA at 90 °C and 160 °C and its corresponding building block in 1,3,5-trichlorobenzene (TCB) as well as a schematic view of the degradation process of such DA step-growth polymers, consisting of macromonomers (blue) and a small molecular dilinker (red), at increasing temperatures, here T_0 = ambient temperature, T_1 = 90 °C, T_2 = 160 °C. Adapted with permission from Reference²⁵⁹. © 2016 WILEY-VCH Verlag GmbH & Co. KGaA, Weinheim. 85
- Figure 3-23** Temperature dependent decrease of DA-PⁱBoA or DA-PMA in comparison with the release of the DA dilinker. Adapted with permission from Reference²⁵⁹. © 2016 WILEY-VCH Verlag GmbH & Co. KGaA, Weinheim. 86
- Figure 4-1** ¹H and ¹³C NMR spectra of MTTA in CDCl₃. Adapted from Ref.¹²³ with permission from The Royal Society of Chemistry. 97
- Figure 4-2** UV/Vis spectrum of the characteristic C=S double bond absorbance of MTTA (10 mg mL⁻¹, 33.5 mmol L⁻¹ in MeCN) at 500 nm. Adapted from Ref.¹²³ with permission from The Royal Society of Chemistry. 98
- Figure 4-3** Kinetic plot of the C=S double bond absorbance at 500 nm of a reaction mixture of 20 mg mL⁻¹ (67 mmol L⁻¹) MTTA in acetonitrile or toluene and several dienes vs. time with different equivalents of diene species as well as reaction temperatures. Adapted from Ref.¹²³ with permission from The Royal Society of Chemistry. 99
- Figure 4-4** ¹H NMR spectra of (top) Cp, (middle) MTTA and (bottom) the resulting HDA adduct in a reaction of both reactants, measured in CDCl₃. An endo/exo ratio of approximately 60:40 can be calculated via the integral ratios of signals of different stereoisomers. Adapted from Ref.¹²³ with permission from The Royal Society of Chemistry. 101
- Figure 4-5** Kinetic plot of the C=S double bond absorbance at 500 nm of a reaction mixture of 20 mg mL⁻¹ MTTA in acetonitrile with equimolar amounts of (a) Cp difunctional poly(*tert*-

butyl acrylate) ($\text{Cp}_2\text{P}^t\text{BuA}$) or (b) isophorone bis(sorbic carbamate) (IPDI-SA) at 50 °C. Adapted from Ref. ¹²³ with permission from The Royal Society of Chemistry.	102
Figure 4-6 SEC trace of (a) $\text{Cp}_2\text{P}^t\text{BuA}$ (---) or (b) IPDI-SA and their DA step-growth adduct (– –) with equimolar amounts of MTTA (20 mg mL ⁻¹ in MeCN), measured in THF at 35 °C. Adapted from Ref. ¹²³ with permission from The Royal Society of Chemistry.	103
Figure 4-7 Demonstration of the thermoreversibility of the DA adduct of (a) MTTA and Cp or (b) MTTA and Cp α,ω -difunctional poly(<i>tert</i> -butyl acrylate) via ¹ H HT NMR measurements in toluene-d ₈ . Adapted from Ref. ¹²³ with permission from The Royal Society of Chemistry.	104
Figure 4-8 SEC trace of the step-growth polymer formed from equimolar amounts of MTTA and $\text{Cp}_2\text{P}^t\text{BuA}$ after multiple thermocycles. The rDA reactions were induced by heating the sample to 100-120 °C, the re-emerging DA reactions were achieved upon cooling to ambient temperature. Inset: fluctuation of the molar mass of the DA step-growth adduct as a function of the bonding/debonding cycles. Adapted from Ref. ¹²³ with permission from The Royal Society of Chemistry.	105
Figure 6-1 Linear fit to determine <i>k</i> as the slope of $\ln BB0AA0 \cdot 1B0 - A0$ vs. <i>t</i> for the Diels–Alder reaction of 1.2 eq. DMBD with MTTA (20 mg mL ⁻¹ in MeCN).....	115
Figure 6-2 ¹ H NMR spectra of the dibromo precursor and Cp difunctionalized polymer building blocks with 50 (a) methyl acrylate or (b) isobornyl butyl acrylate repeating units in CDCl ₃	121
Figure 6-3 ¹ H NMR spectra of the dibromo precursor and Cp difunctionalized polymer building blocks with 10 (a) methyl acrylate or (b) isobornyl butyl acrylate repeating units in CDCl ₃	121
Figure 6-4 ¹ H NMR spectra of the bromo precursor and Cp functionalized polymer building blocks with 50 (a) methyl methacrylate, (b) <i>iso</i> -butyl methacrylate or (c) <i>tert</i> -butyl methacrylate repeating units in CDCl ₃	121
Figure 6-5 ¹ H NMR spectra of the dibromo precursor and Cp difunctionalized polymer building blocks with 50 (a) <i>iso</i> -butyl acrylate, (b) <i>n</i> -butyl acrylate or (c) <i>tert</i> -butyl acrylate repeating units in CDCl ₃	122
Figure 6-6 ¹ H HT NMR spectra of the DA polymer formed from (left) PMA _{large} or (right) P ⁱ BoA _{large} building blocks.	122

Figure 6-7 ^1H HT NMR spectra of the DA polymer formed from (left) $\text{PMA}_{\text{small}}$ or (right) $\text{P}^i\text{BoA}_{\text{small}}$ building blocks.....	122
Figure 6-8 ^1H HT NMR spectra of the DA diblock polymer formed from PMMA or P^iBuMA building blocks.....	123
Figure 6-9 ^1H HT NMR spectra of the DA diblock polymer formed from (left) P^tBuMA or (right) P^nBuA building blocks.....	123
Figure 6-10 ^1H HT NMR spectra of the DA polymer formed from (left) P^iBuA or (right) P^tBuA building blocks.....	123
Figure 6-11 Left: ^1H NMR (400 MHz, CDCl_3) of $\text{CA-P}^n\text{BuA}_{\text{small}}$. The ratio of the integral values of the signals H^1 and H^2 allow for the determination of the CA end-group fidelity as $\sim 98\%$. Right: ^1H NMR (400 MHz, CDCl_3) of $\text{HW-P}^n\text{BuA}_{\text{small}}$. The ratio of the integral values of the signals H^{1+2} and H^3 allow for the determination of the CA end-group fidelity as $\sim 99\%$..	125
Figure 6-12 Left: ^1H NMR (400 MHz, CDCl_3) of $\text{CA-P}^i\text{BoA}_{\text{small}}$. The ratio of the integral values of the signals H^1 and H^5 allow for the determination of the CA end-group fidelity as $\sim 99\%$. Right: ^1H NMR (400 MHz, CDCl_3) of $\text{HW-P}^i\text{BoA}_{\text{small}}$. The ratio of the integral values of the signals H^{1+2} and H^5 allow for the determination of the CA end-group fidelity as $\sim 99\%$..	126
Figure 6-13 Left: ^1H NMR (400 MHz, CD_2Cl_2) of $\text{CA-P}^n\text{BuA}_{\text{med}}$. The ratio of the integral values of the signals H^1 and H^2 allow for the determination of the CA end-group fidelity as $\sim 99\%$. Right: ^1H NMR (400 MHz, CDCl_3) of $\text{HW-P}^n\text{BuA}_{\text{med}}$. The ratio of the integral values of the signals H^{1+2} and H^3 allow for the determination of the CA end-group fidelity as $\sim 99\%$..	126
Figure 6-14 Left: ^1H NMR (400 MHz, CDCl_3) of $\text{CA-P}^i\text{BoA}_{\text{large}}$. The ratio of the integral values of the signals H^1 and H^5 allow for the determination of the CA end-group fidelity as $\sim 99\%$. Right: ^1H NMR (400 MHz, CDCl_3) of $\text{HW-P}^i\text{BoA}_{\text{large}}$. The ratio of the integral values of the signals H^{1+2} and H^5 allow for the determination of the CA end-group fidelity as $\sim 99\%$ (x : residual monomer).....	127
Figure 6-15 Expanded temperature dependent ^1H NMR spectra ($n_s = 128$) of equimolar amounts of left: HW- and $\text{CA-P}^n\text{BuA}_{\text{small}}$ or right: HW- and $\text{CA-P}^i\text{BoA}_{\text{small}}$ in $\text{C}_2\text{D}_2\text{Cl}_4$ ($c = 6 \text{ mmol L}^{-1}$), showing the debonding dependent shift of the CA imide proton resonance (*).	127
Figure 6-16 Expanded temperature dependent ^1H NMR spectra ($n_s = 128$) of equimolar amounts of left: HW- and $\text{CA-P}^n\text{BuA}_{\text{med}}$. or right: HW- and $\text{CA-P}^i\text{BoA}_{\text{large}}$ in $\text{C}_2\text{D}_2\text{Cl}_4$	

($c = 6 \text{ mmol L}^{-1}$), showing the debonding dependent shift of the CA imide proton resonance (*).	128
Figure 6-17 Left: Expanded ^1H NMR spectra of CA plus HW Small Molecule (6 mM) without (blue) and with (red) additional non-functional P ⁱ BoA (50 kDa) in $\text{C}_2\text{D}_2\text{Cl}_4$ (6 mM), showing the CA imide proton signal (*). Right: Expanded ^1H NMR spectra of CA plus HW Small Molecule (2 mM) without (blue) and with (red) additional non-functional P ⁿ BuA (7 kDa) in $\text{C}_2\text{D}_2\text{Cl}_4$ (2 mM), showing the CA imide proton signal (*).	128
Figure 6-18 Chemical shifts observed for different ratios of HW/CA species of different molecular weights at 100 °C ($c_{\text{CA}} = 2 \text{ mmol L}^{-1}$).	129
Figure 6-19 Exemplary SEC chromatograms of the dibromo precursor polystyrene (····), Cp difunctional polystyrene (----), Diels–Alder polystyrene (—) and control sample of heated Cp difunctional polystyrene without CDTE dilinker (---) in THF at 35 °C.	130
Figure 6-20 ^1H NMR (400 MHz, CDCl_3) of HW-P ⁱ BoA (60 kDa). The ratio of the integral values of the signals H^{1+2} and H^5 allow for the determination of the CA end-group fidelity as ~99 % (x: residual monomer).	131
Figure 6-21 Expanded temperature dependent ^1H NMR spectra of equimolar amounts ($c = 6 \text{ mmol L}^{-1}$) of $\text{CA}_{\text{small molecule}}$ and HW-P ⁱ BoA (60 kDa) in $\text{C}_2\text{D}_2\text{Cl}_4$ ($n_s = 128$) showing the debonding dependent shift of the CA imide proton resonance (*).	132
Figure 6-22 Chemical shifts observed for different ratios of $\text{CA}_{\text{small molecule}} + \text{HW-P}^i\text{BoA}$ (60 kDa) at 100 °C ($c_{\text{CA}} = 1 \text{ mmol L}^{-1}$ in $\text{C}_2\text{D}_2\text{Cl}_4$).	132
Figure 6-23 ^1H NMR (400 MHz, CDCl_3) of the DA adduct of MTTA and cyclopentadiene.	135
Figure 6-24 ^1H NMR (400 MHz, CDCl_3) of the DA adduct of MTTA and 2,3-dimethyl-1,3-butadiene.	135
Figure 6-25 ^1H NMR (400 MHz, CDCl_3) of the DA adduct of MTTA and sorbic alcohol; x: residual sorbic alcohol.	136
Figure 6-26 ^1H NMR (400 MHz, CDCl_3) of the DA adduct of MTTA and ethyl sorbate.	136
Figure 6-27 ^1H NMR (400 MHz, CDCl_3) of IPDI-SA (top), MTTA (middle) and their step-growth adduct (bottom).	137

Tables

Table 3-1 List of the synthesized bromo and Cp difunctional polyacrylates, their number average molecular weight M_n , dispersity \mathcal{D} and average number of repeating units n	51
Table 3-2 List of the synthesized bromo and Cp (di-)functional polymers, their number average molecular weight M_n , dispersity \mathcal{D} and average number of repeating units n	63
Table 3-3 The different poly(butyl acrylates) investigated in the current section and the corresponding literature values for their glass transition temperatures T_g as well as measured persistence lengths (l_p) in toluene- d_8	65
Table 3-4 Values for the translational and rotational entropy ^a for de-bonding of simple geometric models determined via statistical thermodynamics methods.	81
Table 4-1 List of computationally determined temperatures for DA reaction equilibrium constants of a dithiooxalate with different diene species in MeCN corresponding to a degree of debonding of 20 %. ^a	94
Table 4-2 List of computationally determined temperatures for DA reaction equilibrium constants of full MTTA with different diene species in MeCN corresponding to a degree of debonding of 20 %. ^a	95
Table 4-3 List of rate coefficients ($\pm 15\%$) for the DA reaction of MTTA with different equivalents of dienes in MeCN at ambient or elevated (50 °C) temperature.	100
Table 4-4 Sum formulae and experimental as well as theoretical m/z ratios of reaction products of MTTA + diverse small molecular dienes in ESI-MS.....	101
Table 6-1 Applied Mark-Houwink-Kuhn-Sakurada parameters:.....	113
Table 6-2 List of ARGET ATRP synthetic conditions for the generation of bromo functional polymethacrylates.....	118
Table 6-3 List of ARGET ATRP synthetic conditions for the generation of bromo difunctional polyacrylates.	118
Table 6-4 List of reaction conditions for the Cp functionalization reactions of the bromo (di-) functional poly(meth-)acrylates.....	119
Table 6-5 List of synthetic conditions for the DA linkage reactions.	120
Table 6-6 List of experimental debonding values determined via HT NMR.	120

Table 6-7 Experimental equilibrium constant values for association (K_{ass}) and dissociation (K_{diss}) of differently sized hydrogen bonding diblocks determined via ^1H HT NMR titration ($c_{\text{CA}} = 2 \text{ mmol L}^{-1}$).....	129
Table 6-8 Calculated entropies, enthalpies and free energies of DA reactions in the gas phase and in toluene solution at 25 °C.....	139
Table 6-9 Contributions to the free energies of all species at 25 °C. ^a	140

LIST OF ABBREVIATIONS

a.u.	arbitrary units
Ar	Argon
ARGET	activators regenerated by electron-transfer
ATRP	atom transfer radical polymerization
avg.	average
<i>c</i>	concentration
CA	cyanuric acid
CDCl ₃	deuterated chloroform
CDTE	cyanodithioester
Cp	cyclopentadiene
Cu	copper
CuBr ₂	copper(II) bromide
C ₂ D ₂ Cl ₄	deuterated tetrachloroethane
<i>C</i> _∞	characteristic ratio
δ	chemical shift
\bar{D}	dispersity
Da	Dalton
DA	Diels–Alder
DMAc	dimethylacetamide
DMBD	2,3-dimethyl-1,3-butadiene
DMF	dimethylformamide
DNA	deoxyribonucleic acid
<i>DP</i> _n	degree of polymerization
eq.	equivalents
ESI-MS	electrospray ionization mass spectrometry
FMO	frontier molecular orbital
FRP	free radical polymerization
g	grams

List of Abbreviations

ΔG	free enthalpy
h	hours
ΔH	enthalpy
HDA	hetero Diels–Alder
HOMO	highest occupied molecular orbital
HT	high temperature
HW	Hamilton wedge
ⁱ BoA	isobornyl acrylate
ⁱ BuA	<i>iso</i> -butyl acrylate
ⁱ BuMA	<i>iso</i> -butyl methacrylate
IPDI-SA	isophorone bis(sorbic carbamate)
J	Joule
K	Kelvin
K_a	association constant
K_{diss}	dissociation constant
k_d	rate coefficient of the initiator decomposition
k_i	rate coefficient of initiation
k_p	rate coefficient of propagation
k_t	rate coefficient of termination
k_{tr}	rate coefficient of transfer
λ	wavelength
L	liters
l_k	Kuhn length
l_p	persistence length
LUMO	lowest unoccupied molecular orbital
M	molar
MA	methyl acrylate
MADIX	macromolecular design via the interchange of xanthates
MeCN	acetonitrile
MeI	methyl iodide
Me ₆ TREN	tris[2-(dimethylamino)ethyl]amine

min.	minutes
MMA	methyl methacrylate
M_n	number average molar mass
MTTA	ethane-1,2-diyl bis(2-(methylthio)-2-thioacetate)
M_w	weight average molar mass
mV	millivolts
m/z	mass-to-charge ratio
n BuA	<i>n</i> -butyl acrylate
NaI	sodium iodide
NEt ₃	triethylamine
NiCp ₂	nickelocene/bis(cyclopentadienyl)nickel
nm	nanometers
NMP	nitroxide mediated polymerization
NMR	nuclear magnetic resonance
PBuA	poly(butyl acrylates)
PBuMA	poly(butyl methacrylates)
P ^{<i>i</i>} BoA	poly(isobornyl acrylate)
P ^{<i>i</i>} BuA	poly(<i>iso</i> -butyl acrylate)
P ^{<i>i</i>} BuMA	poly(<i>iso</i> -butyl methacrylate)
PMA	poly(methyl acrylate)
PMMA	poly(methyl methacrylate)
P ^{<i>n</i>} BuA	poly(<i>n</i> -butyl acrylate)
ppm	parts per million
P ^{<i>t</i>} BuA	poly(<i>tert</i> -butyl acrylate)
P ^{<i>t</i>} BuMA	poly(<i>tert</i> -butyl methacrylate)
PPh ₃	triphenylphosphine
PS	polystyrene
RAFT	reversible addition-fragmentation chain-transfer
rDA	retro Diels–Alder
RDRP	reversible deactivation radical polymerization
Ref.	reference

List of Abbreviations

RI	refractive index
rt	ambient temperature
s	seconds
S ₈	sulphur
$\Delta S_{(\text{trans/rot/vib})}$	(translational/vibrational/rotational) entropy
SEC	size exclusion chromatography
Sn(EH) ₂	tin(II) 2-ethylhexanoate
<i>t</i>	time
<i>T</i>	temperature
^t BuA	<i>tert</i> -butyl acrylate
^t BuMA	<i>tert</i> -butyl methacrylate
TCB	1,2,4-trichlorobenzene
TD	temperature dependent
<i>T_g</i>	glass transition temperature
THF	tetrahydrofuran
TMS	tetramethylsilane
UPy	2-ureido-4[1H]-pyrimidinone
UV	ultraviolet (light)
Vis	visible (light)
% _{debond}	degree of debonding

CURRICULUM VITAE

Not available in the electronic version.

PUBLICATIONS AND CONFERENCE CONTRIBUTIONS

Publications Arising from this Thesis

- [4] *A Mild, Efficient and Catalyst-Free Thermoreversible Ligation System Based on Dithiooxalates*
K. Pahnke, N. L. Haworth, J. Brandt, U. Paulmann, C. Richter, F. G. Schmidt, A. Lederer, M. L. Coote, C. Barner-Kowollik, *Polym. Chem.* **2016**, *7*, 3244-3250.
- [3a] *Entropy-Driven Selectivity for Chain Scission: Where Macromolecules Cleave*
K. Pahnke, J. Brandt, G. Gryn'ova, C. Y. Lin, O. Altintas, F. G. Schmidt, A. Lederer, M. L. Coote, C. Barner-Kowollik, *Angew. Chem. Int. Ed.* **2016**, *55*, 1514-1518.
- [3b] *Entropisch bedingte Selektivität der Kettenspaltung oder: Wo Makromoleküle sich trennen*
K. Pahnke, J. Brandt, G. Gryn'ova, C. Y. Lin, O. Altintas, F. G. Schmidt, A. Lederer, M. L. Coote, C. Barner-Kowollik, *Angew. Chem.* **2016**, *128*, 1537-1541.
- [2] *Entropic Effects on the Supramolecular Self-Assembly of Macromolecules*
K. Pahnke, O. Altintas, F. G. Schmidt, C. Barner-Kowollik, *ACS Macro Lett.* **2015**, *4*, 774-777.
- [1] *Entropy Driven Chain Effects on Ligation Chemistry*
K. Pahnke, J. Brandt, G. Gryn'ova, P. Lindner, R. Schweins, F. G. Schmidt, A. Lederer, M. L. Coote, C. Barner-Kowollik, *Chem. Sci.* **2015**, *6*, 1061-1074.

Patents Arising from this Thesis

- [1] *Neuartige Hetero-Diels-Alder-Vernetzer und deren Verwendung in reversibel vernetzenden Polymersystemen*

F. G. Schmidt, U. Paulmann, C. Richter, M. Inhestern, C. Meier, C. Barner-Kowollik, **K. Pahnke**, M. A. Sanz, S. Umbreen, IP-Nr. to be advised.

Additional Publications

- [1] *Consecutive Modular Ligation as an Access Route to Palladium Containing Polymers*

C. Lang, **K. Pahnke**, C. Kiefer, A. S. Goldmann, P. W. Roesky, C. Barner-Kowollik, *Polym. Chem.* **2013**, *4*, 5456-5462.

Invited Talk and Conference Contributions

- [4] *Entropic Chain Effects on Covalent and Supramolecular Association Chemistries* (poster presentation)

K. Pahnke, J. Brandt, G. Gryn'ova, N. L. Haworth, O. Altintas, F. G. Schmidt, A. Lederer, M. L. Coote, C. Barner-Kowollik, *Warwick Polymer Conference*, July **2016**, Warwick, **Great Britain**.

- [3] *Entropic Chain Effects on Ligation Chemistry: An Overview* (oral presentation)

K. Pahnke, J. Brandt, G. Gryn'ova, C. Y. Lin, F. G. Schmidt, A. Lederer, M. L. Coote, C. Barner-Kowollik, *Australian National University*, January **2016**, Canberra, **Australia**.

[2] *Entropic Chain Effects on Ligation Chemistry* (oral presentation)

K. Pahnke, J. Brandt, G. Gryn'ova, F. G. Schmidt, A. Lederer, M. L. Coote, C. Barner-Kowollik, *EPF Congress*, June **2015**, Dresden, **Germany**.

[1] *Entropy Driven Chain Effects on Ligation Chemistry* (poster presentation)

K. Pahnke, J. Brandt, G. Gryn'ova, P. Lindner, R. Schweins, F. G. Schmidt, A. Lederer, M. L. Coote, C. Barner-Kowollik, *Evonik Chemtogether*, November **2014**, Darmstadt, **Germany**.

ACKNOWLEDGEMENTS

Zu allererst gilt mein Dank natürlich meinem Doktorvater, Prof. Dr. Christopher Barner-Kowollik – für dieses spannende und herausfordernde Thema, seine sehr direkte Betreuung und immerwährende Unterstützung sowie seinen vollen Einsatz für die Gruppe und für jeden Einzelnen. Diese außergewöhnliche Motivation in Kombination mit dem entgegengebrachten Vertrauen macht ein selbstständiges Arbeiten und die eigene Weiterentwicklung auf beste Weise möglich.

Ein besonderer Dank gilt meinen Kooperationspartnern bei Evonik Industries für die ausgezeichnete fachliche und jederzeit sehr menschliche Zusammenarbeit – besonders mit Dr. Friedrich Georg Schmidt, aber auch mit Dr. Stefan Hilf und Dr. Christian Meier, um nur diejenigen zu nennen, die am häufigsten Teil der Diskussionsrunde waren. Durch ihre Unterstützung, Impulse und geteilten Ansätze wurde diese Arbeit nicht nur ermöglicht, sondern auch bereichert.

Thanks to the whole macroarc group and all former members for the great working atmosphere and team spirit. Danke insbesondere an Evelyn Stühling, Dr. Maria Schneider, Dr. Anja Goldmann, Peter Gerstel und Vincent Schüler, ohne deren außerordentliche organisatorische Arbeit die reibungslose Funktion der Gruppe nicht möglich wäre!

I especially want to thank my Evonik teammates Dr. Nathalie Guimard, Kim Öhlenschläger and Jan Müller – as well as our latest member, Astrid Hirschbiel – for the productive scientific discussions and the great times on our way to or after the meetings.

A big thank you goes to Prof. Michelle Coote and her team with Dr. Naomi Campbell and Dr. Ganna Gryn'ova amongst them for providing plentiful scientific discussions and excellent theoretical calculations to substantiate the experimental work as well as for my cordial welcome at the Australian National University in Canberra. Thanks to Dr. Leesa Smith for her great help with all laboratory-related and organizational issues at the ANU as well as to all my other new friends in Canberra who made my time Down Under special. Ich danke dem Karlsruhe House of Young Scientists (KHYS) für die Finanzierung meines Auslandsaufenthalts an der Australian National University.

Ein großes Dankeschön geht auch an Dr. Albena Lederer und Josef Brandt vom Leibniz-Institut für Polymerforschung in Dresden für ihre unkomplizierte Zusammenarbeit und die vielen Messungen und Diskussionen in unserem gemeinsamen Projekt.

Thanks to all other co-authors of my publications for your valuable contributions, discussions, comments and support: Dr. Ching Yeh Lin, Dr. Uwe Paulmann, Dr. Christian Richter, Dr. Paul Lindner and Dr. Ralf Schweins. A special thanks goes to Dr. Özcan Altintas for his great assistance with polymerization techniques and hydrogen bonding systems.

Danke Arthur Turkin für die gute Zusammenarbeit und die Unterstützung meiner Dissertation durch eine Bachelorarbeit, alles Gute für die Zukunft!

Thanks Tanja Claus, Michael Kaupp, Bryan Tuten and Rouven Müller for proofreading my thesis as well as Andrew Vogt for always correcting my English.

Thank you Westies for being the best lab- and office-team ever! Without being exhaustive, the long list of great co-workers in the Westhochschule include Dr. Christiane Lang, Dr. Lebohang Hlalele, Dr. Andrew Vogt, Dr. Christoph Dürr, Tanja Claus, Carolin Heiler, Rouven Müller, Paul Lederhose, Marcus Zieger, Dr. Alex Soeriyadi, Jeroen de Neve, Tanja Rieder and – since lately – also Marcel Langer. It was a pleasure to share time with you during work, coffee breaks and also after hours.

Danke liebe Freunde, danke meine liebe Familie für eure Unterstützung, eure Geduld und euren Glauben an mich. Danke Mirijam, dass du auch in schwierigen Zeiten zu mir hältst. Ohne euch wäre diese Arbeit nicht möglich gewesen.

DECLARATION

Hiermit erkläre ich wahrheitsgemäß, dass diese Arbeit im Rahmen der Betreuung durch Prof. Dr. Christopher Barner-Kowollik selbstständig von mir verfasst wurde, keine anderen als die angegebenen Quellen und Hilfsmittel verwendet, die wörtlich oder inhaltlich übernommenen Stellen als solche kenntlich gemacht sowie die Regeln zur Sicherung guter wissenschaftlicher Praxis des Karlsruher Instituts für Technologie (KIT) beachtet wurden, die elektronische Version der Arbeit mit der schriftlichen übereinstimmt und die Abgabe und Archivierung der Primärdaten gemäß Abs. A (6) der Regeln zur Sicherung guter wissenschaftlicher Praxis des KIT beim Institut gesichert ist.

Karlsruhe, 07.06.2016